Precursors of “Enteric” Smooth Muscle: from developmental origin to regenerative medicine

---

by Silvia Perin

To be submitted for a degree of

Doctor of Philosophy

University College London

August 2019

I, Silvia Perin, confirm that the work presented in this thesis is my own. Where information has been taken from other sources, I confirm that this has been stated.

Table of contents

Abstract

A tissue-engineered intestine could be the ideal solution to overcome two of the main constrains of transplantation, such as donor shortage and life-long immunosuppression, to treat intestinal failure in children and in adults. In order to build a functional intestine, all its layers need to be regenerated. Unfortunately, while the precursors of the epithelium and the enteric nervous system have been already identified, the origin of intestinal smooth muscle cells is still undetermined. Thus, the purpose of my research was twofold: i) investigate the origin of smooth muscle cells during mouse and human intestinal development to identify putative smooth muscle precursors; ii) isolate and characterise intestinal mesoangioblasts as a vascular source of smooth muscle cells for regenerative use.

In this study, a population of cells co-expressing cKit and PDGFRα was identified as the putative smooth muscle precursor population using immunofluorescence and RNA-sequencing techniques at different developmental stages. Intestinal mesoangioblasts were successfully isolated from foetal and paediatric intestinal biopsies and showed similarities with pericytes. Upon different treatments mesoangioblasts were able to differentiate into smooth muscle cells as confirmed by immunofluorescence, western blotting, qPCR and transcriptome analyses. Moreover, cells showed an innate differentiation potential towards smooth muscle *in vivo*. When seeded into decellularised foetal midguts, mesoangioblasts successfully regenerated two orthogonal smooth muscle layers resembling the native layers.

Overall, the work reported in this PhD provided new insights into the origin of the longitudinal smooth muscle layer of the gut and identified in intestinal mesoangioblasts a source of smooth muscle precursors, that can be easily isolated from intestinal biopsies and can be used in regenerative medicine.

Impact Statement

Although the advancements in medical and surgical managements of several congenital and acquired diseases of the intestine have slightly improved patients' quality of life, frequently they still fail in overcoming the inevitable progression of such diseases leading to intestinal failure (IF). IF is a clinical challenge mainly for the poor outcome and the high morbidity and mortality, offering survivors a very poor quality of life. When dealing with intestinal failure in children, the last resource remains intestinal transplantation. As very well known, transplantation has some drawbacks, like the need of donors and of life-long immunosuppression. Nevertheless, the massive improvement in the field of regenerative medicine gave researchers something to look forward with the aim of building a fully functional intestine using patients' own cells in order to avoid most of the complications associated with transplantation.

So far, a suitable intestinal replacement is still missing due to a lack of proper pre-vascularisation and the absence of a mature and contractile neuromuscular wall. The work described here was driven by the idea that in order to build a fully functional intestinal replacement, which would massively improve the management of children affected by IF, all the different cell types need to be used. However, while for most of the components of the multilayer intestinal structure, the appropriate stem/precursor cells have been identified, there is no agreement in regards to the proper cell type that is required for the regeneration of the smooth muscle layers.

In this study, attention was drawn on the isolation and characterisation of a source of smooth muscle precursors that could be easily isolated from intestinal biopsies, which are routinely taken during the diagnostic process and during treatment of the aforementioned diseases. We believe that these smooth muscle precursor cells, used in combination with the well characterised epithelial and neural precursor cells, will allow the generation of a functional intestine with a contractile wall.

This approach will have a huge economic impact on the health system, helping to reduce the costs of current treatments and of the frequent

hospitalisations that our little patients need. Moreover, the use of such advance and personalised therapeutic substitutes, might offer a one-off therapy, that will transform surgical treatments, saving costs for families as well as health services and offering commercial opportunities to pharmaceutical companies.

List of publications

The work described in this thesis will be included in the following manuscripts, currently under preparation:

Perin, S., Peruzza, L., McCann, C.J., Natarajan, D., Chapman, C., De Coppi, P. and Thapar, N. *Intestinal mesoangioblasts can successfully generate orthogonally orientated muscle layers in a decellularised scaffold.*

Perin, S., Peruzza, L., McCann, C.J., Natarajan, D., Khalaf, S., De Coppi, P. and Thapar, N. *PDGFRa^{+}/cKit^{+} cells of the developing gut: putative smooth muscle precursors.*

Perin, S., McCann, C.J., Khalaf, S., De Coppi, P. and Thapar, N. *Human development of PDGFRa positive interstitial cells.*

Additional contribution to the following publications was made during the three-years PhD period:

McCann, C.J., Alves, M.M., Brosens, E., Natarajan, D., **Perin, S.**, Chapman, C., Hofstra, R.M., Burns, A.J., Thapar, N., 2019. *Neuronal Development and Onset of Electrical Activity in the Human Enteric Nervous System.* Gastroenterology 156, 1483-1495 e1486.

Perin, S., McCann, C.J., De Coppi, P., Thapar, N., 2019. *Isolation and characterisation of mouse intestinal mesoangioblasts.* Pediatric surgery international 35, 29-34.

Urciuolo, A., Urbani, L., **Perin, S.**, Maghsoudlou, P., Scottoni, F., Gjinovci, A., Collins-Hooper, H., Loukogeorgakis, S., Tyraskis, A., Torelli, S., Germinario, E., Fallas, M.E.A., Julia-Vilella, C., Eaton, S., Blaauw, B., Patel, K., De Coppi, P., 2018. *Decellularised skeletal muscles allow functional muscle regeneration by promoting host cell migration.* Sci Rep 8, 8398.

Perin, S., McCann, C.J., Borrelli, O., De Coppi, P., Thapar, N., 2017. *Update on Foregut Molecular Embryology and Role of Regenerative Medicine Therapies.* Frontiers in pediatrics 5, 91.

List of abbreviations

αSMA: alpha smooth muscle actin

AP: alkaline phosphatase

ASCs: adult stem cells

BMP: bone morphogenetic protein

BMPr: bone morphogenetic protein receptor

BSA: Bovine serum albumin

CIPO: chronic intestinal pseudo-obstruction

CM: circular muscle

CPM: count per million

DEGs: differentially expressed genes

DET: detergent enzymatic treatment

DMP: deep muscular plexus

dpc: day post conception

EDNRB: endothelin receptor

EMT: epithelial-mesenchymal transition

ENCs: enteric neural cells

ENS: enteric nervous system

EpCAM: Epithelium Cell Adhesion Molecule

ESCs: embryonic stem cells

EtOH: ethanol

FACS: Flow activated cell sorting

FBS: foetal bovine serum

FGF: fibroblast growth factor

FLC: fibroblast-like cells

GI: gastrointestinal

GLP-2: glucagon-like peptide-2

GO: gene ontology

H&E: Haematoxylin and Eosin

HDBR: Human Developmental Biology Resource

hFtLIMB_MABs: human foetal limb mesoangioblasts

hFtSI_MABs: human foetal small intestinal mesoangioblast-like cells

Hh: Hedgehog

hPaedSI_MABs: human paediatric small intestinal mesoangioblast-like cells

HS: horse serum

hSI_MABs: human small intestinal mesoangioblast-like cells

ICCs-DMP: interstitial cells of Cajal of the deep muscular plexus

ICCs-IM: intramuscular interstitial cells of Cajal

ICCs-MY: myenteric interstitial cells of Cajal

ICCs-SEP: septal interstitial cells of Cajal

ICCs-SM: submucosal ICCs

ICCs-SS: subserosal interstitial cells of Cajal

ICCs: interstitial cells of Cajal

IF: intestinal failure

Ihh: Indian hedgehog

iPSCs: induced pluripotent stem cells

LILT: Longitudinal Intestinal Lengthening and Tailoring

LM: longitudinal muscle

LMCs: longitudinal muscle cells

MABs: mesoangioblasts

MSCs: mesenchymal stem cells

NCCs: neural crest cells

O/N: overnight

PBS: phosphate buffer solution

PBT: Triton-X in phosphate buffer solution

pcw: post conceptional week

PDGF: platelet derived growth factor

PDGFRs: platelet-derived growth factor receptors

PDGFRα-IM: intramuscular PDGFRα^{+} cells

PDGFRα-MY: myenteric PDGFRα^{+} cells

PDGFRα: platelet-derived growth factor receptor alpha

PFA: paraformaldehyde

PIPO: paediatric intestinal pseudo-obstruction

RIN: RNA integrity number

RT: room temperature

SBS: short bowel syndrome

SCFr: stem cell factor receptor

Shh: Sonic hedgehog

SILT: Spiral Intestinal Lengthening and Tailoring

SIP: SMCs / ICCs / PDGFRα^{+} cells

SM-MHC: smooth muscle myosin heavy chain

SM: smooth muscle

SM22: smooth muscle protein 22

SMCs: smooth muscle cells

SNP: Single nucleotide polymorphism

SRF: serum response factor

STEP: Serial Transverse Enteroplasty

TE: tissue engineering

TGFß: transforming growth factor beta

TSSCs: tissue specific stem cells

WT: wild type

List of figures

Chapter 1. Introduction

Chapter 2. Materials and Methods

Chapter 3. Human intestine: development of the smooth muscle layers

Chapter 4. Mouse enteric smooth muscle: origin and development

Chapter 5. Human small intestinal mesoangioblast-like cells (hSI_MABs): isolation, characterisation and regenerative medicine application

Chapter 6. Human small intestinal mesoangioblast-like cells (hSI_MABs): smooth muscle differentiation

List of Tables

Chapter 2. Materials and Methods

Chapter 3. Human intestine: development of the smooth muscle layers

Chapter 4. Mouse enteric smooth muscle: origin and development

Chapter 1

Introduction

1. Introduction

1.1 The intestine: anatomy and functions

The hollow organs of the digestive system, namely pharynx, oesophagus, stomach, intestine and colon, usually termed the “gut”, together with thyroid, thymus, parathyroid, lungs, liver, biliary apparatus, spleen and pancreas, constitute a complex physiological system, called gastrointestinal (GI) tract. The gut has several functions, of which, the main ones, are to process food by assimilating water and nutrients and finally to eliminate waste. To fulfil these functions, a healthy muscular gut wall is needed to mix and propel food and waste along the tubular organs, while different specialised epithelia are needed to absorb nutrients and water throughout the length of the small and large intestine (Sanders et al., 2012). In addition, given that the intestine is constantly exposed to external antigens and immune stimuli it houses the largest compartment of the immune system (Mowat and Agace, 2014).

The intestine is made up of two major segments in continuity with each other, the small and large intestine. The former begins at the level of the pylorus, just after the stomach, and terminates with the ileocecal valve from which the large intestine starts, ending with the anus. The small intestine is divided into three segments; the duodenum, the jejunum and the ileum and, in the human adult, has a total length of 6-7 meters configured as multiple loops (Mowat and Agace, 2014). Compared with the small intestine, the large intestine has a wider diameter, but shorter length (around 1.5 meters) (Mowat and Agace, 2014). The large intestine starts proximally with the caecum, followed by the ascending colon, transverse colon, descending colon, sigmoid colon, rectum and terminates distally with the anus (Fig. 1-1).

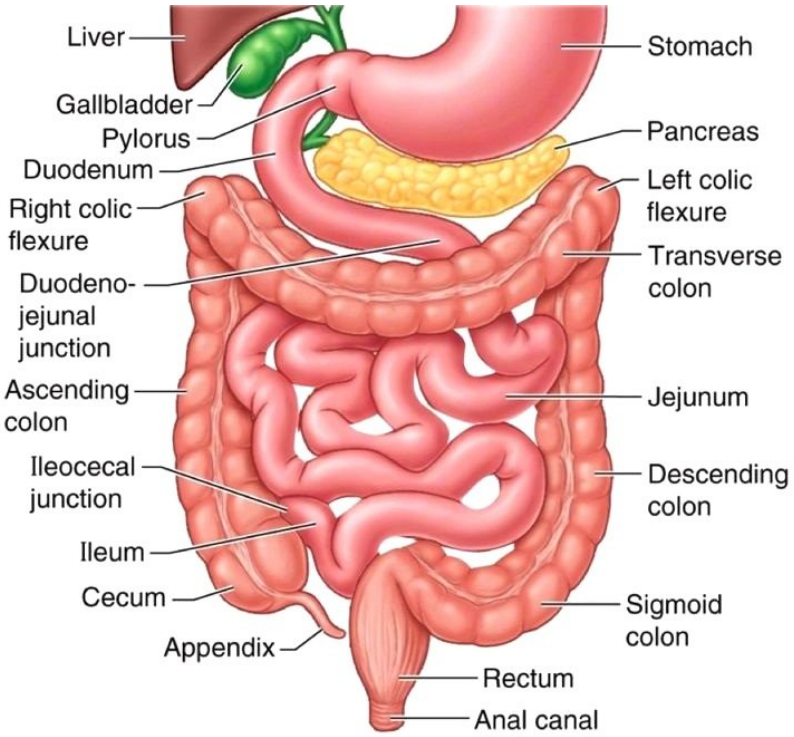

Figure 1-1: Intestine gross anatomy

Picture taken from https://www.advancedhealing.com/small-intestine-enterocyte-leaky-gut-digestion/

Histologically, the intestine is a multi-stratified organ composed of different layers. The first layer on the luminal surface is the mucosa, a specialised columnar epithelium lying on the *lamina propria.* Underneath this is the *muscularis mucosae,* a thin layer of muscle cells, which separates the mucosa from the submucosa. The submucosa sits adjacent to the *muscularis externa* and contains the submucosal plexus of the Enteric Nervous System (ENS). The muscularis externa is composed of two muscle layers, an inner circular and an outer longitudinal, with the myenteric plexus of the ENS located between them (Fig. 1-2). Finally, a thin outer layer of cells, the serosa, encases the entire structure (Standring, 2016).

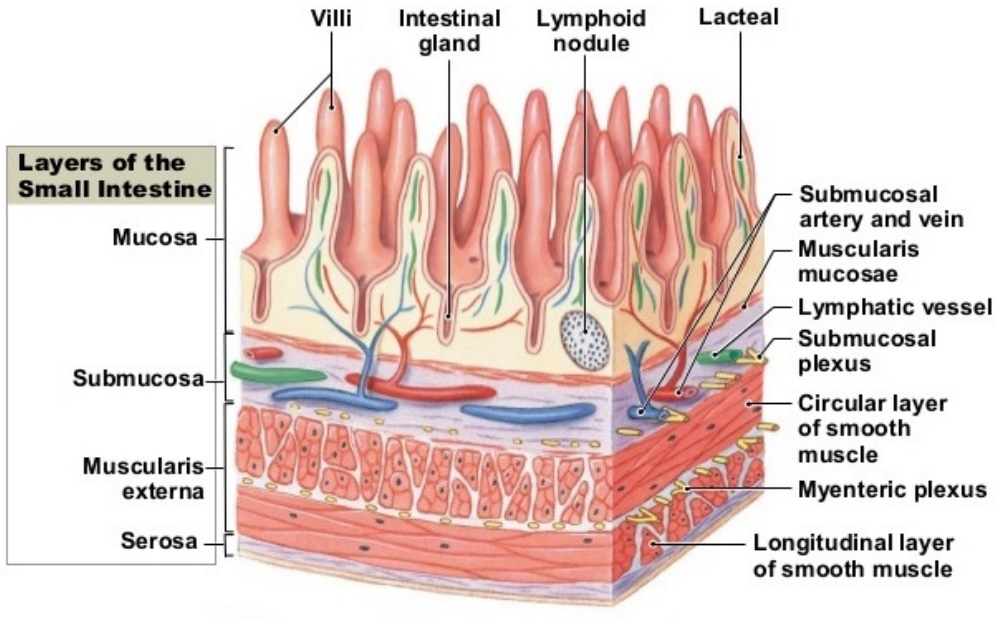

Figure 1-2: Histology of the small Intestine

Subdivision of small intestinal wall into four main layers: mucosa, submucosa, muscularis externa or propria and serosa. Picture taken from https://socratic.org/questions/from-the-lumen-outward-what-are-the-layers-of-the-gastrointestinal-tract

As mentioned previously, the intestinal epithelium is specialised along the different regions designed to fulfil different functions. Small and large intestinal epithelia differ in the presence/absence of villi, finger-like projections that are present in the small intestine only and function to increase the surface area in contact with luminal contents (Mowat and Agace, 2014). The villi also have an additional layer of microvilli, full of digestive enzymes and nutrient transporters, forming the “brush border”, intended to further increase the absorptive function of the small intestine (Crawley et al., 2014). The large intestine, however, has little digestive function, but mainly absorbs water and eliminates undigested food. It is also the reservoir of a commensal community of bacteria that appears to have major functions, essential for the individual’s health, some of which still unknown, (Fig. 1-3) (Gerritsen et al., 2011).

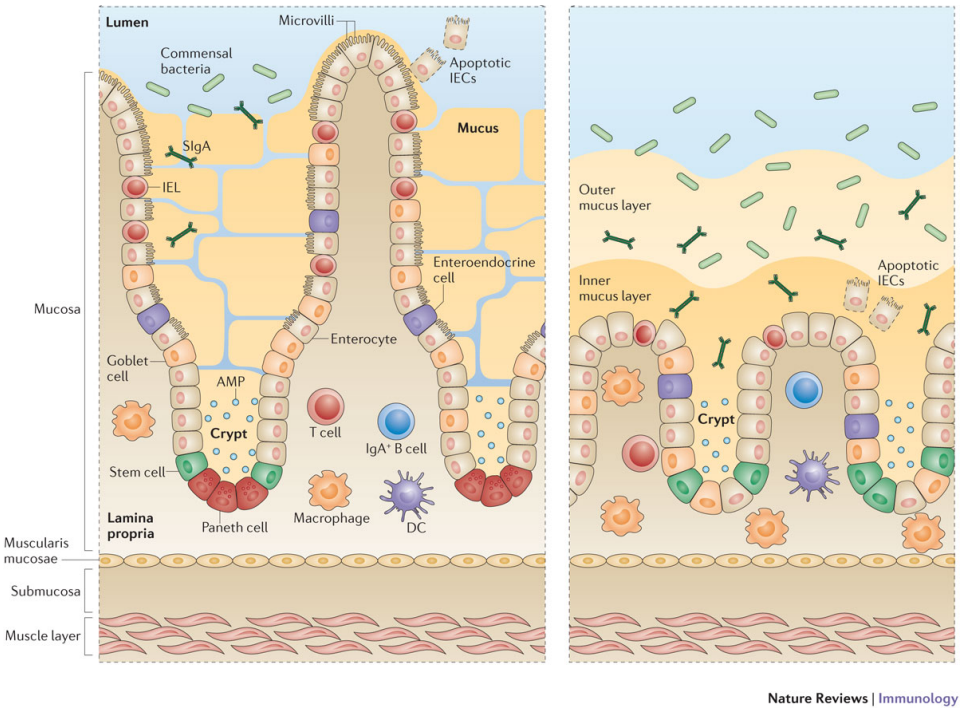

Figure 1-3: Schematic histology of the small and large intestinal epithelium

Representation of the different cell types localised in the small and large intestinal epithelium. Adapted from Mowat and Agace (2014).

The epithelium is formed of several cell types exerting different functions, which originate from a common population of multipotent stem cells located in the crypts (Fig. 1-3) (Barker et al., 2007b). In fact, the absorptive enterocytes, which make up the vast majority of cells, are intercalated with Paneth and Goblet cells, associated with the immune function, and enteroendocrine cells (Fig. 1-3). All these cells, with the exception of Paneth cells, have a fast turn-over of about 4-5 days, when after originating from stem cells near the bottom of the crypt, they move upwards along the length of the villus, mature, and acquire their specific function before being extruded and ejected into the intestinal lumen (Gehart and Clevers, 2019).

Given the vast surface in contact with the external environment, the intestine exerts an important immune action within the body. The immune function is mainly exerted by the epithelium and the *lamina propria*. A mixture of T- and B-lymphocytes and other innate immune cells, such as dendritic cells, macrophages, eosinophils and mast cells, are located within the *lamina propria*, whereas, only T-lymphocytes are localised within the epithelium (Fig. 1-3) (Mowat

and Agace, 2014). In the small intestine, the immune system acts mainly to maintain the sterility and barrier function of the absorptive epithelium. In addition, it is the mediator of tolerance mechanisms towards food antigens that are absorbed and disseminated throughout the body (Mowat and Agace, 2014). In the colon, on the other hand, the immune system maintains and controls the commensal microbiota, resident in the mucus layer, by preventing immune responses against them (Mowat and Agace, 2014).

The main function of the intestine, however, is to assimilate food and this function is accomplished by moving it along the intestine as a result of a neuromuscular wall described in detail in the next section.

1.2 The neuromuscular compartment

The intestine is a neuromuscular organ that mixes and propels food and waste along its entire length. To fulfil this function, the intestine is made of a neuromuscular wall with the myenteric plexus located in between the inner circular and the outer longitudinal muscle layers (Fig. 1-2). The myenteric plexus, together with the submucosal plexus, located in the submucosal layer in close proximity with the circular muscle layer, constitute the ENS (Fig. 1-4) (Furness, 2012). While the submucosal plexus, by sending projections towards the epithelium, is mainly involved in gastrointestinal secretion by innervating glandular epithelium and intestinal endocrine cells, the myenteric plexus is implicated in the control of the gastrointestinal motility. A clear idea on how the entire gastrointestinal motility system works has not been fully determined, however, in the past decades several studies have been performed to better understand this process and underpin neuronal circuits underling motility patterns (Hao et al., 2016).

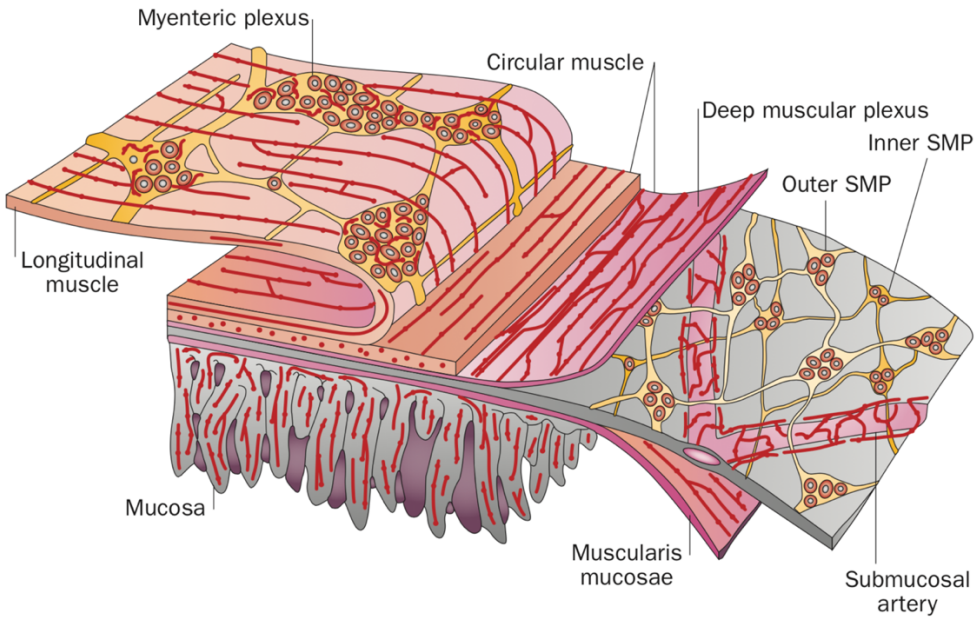

Figure 1-4: The Enteric Nervous System (ENS)

Schematic of the position and structure of the ENS. From Furness (2012).

The ENS is a well organised intrinsic nervous system arranged into enteric ganglia, which are aggregations of nerves and glial cells localised in the submucosal and myenteric plexuses and joined by neural connections and neural fibres that innervate muscle cells, the epithelium and the blood vessels supplying the intestine (Furness, 2012; Sasselli et al., 2012). The main function of the ENS is the regulation of enteric contractility. In particular, the ENS controls peristalsis, that allows slow and rapid propulsion as well as segmentation of food to allow its mixing and propagation (Furness, 2012). These functions are exerted by a complex circuit composed of intrinsic sensory neurons that respond to changes in luminal chemistry or mechanical stretch, ascending and descending interneurons and both excitatory and inhibitory motoneurons acting on the enteric musculature (Furness, 2012). The functional maturation of these complex systems has not been fully identified yet. However, it has been demonstrated that partial intestinal neuromuscular activity is present before birth (Roberts et al., 2010; Roberts et al., 2007). In fact, spontaneous gut motility has been recorded at E13.5 in the mouse duodenum (Roberts et al., 2010), while proper neural-induced motility has been reported in the mouse duodenum at E18.5 (Roberts et al., 2010) and in the colon at P10 (Roberts et al., 2007). In humans, recently it

has been shown that in the ENS the emergence of evoked electrical activity is evident at week 16 of gestation (McCann et al., 2019), however further investigations are needed to determine the ontogeny of human gut motility.

The ENS is derived mainly from the vagal neural crest cells (NCCs), as was first suggested by Yntema and Hammond (1954) and further confirmed in the seventies in chick (Le Douarin and Teillet, 1973) and in the nineties in mammals (Anderson et al., 2006; Durbec et al., 1996; Kapur, 2000). Vagal NCCs migrate from the neural tube to the developing gut in a rostrocaudal manner and, in mouse, fully colonise the entire gut by E15.5 (Sasselli et al., 2012). An additional contribution to the ENS comes from the sacral NCCs that are partially responsible for the innervation of the hindgut (Burns and Douarin, 1998; Kapur, 2000; Serbedzija et al., 1991; Wang et al., 2011). Migratory enteric NCCs, both vagal and sacral, can be identified by their expression of the transcription factor SOX10 (Anderson et al., 2006) and the cell receptor endothelin receptor B (EDNRB) (Nataf et al., 1996). Shortly after moving out from the neural tube, enteric NCCs start expressing the low-affinity nerve growth receptor p75 (Anderson et al., 2006; Wilson et al., 2004) when in proximity of the dorsal aorta, and whilst entering the developing foregut, they express the tyrosine kinase receptor RET (Anderson et al., 2006; Durbec et al., 1996; Natarajan et al., 2002; Pachnis et al., 1993) and the transcriptional regulator Phox2b, that will be expressed also after differentiation (Pattyn et al., 1999). Once NCCs have migrated into the gut, they differentiate into neurons, identified by the expression of a pan-neuronal marker, beta Tubulin-III, and glial cells, characterised by the expression of s100 and GFAP (Sasselli et al., 2012).

The cells responsible for effecting gastrointestinal motor function are the enteric smooth muscle cells (SMCs). These are organised in two muscle layers, which accomplish their motility function by means of coordinated peristaltic movements in which the circular muscle layer contracts behind the food bolus material to prevent it from moving backward, while the longitudinal muscle layer contracts to push food along the intestine (Bitar, 2003). In addition, SMCs act to maintain organ shape and dimensions against the load imposed by food by generating a tonic contraction (Bitar, 2003). SMCs are elongated spindle-like

cells rich in endoplasmic reticulum and mitochondria (Gabella, 2002), 200-300 μm in length and 4-15 μm wide (Bitar, 2003). In contrast to cardiac and skeletal muscle cells, SMCs lack visible cross-striation, although 80% of the cell is made of dense bodies and contractile filaments subdivided into thin actin filaments, intermediate filaments and thick myosin filaments that run along the longitudinal axis of the cell (Bitar, 2003). SMCs contraction is induced by a massive release of calcium into the cytosol, which causes the overlapping thin and thick filaments to slide on each other resulting in cell contraction and hence shortening the gut segment (Somlyo and Himpens, 1989).

However, other cell types are also involved in gut motility. In fact, several cells defined as “interstitial” cells, due to their physical location in the interstitium within specific tissues (Sanders et al., 2014), take part in the complex system regulating the gastrointestinal motility. In particular, the interstitial cells of Cajal (ICCs), and cells described as “fibroblast-like cells”, from now on referred as PDGFRα$^+$ cells since they are specifically labelled with an antibody against platelet-derived growth factor receptor alpha (PDGFRα), constitute, together with smooth muscle cells, a functional structure called SMC / ICC / PDGFRα$^+$ cell (SIP) syncytium (Fig. 1-5) (Sanders et al., 2014). The ENS is linked to the SIP syncytium, regulating and co-ordinating its function.

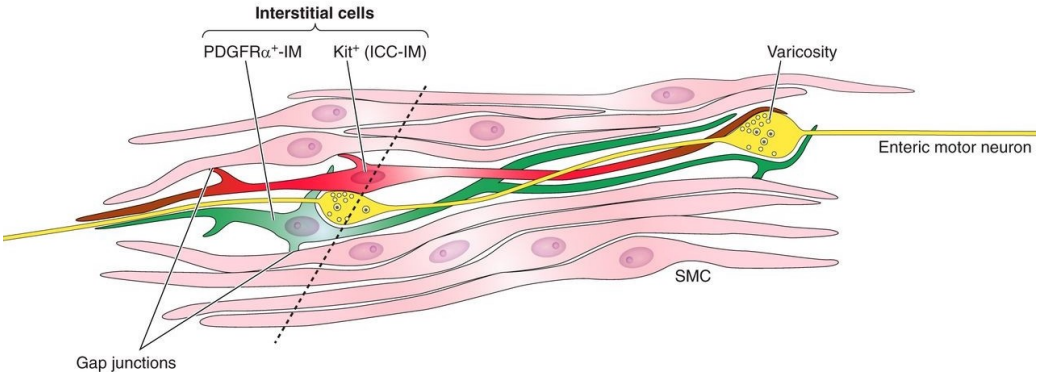

Figure 1-5: SMCs / ICCs / PDGFRα$^+$ (SIP) syncytium

Representative schematic of the connection between an enteric motor neuron of the ENS and the SIP syncytium. From Sanders et al. (2014).

Firstly described by Santiago Ramón y Cajal as accessory neurons (Cajal, 1893), the identity of interstitial cells of Cajal (ICCs) has been debated for years,

and ranged from neuronal-like cells, due to their propensity to co-stain with neuronal markers (Taxi, 1952), to fibroblasts. Then, the idea that ICCs were involved in the communication between neurons and smooth muscle cells was introduced (Cajal, 1911). Furthermore, due to the abundance of smooth endoplasmic reticulum compared to rough reticulum and the presence of filaments identified at ultrastructural level, ICCs were defined as specialised SMCs (Faussone Pellegrini, 1977) and proposed as pacemakers of the gastrointestinal tract for their structural similarity with cardiac pacemaker cells (Faussone Pellegrini, 1977). Finally, the discovery that ICCs could be identified using a specific antibody against the tyrosine kinase receptor KIT helped to characterise different subpopulations of ICCs within the gut (Fig. 1-6) (Blair et al., 2014; Komuro, 2006; Torihashi et al., 1995; Ward et al., 1994).

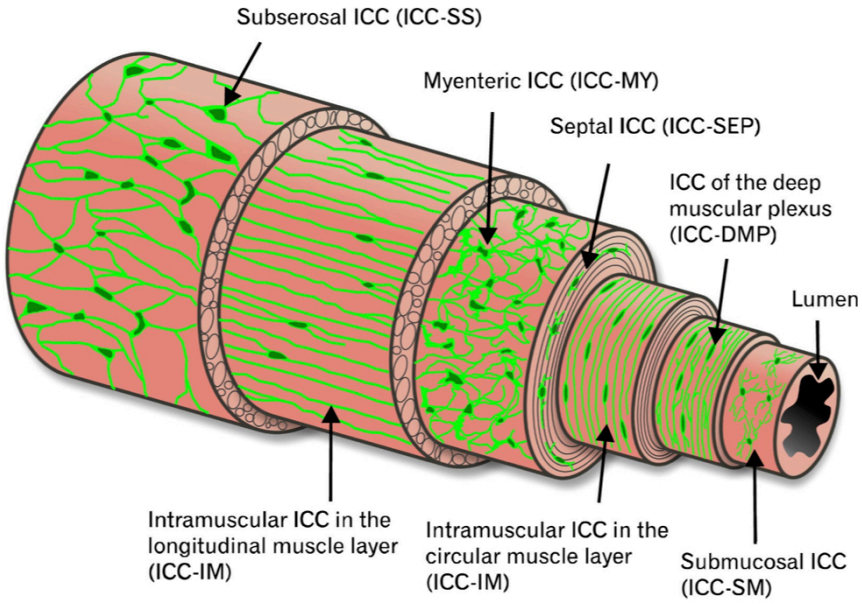

Figure 1-6: ICCs classification and anatomical position

Schematic of the localisation of the different sub-types of ICCs. From Blair et al. (2014).

Moving from the outer surface of the gut, the serosa, to the epithelium, the first population of ICCs identified, just beneath the serosa, is the subserosal interstitial cells of Cajal (ICCs-SS) (Vanderwinden et al., 2000). ICCs-SS do not seem to have a close relation with enteric neurons in mice (Blair et al., 2014), although it has been shown that some connections are present at the level of

taenia coli, thicker regions of longitudinal smooth muscle, characteristic only of primates and humans colon (Blair et al., 2014). It has been suggested that their role might be of stretch receptors (Aranishi et al., 2009), but more studies are needed to clarify their function. Between the longitudinal and circular muscle layers, where the myenteric plexus is found, a second group of ICCs called ICCs-MY (Myenteric) (Blair et al., 2014) is localised. These are multipolar cells that surround the ganglia and the nerve fibres without penetrating them. Moreover, ICCs-MY have several cellular processes that branch out and connect to other cells to create a complex network (Komuro, 2006). Intermingled with SMCs, both in the circular and longitudinal muscle layers, intramuscular ICCs (ICCs-IM) can be recognised as elongated cells running parallel to SMCs (Blair et al., 2014). ICCs-IM have been proposed to be enteric neurotransmission mediators (Burns et al., 1996), as well as pacemaker cells in the stomach (Suzuki et al., 2003). A subgroup of ICCs-IM, located in the deep muscular plexus (DMP, a non-ganglionated neural plexus located in the circular muscle layer) close to the submucosa from which it is separated just by a thin layer of smooth muscle cells, have also been described and classified as ICCs-DMP (Blair et al., 2014). Between muscle bundles of large animals and humans, an additional population of cells, called septal interstitial cells of Cajal (ICCs-SEP) is localised and thought to have a role in the slow wave propagation through the muscle layers, as the "Purkinjie-cells" of the gut (Lee et al., 2007; Ward and Sanders, 1990). The last described population of ICCs, called submucosal ICCs (ICCs-SM), are thought to have pacemaker functions. ICCs-SM have been found only in stomach and colon and run parallel to the circular SMCs on the submucosal surface (Blair et al., 2014; Komuro, 2006).

The second class of interstitial cells residing in the gut has been described for years as fibroblast-like cells (FLC) (Faussone Pellegrini and Cortesini, 1984). When it was discovered that these cells could be specifically identified using an antibody against PDGFRα, they were renamed as PDGFRα$^+$ cells (Iino et al., 2009; Kurahashi et al., 2011). PDGFRα$^+$ cells, contrary to ICCs, have more rough endoplasmic reticulum, are closely associated with neural varicosities and form gap junctions with both circular and longitudinal SMCs (Blair et al., 2014;

Kurahashi et al., 2011). Similar to ICCs, PDGFRα+ cells have also been subdivided into intramuscular PDGFRα+ cells (PDGFRα-IM) situated between muscle bundles, and myenteric PDGFRα+ cells (PDGFRα-MY) in close relation with the myenteric plexus (Blair et al., 2014). Studies have been performed to assess the function of this subpopulation of interstitial cells within the gut and determined that PDGFRα+ cells have a role as mediators of inhibitory neurotransmission, specifically referred to purinergic neurotransmission (Kurahashi et al., 2011; Peri et al., 2013).

All together, these cells located within the neuromuscular wall of the intestine guarantee a normal enteric motility. SMCs, ICCs and PDGFRα+ cells, present several gap junction proteins that allow them to communicate with each other, although so far little is known about the level of this communication (Blair et al., 2014). Nevertheless, this electrical connectivity allows these cells to behave as a single unit, a multicellular electrical syncytium, the aforementioned SIP (Sanders et al., 2012; Sanders et al., 2014). ICCs' pacemaker activity is conducted onto smooth muscle cells generating electrical slow waves and phasic contraction, while, neural inputs on both ICCs and PDGFRα+ cells are transferred to SMCs coordinating gastrointestinal motility (Blair et al., 2014). Therefore, alterations on any one cell type can impact the activity of the entire syncytium leading to motility disorders of the GI tract.

1.3 Gut development

1.3.1 Morphology

Each region of the GI tract is a multi-layered system composed of a mucosal layer, neural plexuses and three muscle layers. From an embryonic point of view, all three germ layers contribute to the formation of the GI tract: the ectoderm originates the ENS, the endoderm forms the epithelial layer and the mesoderm, in particular the visceral splanchnic mesoderm derived from the lateral plate mesoderm, generates the muscle layers (de Santa Barbara et al., 2002).

Human and murine gut develops as a result of cephalocaudal and lateral embryo folding and incorporation of the endoderm lined yolk sac around the fourth week of human gestation. This leads to the formation of two blind-ended endodermal invaginations at the anterior and posterior end of the embryo, which fuse to give rise to the primitive gut tube. At this stage the gut is temporarily bounded by two ectodermal-endodermal membranes, called the oropharyngeal and cloacal membranes, that rupture at the fourth and seventh week of gestation respectively (Moore KL et al., 2016). This primitive gut structure is descriptively subdivided into 4 main areas: the pharyngeal gut (pharynx), the foregut (oesophagus and stomach and proximal duodenum), midgut (small intestine from the eminence of the bile duct in the duodenum to the proximal two-thirds of the transverse colon) and hindgut (the remaining part of the colon). While the foregut and the hindgut are established at this point, the midgut remains connected with the yolk sac by the vitelline duct, which will, over time, become narrow and longer and finally obliterate, allowing the midgut to gain its free position in the abdominal cavity (Sadler, 2011).

The foregut undergoes major modifications between week four and six of human gestation, when a compartmentalisation process takes place with the formation of the respiratory diverticulum (lung buds) and the appearance of the oesophago-tracheal septum, ultimately resulting in the development of two independent and separate systems: the trachea and the oesophagus (de Santa Barbara et al., 2002; Perin et al., 2017). At the same time the stomach changes appearance and position inside the body following two rotations, the first one along its longitudinal axis and the second along its anterior-posterior axis. Around week five of gestation, the spleen primordium appears and it is followed by the pancreas, which will develop further in the following weeks. The caudal portion of the foregut, together with the cephalic part of the midgut, will form the duodenum, the first portion of the small intestine just distal to the origin of the liver bud. While the stomach is rotating, the duodenum assumes its form as a C-shaped loop, and gains its position on the left side of the abdominal cavity, fixed to the dorsal body wall (Moore KL et al., 2016; Sadler, 2011).

After week five of human gestation the midgut rapidly elongates together with its mesentery, double layers of peritoneum that enclose the gut and connect it to the body wall, forming the primary intestinal loop. The cephalic part of this loop will give rise to the distal portion of the duodenum, the jejunum and the proximal part of the ileum, while the caudal portion of the loop will generate the lower part of the ileum, the caecum, the appendix, the ascending colon and the first two-thirds of the transverse colon. During the development of this loop, the cephalic portion has a faster growth rate in comparison to the enlargement of the abdominal cavity. For this reason, around week six of gestation (E9.5 of mouse development), the midgut enters the extraembryonic coelom in the umbilical cord in a process called physiological umbilical herniation. Throughout this period of time, the midgut keeps elongating to form a number of coiled loops. It is only during week ten of gestation that the herniated intestinal loops start returning into the abdominal cavity, with the ceacal bud being the last portion to re-enter the abdominal cavity (Moore KL et al., 2016; Sadler, 2011).

Until week seven of gestation, the urogenital and the GI system share a common end, the cloaca, enclosed by the cloacal membrane, and their separation happens thanks to the formation of a layer of mesoderm, called urorectal septum. At week seven of gestation, the cloacal membrane breaks forming the anal opening of the hindgut dorsally and the urogenital sinus ventrally. However, at this time, proliferation of the ectoderm closes the caudal end of the anal canal, which will be re-canalized only at week nine of gestation (Moore KL et al., 2016; Sadler, 2011). As soon as the re-canalisation, herniation and the rotation processes have all occurred, the organogenesis of the GI tract is completed and an additional process of growth and enlargement will take place in the subsequent foetal and early post-natal life.

1.3.2 Molecular regulation

The entire developmental process of generation, elongation and regional specification of the gut is, as for every other biological process, strictly controlled and regulated by the activation of specific molecular markers in different regions of the GI tract. Unfortunately, while there is a great corpus of research focussing

on epithelial specialisation and regionalisation, less attention has been paid on the muscular compartment during gut development. Early during embryogenesis, the embryo elongates and differences along the anterior/posterior axis will appear together with the development of a right/left symmetry (mainly via *Sox17* (Saund et al., 2012; Viotti et al., 2012)). In the process of anterior-posterior patterning (responsible for the division into foregut, midgut, hindgut) the importance of *FGF* (Dessimoz et al., 2006), *WNT* (Sherwood et al., 2011), *Sox2* and *Cdx2* have been documented: for example, at E7.5 of mouse development *Sox2* is expressed at the anterior end of the gut while the expression of *Cdx2* is found at the opposite end of the gut (Sherwood et al., 2009). At E9.5 a clear and distinct line separating Sox2 and Cdx2 is visible at the level of the future pylorus while by E14.5 the separation becomes less demarcated, with the expression of Sox2 gradually diminishing from the stomach to the duodenum with an opposite pattern for Cdx2 (Li et al., 2009).

At birth, the human intestine is already 40% of its final adult length given that the process of elongation starts very early during development. During the initial elongation stage (from E10.5 to E14.5 of mouse development), when intestinal villi are still absent, the size of the small intestine from pylorus to caecum increases more than 11-fold (Wang et al., 2019). It has been shown that WNT5A, mainly expressed by the mesenchymal cells, is important for the correct proliferation of the columnar epithelium and its loss results in ~70% reduction of small intestine length (Cervantes et al., 2009). Similarly, but to a lesser extent in comparison to WNT5A, loss of ROR2 (the WNT5A receptor present in both epithelial and mesenchymal cells) and GATA4 (a transcription factor expressed by epithelial cells and required for proliferation) result in intestinal length reduction (Cervantes et al., 2009; Kohlnhofer et al., 2016; Yamada et al., 2010). Interestingly, mutations in FLNA (Filamin A), an actin-binding protein acting downstream of WNT5A/ROR2, has been associated in patients with congenital short-bowel syndrome (Van Der Werf et al., 2013).

Intestinal length reduction has also been associated with reduced proliferation of mesodermal cells. In this context, the hedgehog (Hh) pathway has been identified as a key pathway since loss of both sonic hedgehog (Shh) and

Indian hedgehog (Ihh) leads to a final intestinal length of only ~10% the length of wild type mice by E12.5 (Kim et al., 2011; Mao et al., 2010; Ramalho-Santos et al., 2000). Altered Hh signalling has additional severe consequences on the normal GI development: its loss results in duodenal stenosis, abnormal innervation, loss of smooth muscle, loss of villi and malrotation (Madison et al., 2005; Mo et al., 2001; Ramalho-Santos et al., 2000; Sukegawa et al., 2000), while its constitutive activation gives rise to a huge expansion of the mesenchyme and an increase of smooth muscle differentiation (Zacharias et al., 2011).

Another factor*, Fgf9*, has been linked to intestinal lengthening since lack of *Fgf9* resulted in lowered mesenchymal proliferation and an overall reduction in small intestinal length (Geske et al., 2008). FoxF2, a member of the transforming growth factor ß (TGFß) pathway, is also a determinant of intestinal elongation. In fact, when FoxF2 is selectively knocked-out from SMCs, there is a reduction in intestinal length with thickening of the longitudinal muscle layer (Bolte et al., 2015). The overall growth of the intestine in terms of the number and size of intestinal loops is species-specific and evidence using chick gut, seems to suggest that BMP2, expressed by the dorsal mesentery, regulates the rate of growth of the mesentery (Nerurkar et al., 2017). In fact, more and tighter loops develop when the growth rate of mesentery is reduced causing more tension on the intestine (Nerurkar et al., 2017).

To fulfil the various physiological functions, the intestine requires a certain degree of regionalisation and several molecular markers have been associated with this process. The mesoderm along the antero-posterior axis expresses multiple *Hox* genes, with each morphological region (i.e. foregut, midgut, hindgut) expressing a distinct combination of different *Hox* genes (Sakiyama et al., 2001; Sekimoto et al., 1998). Interestingly, sphincters have been hypothesised to be located anatomically at the level of the rostral area of some *Hox* domains, with functional evidence showing the role of *Hox* genes in the morphogenesis of the pyloric, ileocecal and anal sphincters (Wang et al., 2019). In spite of the attention directed toward *Hox* genes, they do not seem to be the primary determinants of regional patterning in the intestine (Gao et al., 2009). In fact, in the distal intestine (i.e. ileum and colon) Cdx2 is essential in generating a normal phenotype with

Cdx2 loss in these regions resulting in the formation of a squamous oesophageal-like epithelium with minimal changes in the expression of Hox code but substantial ones in both Wnt and Hedgehog signalling (Gao et al., 2009).

Other GI regions seems to depend on other molecular cues for their correct development. The specification of the duodenum relies on the expression of Parahox factor PDX1, known to be crucial also for pancreas development (Offield et al., 1996). Loss of Pdx1 affects the proximal duodenum where villi fail to form and the epithelium grows as a cuboidal cell sheet (Wang et al., 2019). The jejunum and ileum seem to rely on the GATA family of transcription factors for their specification. In fact, GATA4 is essential for jejunal determination, since its deficit transforms the jejunum into an ileum domain (Kohlnhofer et al., 2016; Walker et al., 2014), while GATA6, expressed throughout the entire intestine (Battle et al., 2008; Beuling et al., 2012; Bosse et al., 2006; Fang et al., 2006), seems to be necessary for the formation of ileum since its loss results in a colonic transformation of the ileum epithelium (Beuling et al., 2011; Walker et al., 2014).

The regionalisation process has not been fully understood; however, it is clear how critical the crosstalk that takes place during development between endoderm and mesoderm is. Actually, several studies, performed with combinations of enzymatically-separated endoderm and mesoderm from different regions of the gut in different species, showed the different roles of the two tissues. Intestinal pre-villus endoderm cultured alone, in a vascularised environment, gave rise to intestinal epithelium where villi did not form (Mizuno and Yasugi, 1990); conversely, the villi structure could be identified when intestinal endoderm was cultured with isolated mesenchyme from any origin (Duluc et al., 1994; Kedinger et al., 1998). Interestingly, the origin of the endoderm exercised a certain degree of dominance in the outcome: for example when rat endoderm from proximal jejunum was cultured with rat mesenchyme from distal ileum (or *vice versa*) the final epithelial phenotype resembled the tissue from which the endoderm was taken (Duluc et al., 1994).

1.4 Paediatric Intestinal Failure

If the intestine becomes unable to fulfil nutritional demands and parenteral nutrition is needed, a condition called intestinal failure (IF) is said to occur (Kappus et al., 2016). IF is a common complication of short bowel syndrome (SBS), dysmotility disorders, such as intestinal pseudo-obstruction, and different mucosal enteropathies (Mangalat and Teckman, 2018). SBS is a complex congenital or acquired condition resulting from failed development or physical loss, usually by surgical resection, of functional intestinal mass. Causes of SBS include necrotizing enterocolitis, inflammatory diseases such as Crohn's disease, intestinal obstruction, dysmotility, or congenital defects, such as gastroschisis and intestinal atresia (Duggan and Jaksic, 2017; Goldstein et al., 2016; Kappus et al., 2016).

Among the different dysmotility disorders of the GI tract (Burns and Thapar, 2014), intestinal pseudo-obstruction (CIPO) is a rare syndrome characterised by a clinical picture of repetitive mechanical obstructions in the absence of occluding lesions (Antonucci et al., 2008; Burns and Thapar, 2014). Recently, paediatric forms of CIPO have been reviewed and have been recognised as a separate group, called paediatric intestinal pseudo-obstruction (PIPO) (Thapar et al., 2018). PIPO can be classified into primary PIPO, more frequently sporadic although some familial forms have been described, or, more rarely, secondary to recognizable diseases. Based predominantly on histological findings, CIPO disorders have been subdivided into three main groups depending on the main involvement of neurons, interstitial cells or SCMs, respectively called neuropathies, "mesenchymopathies" and myopathies (Antonucci et al., 2008; Di Nardo et al., 2008). Similar classification has been adopted also for PIPO. Among the different groups, neuropathies constitute the vast majority of PIPO (~ 70%), with the myopathic group being second for incidence (~ 30%) (Thapar et al., 2018). Within the myopathic group, a variety of phenotypes can be identified, which can be subdivided into two main classes: the first one characterised by alterations of SMCs such as vacuolar alteration, fibrosis (Smith and Milla, 1997), increased mitotic activity and changes in smooth muscle actin expression (Knowles et al., 2004); the latter involving alteration of the entire muscularis

propria, such as atrophy (De Giorgio et al., 2004), hypertrophy (Koh et al., 2008) or, more rarely, abnormal layering (i.e. presence of additional muscle layers) (Munoz-Yague et al., 2006; Smith and Milla, 1997). Unfortunately, PIPO is frequently misunderstood and leads to useless and potentially dangerous surgical resections increasing the risk of intestinal failure (Antonucci et al., 2008; Thapar et al., 2018).

Amongst the paediatric population, IF afflicts tens out of thousands of children (Duggan and Jaksic, 2017) and the overall mortality rate is around 25%, mainly due to multi-organ system failure, sepsis and haemorrhage caused by prolonged parenteral nutrition and complications associated with intestinal transplantation (Squires et al., 2012). Current treatments of SBS are aimed at increasing the absorptive capacity of remnant bowel or expanding bowel length either with intestinal-lengthening procedures or intestinal transplant (Martin et al., 2018). At present, for children aged above 12 months, a hormonal pharmacologic agent, Teduglutide, a glucagon-like peptide-2 (GLP-2) analogue (Jeppesen, 2012), has been used to increase intestinal absorption by facilitating intestinal adaptation after resection, increasing villous height and crypt depth. However, the effect is reversed when the drug is withdrawn (Chandra and Kesavan, 2018). Unfortunately, some patients may never recover bowel function and if 10-50% of caloric intake is not obtained by 6 months of parenteral nutrition, surgical management is indicated (Chandra and Kesavan, 2018).

Currently, surgical options aim to increase length and motility of the small intestine and include the “Longitudinal Intestinal Lengthening and Tailoring” (LILT) or “Bianchi procedure” (Bianchi, 1984), the “Serial Transverse Enteroplasty” (STEP) procedure (Kim et al., 2003) and the “Spiral Intestinal Lengthening and Tailoring” (SILT) (Cserni et al., 2011). With the LILT procedure, a segment of viable small bowel is doubled in its length but halved in its circumference by dividing the original segment along its longitudinal axis and then anastomosing the two loops in an isoperistaltic fashion (Bianchi, 1984) (Fig. 1-7a,b,c). STEP procedure allows the extension of the intestine without the need of anastomosis, but simply transecting a portion of bowel in a “zigzag” fashion (Kim et al., 2003) (Fig. 1-7d,e). The SILT procedure is the newest surgical procedure

for SBS whereby a spiral incision along the intestine is made, then the intestine is stretched longitudinally and re-tabularised by suture (Cserni et al., 2011). Overall, a meta-analysis study comparing LILT and STEP procedures showed capacity to wean off from parenteral nutrition after 9 months in 58.1% of patients that underwent STEP procedure and 71.5% of patients that underwent LILT procedure (Frongia et al., 2013). When both medical and surgical treatments fail, the last resort remains small bowel transplantation, frequently coupled with liver transplantation (Chandra and Kesavan, 2018).

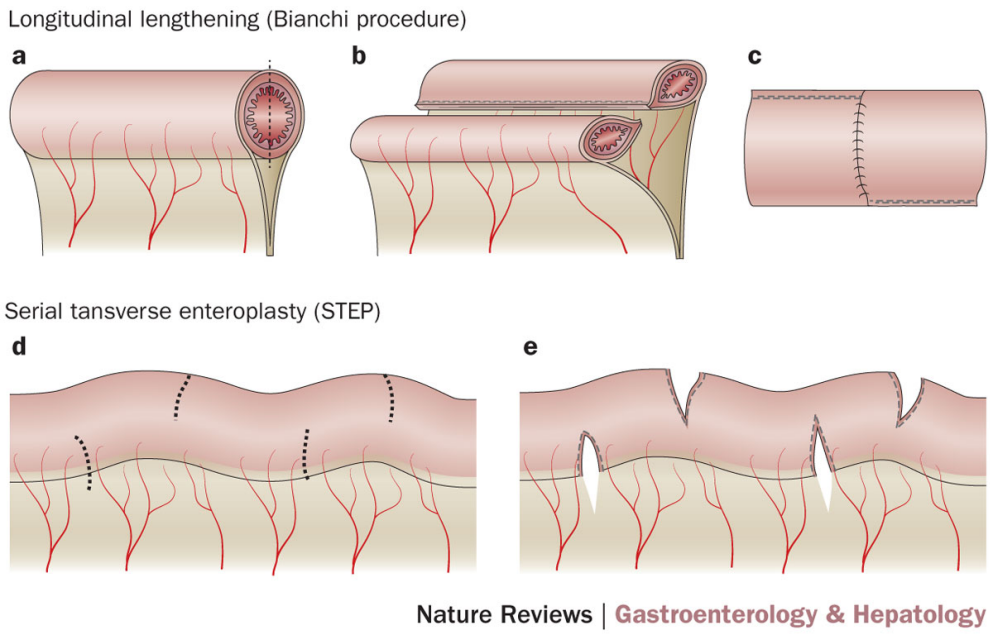

Figure 1-7: Intestinal lengthening procedures

Schematics of the Bianchi and SPET procedures. From Kim et al. (2003).

Transplantation of the small bowel remains a very challenging approach because of the poor rate of success. In fact, the incidence of acute rejection in children within the first two years after transplantation is very high, up to 45% in isolated small bowel transplantation and slightly less, around 35-38%, in case of multi-organ transplantation (Boluda, 2015). Furthermore, in children undergoing small bowel transplantation, rates of the graft versus host disease have been shown to be very high, leading to very high morbidity and mortality (Andres et al., 2010; Boluda, 2015). In addition, transplantation itself has major constraints, such as the lack of sufficient numbers of available organs (a problem which is

increasingly encountered given the ageing of the population (Glotzbach et al., 2011)), the morbidity at the donor site and the necessity for life-long immunosuppression.

Current multidisciplinary approaches for complex diseases and advances in intestinal rehabilitation have slightly improved patients' outcomes and quality of life, but still carry significant levels of morbidity and mortality. Therefore, novel treatments are needed (Duggan and Jaksic, 2017; Martin et al., 2018). A tissue engineering approach, aimed at the production of autografts that resemble the native tissue, structurally and functionally, could provide an alternative strategy to small bowel transplantation with potential to overcome its major challenges, donor shortage and life-long immunosuppression (Grant et al., 2015).

1.5 Intestinal Tissue Engineering

Tissue engineering (TE) is a relatively recent branch of science, arguably born in the early nineties with work from Joseph Vacanti and Robert Langer, who aspired to generate "biological equivalents through the combination of cells and scaffold matrices in appropriate environments" to replace diseased or injury-impaired tissues (Langer and Vacanti, 1993). TE is of high clinical relevance because, by recreating an autologous artificial organ, it addresses the major problems linked to organ transplantation, such as organ shortage (Katari et al., 2014; Langer and Vacanti, 1993) and the necessity of lifelong immunosuppression (Katari et al., 2014). Moreover, TE could address the difficulties, especially for paediatric patients, in finding organs of the right size and that will grow with them. In 1993, Langer and Vacanti postulated three minimal concepts that represent the starting point for the creation of new tissues, which could be used separately or in combination: the use of matrices as scaffold for cell growth; the identification of appropriate cell types; and the introduction of tissue-inducing substances (Langer and Vacanti, 1993).

1.5.1 Scaffolds

To produce a functional intestine, a critical step is the generation of a biocompatible scaffold that should support cell attachment, proliferation, differentiation, angiogenesis and vascular ingrowth, as well as incorporate into the host without inducing an acute inflammatory reaction or chronic immune response (Martin et al., 2018). To date, researchers have focused on synthetic polymers, biological materials or decellularised organs. Synthetic polymers are most commonly used due to their unlimited source and their custom-made characteristics in terms of structural, mechanical and degradation properties (Place et al., 2009). However, induction of chronic inflammation remains a major issue in their use (Martin et al., 2018). Biological materials represent an alternative source, being of natural origin. The best hope perhaps resides in the use of biological material for decellularised scaffolds as they are of natural origin, with both the native structure and the molecular cues of the original organ preserved, helping in the maintenance of the cellular niche (Martin et al., 2018). The regeneration of several organs has been attempted using decellularised scaffolds, including the intestine. Totonelli et al. (2012) have shown the capacity to preserve the intestinal extracellular components after the decellularisation process, reporting epithelial cell adherence, and the maintenance of angiogenic properties. Furthermore, the absence of an immune response following *in vivo* implantation has been shown (Kitano et al., 2017; Totonelli et al., 2012), making intestinal scaffolds a potentially safe option for clinical use.

1.5.2 Tissue-inducing factors

In the body, after an injury, the natural regeneration of tissues is orchestrated by the complex production of numerous molecules, called inductive factors, which regulate cellular activity and guide the regeneration process. Inductive factors represent a vast group (with more than hundreds of molecules discovered so far) of growth factors and other molecules that transmit signals to modulate cellular activities, such as cell proliferation, differentiation, migration and adhesion, and also to influence matrix remodelling (Babensee et al., 2000; Vasita and Katti, 2006). Their application can be finely regulated, since their

concentration can be temporally and spatially controlled (Babensee et al., 2000): in example growth factors can be added at different times to cell culture medium to generate modifications on cells' behaviour (Babensee et al., 2000). Growth factors and other chemical signals can be applied alone or in combination. For example, scaffolds added with fibroblast growth factor 2 (FGF2) and vascular endothelial growth factor (VEGF) have been used in combination to increase angiogenesis and blood vessel maturation *in vivo* (Nillesen et al., 2007).

Inductive factors, in order to perform their function, must be conveyed inside tissues. Direct delivery at the site of action with the help of a carrier (e.g. scaffold) is the most popular method in TE. Researchers are able to deliver these inductive factors by using polymeric scaffolds, biodegradable microspheres (that with their controlled degradation allow a continuous release of the growth factor), and lipid-based drug delivery (Glotzbach et al., 2011). For instance, many natural materials deriving from animals and plants, such as alginate, chitosan, fibrin, hyaluronic acid and collagen, have been investigated for the delivery of growth factors (e.g. hyaluronic acid scaffolds have been employed for the delivery of bFGF; results demonstrated that hyaluronic acid-heparin conjugate gels increased both stability and activity of the growth factors (Liu et al., 2002)). Additional approaches to deliver inducing factors are based on gene delivery (e.g. cell based gene delivery or direct gene delivery). In the first approach cells are transfected *in vitro* with the gene of interest, allowed to grow and then administered (e.g. myocardial cells, transfected with VEGF, have been transplanted in rats' myocardial injury site, demonstrating an improved angiogenic effect (Yau et al., 2005)). On the other hand, in direct gene delivery genes are conveyed using vectors, alone or in combination with polymeric scaffolds (Vasita and Katti, 2006).

Inducing factors are not limited to biochemical approaches, but can also be mechanical, electrical and/or magnetic signals (Wong et al., 2012). For this purpose, particular devices called bioreactors have been designed to permit long-term tissue growth by providing appropriate conditions for cell growth and, at the same time, delivering tissue-specific biochemical and biophysical cues (Rangarajan et al., 2014), such as electrical and mechanical stimulations (Martin

et al., 2004). This last consideration is an important aspect, especially in musculoskeletal and cardiovascular tissues. In fact, mechanical stimuli (mechanical loading, dynamic or pulsatile distension, etc.) are known to ameliorate cell proliferation, cell orientation (Huycke et al., 2019) and matrix production both *in vitro* and *in vivo* (Brown et al., 2008; Jeong et al., 2005).

1.5.3 Cell types

The choice of the appropriate cell type is a critical step in TE. Cells have been largely studied over the past decades and the knowledge derived from these studies has increased the possible applications of both stem and somatic cells in TE. Stem cells are classically defined by their self-renewal capabilities, their ability to differentiate into specific cell types and the fact they reside inside a specific niche (Cosgrove et al., 2009; Sailaja et al., 2016; So and Cheung, 2018; Wu et al., 2010). They are present in almost all tissues and are maintained in the body thanks to their self-renewal ability, which implies that some cells of their progeny will retain stem cell capacity, while others terminally differentiate. The classification of stem cells is based on their tissue of origin and their potency, which refers to the possibility of giving rise to a mature lineage (Glotzbach et al., 2011). In mammals, only the zigote is a *totipotent* cell that can generate all cell types of the adult organism, including the extra embryonic tissues, while Embryonic Stem Cells (ESCs), which are considered *pluripotent* cells, can differentiate into all three germ layers (ectoderm, mesoderm and endoderm) but research has demonstrated that they are not stable enough to undergo embryogenesis on their own (Martin et al., 1977). ESCs were isolated for the first time in mice in 1981 (Evans and Kaufman, 1981) and from the human blastocyst solely in 1998 (Shamblott et al., 1998). Even if ESCs show the highest regenerative potential amongst all stem cells that can be expanded *in vitro*, ethical debate about their use has arisen due to the necessity to destroy human embryos to obtain them. This ethical issue has pushed researchers to look for other types of stem cells able to be used in TE, like so-called Adult Stem Cells (ASCs) or Tissue-Specific Stem Cells (TSSCs).

ASCs are defined as *multipotent* cells given they can generate different cell types within a single germ layer (i.e. hematopoietic stem cells, giving rise to all cell types circulating in the blood), or even as *unipotent* cells, since in some cases their potential is restricted to differentiation into a single cell type (i.e. keratinocyte stem cells, able to exclusively generate the epidermis). They appear at the end of embryogenesis when the pluripotent stem cells no longer exist and their role is to maintain the homeostasis of adult tissues. Adult stem cells reside in instructive, tissue-specific microenvironments defined as *niches*. A stem cell *niche* is the local microenvironment of the adult stem cells, which permits them to stay as stem cells, maintains a steady state level of slowly dividing cells during homeostasis, and controls their functions by activating them in response to injury. The niche consists of unique combinations of cellular (stem and other supporting cells), biochemical and biophysical components (Cosgrove et al., 2009; So and Cheung, 2018; Spangrude et al., 1988). In fact, stem cells remain quiescent in normal conditions, but are rapidly activated in cases of stress or injury to regenerate the damaged tissue. So far different types of ASCs have been discovered. The first was the Hematopoietic Stem Cell described by Spangrude et al. (1988) even if in 1961 Mauro described the satellite cells in the muscle (Mauro and Adams, 1961), although, their stemness was proved many years later; Caplan coined the term Mesenchymal Stem Cells in 1991 to describe the bone marrow-derived cells (Caplan, 1991); Endothelial Progenitor Cells (Asahara et al., 1997) were described in 1997; and finally in 2001 Adipose-Derived Stromal Cells (Zuk et al., 2001) were reported.

ASCs have been extensively studied and used in TE, but to achieve the pluripotent capacity of the ESCs researchers have developed different techniques to generate pluripotent stem cells from differentiated cells. It was in 2006 when Takahashi and Yamanaka succeeded in the reprogramming of a mouse fibroblast into a pluripotent cell using viral vectors (Takahashi and Yamanaka, 2006). After this first description many other reprogrammed cells have been produced and these cells have been collectively named Induced Pluripotent Stem Cells (iPSCs) (Brown et al., 2010; Loh et al., 2010; Maherali et al., 2007; Okita et al., 2007; Seki et al., 2010; Staerk et al., 2010; Sugii et al.,

2010; Sun et al., 2009; Takahashi et al., 2007; Wernig et al., 2007; Yu et al., 2007). At first the use of iPSCs was debated because of the possible tumorigenicity linked to viral integration and incomplete differentiation of cells leaving stem cells to proliferate. For this reason, different strategies to reprogram cells have been developed, such as the usage of plasmids, small molecules and non-viral minicircles (Glotzbach et al., 2011). Although iPSCs are very similar to ESCs, it has been shown that they are not strictly identical (Glotzbach et al., 2011). Until now, the broader use of ESCs and iPSCs is still limited due to ethical concerns and difficulty of production, respectively. In both cases, there is a potential threat of tumorigenesis that accompanies the direct implantation of these cells *in vivo*.

Somatic cells are differentiated cells able to fulfil a specific task in a particular tissue. Their application in TE has the advantage of exploiting their tissue-specific function without any manipulation, although their regenerative potential remains very low. However, paracrine communication between stem cells and differentiated cells has proven to be a crucial factor in maintaining the correct homeostasis of the tissue and the correct function of each subpopulation of cells present in the tissue, including stem cells (Bianco and Robey, 2001).

So far from the above descriptions, it is clear that there are several options for scaffolds and cell types. However, the intestine is an organ that is made up of a complex combination of cells and tissues which varies along its length. Therefore, in order to create a functional intestine, each intestinal layer will need to be regenerated to provide an appropriate absorptive epithelium, with barrier and immune functions, and a motile neuro-muscular wall. For this scope, the correct anatomical structure needs to be recreated and the appropriate cell types need to be identified between stem and somatic cells.

The epithelium of the adult intestine is subjected to a constant physicochemical insult due to its digestive and absorptive functions during the transit of food, therefore requiring a constant turnover of cells which is sustained by a resident population of intestinal epithelial stem cells (Clevers, 2013; Guiu and Jensen, 2015). Intestinal epithelial columnar stem cells, located between Paneth cells at the bottom of the crypts, as described in section 1.1 (Fig. 1-3),

are known for the expression of specific markers, such as Leucine-rich repeat-containing G-protein coupled receptor 5 (Lgr5) (Barker et al., 2007a), Olfactomedin4 (Olfm4) (van der Flier et al., 2009a) and Achaete scute-like2 (Ascl-2) (van der Flier et al., 2009b). These stem cells have a high self-renewal capacity and sustain the generation of all cells of the intestinal epithelium. When needed, in a stochastic manner, a freshly divided stem cell leaves the crypt stem cell niche to differentiate, initially becoming a transient amplifying cell, located just above the crypt. Transient amplifying cells will then divide and migrate upwards the villi, finally differentiating into one of the different epithelial cells, such as enterocytes, goblet cells, tuft cells, endocrine cells (Lander et al., 2012). Only when differentiating into Paneth cells, which have a slower turnover, cells will migrate downward the crypt to locate between columnar stem cells (Lander et al., 2012). Intestinal stem cells have been successfully isolated and cultured, both from mouse (Barker et al., 2007a) and human intestine (Sato et al., 2011) and used in different TE approaches (Clevers et al., 2019; Schlieve et al., 2017). Similarly, also stem cells originating the ENS have been isolated from mouse and human intestine (Bondurand et al., 2003; McCann et al., 2017; Natarajan et al., 2014) and used in gastrointestinal TE (Schlieve et al., 2017; Urbani et al., 2018).

Unfortunately, while the precursors of the intestinal epithelium and the neural plexus have already been described and characterised (Barker et al., 2007b; Bondurand et al., 2003), **the origin of the smooth muscle layers of the gut is still debated and additional work is required to identify the enteric visceral smooth muscle precursors.**

1.6 Intestinal smooth muscle cells origin

1.6.1 Canonical smooth muscle precursors

Hitherto gut smooth muscle development has not been extensively investigated, especially in humans. According to Wallace and Burns (2005), the smooth muscle layers first appear with a rostrocaudal gradient identified by anti-α-smooth muscle actin (αSMA) immunoreactivity from week 8 of human development. In particular, they described the presence of a thin layer of αSMA

positive cells in the proximal and distal intestine corresponding to the circular smooth muscle layer. By week 11 the immunoreactivity extended to both layers, circular and longitudinal, and by week 14 smooth muscle layers were condensed and discrete. Furthermore, at this stage of development, weak αSMA immunostaining was observed in the *muscularis mucosae*, just beneath the epithelium (Wallace and Burns, 2005). However, the precise cellular origin of the smooth muscle layers in humans is still unclear.

As opposed to the scarce knowledge in humans, more studies in mice have attempted to identify the precursors that give rise to smooth muscle cells of the gut. Torihashi et al. (1997) and Kluppel et al. (1998) reported the presence of a common cKit positive precursor capable of generating both longitudinal muscle cells (LMCs) as well as the myenteric interstitial cells of Cajal (ICCs-MY). The former study described the precursor as expressing cKit, a receptor tyrosine kinase (located in the W locus) activated by its ligand called stem cell factor or steel factor, which appeared around embryonic day 12 (E12) of mice development. By E18, ICCs and LMCs arose from this precursor, with ICCs maintaining the expression of cKit and LMCs losing its expression and differentiating into vimentin$^+$ smooth muscle cells. The authors suggested that the fate of these cKit$^+$ precursor cells rely on their proximity to the enteric neural cells (ENCs) which produce stem-cell-factor, the endogenous ligand for cKit. This hypothesis suggested that cells in close contact with ENCs would experience signalling via the cKit pathway and become ICCs, while cells not in close contact would lose the expression of cKit and become LMCs (Torihashi et al., 1997) (Fig. 1-8, Fig. 1-10 middle). Using a different approach, Kluppel et al. (1998) came to a similar conclusion that both ICCs and LMCs originated from a common precursor. They evaluated mRNA expression and showed that at E14.5 both the circular muscle (CM) and LM layers co-expressed c*Kit* and smooth muscle myosin heavy chain (*SM-MHC*). Subsequently they found that the CM layer lost c*Kit* expression, while the divergence began between ICCs and *SM-MHC*$^+$ LMCs in the LM layer and was completed by E18 (Fig. 1-9).

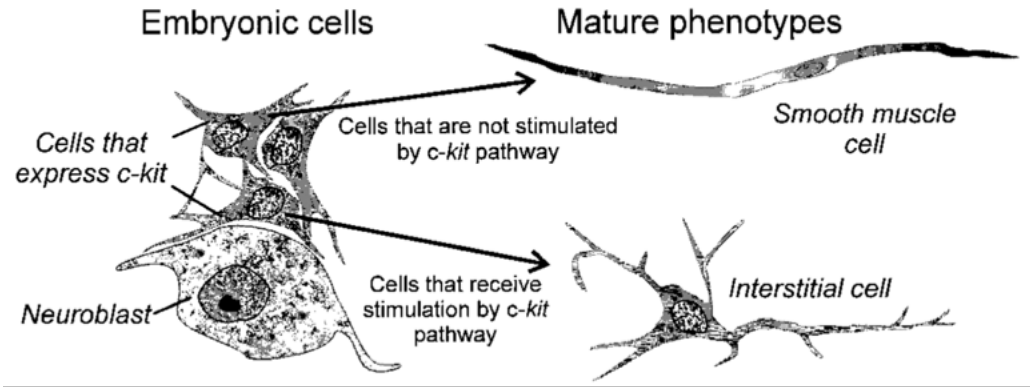

Figure 1-8: Current theory of LMCs and ICCs development

Schematic image describing the theory of a common precursor giving rise to both LMCs and ICCs, depending on the vicinity to the stem cells factor expressing neuroblasts. From Torihashi et al. (1997).

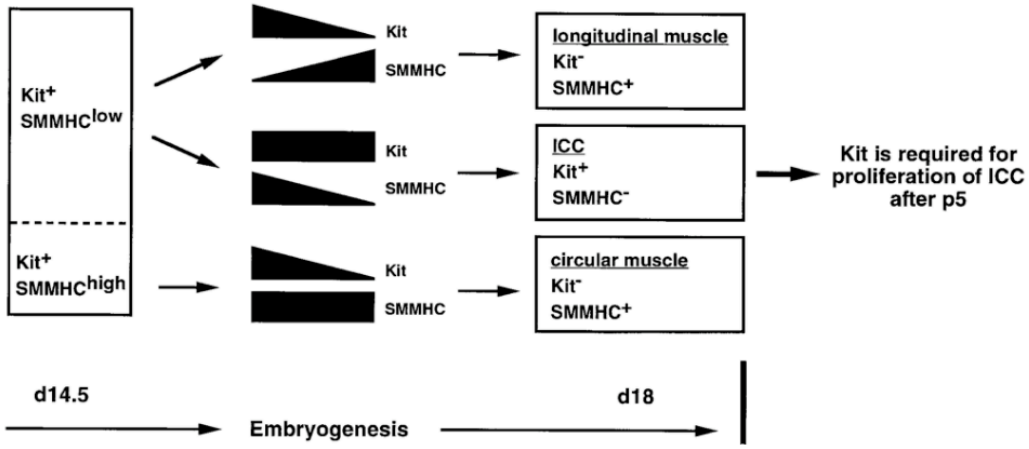

Figure 1-9: The development and lineage relationship of ICCs and SMCs

Schematic describing the variation of Kit and SM-MHC expression in circular and longitudinal SMCs as well as in ICCs during mouse development. From Kluppel et al. (1998).

An additional study, conducted by blocking cKit receptors after birth with an antibody, showed that ICCs lost cKit and transdifferentiated to take the ultrastructural form of smooth muscle cells, further suggesting the connection between ICCs and LMCs (Torihashi et al., 1999). cKit seems to be necessary for the development and maintenance of ICCs, as suggested by the failure in the development of ICCs in W locus mutants with missing or defective *ckit* as well as in *steel* locus mutants with a deficient soluble isoform of steel factor. However, it

is not necessary for the development of LMCs, as these develop normally in W and steel mutants (Torihashi et al., 1997).

Another important pathway proved to have a role in the proliferation and differentiation of different cell types, including smooth muscle cells, is via platelet-derived growth factor (PDGF) signalling. The PDGF family is composed of four ligands, A, B, C and D, and two receptors, alpha and beta, which are major mitogens for different cell types of mesenchymal origin (Fredriksson et al., 2004). Kurahashi et al. (2008) showed that alpha and beta PDGF receptors (PDGFRs) were co-expressed with cKit in ICCs and LM precursor cells during mouse development in a narrow window between E13 and E15. Furthermore, taking advantage of an *in vitro* organ culture system, they managed to completely block both PDGFR alpha and beta in the embryonic gut, showing that the LM layer did not develop when a PDGFR alpha inhibitor was applied between E12.5 and E13.5; instead a broad layer of cKit^{+} cells was still present. If the inhibitor was applied after E14, no changes in the LM layer development were observed. Thus, they concluded that PDGF signals play a crucial role in the differentiation of LMCs between E13 and E14 of development (Fig. 1-10 lower).

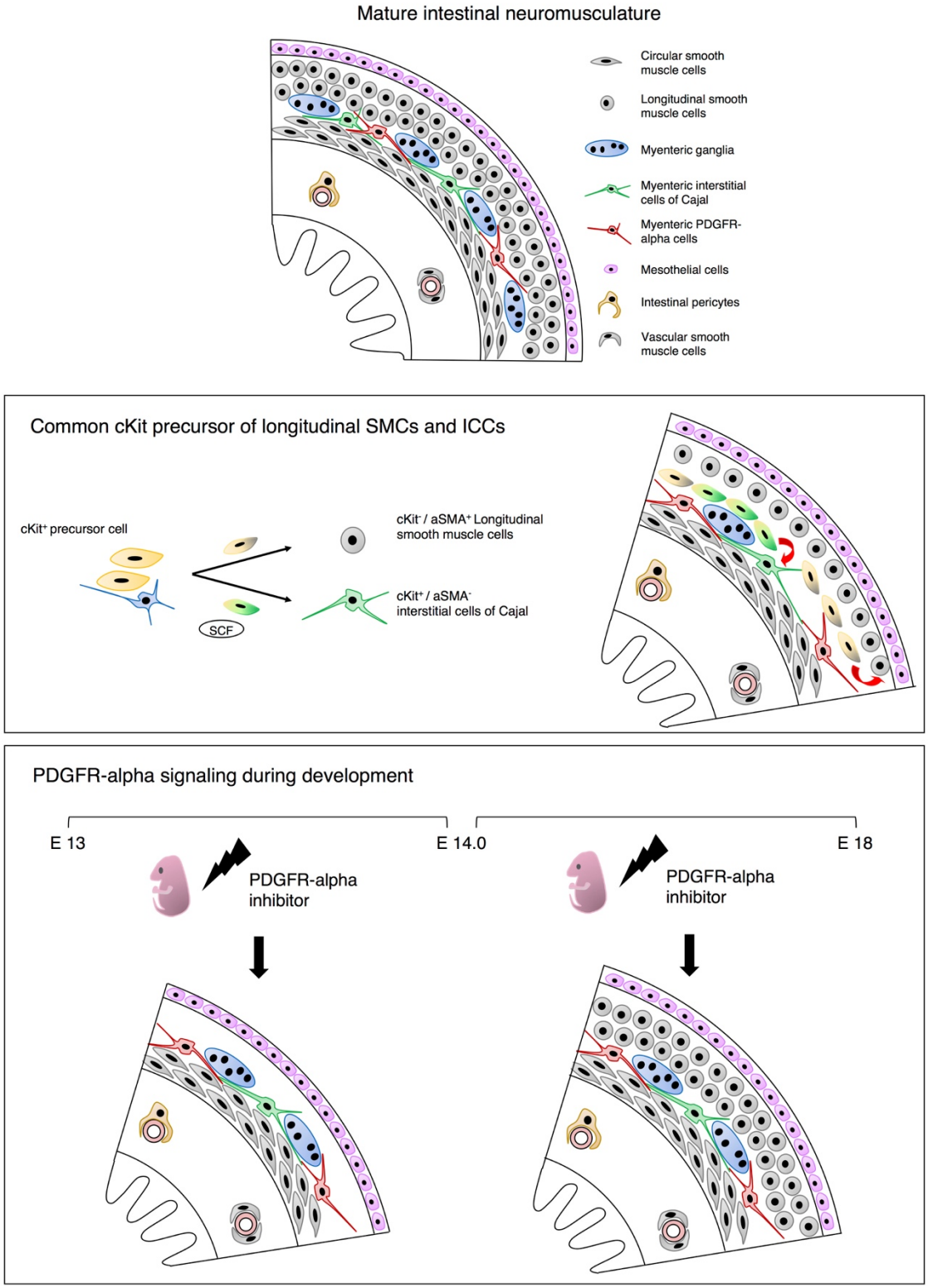

Figure 1-10: Schematic of canonical longitudinal smooth muscle origin

The **upper panel** shows a schematic representation of the mature neuromuscular intestinal wall. The **middle panel** illustrates the theory by which a cKit positive precursor, located outside the circular SM layer when the intestine develops, can give rise to an ICC or a longitudinal SMC depending on its vicinity to the neuroblasts secreting the stem cells factor (SCF). The **lower panel** represent the role of PDGFR-alpha signalling during longitudinal SM development, showing how

the inhibition of the signal ("thunder" symbol) in a time window between E13 and E14 results in the absence of the longitudinal SM layer while there is no effect if inhibition occurs after E14.

The bone morphogenetic protein (BMP) signalling has also been suggested to be involved in enteric smooth muscle differentiation (De Santa Barbara et al., 2005). In fact, work on chick showed that during development pSMAD proteins (components of the endogenous BMP signalling pathway) were broadly expressed in the mesoderm and following smooth muscle differentiation, their expression was highly down-regulated (De Santa Barbara et al., 2005). If the BMP pathway was experimentally induced, undifferentiated mesenchymal cells would remain due to a failure of smooth muscle differentiation (De Santa Barbara et al., 2005). Further, it has been demonstrated that mesenchymal smooth muscle precursors, when starting to express αSMA, transiently expressed RNA-binding protein for multiple splicing 2 (*RBPMS2*), a regulator in RNA metabolism (Notarnicola et al., 2012). Additionally, Notarnicola et al. (2012) demonstrated that a sustained expression of *RBPMS2*, both *in vivo* and *in vitro* cultured SMCs, represses smooth muscle differentiation by up-regulation of *Noggin,* the major inhibitor of the BMP pathway.

The role of BMP pathway was also investigated in mice and it was shown that BMP2 and the receptor BMPr-Ib and BMPr-II are expressed at E12 and E13 in the developing mouse gut (Torihashi et al., 2009). In particular, BMPr-Ib is expressed in the newly formed CM layer, while BMP2 and BMPr-II are localised in the outer region of the future LM layer (Torihashi et al., 2009). BMP is thought to signal the developing SMCs in a autocrine/paracrine manner, as evidenced by expression of pSMAD at E12.5 and E13 in the same regions (Torihashi et al., 2009). Torihashi et al. (2009) further confirmed the BMP signalling role in smooth muscle differentiation, showing, in an *in vitro* system, that beads soaked with BMP2 increased gut-like structure contractility and induced upregulation of smooth muscle protein 22 (SM22) and γ-enteric actin mRNA, and that this process was inhibited by noggin. Interestingly, they noted, in the short window between E12 and E13, the effect of an interaction between BMP and PDGF signalling on smooth muscle differentiation. Comparing their findings with the work of Kurahashi et al. (2008), they highlighted that the CM layer expresses

PDGF-A and BMPr-Ib, whereas the precursors of the LM layer express PDGFR alpha and BMP2 (Fig. 1-11) (Torihashi et al., 2009).

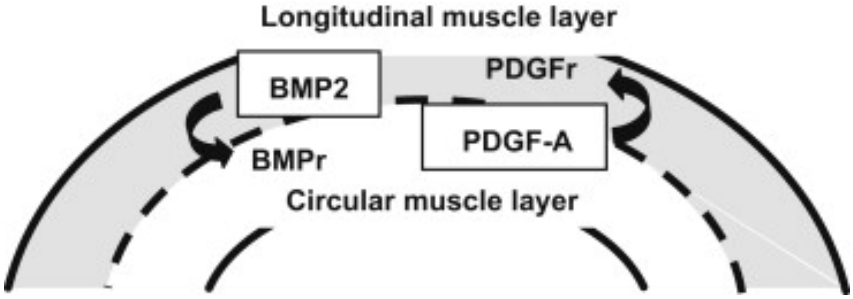

Figure 1-11: BMP and PDGF regulation between SMCs of the LM and the CM layers
Schematic of theory proposed by Torihashi et al. (2009) on the reciprocal signalling between CM and LM layers. From Torihashi et al. (2009).

1.6.2 Mesothelial contribution

Other researchers have been looking for an alternative origin of smooth muscle cells of the intestine from the mesothelium, an epithelial monolayer that covers the coelomic cavity and furnishes a non-adhesive layer that helps the frictionless movement of organs (Rinkevich et al., 2012). In fact, mesothelial cells of different organs have been shown to undergo epithelial-mesenchymal transition (EMT), a process by which coelomic epithelial cells convert to mesenchymal cell phenotype and migrate throughout to contribute at least to the vascular smooth muscle of the intestine (Wilm et al., 2005). By employing genetic lineage tracing techniques using mesothelin (MSLN), a membrane glycoprotein expressed on normal mesothelium, Rinkevich et al. (2012) demonstrated an important role of mesothelium in visceral smooth muscle generation. They showed how $MSLN^+$ mesothelial cells were involved in development, post-natal growth and maintenance of intestinal smooth muscle layers as well as in smooth muscle regeneration following irradiation-induced injury. Subsequently, Carmona and co-workers (2013) pursued this theory of mesothelial origin of smooth muscle cells taking advantage of previous work from Wilm et al. (2005). Using the Wilms' tumour suppressor gene *Wt1*, they created a more efficient *Wt1* reporter line, which allowed them to demonstrate that $Wt1^+$ cells have a huge potential, being able to differentiate into different cell types: endothelial, vascular and visceral

smooth muscle and interstitial cells of the intestine (Carmona et al., 2013)(Fig. 1-12).

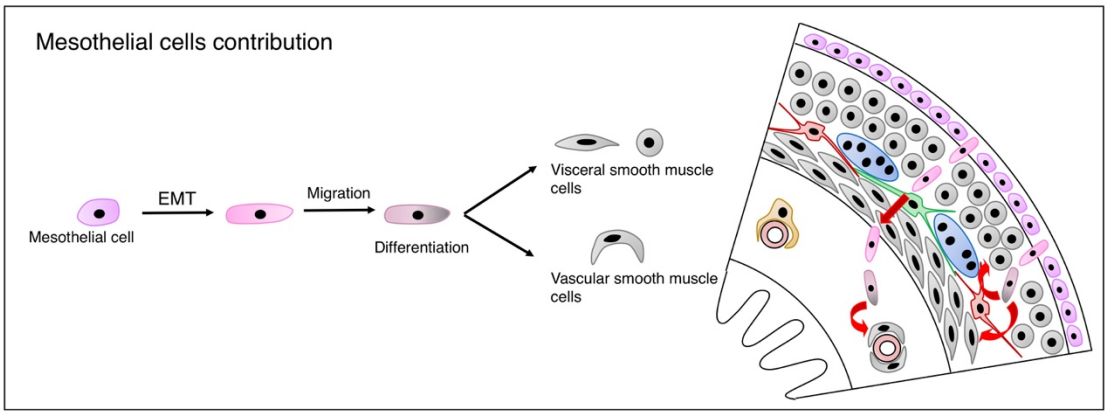

Figure 1-12: Schematic of mesothelial cell contribution to visceral SMCs

The schematic shows how a mesothelial cell can contribute to the formation of both vascular and visceral SMCs, by undergoing an EMT transition, migrating and differentiating into SMCs. The shape and colour of cells matches the legend in Figure 1-10 upper.

Despite all the aforementioned studies, hitherto, there is no agreement on a common origin for intestinal smooth muscle cells. **Therefore, further studies are needed to underpin the identity of the smooth muscle precursor cells of the intestine.**

1.6.3 Vascular compartment as source of smooth muscle precursors

As discussed in section 1.6.2, the origin of part of the vascular smooth muscle cells of the gut has been ascribed to the mesothelium (Wilm et al., 2005). This process has also been described in other coelomatic organs, such as liver (Asahina et al., 2011) and lung (Que et al., 2008). However, from several other lineage-tracing studies, it is now clear that this developmental origin is only one of many, with the suggestion that the mural wall of a vessel could be considered a mosaic from a developmental point of view (Armulik et al., 2011).

Pericytes, specialised cells of vessel mural wall, defined by their position underneath the basal lamina of micro vessels, have recently been suggested to be vascular smooth muscle progenitors, and also constitute multipotent stem/progenitor cells such as adipocyte progenitors (Olson and Soriano, 2011),

osteoblasts, chondrocytes (Collett and Canfield, 2005) and skeletal muscle stem cells (Dellavalle et al., 2007). In this respect, pericytes resemble mesenchymal stem cells (MSCs). MSCs were described to reside in a vascular niche in bone marrow and dental pulp (Shi and Gronthos, 2003) and generate osteoblasts, chondrocytes and adipocytes *in vitro*. Similarly, pericytes have shown the same differentiation capacity *in vitro* and, in addition, can generate vascular and skeletal muscle cells (Armulik et al., 2011). From these analogies, a new concept for a perivascular niche of MSCs was developed (Armulik et al., 2011). In support of this theory, further research by Bianco's group suggested that, rather than a ubiquitous population of MSCs with identical capacities, pericytes constitute tissue-specific mesodermal progenitors able to generate cells of the mural wall (Sacchetti et al., 2016). Considering all these data, they speculated that pericytes could be local progenitors capable of generating both vascular smooth muscle cells and the mesoderm of the organ from which they originate.

A different source of pericytes has been identified in a relatively new population of cells named mesoangioblasts (MABs). These cells were first isolated from the embryonic murine dorsal aorta (De Angelis et al., 1999), and later described by Minasi et al. (2002) as cells assigned to a perivascular origin that give rise to vascular and other mesodermal derivatives *in vivo*. MABs are thought to arise from an "angiopoietic" ancestor similar to hemoangioblasts. According to this theory, angioblasts generate hematopoietic and mesodermal progenitors by asymmetric division, as well as endothelium restricted precursors (Cossu and Bianco, 2003) (Fig.1-13). However, postnatal MABs lose expression of endothelial markers, such as CD34 and Flk1 (Foetal Liver Kinase 1), but share features of pericytes in their differentiation capabilities/origin, suggesting that they can be referred to as pericyte-derived cells. However, it should be noted that pericytes cannot be identified univocally by a defined set of markers, since their expression is not consistent and can differ throughout the life of the same cell (Armulik et al., 2011).

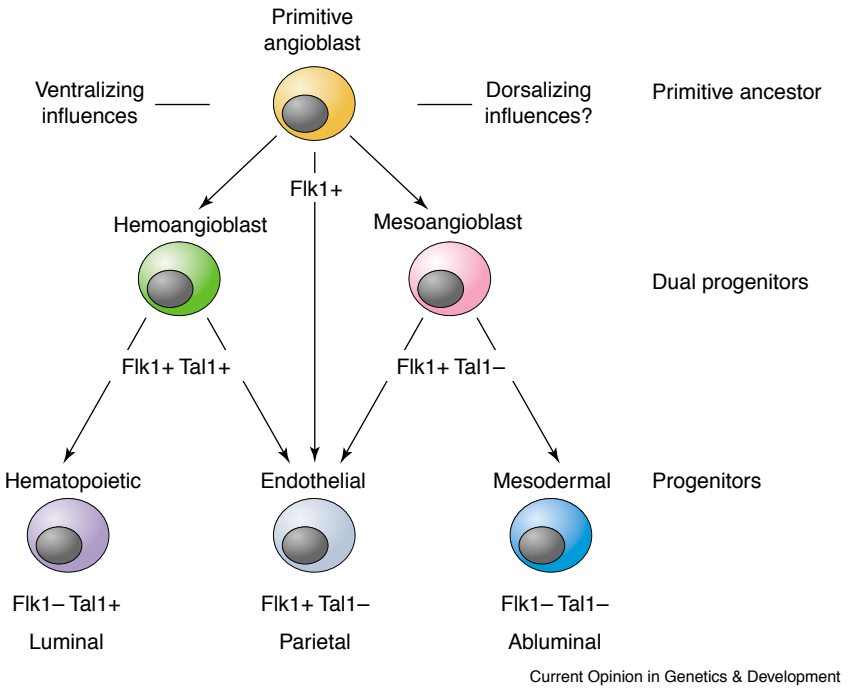

Figure 1-13: Origin of mesoangioblasts in the embryonic dorsal aorta

Schematic of hematopoietic endothelial and mesodermal progenitors originating from the primitive angioblast ancestor. From Cossu and Bianco (2003).

Postnatal pericyte-derived cells have been efficiently isolated from skeletal muscle biopsies showing high growth capacity and ability to differentiate into mesodermal tissues in culture under specific conditions (Tonlorenzi et al., 2007). Specifically, they differentiate into a smooth muscle lineage, as pericytes do, and also in skeletal muscle as their mesodermal lineage of origin (Dellavalle et al., 2011). *In vitro*, MABs efficiently differentiate towards smooth muscle cells in response to TGFß, a cytokine well-known in the smooth muscle differentiation pathway. Nevertheless, even if with lower efficiency, spontaneous smooth muscle myogenesis has been reported by foetal MABs *in vitro*, further suggesting this may be a default mechanism *in vivo* (Minasi et al., 2002).

Taking into account all these considerations, it could be speculated that MABs and pericyte-derived cells may conceivably constitute a source of intestinal vascular and visceral smooth muscle cells (Perin et al., 2019). Therefore, their use for intestinal tissue engineering approaches could be promoted, in the light of their tendency towards smooth muscle formation (Fig. 1-14).

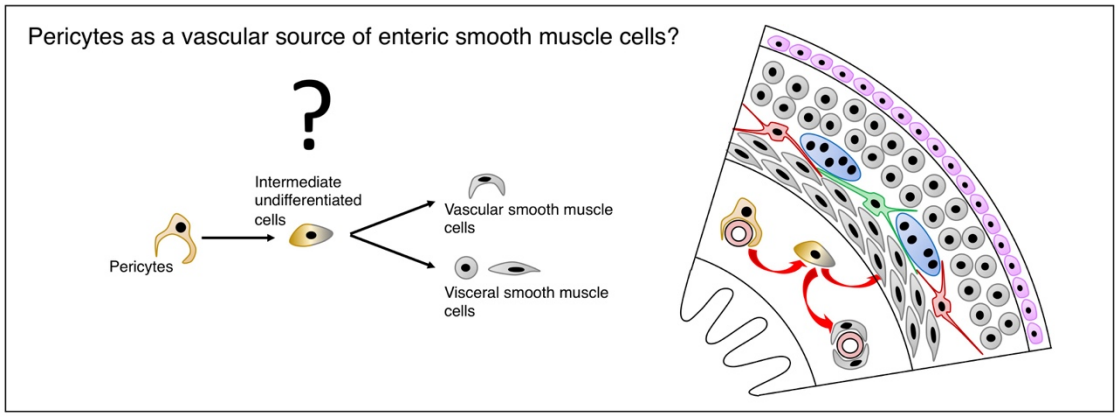

Figure 1-14: Schematic of the hypothesis of intestinal SM formation from the pericytes
The schematic describes the hypothesis by which a pericyte could be giving rise to both the vascular and visceral SMCs. Question mark underlines the fact that this mechanism has not been demonstrated. The shape and colour of cells matches the legend in Figure 1-10 upper.

1.7 Smooth Muscle Cell (SMC) differentiation

Our understanding of how SMCs proliferate and differentiate is mainly based on studies focussed on vascular SMC differentiation, although some studies have also been done to underpin enteric smooth muscle (SM) differentiation. The cellular process of SM differentiation is usually associated with the presence of specific muscle contractile proteins, such as αSMA, SM22, calponin and SM-MHC. The expression of such markers within the cells has been correlated with the activation of different pathways, which can dynamically interact with each other in order to fine-tune SMC differentiation.

As it is well known, studies on vascular SMCs have shown that these cells do not terminally differentiate and, both during development or in adulthood following injuries, SMCs can de-differentiate, proliferate and differentiate again to fulfil the needs of the body (Bengal, 2017). Among all pathways, TGFß signalling is recognized as pivotal in SMC differentiation (Guo and Chen, 2012) by acting through Smad proteins that bind to Smad-binding elements (SBEs) on promoters of SMC genes (Bengal, 2017). However, it is clear that rather than a single mechanism/pathway responsible for SM differentiation, a complex interaction between different pathways is in place. For instance, the Hippo pathway, serum response factor (SRF)/Myocardin signalling, NOTCH signalling and the Hh

pathway have all been associated with SM differentiation (Cotton et al., 2017; Pagiatakis et al., 2017; Pipes et al., 2006; Tang et al., 2010; Wang et al., 2002).

The complex SRF/Myocardin is involved in the regulation of cell proliferation as well as in myogenesis. SRF is a transcription factor that acts by binding to specific sequences, the CArG-box (i.e. $CC(A/T)_6GG$), also known as serum response element (SRE), on the promoters of genes (Pipes et al., 2006). It has been demonstrated that SRF perfectly matches the CArG box of genes involved in cell growth, while the sequences on promoters of SM genes deviate from the consensus sequence by one or more residues (Chang et al., 2001). Therefore, an additional co-activator is needed for the stable binding of SRF to trigger their transcription (Pipes et al., 2006). In fact, Wang et al. (2002) demonstrated the ability of myocardin, expressed in cardiac and SMCs, to create a stable bond with SRF on the CArG-boxes of promoters of SM genes, some of which include: αSMA, γSMA, SM-MHC, calponin, SM22 and TGFß1-induced transcript 1 (TGFB1I1) (Zheng, 2014). In contrast, binding of SFR to the transcription activator Elk1, silences transcription of SM genes and induces SMCs de-differentiation (Scirocco et al., 2016). It is interesting to note, that the canonical TGFß/Smad pathway increases the binding of transcriptional complexes to the CArG elements, therefore increasing SRF/myocardin SM induction.

An important role during development of SM in the gut is played by Hh pathway. The major ligands of this pathway are Sonic Hh (Shh) and Indian Hh (Ihh) that are produced by the endodermal epithelia to target adjacent mesenchymal cells. These ligands bind to the receptor Patched (Ptch) which causes the release of Smoothened (Smo), which in turn activates the Gli transcription factors, triggering the downstream transcription (Mao et al., 2010; Sailaja et al., 2016). This paracrine mechanism of action of Hh is thought to play an important role in triggering SM differentiation and regulation of mesenchymal growth (Huang et al., 2013; Kolterud et al., 2009; Mao et al., 2010; Zacharias et al., 2011) via interaction with the Hippo pathway (Cotton et al., 2017).

In the Hippo pathway, an evolutionarily conserved pathway discovered in Drosophila that controls organ size from flies to humans (Varelas, 2014), the core

signal is transduced by two kinases Mst1/2 and Lats1/2. The activation of these kinases induces the degradation of the transcription coactivators YAP/TAZ (Cotton et al., 2017). The inactivation of the Hippo pathway allows the nuclear translocation of YAP/TAZ and their association with the transcription factors of the Tead family, which in turn regulates downstream gene transcription (Cotton et al., 2017). In support of its role in controlling organ size, Cotton et al. (2017) demonstrated that inhibition of the pathway (and consequent activation of YAP/TAZ) stimulates mesenchymal growth, and, when YAP was conditionally activated in a specific mouse model, there was disruption of cell organization and massive mesenchymal expansion. Furthermore, research proved that high levels of YAP/TAZ are able to block SM differentiation, while low levels of YAP/TAZ allow Hh-induced SM differentiation (Cotton et al., 2017). In contrast, Pagiatakis et al. (2017) demonstrated the role of TAZ in the TGFß/Smad pathway related with SM differentiation. In particular they observed that TGFß increases TAZ expression in mesenchymal cells and the mRNA levels of SM genes. When TAZ is absent, there is a reduction in transcription of SM genes, while when TGFß is active, recruitment of SRF and TAZ on the CArG element increases. Finally, TAZ interacts directly with Myocardin to enhance SM gene transcription and induce an upregulation of *myocardin* mRNA (Pagiatakis et al., 2017).

Another important pathway involved with SM differentiation is the NOTCH pathway. Tang et al. (2008) demonstrated the induction of SM phenotype following NOTCH activation and found that the phenotype is inhibited by hairy-related transcription factors, HRT, downstream effectors in the Notch pathway, which suggest the presence of a negative feedback within the pathway. They further investigated HRT role as transcriptional repressor and found that HRT is able to exert negative regulation of TGFß1 SM differentiation (Tang et al., 2010). Moreover, Tang et al. (2010) revealed an intriguing relationship between NOTCH and TGFß pathways as both pathways cooperatively affect SM phenotype differentiation via their effects on Smad activity, which in turn is correlated with higher mRNAs encoding for SMA, calponin1 and SM22.

Overall, the findings reported so far suggests that the process of proliferation and differentiation of SMCs is complex, with the involvement of several interconnected mechanisms.

1.8 Aim

The treatment of intestinal failure remains a considerable clinical challenge and the most severe disorders may require significant interventions such as small bowel transplantation. Unfortunately, small bowel transplantation in children is restrained by the very limited availability of organs and variable outcomes. Therefore, a tissue engineering approach aimed at the generation of a functional intestine is a promising solution, but requires the identification of appropriate sources of cells for its generation.

Thus far, researchers have identified multiple potential sources of intestinal smooth muscle cells. Agreement on the origins of both layers of smooth muscle cells in the intestine, however, is lacking. The aim of this project is focused on the identification of possible cell sources for intestinal muscle regeneration and their characterisation in order to determine specific molecular markers and cues that may be useful for the isolation and manipulation of these cells.

The initial part of the thesis describes the development of the muscle layers in the human intestine and then, in mice, it focuses on the “canonical” precursors in order to identify their molecular signature.

Objectives part 1:

- Characterisation of the human intestinal development, by means of immunohistochemistry, to identify the most important timing in the formation of the intestinal smooth muscle layers;
- Study the formation of the longitudinal smooth muscle layer in mouse using immunofluorescence staining and flow cytometry analysis for known markers of the putative enteric smooth muscle precursors;

- Study the whole transcriptome profile of the subpopulations of intestinal cells identified by flow cytometry analysis throughout mouse gut development to try to identify a subpopulation that may likely be (or contain) the enteric smooth muscle precursors;

In the second part, attention is drawn to the vascular contribution to smooth muscle cells of the intestine, with the isolation and characterisation of human intestinal mesoangioblasts and with the assessment of their possible use in tissue engineering.

Objectives part 2:

- Isolation and characterisation of human mesoangioblasts from intestinal samples by means of immunofluorescence and flow cytometry analysis;
- Evaluation of the capacity of these cells to differentiate into smooth muscle via immunofluorescence, western blotting, transcriptomic analysis, qPCR analysis and functional assay (calcium imaging);
- *Ex-vivo* and *in-vivo* assessment of smooth muscle regeneration capacity of intestinal mesoangioblasts in an injured intestinal model;
- *In vitro* generation of an intestinal smooth muscle wall using a human foetal decellularised scaffold.

Chapter 2

Materials and Methods

2. Materials and Methods

2.1 Animal samples collection

Animal tissues used to study gut smooth muscle development were isolated from C57BL/6J wild type (WT) mice. Guts were isolated from embryos, foetal and adult mice. Embryos were staged according to the "Days post conception" (dpc) method, where, the morning in which vaginal plug is found, is designated as 0.5 dpc (E0.5). To isolate guts, a midline incision on the abdominal wall was made and gut was carefully dissected from the stomach till the colon. The entire gut or specific regions of the gut were analysed and this is specifically mentioned for each experiment.

All experimental procedures performed were in accordance with Animals (Scientific Procedures) Act 1986 and all the experimental protocols approved by the UK Home Office, Project Licence PPL P8D8E806D.

2.2 Human gut samples collection

Human foetal gut samples were obtained from voluntary medical or surgical termination of pregnancy through the Joint MRC/Wellcome Trust Human Developmental Biology Resource (HDBR) under informed ethical consent with Research Tissue Bank ethical approval (08/H0712/34+5 and 08/H0906/21+5). Gut samples used in this study were between Carnegie Stage 23 (cs23) and 20 post conceptional weeks (pcw). Developmental stages were determined following Carnegie staging for embryos (Bullen and Wilson, 1997) and measuring foot length for foetuses.

Paediatric full thickness biopsies were taken during surgeries at the Great Ormond Street Hospital, London, under informed ethical consent (ethical approval REC Ref Q0508/79).

2.3 Histology and Immunostaining

2.3.1 Sample preparation and sectioning

Embryonic, foetal and post-natal gut samples, both human and murine, were fixed after dissection for 1-2 hours with 4% paraformaldehyde (PFA) made in phosphate buffer solution (PBS) at room temperature (RT) and washed overnight (O/N) with PBS at 4°C. They were embedded either in gelatine for cryosection, paraffin-embedded or flat opened longitudinally along their mesentery for whole mount staining.

For cryosections, samples were cryoprotected/dehydrated using 30% sucrose in PBS at 4 ºC O/N, embedded in 7.5% gelatine (300 bloom, Sigma)/15% sucrose in PBS, frozen in dry ice-cooled isopentane and stored at -80 ºC till their use. Samples were cut at 10-12 μm using a Cam 1900 Uv Cryostat (Leica Microsystem) and superfrost slides (Thermo Scientific) with sections were first dried at RT and then stored at -20 °C. Before immunohistochemistry was performed, slides were left to thaw at RT, then kept for 20 minutes in PBS at 37 °C to remove gelatine, post-fixed with 4% PFA in PBS for 10 minutes at RT and finally washed 3 times for 5 min with PBS.

For paraffin embedding, samples were dehydrated through a graded ethanol series before embedding. Then, paraffin-embedded samples were sectioned at 5-7 μm (using a HM 325 Rotary Microtome, Thermo Scientific) and left to dry O/N at 37 °C. Slides were deparaffinised for 5-6 minutes in xylene, rehydrated in a graded ethanol (EtOH) series (100% 5 min twice, 90% 5 min, 70% 5 min) and washed in tap water before being processed for histology or immunostaining. For immunostaining, heat mediated antigen retrieval was performed in citrate/EDTA buffer at 6.2 pH using The Menapath Antigen Access Unit pressure cooker.

2.3.2 Histology

For Haematoxylin & Eosin (H&E) staining, slides were stained with Modified-Harris Haematoxylin for 5 to 10min, then rinsed with running tap water and dipped in 1% Acid Alcohol (1ml 37% HCl in 100ml 70% Ethanol) to remove

excess dye. After washing in tap water, sections were counterstained with 1% Eosin Y (1g in 100ml of milliQ water, Sigma) for 5 to 10min. Sections were then dehydrated in a graded ethanol series (50% 1 dip, 70% 1 dip, 90% and 100% EtOH for 1 min) and finally cleared in Xylene for 6 min before being mounted in D.P.X (Sigma). Sections were imaged using a Zeiss Axioplan microscope.

2.3.3 Immunostaining

For immunofluorescence staining, sections were blocked for 1h with 1% Bovine Serum Albumin (BSA, Sigma)/ 0.1% Triton-X in PBS (PBT) at RT. Sections were incubated O/N at 4 °C with primary antibodies (Tab. 2-1) diluted in the block solution, washed three times for 5 minutes with PBS and then detected with secondary antibodies (Tab. 2-2) diluted in block solution for 1h at RT. They were then mounted using vectashield mounting medium (Vector Labs) after being washed three times for 5 minutes with PBS. Negative control tissues were prepared by omitting primary antibodies.

For whole mount staining, tissues were blocked for 2h with 1% BSA / 1% Triton-X in PBS (whole mount block) rolling at RT. Tissues were then incubated O/N rolling at 4 °C using primary antibodies listed in Tab 2-1, washed three times for 30 min with PBS and then detected with secondary antibodies (Tab. 2-2) diluted in whole mount block solution for 2h at RT. Finally, tissues were washed three times for 30 minutes with PBS before being mounted.

Tissues were imaged using Olympus IX71 inverted microscope, Zeiss Observer microscope or Zeiss LSM710 confocal microscope.

Table 2-1: Immunofluorescence primary antibody list

Antibody	Company	Concentration
Goat anti human PDGFRα	R & D	1:100 - 1:500
Rabbit anti SM22	abcam	1:1000
Mouse anti Calponin	Sigma-Aldrich	1:1000
Mouse anti SM-MHC	Sigma-Aldrich	1:200 - 1:400
Mouse anti αSMA	Sigma-Aldrich	1:250
Rabbit anti αSMA	abcam	1:250
Rabbit anti cKit	Dako	1:250
Mouse anti TuJ1	Biolegend	1:500

Rabbit anti TuJ1	Biolegend	1:500
Goat anti SCFR	R & D	1:500
Rabbit anti PDGFRß	Abcam	1:100
Rabbit anti NG2	abcam	1:100
Goat anti mouse PDGFRα	R &D	1:100 - 1:500
Rabbit anti Ki67	Novocastra	1:250
Rabbit anti MyHC	Abcam	1:100
Rabbit Anti MyoD	Santa Cruz	1:80

Table 2-2: Immunofluorescence secondary antibody list

Antibody	Company	Concentration
Donkey anti Gt 568	Invitrogen	1:500
Donkey anti Ms 568	Invitrogen	1:500
Donkey anti Ms 647	Invitrogen	1:500
Goat ant Ms 488	Invitrogen	1:500
Goat anti Ms 568	Invitrogen	1:500
Goat anti Rb 488	Invitrogen	1:500
Goat anti Rb 568	Invitrogen	1:500
Goat anti Rb 647	Invitrogen	1:500
Dapi	Sigma	1:1000 (1mg/ml)

2.4 Flow Cytometry analysis and Fluorescence Activated Cell Sorting (FACS) of mouse embryonic guts

2.4.1 Mouse guts preparation

Guts from embryos staged E12.5, E14.5, E16.5 and E18.5 were carefully dissected under a stereomicroscope using fine forceps. Embryonic guts isolated from one litter, were collected, pooled and dissociated, before starting the staining process, using 1 mg/mL dispase/collagenase solution or using Tumour Dissociation kit (Miltenyi). Dissociation time was increased according to the stage and size of the samples, varying between 4 and 8 min when using dispase/collagenase for younger staged guts and between 40 and 60 minutes when using Tumour dissociation Kit for older guts. After digestion, samples were washed with medium to remove enzymes.

2.4.2 Cell staining

For flow cytometer analysis, cells were strained through a 40 μm mesh and then stained with one or more different conjugated antibodies listed in Tab. 2-3, for 20-30 min at 4 °C in ice-cold 2% FBS/ 0.05mM EDTA in PBS, according to the experiment. Then cells were washed and re-suspended in sterile ice-cold 2% FBS/ 0.05mM EDTA in PBS for analysis. Unstained cells, as negative control, were treated in the same way. Beads were stained and used for compensation.

For FACS, two additional steps were performed. After the first stage of staining, cells were washed in ice-cold 2% FBS/ 0.05mM EDTA in PBS and stained for 5 min at 37°C wrapped in foil to prevent sample to be exposed to the light with 1:400 Draq5 (Biolegend) to identify nucleated cells and washed again with ice-cold 2% FBS/ 0.05mM EDTA in PBS. Finally, just before sorting, cells were stained 1:200 with dapi.

For flow cytometer analysis, LSRII cell analyser or FACS AriaIII were used and analyses were conducted using FlowJo™ V10.

Table 2-3: List of antibodies for mouse flow cytometry analysis

Antibody	Company	Concentration
CD140a – PE	Biolegend	1:200
CD117 – PE/Cy7	Biolegend	1:200
EpCAM – BV605	Biolegend	1:200

2.5 Mouse subpopulation RNA-sequencing

2.5.1 RNA isolation from mouse embryonic gut cells

Sorted cells were collected, resuspended in RLT buffer provided with the RNeasy micro kit Plus (QIAGEN) and stored at -80 °C until ready for RNA isolation. RNA was isolated with the mentioned kit following manufacturer instructions. RNA quantity and quality were assessed using NanoDrop™ (ThermoFisher) and Bioanalyser (Agilent Thecnologies). All RNA samples used for sequencing were of good quality as confirmed by an RNA Integrity Number (RIN) > 7.5 using the total RNA pico Kit (Agilent Thecnologies).

2.5.2 Library preparation and sequencing

RNA sequencing was performed using a 3' tag library. This sequencing technology does not generate fragments across the whole mRNA transcript, but is centred on generating sequences towards the polyA tail of the mRNA. This allows the detection of different transcripts (and thus allowing differential gene expression) while it decreases the need for high sequencing depth in each sample because reads are not spanning the whole transcript (Ma et al., 2019). Libraries were generated by UCL Genomics using QuantSeq 3' mRNA-Seq Library Prep Kit FWD for Illumina (Lexogen) with UMI add-on and dual indexing to allow for multiplexing. Libraries (1x75bp) were produced following manufacturer protocol and, when necessary due to low yield of RNA from some samples, adjustments were performed as recommended by the manufacturer. Sequencing was performed on a NextSeq 500 (Illumina).

2.5.3 RNA-sequencing analysis

Bioinformatics analyses carried out in this study were performed in collaboration with Dr. Luca Peruzza (University of Southampton, UK).

Raw reads were quality checked using FastQC/v0.11.3 (https://www.bioinformatics.babraham.ac.uk/projects/fastqc/) and trimmed using Trimmomatic/v0.32 (Bolger et al., 2014) with default parameters to remove low quality bases and adaptors. High quality, clean reads were mapped against the mouse genome (Ensembl assembly version GRCm38.p6 96.38) using STAR/v2.7.0e (Dobin et al., 2013) and the raw count matrix was generated using featureCounts/v1.6.3 (Liao et al., 2014) excluding multi-mapping reads. The count matrix was imported into R/v3.6.0 (R Development Core Team, 2008) using the library edgeR/v3.22.5 (Robinson et al., 2010) and was subsequently filtered (to remove transcripts with low coverage) to retain transcripts with counts per million >1 in at least two libraries and normalized using the trimmed mean of M values (TMM) method (Robinson and Oshlack, 2010). After filtering, a CPM table was generated with all genes that passed the filtration criterion by using the "cpm" function of edgeR. For each developmental stage, Differentially Expressed Genes (DEGs) were identified using edgeR by comparing the overall expression

of one cell population against the average of the other three populations and were deemed significant using a cut-off p-value < 0.01 and a Fold Change ≥ |2|. This analysis was performed for all cell populations at all developmental stages.

For each developmental stage, all up-regulated and down-regulated DEGs were subsequently tested for the presence of enriched categories by using the Gene Ontology (GO, http://geneontology.org), Kegg (https://www.genome.jp) and Reactome (https://reactome.org) databases with the function "compareCluster" from the R library clusterProfiler/v3.8.1 (Yu et al., 2012) with a cut-off FDR < 0.01.

Figures were plotted using R or Prism/v8.0.2 (GraphPad Software, California USA, www.graphpad.com) software.

2.6 Cell culture: mesoangioblasts (MABs)

2.6.1 Isolation and expansion of human small intestinal MABs

Human foetal small intestinal mesoanglioblast-like cells (hFtSI_MABs) were isolated from foetal biopsies, between 10 and 20 pcw, collected through HDBR resources (see section 2.2 above), while paediatric small intestinal mesoanglioblast-like cells (hPaedSI_MABs) were isolated from ileum full thickness biopsies obtained from patients in the first year of life undertaking surgery (see section 2.2 above). A list of biopsies used in this study is provided in Table 2-4.

Table 2-4: List of human gut biopsies used for intestinal MABs isolation

# Biopsy	Donor age	Sex
# 1	12 pcw	male
# 2	16 pcw	male
# 3	20 pcw	male
# 4	12 pcw	male
# 5	12 pcw	female
# 11	1 year	male
# 12	1 year	male

Cells were isolated with a few adaptations from the protocol published by Tonlorenzi et al. (2007) and recently used to isolate MABs from murine intestine (Perin et al., 2019). Following washes with sterile phosphate buffer saline (PBS), smooth muscle layers of midgut and ileum were carefully dissected from the submucosa and mucosa layers, using fine forceps under a stereomicroscope and cut into small pieces of around 2 mm each. These pieces were transferred into a 6 well dish, pre-treated with 1:100 growth factor reduced Matrigel (MRF, BD) to favour attachment and cell outgrowth, with maximum 3 pieces per well. Megacell medium (Sigma) supplemented with 5% Foetal Bovine Serum (FBS, Gibco), 1% non-essential amino acids (Gibco), 1% L-glutamine (Gibco), 1% Pen-Strep (Gibco), 0.05mM β-mercaptoethanol (Sigma) and 5ng/ml basic Fibroblast Growth Factor (FGF, Peprotech) was gently added, to avoid fragment detachment, until the muscle pieces were covered. Dishes were placed inside an incubator at 37°C, 5%CO_2. The following day, fresh medium was added on each well.

For the first two days, plates were left in the incubator, avoiding any movements to prevent tissue detachment. After 3 days, cultures were checked for preliminary outgrowth and the medium was changed. Timing of cell outgrowth was sample specific and varied from 5 to 10 days. In general, when cells from the outgrowth covered a 10x field of view, they were trypsinized and placed into flasks and expanded using the same enriched Megacell medium as for outgrowth.

For cell expansion, when human small intestinal mesoangioblast-like cells (hSI_MABs) reached 60-70% confluency, they were detached, always recovering both the adherent and the floating population. After gentle rinsing with PBS, TripleE solution (Gibco) was added and incubated at 37°C for 3 minutes, when all cells detached from the flask. Usually, between 1:6-1:8 passaging was performed.

Cultured cells were characterised via immunofluorescence staining after being fixed for 8- 10min with 4% PFA in PBS following the protocol described above (section 2.3.3).

2.6.2 Single nucleotide polymorphism (SNP) genotyping array

To assess genomic stability of human small intestinal MABs after several passages in culture, an SNP genotyping array was carried out. First, DNA was extracted from two hFtSI_MABs lines (# 4; # 11) kept in culture for 8-9 passages, using DNasy Blood & Tissue Kits (QIAGEN). Purified DNA was then processed by UCL Genomics using Infinium Core-24 Kit (Illumina) and data were processed using GenomeStudio Software (Illumina).

2.6.3 Other MABs used in the study

MABs isolated from other tissues were used for comparison with hSI_MABs. For this purpose, human MABs isolated from foetal limbs staged between 7 and 22 pcw were used (hFtLIMB_MABs). These cells were a gift from Dr. Carlotta Camilli, from Prof. Paolo De Coppi's lab.

2.6.4 Alkaline Phosphatase

Alkaline Phosphatase (AP) staining was performed using the Vector® Red Alkaline Phosphatase Kit (Vector Laboratories), following manufacturer protocol. Briefly, plated cells were washed in PBS, then incubated in the dark at RT for 20 to 30 minutes with the working solution made of 20 µl of each reagent (Reagent 1, 2, 3 provided in the kit) every ml of 200 mM Tris-HCL buffer adjusted to a final pH of 8.3. Then cells were washed for 10 minutes with the buffer solution and mounted or counterstained following immunofluorescent protocol described in section 2.3.3.

2.6.5 hSI_MABs flow cytometer analysis and FACS

Analysis and FACS were performed with foetal or paediatric hSI_MABs. hSI_MABs were analysed at passage 3 or 4 of culture. hSI_MABs were detached using a cell scraper, to reduce internalisation of some cell membrane receptors particularly sensitive to TripleE solution. Cells were treated for flow cytometry as described in section 2.4.2. A list of antibodies used for hSI_MABs characterisation and their concentration is provided in Table 2-5.

Table 2-5: hSI_MABs flow cytometry antibody list

Antibody	Company	Concentration
CD34 – APC	Miltenyi	1:100
CD34 – BV605	Biolegend	1:100
CD90 – PE/Cy7	Biolegend	1:200
CD146 – BV710	Biolegend	1:200
CD140b - PE	Biolegend	1:200
CD140b -APC	Biolegend	1:200
NG2 – AF488	Biolegend	1:200
CD56 – AF488	Biolegend	1:200
CD56 – BV510	Biolegend	1:200
AP – AF647	Biolegend	1:200

2.6.6 Cell transduction

Plated hSI_MABs were transduced using a lentivirus carrying eGFP reporter, previously produced in the lab (Natarajan et al., 2014) (Fig. 2-1). For every 10^6 cells, 100μl of virus was added to culture media and left for at least 36 hours to allow viral transduction and inactivation. GFP-positive cells were then selected via Fluorescence Activated Cell Sorting (FACS) and cultured for at least three days before experimental uses.

Figure 2-1: Lentiviral construct

Schematic of the lentiviral construct. Adapted from Natarajan et al. (2014)

2.6.7 hSI_MABs differentiation protocols

hSI_MABs were tested in their capacity to generate SMCs, as well as to differentiate towards skeletal muscle as previously shown for MABs isolated from skeletal muscle biopsies by Tonlorenzi et al. (2007). Initially cells were cultured in expansion medium (enriched Megacell; see section 2.6.1) for 24 hours before medium was changed for differentiation. Differentiation protocols used were:

- **Smooth Muscle**

  Medium used was based on High Glucose DMEM (Gibco) enriched with 1% L-Glutamine, 1% Pen-Strep and 2% Horse Serum (HS, Gibco), with or without daily addition of 5ng/ml of Transforming Growth Factor - ß (TGFß, Sigma) for 7 or 14 days. Moreover, TGFß1 - Inhibitor (Sigma) was added to the media (at a final concentration of 5 μM) as control to inhibit TGFß induced smooth muscle differentiation. (This TGFß1 – Inhibitor works by inhibiting the activity of the TGFβ kinase/activin receptor-like kinase (ALK 5), therefore preventing the phosphorylation of Smad2/3 and downstream effects). Differentiation protocols were performed by plating cells in 6- 12- or 24-wells dishes.

- **Skeletal Muscle**

  To assess skeletal muscle differentiation potency, cells were cultured for 7 days in differentiation medium. Differentiation medium was based on High Glucose DMEM enriched with 1% L-Glutamine, 1% Pen-Strep and 2% HS.

Quantification of cells positive for SM markers was assessed by counting the number of positive cells per high-power field (five images per biological samples, n =5). Statistical difference between cells cultured in different smooth muscle differentiation media was evaluated by means of t-test and significance was assessed with p-value <0.05.

2.6.8 C2C12 – hSI_MABs co-culture

C2C12, an immortalized mouse myoblast cell line, was used to co-culture hSI_MABs in order to determine their skeletal muscle potency. C2C12 cells were expanded into flasks using High Glucose DMEM enriched with 1% L-glutamine, 1% Pen-Strep and 20% FBS. For co-culture experiments, C2C12 cells were plated onto 6- wells dishes pre-coated with 1% MRF and cultured until they reached confluence and started differentiating to form myotubes. At this point, different GFP-labelled hSI_MABs lines were seeded on top of the C2C12 cultures. For the first day, the co-cultured cells were cultured in a 50% C2C12 medium / 50% Megacell enriched medium. After 24 hours, cells were cultured in

Megacell enriched medium which was changed every other day for 12 days. For the duration of the experiment, GFP-labelled cells were monitored using a fluorescent microscope to assess fusion of hSI_MABs with already formed mouse myotubes by means of appearance of GFP^+ myotubes. After 12 days of co-culture, cells were fixed for 8- 10 minutes with 4% PFA before being processed for analysis. Cells were stained for skeletal muscle marker, myosin heavy chain and human nuclei as described in section 2.3.3.

2.6.9 Calcium imaging

For calcium imaging analysis, hSI_MABs were cultured using custom-made super-frost slides equipped with silicon rings and coated with 1% rat tail Collagen I (Sigma) (Fig. 2-2). After 8 days in culture (i.e. 24 hours in expansion medium and 7 days of differentiation protocol), undifferentiated hSI_MABs and differentiated cells were submerged in oxygenated Krebs solution (in mM: 120.9 NaCl, 5.9 KCl, 1.2 $MgCl_2$, 2.5 $CaCl_2$, 11.5 glucose, 14.4 $NaHCO_3$ and 1.2 NaH_2PO_4) and incubated with 1 μM CalBryte® 520 dye in Krebs, for 20 min at RT. Following 3 washes of 5 min with Krebs solution, a microscope (Olympus BX51) equipped with 20x water dipping lens and an EMCCD camera (iXon Ultra897, Andor Technology) was used to detect and live-image fluorescence activity. Basal calcium activity and calcium activity in response to local application of 1μM Carbachol, were imaged at 2Hz for 60 seconds. Differences in fluorescence among treatments were assessed in GraphPad Prism 8.2.1 with non-parametric Kruskal-Wallis Test with multiple comparisons using undifferentiated cells as reference. p-value <0.05 was deemed statistically significant.

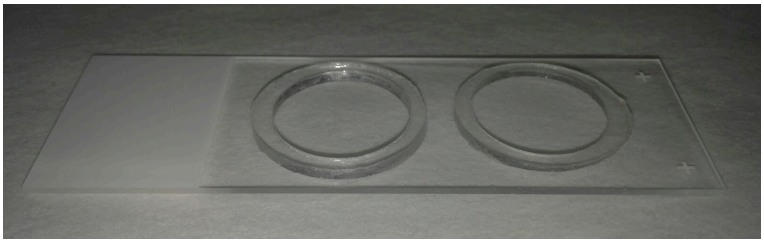

Figure 2-2: Calcium imaging cell culture chambers

Superfrost slides with custom-made silicon rings.

2.6.10 Ex Vivo cell transplantation

Pieces of small intestine (~ 8 mm^2) from C57BL/6J WT mice were used as *ex vivo* models for transplantation of hFtSI_MABs. To avoid tissue contraction, mouse gut pieces were hung between a metal structure and a rubber ring as shown in Figure 2-3, with the serosa facing up.

A cryoinjury was performed in the middle of a tissue piece using a metal instrument with a round smooth end of around 2 mm circumference. The metal instrument was pre-cooled in dry ice for 2 minutes, before being placed on the tissue for 20 seconds to induce the injury. Each ring with the tissue was then placed singularly into a 6-multiwell plate with high glucose DMEM (Gibco) with 1% Pen/Strep and 0.1 mg/ml Primocin™ (InvivoGen) to avoid bacterial growth and left to recover for 1-2 hours. GFP-labelled hSI_MABs were resuspended in 10% rat tail collagen I / 13% fibronectin in PBS and 5x10^4 cells were then seeded within each ring on top of the injury site of tissue using an insulin syringe (Fig. 2-3).

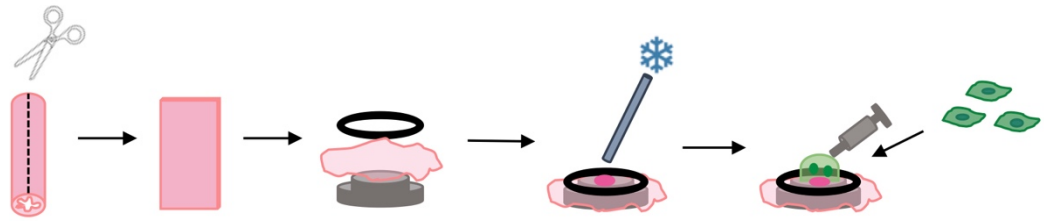

Figure 2-3: Ex vivo schematic

Drawings describes the flat-opening of mouse small intestines, the apposition of pieces of guts between a metal and a rubber ring to secure them. Then the surface of the serosa is cryoinjured and finally GFP-labelled hSI_MABs are injected on top of the injured gut.

For few hours, the tissues were left in very little amount of medium to avoid washing off of the cells, and allow them to settle on tissue, then medium was added to fully cover the surface of the tissues (around 4 mL/ well of the 6-multiwell plate). Tissues with transplanted cells were left in culture for 7-10 days, changing media every other day, before being fixed for 1 hour in 4% PFA and used for immunofluorescence analysis.

2.6.11 In Vivo cells transplantation

GFP-labelled hSI_MABs were transplanted into the distal portion of the ileum, up to 5 centimetres proximal to the caecum, of immune-deficient $Rag2^{-}/\gamma c^{-}/C5^{-}$ knockout mice aged between postnatal day 21 and 42, via laparotomy under isoflurane anaesthetic. Briefly, the caecum and the distal portion of the small intestine were exposed and cells, one million suspended in 10% rat tail collagen I/13% Fibronectin in PBS, were injected with a 30G needle syringe. For each animal (n=5) 5 injections were made 1 cm apart from each other starting 1 cm proximally to the caecum. Mice were maintained for 4 weeks post transplantation before they were sacrificed and intestines dissected for the analyses.

Dissected intestines were fixed for 1 to 2 hours with 4% PFA in PBS. Some were processed for whole mount staining, while others were processed for cryosection and stained as described in sections 2.3.1 and 2.3.3.

2.6.12 Recellularization of human foetal decellularized intestinal scaffolds in vitro

Decellularized scaffolds were obtained using foetal midguts staged between 16 and 20 pcw. To remove all cellular components, pieces of around 3 cm in length were processed using a well-established Detergent Enzymatic Treatment (DET) (Conconi et al., 2005).In brief, tissues were decellularized by submerging them in a series of solutions and left rolling at 4 °C for different period of times. Firstly, after dissection, tissues were left in de-ionised water (resistivity 18.2 MΩ/cm) O/N, followed by 4% sodium deoxycholate (Sigma) for 4 hours and then left washing in de-ionised water O/N. The second day, tissues were immerged in 34 kU/ml DNase-I (Sigma) in 1 M NaCl (Sigma) for 3 hours and finally left washing in de-ionised water for additional 48 hours. Before being sterilised by gamma irradiation, pieces of midgut were cut open along the mesentery insertion and placed in PBS with 1% pen-strep to help maintaining sterility. Removal of DNA content was evaluated measuring the residual DNA content per mg of wet tissue. DNA content of fresh and decellularised samples (n =5 each) was extracted using the DNeasy Blood & Tissue Kits (QIAGEN) and quantified with NanoDrop™ (ThermoFisher). Statistical difference among the two groups was assessed by means of t-test, considering significant p-value <0.05.

Scaffolds were mounted stretched on a Sylgard® coated plate with the serosa surface facing up and left equilibrating with enriched Megacell medium O/N or at least for 2 hours. Half a million cells / half centimetre square ($5x10^5$ / ½ cm^2) resuspended in 10% rat tail collagen I / 13% fibronectin in PBS were injected using an insulin syringe. For a 1 cm long scaffold around 2-3 injections were performed and scaffolds were left without media for two hours to help cell engraftment and avoid washing off of the cells. A schematic of the all process is shown in Figure 2-4.

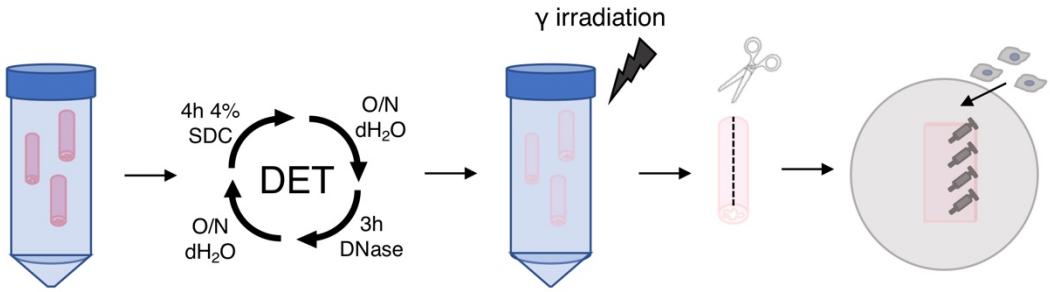

Figure 2-4: Re-cellularisation schematic

Drawings describe the overall re-cellularisation process. The first step is the decellularisation process with the specific DET method protocol; The second step is the irradiation phase, followed by the opening of the gut and finally the injection of hSI_MABs.

Scaffolds were cultured for 2 days in enriched Megacell medium and for the following 7 days with high-glucose DMEM enriched with 2% HS with or without daily addition of 5 ng/ml of TGFß. After the 9 days of culture, scaffolds were fixed in 4% PFA for 1 hour and used for immunofluorescence analysis.

Distribution of cells inside the scaffold was determined by counting the number of cells ($DAPI^+$) per layer using five high-power images each scaffold (n =2 scaffolds). Similarly, the number of cells positive for SM22 and Calponin per each layer were counted over the total number of cells in that layer ($DAPI^+$). Statistical difference among the two groups was assessed by means of t-test, considering significant p-value <0.05.

2.7 Western Blotting

2.7.1 2.7.1 Buffers and solutions

Cell lysis buffer

50 mM Tris-base (~pH7.6)

150 mM NaCl

1% Triton X-100

0.02% sodium azide

1 mM protease inhibitor cocktail (Roche)

1 mM sodium orthovanadate

25 mM sodium fluoride

4X loading buffer

5ml 0.5M Tris-base (pH6.8)

4ml glycerol

0.8g SDS

0.1% bromophenol blue

10% β-mercaptoethanol

4X stacking gel buffer (SGB) (500ml)

0.5M Tris-base (pH 6.8):

- 30.285g Tris-base
- ~ 21ml HCl
- up to 500ml dH_2O

4X running gel buffer (RGB) (500ml)

1.5M Tris-base (pH 8.8):

- 90.855g Tris-base
- ~ 10ml HCL
- up to 500ml dH2O

10X running buffer (1L)

30.2g Tris-base

144g glycine

100ml 10% SDS

Up to 1L dH2O

- For 1X dilute 1:10 in dH2O

10X transfer buffer (1L)

30.3g Tris-base

144g glycine

Up to 1L dH2O

- For 1X dilute in dH2O with 20% methanol

10X TBS (1L)

24.23g Trizma HCl

5.6g Tris-base

88.06g NaCl

- pH 7.6 using conc, HCl

1X TBST (1L)

100ml 10X TBS

900ml dH2O

2ml Tween-20

- up to 1L dH2O

Running gels (for 2 x 1mm gels)		Stacking gels (for 2 x 1mm gels)	
	10% gel		5% gel
RGB	2.5ml	SGB	1.25ml
30% Acrylamide	3.33ml	30% Acrylamide	0.66ml
10% SDS	100ul	10% SDS	50ul
dH2O	3.983ml	dH2O	3ml
10%APS	75ul	10%APS	50ul
TEMED	12ul	TEMED	6ul

2.7.2 Cell lysis and Bradford Assay

Total protein concentration in the solutions was determined by a colorimetric assay based on the protocol of Bradford (1976). The Bradford dye contains Coomassie brilliant blue R-250 which can display either red or blue colouring. When proteins bind, the blue isoform of the dye is stabilised with an absorption of 595 nm. Therefore, absorbance increase is proportional to the amount of blue dye in the solution, and can be used to measure protein content. A BSA dilution series was used to generate a calibration curve (BIO-RAD). Bradford reagent (BIO-RAD protein assay) was diluted 1:5 in dH_2O. For each μl of sample, 100 μl of diluted Bradford was added, mixed and loaded into a 96 well plate (each sample was done in triplicates for proper quantification).

Cells were washed with ice-cold PBS (Gibco) and pelleted into 1.5 ml tubes (Eppendorf). 100 μl of lysis buffer, with added protease inhibitor, sodium orthovanadate and sodium fluoride, were added to each tube containing the cell pellet and left incubating on ice for 30 minutes before being centrifuged at 14000 rpm for 40 minutes at 4 °C. The supernatants were transferred into fresh tubes. Protein concentration was measured diluting 3 μl of cell lysate into 300 μl of diluted Bradford reagent (1:5 in dH_2O) and all samples were loaded in triplicate into a 96-well plate together with a non-template control (NTC). Absorption was measured using a microplate reader (FLUOstar OPTIMA, BMG LABTECH) at 595 nm and values were analysed based on the BSA standard curve to calculate protein concentrations of samples. For each gel, 4 μg of proteins was loaded.

2.7.3 Gel casting, loading and running

Initially, glass plates and combs were carefully cleaned with 70% industrial methylated spirit (70% IMS) to remove dust which would prevent sealing of the glass chamber (tested with dH_2O). Then running gel solution was prepared as described above, poured into the chamber (TEMED was added just before pouring the solution) and let to set for 20 minutes. Similarly, stacking gel was prepared as shown above (TEMED was added just before pouring the solution) and poured on top of the solidified running gel. Combs were immediately inserted and then the gel was allowed to set for 20 minutes at RT.

Samples were mixed with 4X loading buffer (with added 10% β-mercaptoethanol) and boiled at 100°C for 5 minutes. Samples were then spun down and kept at RT to prevent SDS precipitation until ready to load. Gels were then assembled inside the tank, which was filled with running buffer. Finally, protein ladder (Precision Plus Protein™ Dual Xtra Prestained Protein Standard, BIO-RAD) and samples were loaded and gel was run at 100 V constant for around 90 minutes.

Initially, 1x polyvinylidene difluoride (PDVF) membrane (size 6 x 4 cm) and 6x filter paper (size 9 x 6 cm) were cut for each gel. PDVF membranes only were soaked in methanol for 5 minutes, then both membranes and filter papers were left soaking in transfer buffer.

Cassettes (Bio-Rad) were assembled following the schematic below (Fig. X), ensuring all elements were always soaked in transfer buffer and no air bubbles were trapped between layers.

Figure 2-5: ***Western blotting membrane transfer scheme.***

(From https://www.abcam.com/protocols/general-western-blot-protocol)

Cassettes were then placed in the BIO-RAD tank with ice pack and then transfer buffer was poured into the tank until gel and membranes were fully covered. Transfer was assured by running at 100 V constant for 60 minutes.

2.7.4 Blotting of membranes

Membranes were removed from the tank, soaked in methanol for 1 minute and then transferred to TBST. Membranes were blocked by gentle shaking in 10% milk/ TBST for 60 minutes at RT.

Primary antibodies (Tab. 2-6) were prepared in 5% BSA/ 0.01% Sodium Azide (Sigma)/ TBST. Each membrane was incubated with 5 mL of primary antibody solution in a 50 mL falcon tube, which was left rolling O/N at 4 ºC. The following day, membranes were washed on a shaker 3 times for 10 minutes in TBST at RT and then incubated for 60 minutes on a roller at RT with secondary antibodies (Tab. 2-7) diluted in 10% milk/ TBST. Washing steps were then repeated (3x 10 minutes in TBST).

Protein bands were detected using Pierce™ ECL Plus Western Blotting Substrate (Thermo Scientific) following manufacturer's recommendations. Briefly, detection solution was prepared by mixing 40 parts of solution A and 1 part of solution B and pipetted on top of the membrane (around 1 mL of solution per membrane) and left to incubate in the dark for 5 minutes. Membranes were then wrapped in cling film and detected using X-ray film.

Table 2-6: Western blotting primary antibodies

Antibody	Company	Concentration
Rb anti SM22	Abcam	1:10000
Ms anti Calponin	Sigma-Aldrich	1:5000
Ms anti SMMHC	Sigma-Aldrich	1:250
Ms anti ß-actin	Abcam	1:40000

Table 2-7: Western blotting secondary antibodies

Antibody	Company	Concentration
Polyclonal Goat anti-Ms Immunoglobulins / HRP	Dako	1:5000-1:10000
Polyclonal Goat anti-Rb Immunoglobulins / HRP	Dako	1:5000-1:10000

2.7.5 Stripping of membranes (optional)

If necessary, antibodies were stripped from membranes for membrane re-probing, using the following protocol. Membranes were washed twice in water for 10 minutes on a shaker at RT. Then they were incubated in 0.2 M NaOH at 37 ºC for 20 minutes and for additional 20 minutes on a shaker at RT. Finally, membranes were washed twice in TBST for 10 minutes on a shaker, then re-blocked and re-probed for detection.

2.8 MABs RNA-sequencing

2.8.1 hFtSI_MABs RNA extraction and library preparation and sequencing

Undifferentiated and differentiated hFtSI_MABs were analysed in their gene expression profile. RNA was extracted and its quality assessed as described in section 2.5.1. Libraries were prepared and sequencing performed by UCL Genomics as described in section 2.5.2.

2.8.2 RNA-sequencing analysis

Similarly to section 2.5.3, reads were quality checked, trimmed and mapped on the human genome (Ensembl assembly version GRCh38.p12 96.38), and the count matrix was imported into edgeR. The count matrix was filtered to retain transcripts with CPM > 1 in at least 2 replicates and normalized using the trimmed mean of M values (TMM) method (Robinson and Oshlack, 2010). After filtering, a CPM table was generated with all genes that passed the filtration criterion by using the "cpm" function of edgeR. In order to identify DEGs between the various differentiation protocols, an ANOVA like approach was performed using the functions "glmQLFit" and "glmQLFTest" from the package edgeR; briefly the method compared, for each gene, the read counts of each differentiation protocol against the read counts of the "undifferentiated" cells, used as a reference. Significant genes were identified using a cut-off p-value < 0.01 and a Fold Change ≥ |1.5|.

Up-regulated and down-regulated DEGs from each analysis were subsequently tested for Gene Ontology enrichment analysis using the "Enrichment Analysis with Fisher's Exact test" function from the program Blast2GO/v5.2.5 (Conesa and Götz, 2008) with p-value < 0.01.

Figures were plotted using R or Prism/v8.0.2 (GraphPad Software, California USA, www.graphpad.com) software.

2.9 qPCR validation of selected genes

High quality, not fragmented RNA was isolated and its quality assessed as described in section 2.5.1 and then retrotranscribed using SuperScript™ VILO™ cDNA Synthesis Kit (ThermoFisher Scientific). Briefly, 0.5 µg of total RNA were mixed with 4 µl of 5X VILO™ Reaction Mix and 2 µl of 10X SuperScript™ Enzyme Mix in a total volume of 20 µl. The mix was incubated for 10 min at 25 ˚C, for 60 min at 42 ˚C and finally for 5 min at 85 ˚C. The obtained cDNA was diluted 1:2 by adding 20 µl of water and stored at -20 ˚C.

Real-time qPCRs were performed using Brilliant III Ultra-Fast SYBR® Green QPCR Master Mix (Agilent) by mixing, in a total reaction volume of 10 µl,

1 μl of cDNA, 0.3 μl each of 10 μM forward and reverse primers, 5 μl of Master Mix and 3.4 μl of dH_2O. All reactions were performed using an ABI StepOnePlus System (ThermoFiscer Scientific) following Agilent Master Mix recommendation (i.e. following 3 min at 95 ˚C for enzyme activation, 40 cycles of 5 sec at 95 ˚C and 10 sec at 60 ˚C were performed). All primers used are reported in Table 2-8.

Table 2-8: Human qPCR primers list

Gene	Sequence	Efficiency	R^2
ACTG2	FW - GACAGCTATGTGGGGGATGAG RW - GCTCTTCAGGTGCTACACGC	1.90	0.99
TAGLN	FW - GCTAGGGAAACCCACCCTCT RW - AAGTCATCCGGGGCATTTCA	1.80	0.99
CNN1	FW - GTTCGGAGAGGAGAGGCAAA RW - GCCGTCCATGAAGTTGTTGC	1.83	0.99
MYHC11	FW - CAAGCTCAGGCGAGGAAACGA RW - TGCTTATTCACTGGCCTTGGTTC	1.75	0.99
SMTN	FW - TGTCTAATCCGTCTGTCGGG RW - CTAGCTCCGTCGGTTCCTTT	1.94	0.99
RPL30	FW - ACAGCATGCGGAAAATACTAC RW - AAAGGAAAATTTTGCAGGTTT	1.80	0.98
OAZ1	FW - GGATCCTCAATAGCCACTGC RW - TACAGCAGTGGAGGGAGACC	1.91	0.99

In accordance with Bustin et al. (2009), primers were tested by running a Standard Curve with a series of five 1:10 dilutions of test cDNA to assess primer efficiency and linear amplification (i.e. $R^2 > 0.97$, see Table 8 for primer specific efficiency and R^2). Two genes were used as housekeeping (i.e. Ribosomal protein L30, *RPL30* and Ornithine Decarboxylase Antizyme 1, *OAZ1*) after assessing their stability across all samples with the method “geNorm” implemented in the function “selectHKs” from the R package NormqPCR (Perkins et al., 2012). Expression levels were calculated as Normalised Relative Quantities, in accordance with Hellemans et al. (2007), by using the function “ComputeNRQs” from the package NormqPCR.

Statistical differences in NRQs between treatments were assessed in Prism 8.1 by means of One-way ANOVA with Dunnett's multiple comparisons and deemed significant with a cut-off p-value ≤ 0.05.

Chapter 3

Human intestine: development of the smooth muscle layers

3. Human intestine: development of the smooth muscle layers

3.1 Introduction

The study of developmental processes at the level of organ and body formation have extensively benefited from the use of animal models such as mouse and chick (de Santa Barbara et al., 2002; Perin et al., 2017). While most of the knowledge taken from animal models has been useful to understand the general processes of human development, specific aspects such as accurate timings of development (i.e. when during gestation do the different structural components of the intestine arise) need to be assessed directly on human embryos and foetuses (Ostrer et al., 2006). This assessment is of crucial importance when studying congenital diseases, as knowledge of the exact developmental timings can help focus the research on physiological and cellular processes which are altered in such diseases (Gerrelli et al., 2015).

When considering intestinal development, lots of data can be found on the onset and maturation of the intestinal epithelium (de Santa Barbara et al., 2003; Montgomery et al., 1999) and also on the colonisation and activation of the enteric nervous system (Nagy and Goldstein, 2017). However, the development of the muscular compartment (i.e. muscularis propria) of the intestine has been investigated much less, with only two papers, to the best of my knowledge, studying the onset of the different smooth muscle layers in human development (Fu et al., 2004; Wallace and Burns, 2005).

Therefore, in this chapter attention was focussed on the specific timings of appearance of the longitudinal muscle layer and the overall maturation of the SMCs composing the different muscle layers of the intestine. All the work done was supported by the main Human Developmental Biology Resource (HDBR) bank present within the Great Ormond Street Institute of Child Health (University College London) which is of crucial importance for the advancements of research in the field of human development (http://www.hdbr.org). HDBR is a bank of early

human embryonic and foetal tissues that supports several research projects in different countries. HDBR is strictly regimented by the National Research Ethics Service (NRES) and the Human Tissue Authority ensuring that all activities obey to ethical consents.

3.2 Results

3.2.1 Histology *of human foetal midguts*

Human foetal midguts were stained for haematoxylin and eosin (H&E) to assess differences in gut wall morphology between 8 and 20 post conceptional weeks (pcw). At week 8 of gestation, the presence of the forming neuromuscular compartment was clear at the edges of the gut wall as a dense and darker pink eosin stain, where it was possible to distinguish the presence of circumferentially orientated cells forming the inner circular muscle layer (Fig. 3-1 i). Only from week 10 of gestation, it was possible to distinguish, with the H&E staining, the presence of two distinct muscle layers, the circular and longitudinal SM layers, respectively (Fig. 3-1 iii). Orthogonally orientated cells forming the two muscle layers were distinguishable, thanks to the orientation of the nuclei, from 12 pcw and was maintained throughout the development (Fig. 3-1 iv-viii).

Over time, some modifications were observed also in the developing epithelium. In fact, from a flat monolayer of cells visible at 8 pcw (Fig. 3-1 i), invaginations formed during the 9th and 10th week of gestation to form the future villi (Fig. 3-1 ii-iii). However, only from week 12 of gestation, were more eosin-dense areas at the basis of the epithelium, the crypts, identified (Fig. 3-1 iv-viii, arrowheads).

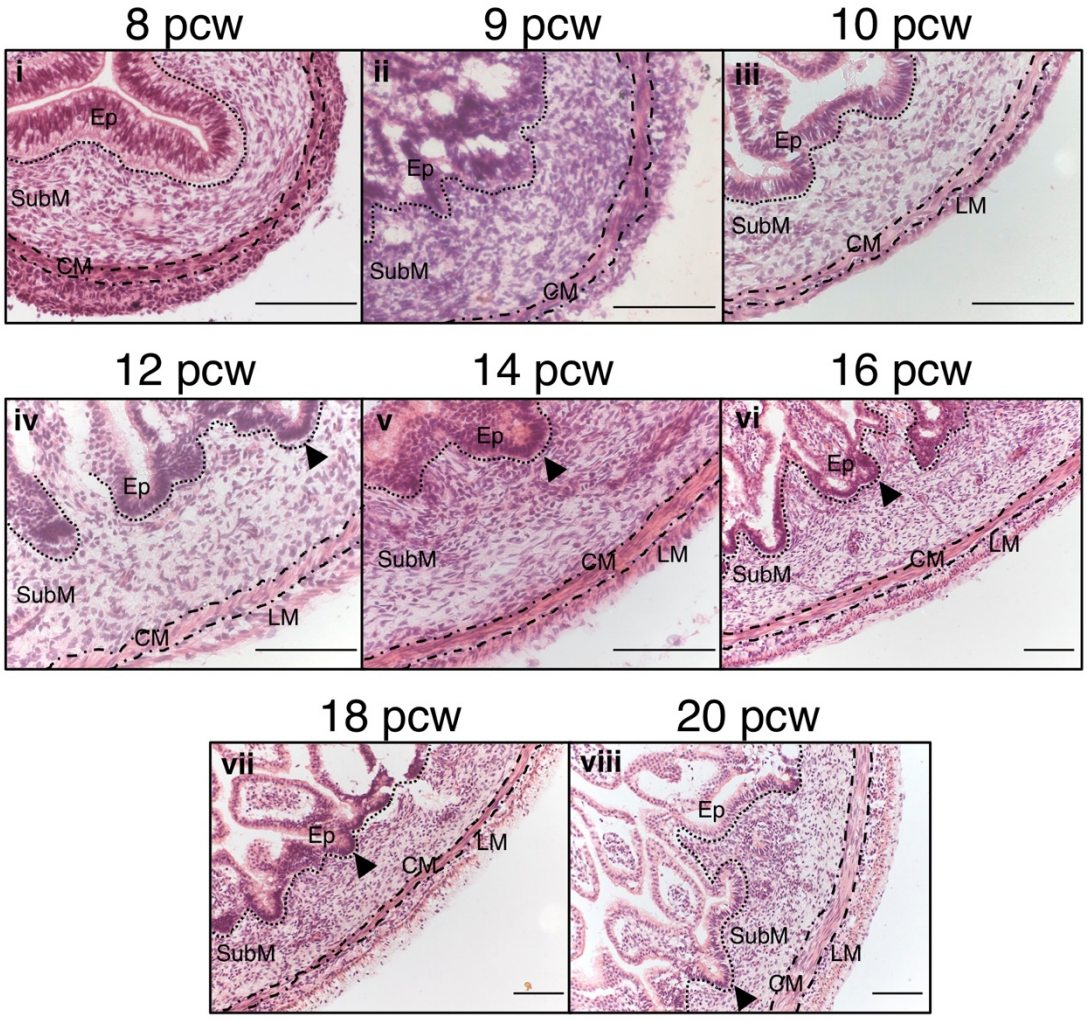

Figure 3-1: Haematoxylin & Eosin staining of human foetal midguts

Representative images of H&E staining of human midguts at different stages of development, starting from 8pcw (top-left) to 20pcw (bottom right). Ep= epithelium, SubM= submucosa, CM= circular muscle layer, LM= longitudinal muscle layer. Dotted lines indicate the separation between epithelium and the submucosa. Dot-dashed lines delimitate the inner circular muscle layer. Arrowheads point to crypt region of the epithelium. Scale bars 100 μm.

3.2.2 Characterisation of the development of the smooth muscle layers via immunofluorescence staining

In order to understand the spatiotemporal development of the enteric neuromusculature (i.e. muscular layers, the enteric nervous system and interstitial cells of Cajal), samples were immunostained for key markers of smooth muscle differentiation, interstitial and neuronal cells. Immunofluorescence staining for alpha smooth muscle actin (αSMA) showed the presence of a broad

band at the centre of the mesoderm region, corresponding to the future circular muscle layer, at week 8 of development (Fig. 3-2a, asterisk). At 8 pcw αSMA positive cells were evidenced also in a second layer of cells localised at the edges of the gut wall in two out of four samples analysed (Fig. 3-2b, arrowheads). By week 9, all samples (n =3) showed the presence of a thin layer of αSMA positive cells outside the inner αSMA positive layer, corresponding to the future longitudinal muscle layer (Fig. 3-2c, arrowheads).

Other important components of the intestinal wall are the interstitial cells, such as the Cells of Cajal, that can be identified by the expression of the receptor tyrosine kinase cKit, and PDGFRα. At week 8, a variable expression of these markers could be identified in different samples. In fact, when αSMA positive cells were detected only in the circular SM layer (Fig. 3-2a), cKit positive cells were detected as two bands, one between the circular muscle layer and the region of the future longitudinal SM layer, the other just beneath the circular SM layer (Fig.3-2a, stars). In this case, the entire submucosa was positive for PDGFRα and other PDGFRα positive cells were identified on the surface of the gut, with co-expression of cKit, αSMA and also PDGFRα at both edges (i.e. inner and outer) of the circular SM layer (Fig. 3-2a, arrows). On the other hand, when αSMA was evidenced in both SM layers (Fig. 3-2b, asterisk and arrowheads), cKit positive cells were identified mainly at the outer surface of the gut while PDGFRα positive cells were present in the submucosa and as scattered cells located between the two muscle layers, in the region of the developing myenteric plexus (Fig. 3-2b). In this case, very few triple positive cells (i.e. cKit, αSMA and PDGFRα) could be identified (Fig. 3-2b, arrows). By week 9, the expression of cKit was restricted to few cells located in the region of the myenteric plexus plus some cells (supposedly mast cells) in the submucosa (Fig. 3-2c). Similarly, PDGFRα positive cells could be identified in the region of the myenteric plexus as well as in the submucosa, with higher expression evidenced near the circular SM layer and beneath the epithelium (Fig. 3-2c and Fig. 3-3, arrowheads). In subsequent developmental stages, the localisation of cKit positive cells remained limited to the myenteric region (Fig. 3-3). Starting from week 10, the expression of PDGFRα varied, in comparison to week 9, with the appearance of an additional

layer of PDGFRα positive cells located at the outer surface of the longitudinal SM layer (i.e. serosa, Fig. 3-3, stars).

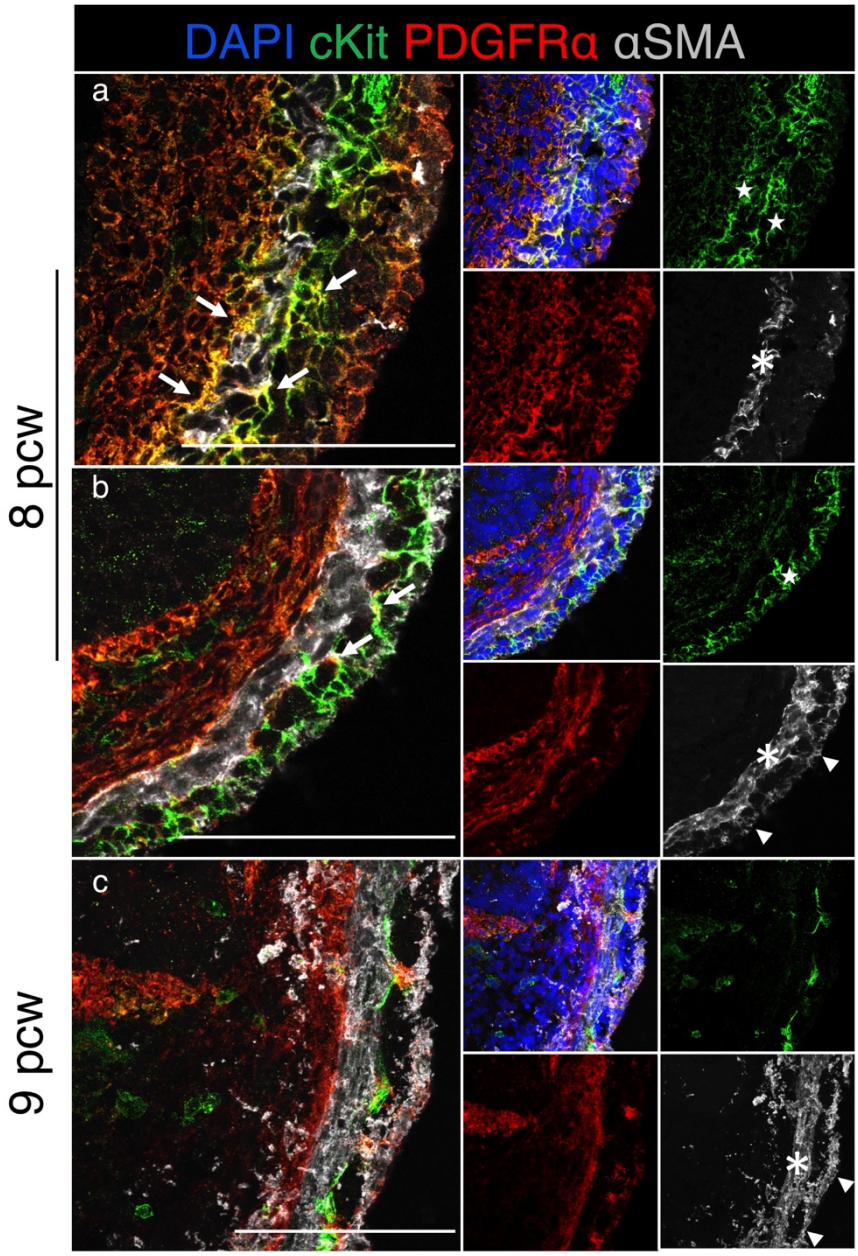

Figure 3-2: cKit, PDGFRα and αSMA assessment of proximal midgut development

Representative immunofluorescence images of proximal midgut sections from 8 (n =4) and 9 (n =3) pcw samples. **a)** 8 pcw proximal midgut showing αSMA positive circular muscle layer (asterisk), two bands of cKit positive cells (stars) and broad expression of PDGFRα in the submucosa and in the outer layer. Arrows point at triple labelled cells. **b)** 8 pcw proximal midgut showing two αSMA positive muscle layers, circular (asterisk) and longitudinal (arrowheads), cKit positivity in the outer layer (star) and PDGFRα positivity in the submucosa and in the myenteric region. Arrows point at triple labelled cells. **c)** 9 pcw proximal midgut showing two αSMA positive muscle layers, circular (asterisk) and longitudinal (arrowheads), ckit expression restricted to

myenteric regions only. cKit in green, PDGFRα in red, αSMA in grey and DAPI, for nuclei, in blue. Scale bar 100 μm.

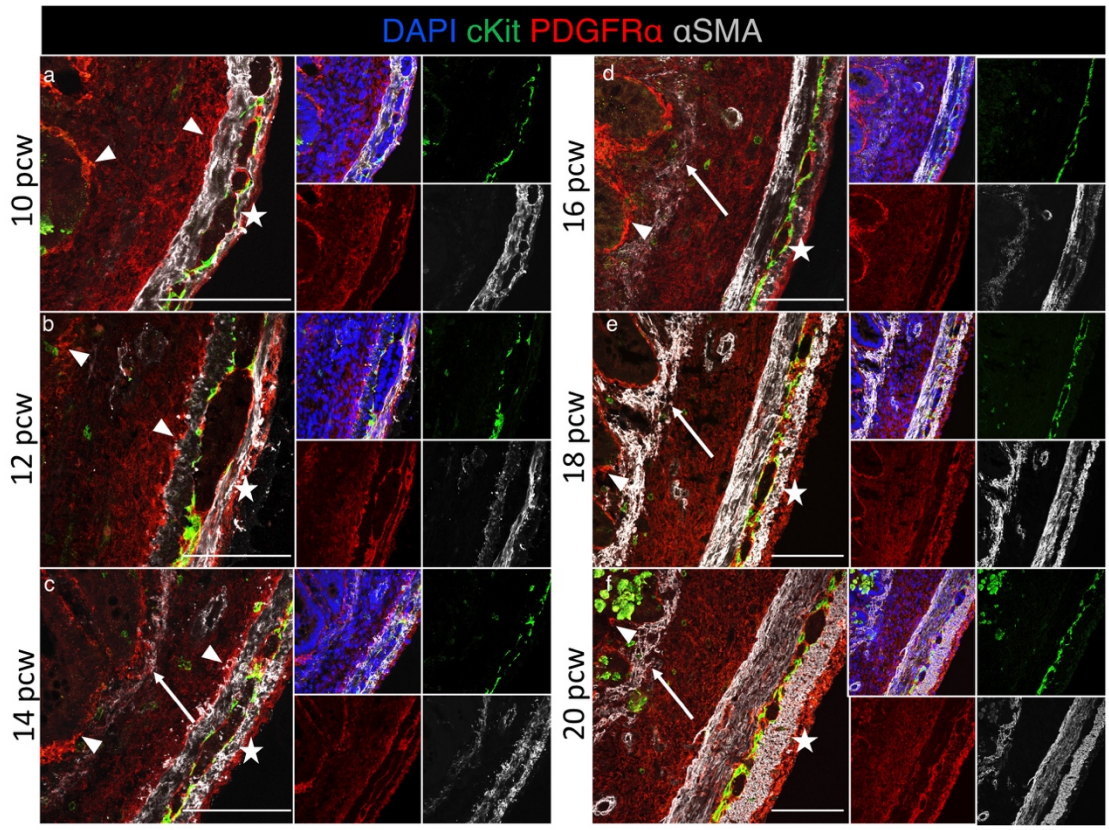

Figure 3-3: cKit, PDGFRα and αSMA assessment of proximal midgut development
Representative immunofluorescence images of proximal midgut sections from samples staged from 10 to 20 pcw. At 10 pcw (n =2), 12 pcw (n =4), 14 pcw (n =2), 16 pcw (n =1), 18 pcw (n =1) and 20 pcw (n =3) samples were analysed for cKit in green, PDGFRα in red, αSMA in grey and DAPI, for nuclei, in blue. White arrows point at the αSMA positive *muscularis mucosae* that is visible from 14 pcw onwards; white arrowheads point at denser PDGFRα staining in the sub-epithelial region and closer to the circular SM layer and white starts identify a layer of PDGFRα cells outside the longitudinal SM layer. Scale bar 100 μm.

Whilst at week 8 the circular muscle layer could be identified as a defined band of smooth muscle myosin heavy chain (SM-MHC, a marker of mature smooth muscle) positive cells in all the samples evaluated (Fig. 3-6a, star; 3-7a, star: n =4), the maturation of the longitudinal SM layer, assessed with different SM markers, was slightly delayed. In fact, at week 8 of gestation, the longitudinal SM layer was positive for SM22 and Calponin (Fig. 3-4a, b, arrowheads; 3-5a, b, arrowheads), intermediate markers of smooth muscle differentiation, in only 2 out

of 4 samples and none of the samples were positive for SM-MHC (Fig. 3-6a; 3-7a, arrowhead). SM22 and Calponin positively stained the longitudinal layer of all samples from 9 pcw (Fig. 3-4c-i; Fig. 3-5c-i), while SM-MHC positivity in the longitudinal layer appeared in all samples only from week 10 of gestation and in 2 out of 3 samples from week 9. (Fig. 3-6b, c, d, arrowheads; 3-7b, c, d, arrowheads). Similarly, the emergence of the third muscle layer of the intestine, the muscularis mucosa, was detected by αSMA positivity beneath the epithelium from week 14 (Fig. 3-3c, arrow). In a similar way, SM22 positive cells were detected only from 14 pcw (Fig. 3-4f, arrow), while Calponin positive cells were found only from 18pcw (Fig. 3-5h, arrow) and SM-MHC expression appeared only in some of the samples from week 20 (Fig. 3-6i; 3-7i). The marker Ki67 was used to assess proliferating cells in the gut throughout development. As expected, at earlier developmental stages a higher number of Ki67 positive cells was found in all regions of the gut (i.e. epithelium, submucosa and muscularis propria) compared to later stages (Fig. 3-5). However, it was interesting to note that across all developmental stages analysed, Ki67 positive cells were evidenced among the Calponin positive cells, suggesting the ability of “mature” SMCs to proliferate (Fig. 3-5).

In a similar fashion, the neuronal compartment is rearranged during development to finally give rise to neuronal plexuses. By immunostaining for ß-Tubulin III (TuJ1), a pan neuronal marker, cell positivity could be seen at week 8 as a broad band between the inner circular layer and the surface of the gut (Fig. 3-7a). Scattered TuJ1 positive cells were found also between the circular muscle layer and the submucosa, in the region of the presumptive submucosal plexus, sending neuronal projections towards the epithelium (Fig. 3-7a). From week 9 the band of TuJ1 positive cells outside the circular muscle layer became narrower and between week 10 and 12 of gestation (Fig. 3-7d, e, asterisks) it acquired a ganglia-like structure, forming the myenteric plexus. In later developmental stages, the number of projections within the submucosal plexus increased significantly (Fig. 3-7f, g, h, i).

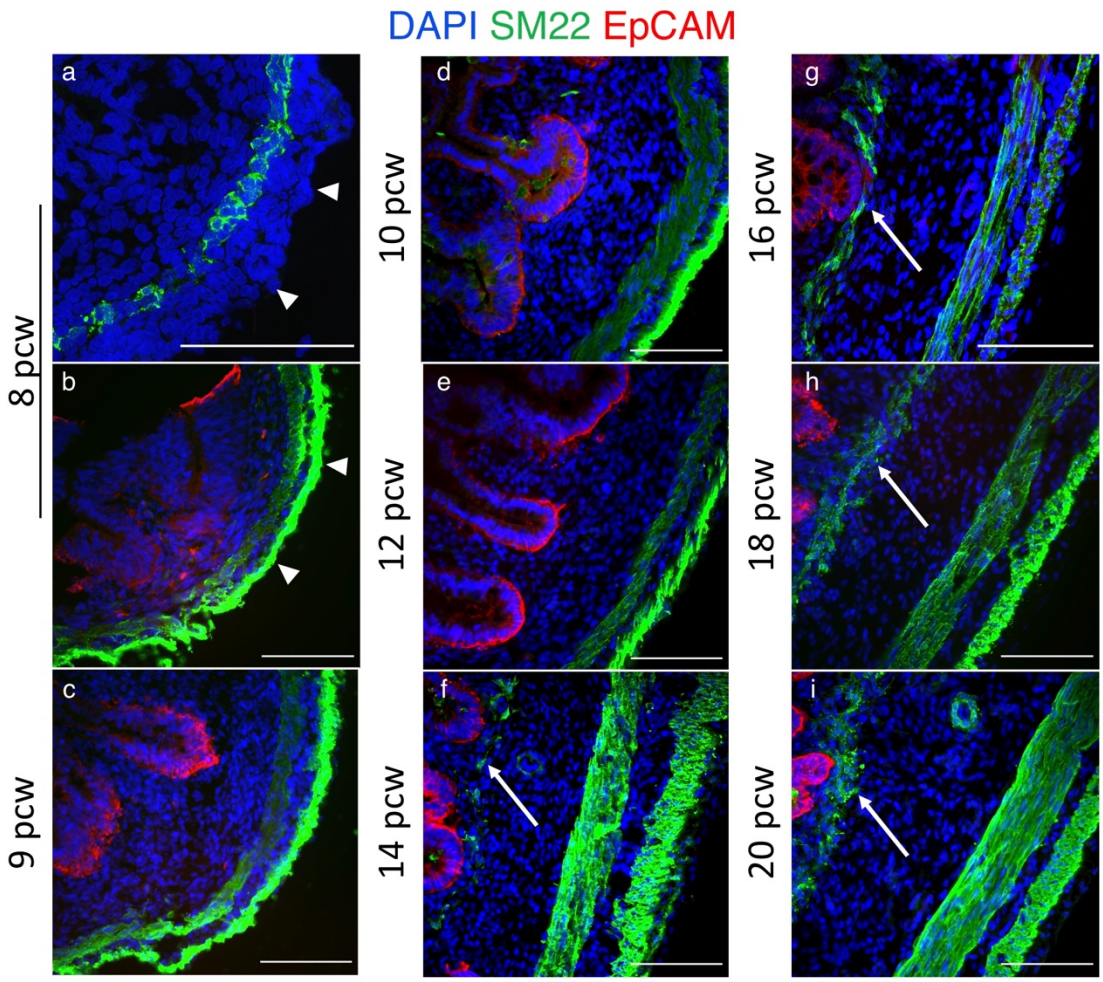

Figure 3-4: SM22 and EpCAM assessment of proximal midgut development

Representative immunofluorescence images of proximal midgut sections from samples staged from 8 to 20 pcw. At 8 pcw (n =4), 9 pcw (n =3), 10 pcw (n =2), 12 pcw (n =4), 14 pcw (n =2), 16 pcw (n =1), 18 pcw (n =1) and 20 pcw (n =3) samples were analysed. In **a)** and **b)** arrowheads point at the SM22 positive longitudinal SM layer evidenced in two out of four 8 pcw samples. In **f, g, h** and **i)** arrows indicate the *muscularis mucosae*. SM22 in green, EpCAM in red and DAPI, for nuclei, in blue. Scale bar 100 μm.

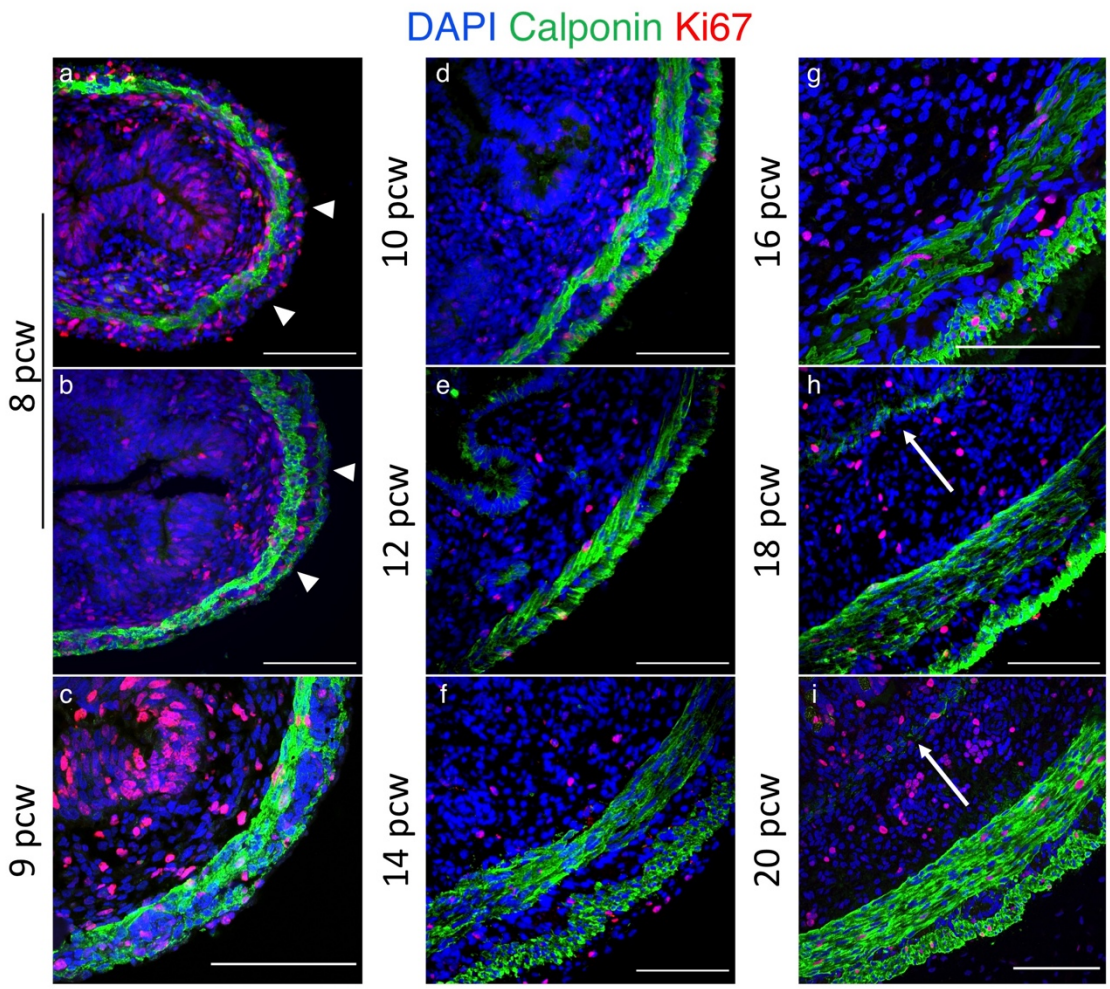

Figure 3-5: Calponin and Ki67 assessment of proximal midgut development

Representative immunofluorescence images of proximal midgut sections from samples staged from 8 to 20 pcw. At 8 pcw (n =4), 9 pcw (n =3), 10 pcw (n =2), 12 pcw (n =4), 14 pcw (n =2), 16 pcw (n =1), 18 pcw (n =1) and 20 pcw (n =3) samples were analysed. **a,b)** two representative 8 pcw samples showing the absence/presence of the longitudinal SM layer by expression of Calponin (arrowheads). **h,i)** 18 and 20 pcw samples showing the emergence of the *muscularis mucosae* (arrows). Ki67/Calponin positive cells are evidenced in all developmental stages. Calponin in green, Ki67 in red and DAPI, for nuclei, in blue. Scale bar 100 μm.

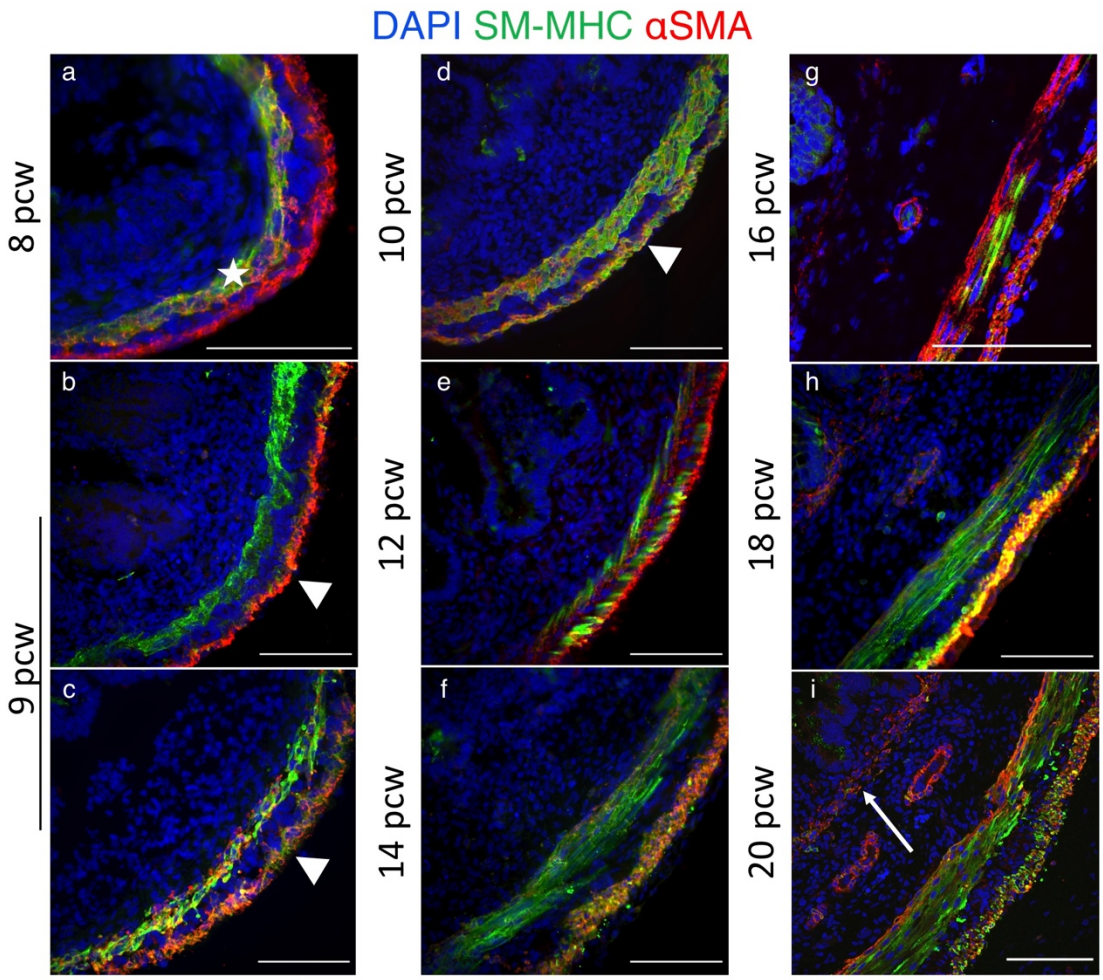

Figure 3-6: SM-MHC and αSMA assessment of proximal midgut development

Representative immunofluorescence images of proximal midgut sections from samples staged from 8 to 20 pcw. At 8 pcw (n =4), 9 pcw (n =3), 10 pcw (n =2), 12 pcw (n =4), 14 pcw (n =2), 16 pcw (n =1), 18 pcw (n =1) and 20 pcw (n =3) samples were analysed. **a)** 8pcw sample showing the presence of an αSMA/SM-MHC positive circular SM layer (star) and an αSMA positive only longitudinal SM layer. **b, c)** Two representative 9 pcw samples revealing the presence/absence of a SM-MHC longitudinal SM layer (2 out of 3; arrowheads). **d)** 10 pcw sample. Arrowhead points at the double positive longitudinal SM layer (arrowhead). **i)** arrow indicates the presence of a SM-MHC positive *muscularis mucosae*. SM-MHC in green, αSMA in red and DAPI, for nuclei, in blue. Scale bar 100 *μ*m.

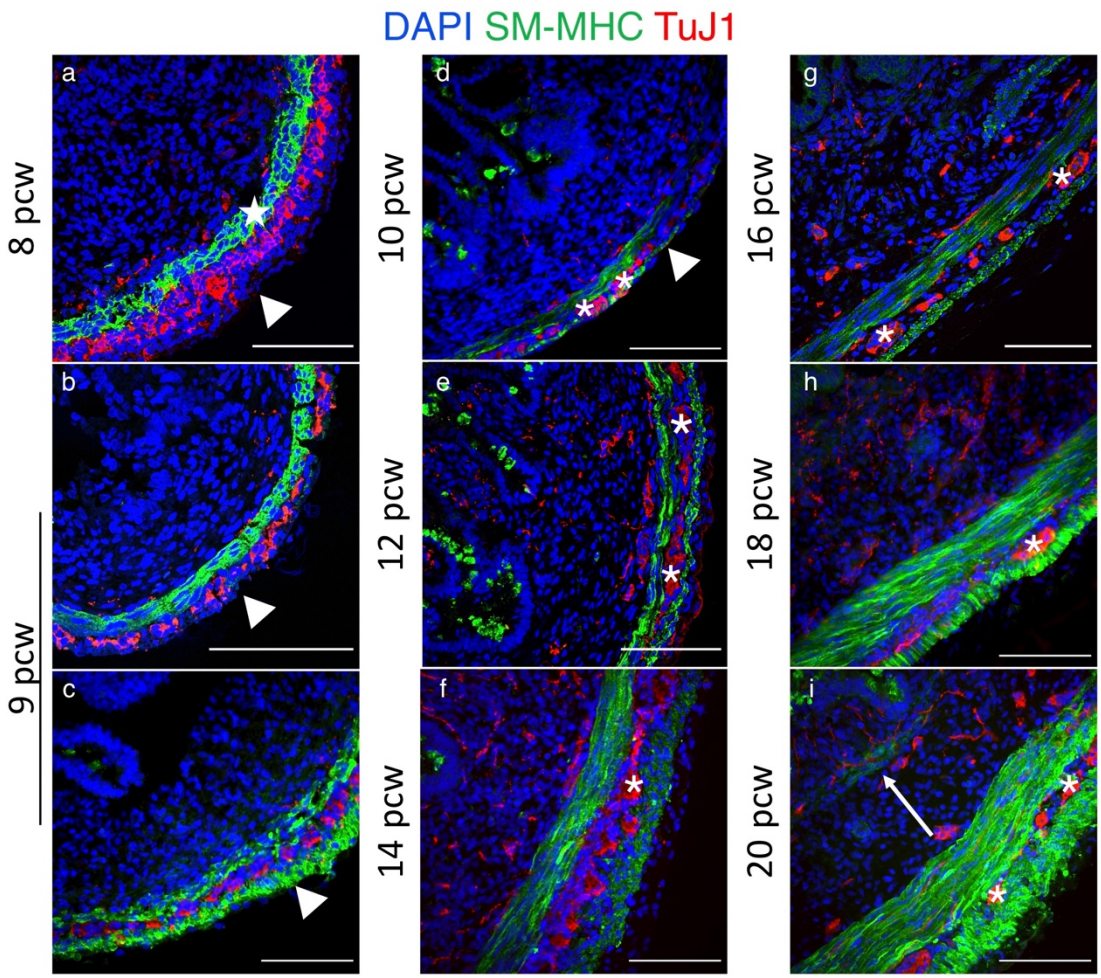

Figure 3-7: SM-MHC and TuJ1 assessment of proximal midgut development

Representative immunofluorescence images of proximal midgut sections from samples staged from 8 to 20 pcw. At 8 pcw (n =4), 9 pcw (n =3), 10 pcw (n =2), 12 pcw (n =4), 14 pcw (n =2), 16 pcw (n =1), 18 pcw (n =1) and 20 pcw (n =3) samples were analysed. **a)** 8 pcw sample showing the presence of a SM-MHC circular SM layer (star) and the absence of a positive SM-MHC longitudinal SM layer (arrowhead). TuJ1 positive neurons are disposed as a broad band outside the circular SM layer. **b, c)** two representative 9 pcw samples showing the absence/presence of a SM-MHC positive longitudinal SM layer (arrowheads). **d)** 10 pcw sample: asterisks indicate the forming myenteric ganglia structures, arrowhead points at the SM-MHC positive longitudinal SM layer. **g-i)** asterisks indicate the myenteric ganglia and arrow indicates the muscularis mucosae. SM-MHC in green, TuJ1 in red and DAPI, for nuclei, in blue. Scale bar 100 μm.

3.3 Discussion

In this study, the development of the muscle layers of the human intestine was assessed by immunofluorescence analyses. Immunofluorescence for

αSMA, SM22, Calponin and SM-MHC, markers of developing SMCs, confirmed the presence of a temporal gap in the development of the circular and longitudinal SM layers. The circular layer was present as a structurally mature layer at week 8 of development, whilst for the LM layer some degree of biological variability was observed. In fact, it appeared between week 8 and week 9 of gestation and fully matured in all samples by week 10 (Tab. 3-1). These results are in contrast with the literature since they only partially agree with conclusions from Wallace and Burns (2005) and Fu et al. (2004). According to Wallace and Burns (2005) the temporal gap in appearance of the two layers is greater, with the LM layer forming only at week 11. On the other hand, Fu et al. (2004) described the advent of the circular and longitudinal SM layers as a contemporary event taking place along the whole gut in a rostrocaudal manner between week 7 and 9 of development. In this study, only the proximal midgut region (i.e. beginning of the intestine) was analysed, therefore only the first appearance of the different components of the neuromuscular wall within the intestine, was evaluated. However, one of the major strengths of this work lies in the fact that, for all critical stages of SM development, multiple biological samples were analysed in order to take into account the biological variability between samples and define the specific time-frame for the formation of SM layers.

Table 3-1: Summary of human intestinal longitudinal SM layer development

Longitudinal SM layer appearance depending on different SM markers (from earlier markers of SM development, αSMA and SM22, to late markers, Calponin and SM-MHC). The presence of a positive layer was evaluated on immunofluorescence images from different biological samples (number in brackets: "positive samples / total samples") and is shown in percentage.

	Longitudinal SM layer			
	αSMA	**SM22**	**Calponin**	**SM-MHC**
8 pcw	50% (2/4)	50% (2/4)	50% (2/4)	0% (0/4)
9 pcw	100% (3/3)	100% (3/3)	100% (3/3)	66% (2/3)
10 pcw	100% (2/2)	100% (2/2)	100% (2/2)	100% (2/2)

In this study, cKit positive cells were initially found as a broad band outside the CM layer at week 8 and by week 10 their expression was restricted to the

area of the myenteric ICCs. It is interesting to note that Wallace and Burns (2005) reported the first appearance of cKit positive cells only at week 9 and their restriction to the areas subsequently were populated by ICCs by week 11. Hence, in comparison to the present study, the same developmental steps were recorded but a week later, arguably as a consequence of differences in the assessment of developmental stages, or maybe due to biological variability between foetuses.

It is noteworthy that, by comparing different biological samples of week 8 (Fig. 3-2a, b), it was apparent that important changes seemed to take place within this gestational week. In fact, when only the circular SM layer was present, the expression of cKit was located in close proximity with this layer, showing co-expression with αSMA as well as PDGFRα (Fig. 3-2a). In this case, PDGFRα positive cells were broadly distributed also at the outer surface of the gut, externally to the cKit positive cells, where the future longitudinal SM layer will arise. In contrast, when both SM layers were identified, as per αSMA expression, cKit was localised more externally, on the outer surface of the gut, co-staining with the longitudinal αSMA positive SMCs, while the expression of PDGFRα was absent in this region (Fig. 3-2b).

From these observations a hypothesis could be drawn: cells that give rise to the longitudinal SM layer are localised in the outer surface of the gut at week 8 of gestation. These cells initially express PDGFRα and dimly cKit, while later they lose the expression of PDGFRα, remaining positive only for cKit and αSMA. In the longitudinal SM layer, by week 9 the expression of PDGFRα and cKit is completely lost. This is in accordance with studies on mice where it was hypothesized that cKit positive cells could diverge towards an ICC fate or a longitudinal SMC fate (Torihashi et al., 1997) and with studies where it was shown that PDGFRα positive cells were found in the outer layer of the developing mouse guts, outside the already formed circular SM layer (Kurahashi et al., 2008). For this reason, it could be argued that a precursor, common to ICCs, PDGFRα expressing cells and longitudinal SMCs, is present in human at week 8 of gestation. An in-depth analysis would be required to validate this hypothesis.

As evidenced from the immunostaining for Ki67 (a marker of proliferation) and Calponin (a marker of SM maturation), double positive cells were identified

in all developmental stages investigated (Fig. 3-5), including the later ones (i.e. week 20) where positive expression for SM-MHC was also evidenced (Fig. 3-6 and 3-7). This observation confirms that mature SMCs of the intestine can proliferate, as reported for vascular SMCs (Alexander and Owens, 2012). The proliferative capacity of mature SMCs could suggest that the presence of a post-natal SM precursor population that resides in the intestine is not needed, as SMCs could proliferate and replace damaged cells during the physiological regeneration process of the intestine. This would be in contrast with what is seen in other muscle tissues, such as in skeletal muscles, where the presence of a specific population of adult stem cells (i.e. satellite cells) has been described as well as the niche where these cells reside (Yin et al., 2013).

However, during post-natal life, additional sources of cells could contribute to the maintenance of intestinal SMCs. In fact, in mouse it was shown that mesothelial cells are able to contribute, after an EMT transition, to the regeneration of vascular and visceral SMCs of the gut (Carmona et al., 2013; Rinkevich et al., 2012; Wilm et al., 2005). In addition, it has been shown that pericytes, which generate vascular SMCs, are multipotent stem/progenitor cells able to form other mesodermal cells, such as adipocytes (Olson and Soriano, 2011), chondroblasts, osteocytes (Collett and Canfield, 2005) and skeletal muscle cells (Dellavalle et al., 2007). Therefore, it could be hypothesised that pericytes may also be able to give rise to visceral SMCs and may contribute to the regenerative process happening during post-natal life (Minasi et al., 2002; Perin et al., 2019; Sacchetti et al., 2016). Investigations of all these different hypotheses would be beneficial for the understanding of intestinal SM regeneration and some aspects of these hypotheses will be discussed in the following chapters.

Chapter 4

Mouse enteric smooth muscle: origin and development

4. Mouse enteric smooth muscle: origin and development

4.1 Introduction

As explained in Chapter 1, the development of the gut is a complex process that involves the elongation of the organ and its regional differentiation in order to give rise to the different parts needed to guarantee the propulsion and absorption of food and the elimination of food waste. While the origin and development of some components of the GI system, such as the migration of the neural crest cells that compose the enteric nervous system (Sasselli et al., 2012), has been well established, a full understanding of SM development in the GI tract is still missing. Although several studies have helped understanding the different contributions of cells to the smooth muscle compartment of the gut as described in section 1.6 (Carmona et al., 2013; Kluppel et al., 1998; Kurahashi et al., 2008; Rinkevich et al., 2012; Torihashi et al., 1997; Wilm et al., 2005), we still don't have a complete understanding of the presence and the characteristics of a common precursor that would give rise to enteric SMCs during development.

As previously mentioned, cKit and PDGFRα positive cells located on the outer surface of E12.5 mice guts, have been suggested to give rise to the LM layer of the gut (Kluppel et al., 1998; Kurahashi et al., 2008; Torihashi et al., 1997). In this study, different analyses on developing mouse guts were performed in an attempt to understand the specific characteristics of the cells expressing the aforementioned receptors as a step to characterise enteric SM precursors. An approach never employed in this field was applied in this study combining flow cytometry analysis to isolate different subpopulations of cells, based on the expression of those markers, and bulk 3'-tag RNA-sequencing to analyse the whole transcriptome of those cells.

4.2 Results:

4.2.1 Mouse enteric smooth muscle development

To determine the characteristics of putative precursors giving rise to the enteric SMCs, guts were carefully dissected from mouse embryos at embryonic day (E) 12.5, 14.5, 16.5 and 18.5. Gross morphology of mouse guts is shown in Figure. 4-1A. Gut length (from stomach to colon) increased during development, from less than 1 cm at E12.5, to over 4 cm at E18.5. Histology (Fig. 4-1B) and further immunofluorescence analysis (Fig. 4-2) of developing guts focused on the midgut region, portion of the intestine between the stomach (Fig. 4-1A, arrowheads) and the caecum (Fig. 4-1A, arrows). At E12.5, the entire gut section was constituted of densely packed cells, of which a layer of circumferentially orientated cells could be identified (Fig. 4-1B; black arrow) by the presence of elongated nuclei. The presence of this layer was evidenced also at later stages, where it became thinner, being comprised of 2-3 layers of circumferentially orientated cells at E18.5 (Fig. 4-1B; black arrows). A layer of cells was present externally to the circular SM layer since E12.5, however, these cells could only be easily distinguished as longitudinally orientated SMCs, constituting the LM layer (black arrowhead), at E18.5 (Fig. 4-1B).

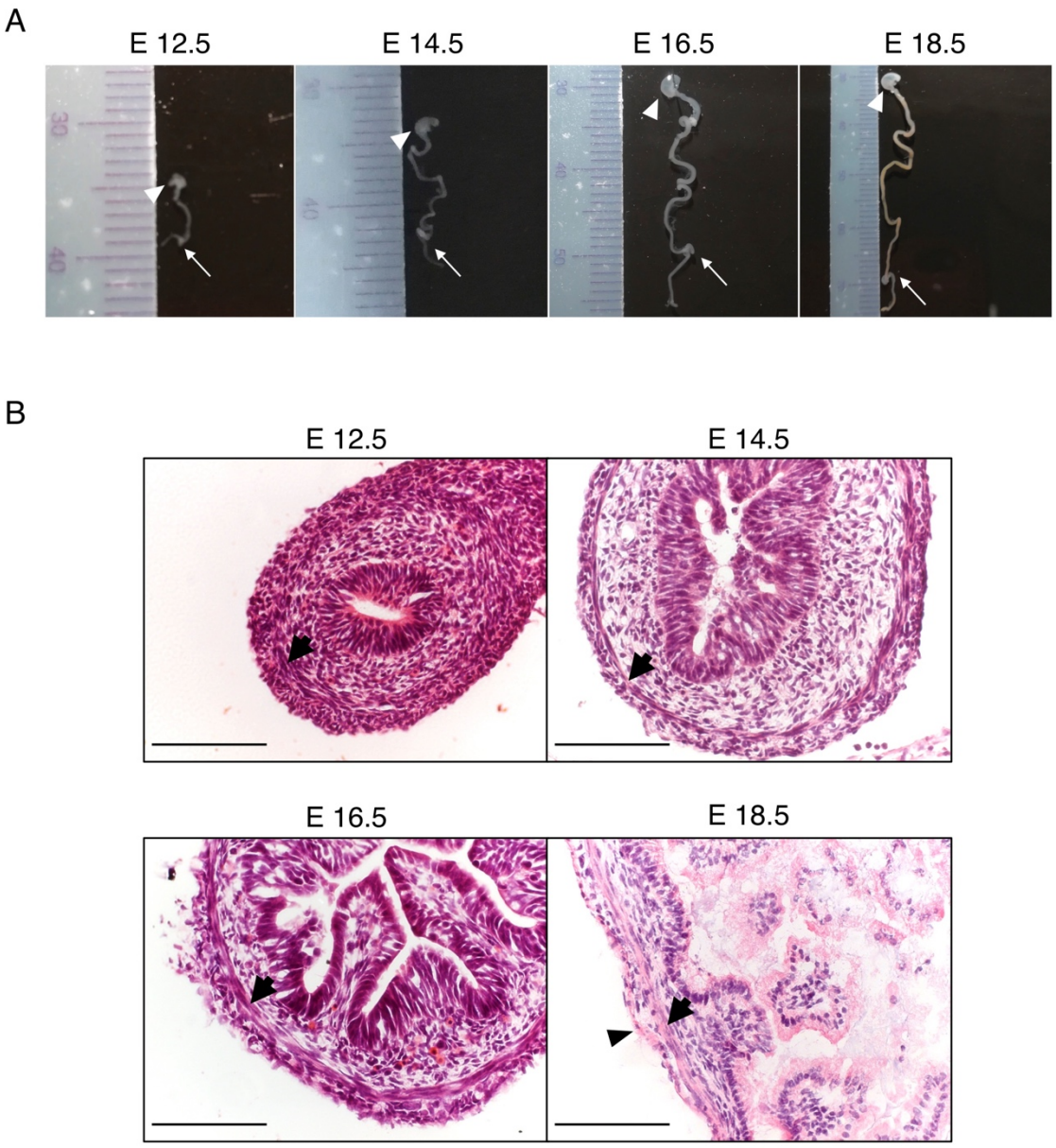

Figure 4-1: Mouse embryonic guts

A) Images showing gross morphology of mouse guts dissected from E12.5, E14.5, E16.5 and E18.5 embryos. White arrowheads point to the stomach, white arrows to the caecum. Rulers in the images are in millimetres. **B)** Haematoxylin and Eosin images of E12.5, E14.5, E16.5 and E18.5 midgut sections. Black arrows point at the circular SM layer, black arrowhead at the longitudinal SM layer. Scale bar 100 μm.

In order to confirm previous studies on the early development of the longitudinal SM layer, embryonic mouse guts between E12.5 and E18.5 were analysed with immunofluorescence staining for two key markers known to be involved in this process: cKit (also known as stem cell factor receptor, SCFr) and

PDGFRα. At E12.5 of development, a single ring of αSMA positive cells was detected in the central portion of the gut mesenchyme (Fig. 4-2), surrounded by a broad layer of cKit positive cells, just beneath the surface of the gut. It is interesting to note that, at the border between the two layers, αSMA and cKit co-staining was present in some cells (Fig. 4-2; white arrowhead). At E14.5 the expression of αSMA was neater in the circular muscle layer, with no co-staining for cKit. Positivity for cKit was restricted to the outer surface of the gut, in the region of the future longitudinal muscle layer, in which αSMA co-staining was observed. During further stages of development (from E16.5 to E18.5), the expression of cKit was progressively restricted to few cells located in between the circular and the longitudinal SM layers (evidenced by the expression of αSMA), maintaining some level of co-expression.

The expression of the second receptor taken into consideration for these analyses, PDGFRα, showed a different pattern during development (Fig. 4-2; right panels). At E12.5, PDGFRα was expressed in two bands, a major one corresponding to the submucosa of the gut and a second one in the developing LM layer. Clear co-staining of PDGFRα and αSMA was not evidenced, although cells expressing the two markers were identified in close proximity to one another. At E14.5, the entire submucosa was still PDGFRα positive, with stronger expression being evidenced in the cells located just beneath the epithelium. Additional cells expressing PDGFRα were also identified in the outer layer of the gut at E14.5. Similarly to what was seen for the expression of cKit, at E16.5 and E18.5 the expression of PDGFRα became more restricted and could be identified in specific regions of the gut structure. In particular PDGFRα positive cells were present in clusters located beneath the epithelium, in between the two muscle layers, and some cells, showing lower levels of PDGFRα expression were also localised in the submucosa.

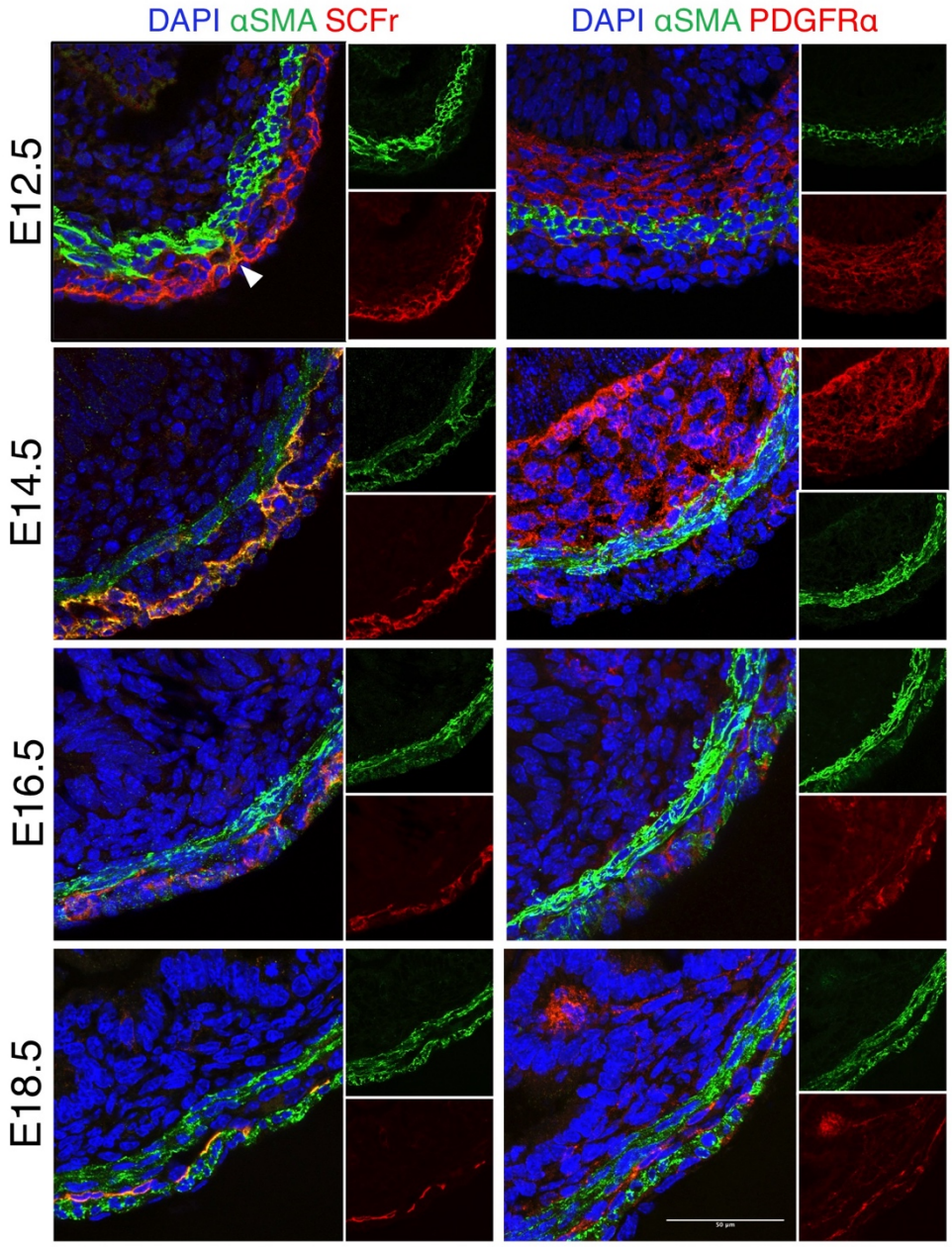

Figure 4-2: Mouse embryonic gut LM layer formation

Representative immunofluorescence images of mouse midgut cryosections, from different developmental stages (i.e. E12.5, E14.5, E16.5 and E18.5), stained for αSMA in green and, in red, for cKit (left panels) and for PDGFRα (right panels). White arrowhead points to αSMA-cKit co-staining. Nuclei, in blue, stained with DAPI. Scale bar 50 μm.

4.2.2 Cell population analysis of potential smooth muscle precursors

Further investigations on the expression of the two major markers known in the literature to be expressed by the presumptive enteric SM precursors, cKit and PDGFRα, were performed via flow cytometry. Embryonic mouse guts were

carefully dissected and enzymatically digested to assess the expression of these two receptors at different developmental stages (E12.5 n =2, E14.5 n =3, E16.5 n =2 and E18.5 n =1). Single cells were selected according to physical parameters by removal of debris and then doublets, finally focusing onto DAPI negative cells to analyse only live cells (Fig. 4-3A). Expression of cKit, also known as CD117, and PDGFRα, or CD140a, was assessed on live cells (Fig. 4-3B). The percentage of cells positive only for CD117 slightly increased over time, from 8.75% at E12.5 to 17.1% at E18.5. The percentage of CD140a positive cells was stable around 20% in all stages apart from E14.5, where its expression was quite variable among the three different samples analysed. In contrast, the percentage of double positive cells (CD117 and CD140a) decreased over time, starting from over 50% double positive cells at E12.5 and E14.5 to around 20% double positive cells at E16.5 and E18.5. cells.

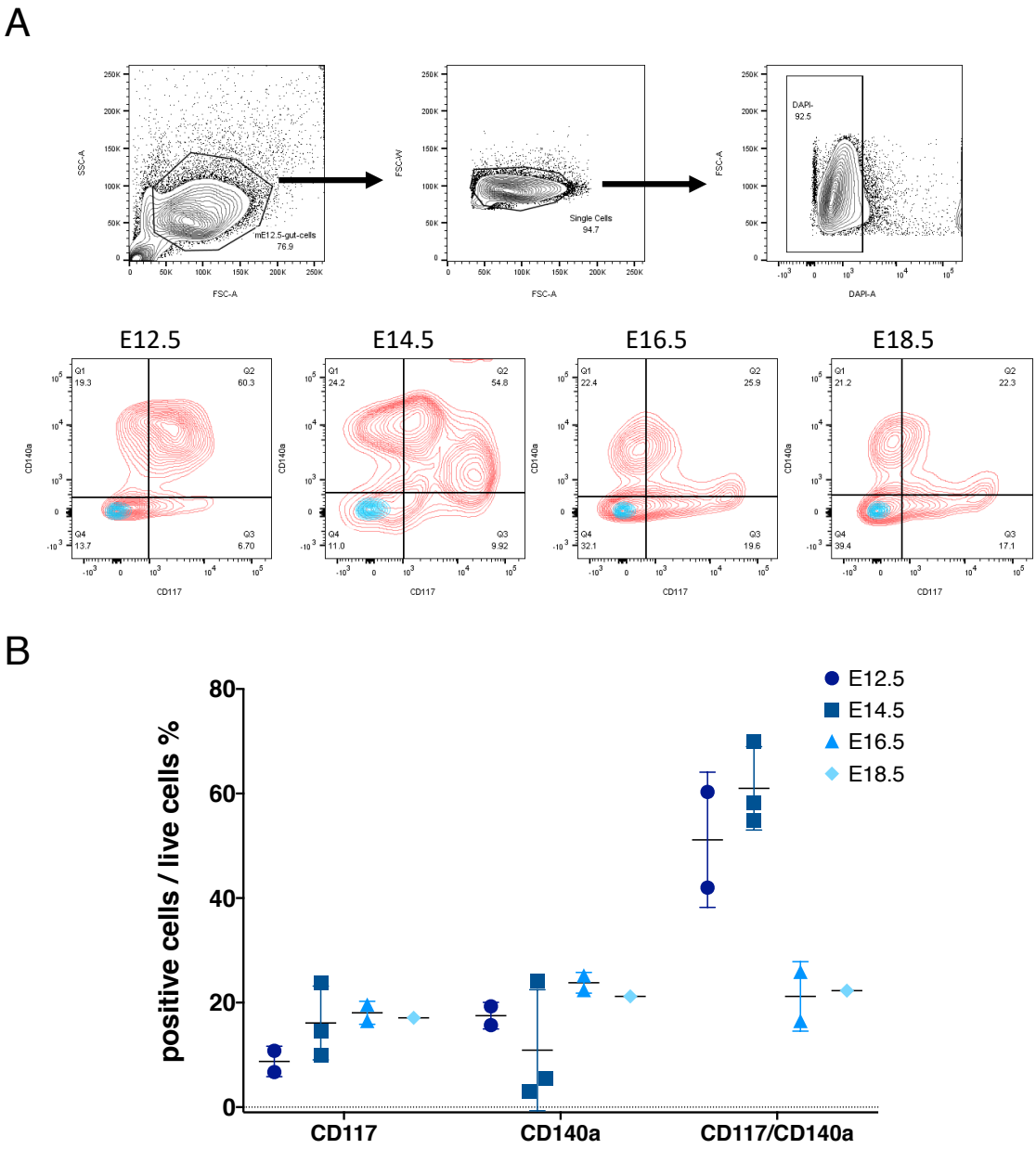

Figure 4-3: Mouse embryonic gut flow cytometry analyses

A) Representative counter plot images of embryonic mouse gut cells and the gating strategy for the analysis, focusing on total cells, single cells and finally on live cells (DAPI negative). Coloured counter plots are representative images of live cells from embryonic mouse guts at different stages of development (E12.5, E14.5, E16.5 and E18.5), showing positivity for CD117 (cKit) or CD140a (PDGFRa). Red clouds represent stained cells and are superimposed on blue clouds representing unstained cells; **B)** Percentage CD117 only, CD140a only or CD117 and CD140a positive cells over live gut cells at different stages of development. Symbols represent different developmental stages (E12.5: circles, n =2; E14.5: squares, n =3; E16.5: triangles, n =2; E18.5: diamond, n =1). Lines show means ±SD.

4.2.3 Cell sorting strategy and analyses

Previous flow cytometry analyses raised several questions regarding the fate of the cellular populations identified, in particular of cKit and PDGFRα double positive cells. Therefore, a whole transcriptomic analysis of these subpopulations at different developmental stages was planned to better characterise these cells. This was done using bulk 3'-tag RNA-sequencing, which allowed to obtain an in-depth representation of the entire cellular gene expression profile. Cells were sorted for 3'-tag RNA-sequencing only from E12.5, E14.5 and E18.5 murine guts due to the high similarity, in terms of percentage of positive cells over total live cells of the gut, between the stages E16.5 and E18.5.

Moreover, in order to reduce unwanted signals coming from red blood cells and the developing epithelium, a specific gating strategy was developed. In particular, as shown in Figure 4-4A, selection of cells was performed by focusing on single cells according to physical parameters (e.g. forward and side scatter), to then focus only on nucleated cells (positive for DRAQ5™) in order to remove red blood cells (possibly present in the vessels of the gut) and finally on live cells (DAPI negative). The last step was to focus only on cells negative for the Epithelium Cell Adhesion Molecule (EpCAM), to avoid endodermal contaminations into our samples.

Collection of cells was based on the presence/absence of CD117 and CD140a, defining a total of four different subpopulations among the mesenchymal compartment of the three stages of the developing gut: $CD117^+$ cells, $CD140a^+$ cells, $CD117^+/CD140a^+$ (DoublePos) cells and $CD117^-/CD140^-$ (Negative) cells (Fig.3-4B). Cells were sorted from the entire gut (from stomach to colon) of all embryos of a pregnant mouse (n =6 at E12.5; n =5 at E14.5; n =5 at E18.5) and selected cells from 3 different females of each developmental stage were used to extract total RNA for whole transcriptome sequencing.

In Figure 4-4C the percentage of cells belonging to the four different subpopulations over the total EpCAM negative cells was plotted for all the samples collected. Overall, the percentage of CD117+ cells remained stable around a median value of 14% during development, with a peak of 23% at E14.5. In contrast, both the $CD140a^+$ and the $CD117^-/CD140^-$ cells showed an increase

with time in the median value from 12.9% to 43.8% and from 7.2% to 35.4%, respectively. On the other hand, a sharp decrease in the percentage of $CD117^{+}/CD140a^{+}$ cells was evidenced during development, from a median value of 66% at E12.5 to 5.1% at E18.5. In general, within each subpopulation, a smaller variability in the percentage of positive cells was observed at E18.5 among different biological samples in comparison to earlier developmental stages.

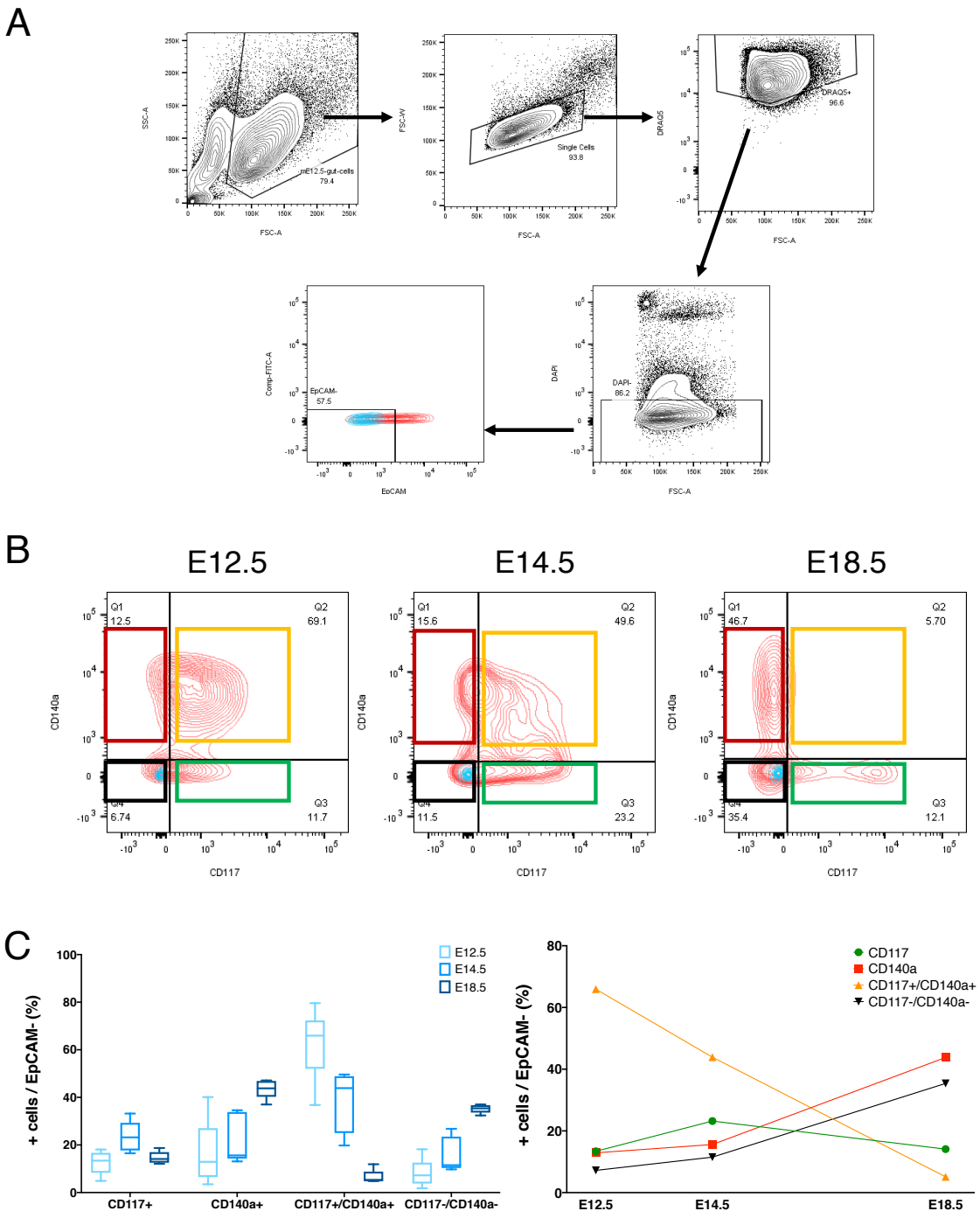

Figure 4-4: Mouse embryonic gut cells Fluorescent activated cell sorting (FACS)

A) Representative counter plot images of embryonic murine gut cells and the gating strategy for cell sorting focusing on total cells, single cells, nucleated cells (DRAQ5™ positive), live cells (DAPI negative) and mesenchymal (EpCAM negative) cells. In the coloured counter plot red clouds represents stained cells and are superimposed on blue clouds corresponding to unstained cells. **B)** Representative coloured counter plots of EpCAM negative cells at E12.5, E14.5 and E18.5 stained for CD117 and CD140a (red clouds =stained cells, blue clouds =unstained cells). Coloured boxes represent gates for the selection of individual populations of interest (red boxes =CD140a$^+$ cells; yellow boxes =CD117$^+$/CD140a$^+$ cells; green boxes =CD117$^+$ cells; black boxes

=CD117^{-}/Cd140a^{-} cells). **C)** Left graph: box and whiskers plots showing the percentage of CD117^{+}, CD140a^{+}, CD117^{+}/CD140a^{+} or CD117^{-}/CD140a^{-} cells over EpCAM^{-} gut cells at different stages of development (E12.5 n =6; E14.5 n =5; E18.5 n =5). Right graph: each symbol represents the median value of the percentage of positive cells in each subpopulation at each time point. Lines connect median values to show trend of expression during development.

4.2.4 Bulk RNA-seq analysis of sorted cell populations

In total, between 2.4 and 9.6 million raw reads were retrieved per sample. After trimming for low quality bases and removal of adaptors, high quality reads were mapped onto the mouse genome (Ensembl assembly version GRCm38.p6 95.38) without ambiguity. The overall mapping rate ranged from 63.2% to 80.8% of high-quality reads. After mapping, lowly expressed genes were removed and only genes with count per million (CPM) >1 in at least 2 of the 36 samples were considered in the analysis (total genes =20,618).

A multi-dimensional scaling (MDS) plot was generated to assess differences among samples (Fig. 4-5). Overall, samples clustered according to their developmental stage, with samples from E12.5, E14.5 and E18.5 being distributed at the bottom-left, middle and top-right of the MDS, respectively (Fig. 4-5; dashed ellipses). Similarly, distribution of the samples according to cell population subtypes was evidenced: from the top-left corner to the bottom-right PDGFRα (red), DoublePos (yellow), Negative (black) and cKit (green). In addition, the variability between sample replicates within the same population subtype was low at E12.5, while it increased at both E14.5 and E18.5. In particular, higher variability among replicates was evident among the DoublePos and Negative subpopulations at E14.5 and E18.5. Finally, it was interesting to note that PDGFRα and DoublePos cells at E12.5 clustered closely, denoting possible similarities between the two subpopulations.

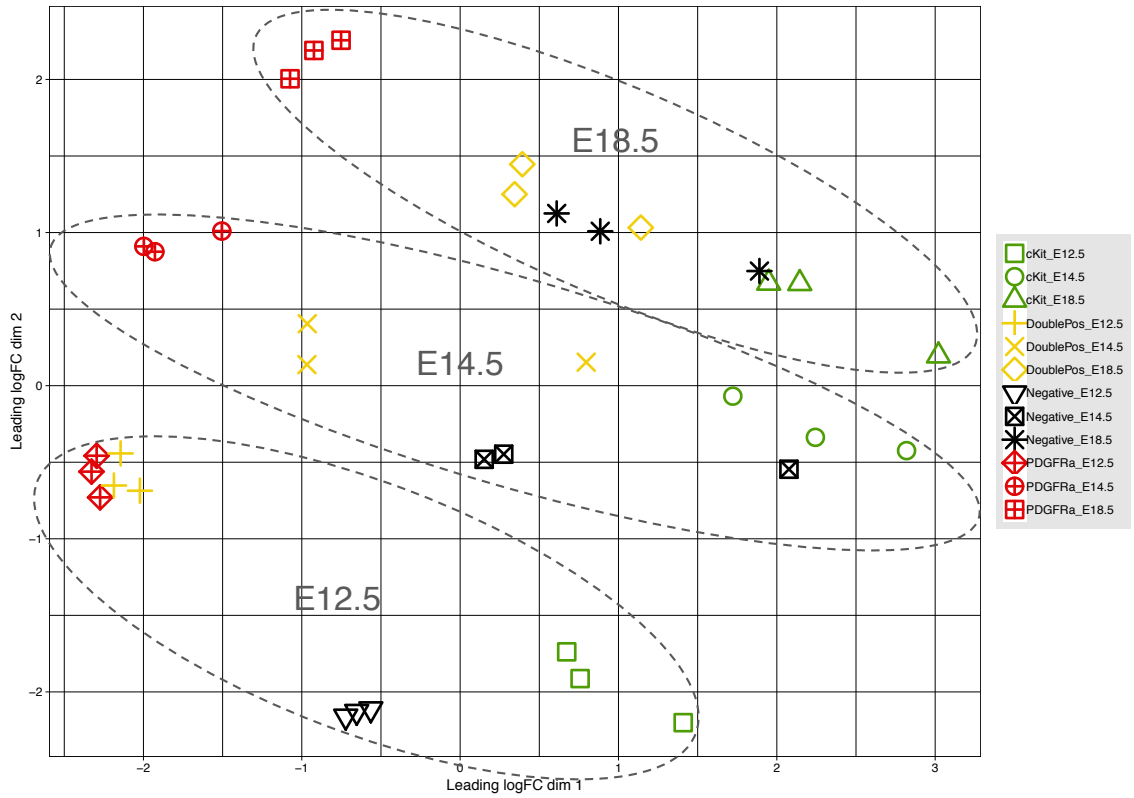

Figure 4-5: Multi-dimensional scaling (MDS) of cKit+, PDGFRα+, DoublePos and double Negative mouse embryonic gut subpopulations

MDS showing the distribution of samples according to the two main sources of variability (x-axis and y-axis respectively). Each symbol represents a combination of a specific cell population (i.e. cKit, PDGFRa, DoublePos and Negative) and a developmental stage (i.e. E12.5, E14.5 and E18.5). Colours identify cell populations throughout developmental stages: green =cKit, red =PDGFRa, yellow =DoublePos and black =Negative). For the sake of clarity, grey dashed ellipses have been drawn around samples from the same developmental stage

Given that samples clustered mainly according to their developmental stage, differentially expressed genes (DEGs) were separately assessed for each developmental stage. In particular, for each developmental stage, DEGs in one cell population were determined by comparing one population against the average of the remaining three populations (e.g. DoublePos compared to the average of PDGFRα, cKit and Negative together; Tab. 4-1). Genes were considered differentially expressed according to a false discovery rate (FDR) cut-off ≤0.01 and a fold change ≥|2|.

Table 4-1: DEGs of different mouse embryonic subpopulations

Number of DEGs of each population in comparison to the average of the other three populations, divided between up- and down-regulated.

Stage	Population considered	# Up-Regulated	# Down-Regulated
E12.5	**cKit**	1266	318
	PDGFRa	202	196
	DoublePos	187	193
	Negative	628	242
E14.5	**cKit**	458	167
	PDGFRa	228	147
	DoublePos	10	-
	Negative	334	59
E18.5	**cKit**	449	181
	PDGFRa	454	340
	DoublePos	54	7
	Negative	499	146

Since populations were isolated based on the expression of cKit and PDGFRα, the genes encoding for such proteins (*Kit* and *Pdgfra*) should have been flagged as differentially expressed when comparing one population against the average of the others. Therefore, the presence of these genes within the DEGs was assessed for each population to validate the overall bioinformatic approach used. As shown in Table 4-2, *Pdgfra* gene was always present in the upregulated DEGs of the PDGFRa and the DoublePos populations in all developmental stages, while it was always downregulated in the cKit and the Negative subpopulations. Similarly, *Kit* gene was upregulated in the cKit and the DoublePos population, while it was downregulated in the PDGFRa and Negative population in all cases except for the population E12.5 – PDGFRa, where it was not differentially expressed.

Table 4-2: Assessment of the bioinformatic approach

For each developmental stage (column 1), the presence/absence of *Kit* and *Pdgfra* within the upregulated or downregulated DEGs (columns 3-6) for each subpopulation (listed in column 2) compared with the average of the other three populations is shown. The presence is indicated by "X", while an empty cell indicates the absence.

		Kit		*Pdgfra*	
Stage	**Population considered**	***UP***	***DOWN***	***UP***	***DOWN***
E12.5	**cKit**	X			X
	PDGFRa			X	
	DoublePos	X		X	
	Negative		X		X
E14.5	**cKit**	X			X
	PDGFRa		X	X	
	DoublePos	X		X	
	Negative		X		X
E18.5	**cKit**	X			X
	PDGFRa		X	X	
	DoublePos	X		X	
	Negative		X		X

In order to characterize the expression profile of the different populations throughout the development of the intestine and investigate the presence of cells from which enteric SMCs may originate, enriched gene ontology categories, Kegg and Reactome pathways were investigated among the DE genes from Table 4-1. Enrichment tests were performed using the R package "clusterProfiler" to directly assess enrichment of categories among DEGs and adjust p-values for multiple comparisons (Yu et al., 2012) and the first 10 enriched results (according to their adjusted p-value) for each list of DEGs were plotted in Figures 4-6; 4-7; 4-8; 4-9; 4-10; 4-11; 4-12.

At E12.5 the most significantly enriched Reactome pathways within the up-regulated cKit cells could be linked with the immune system and immune processes, such as "Toll-like receptor cascade" and "signalling by B cell receptor" (Fig. 4-6). Similarly, the enriched Reactome pathways within the Negative up-regulated DEGs, suggested a link with the neuronal system, with enriched pathways for "neuronal system" and synaptic pathways. While analysis of enriched Reactome pathways for these two populations (i.e. cKit and Negative)

suggested that cells resembled an immune and a neuronal phenotype, PDGFRa and DoublePos cells showed a gene expression profile that could not be immediately associated with a specific cellular phenotype. In fact, the enriched pathways among their up-regulated DEGs were linked with more general pathways connected with the ECM and cell junction (e.g. “Extracellular matrix organisation” and “integrin cell surface interactions”). Among the enriched pathways of the PDGFRa and DoublePos cells, additional pathways such as “axon guidance” as well as MAPK signalling were also evidenced. It is interesting to note that most of the enriched Reactome pathways within the up-regulated DEGs of PDGFRa and DoublePos were enriched within the down-regulated DEGs of cKit and Negative cells, suggesting, as shown by the MDS plot (Fig. 4-5), that at E12.5 PDGFRa and DoublePos cells were very similar in their gene expression profile.

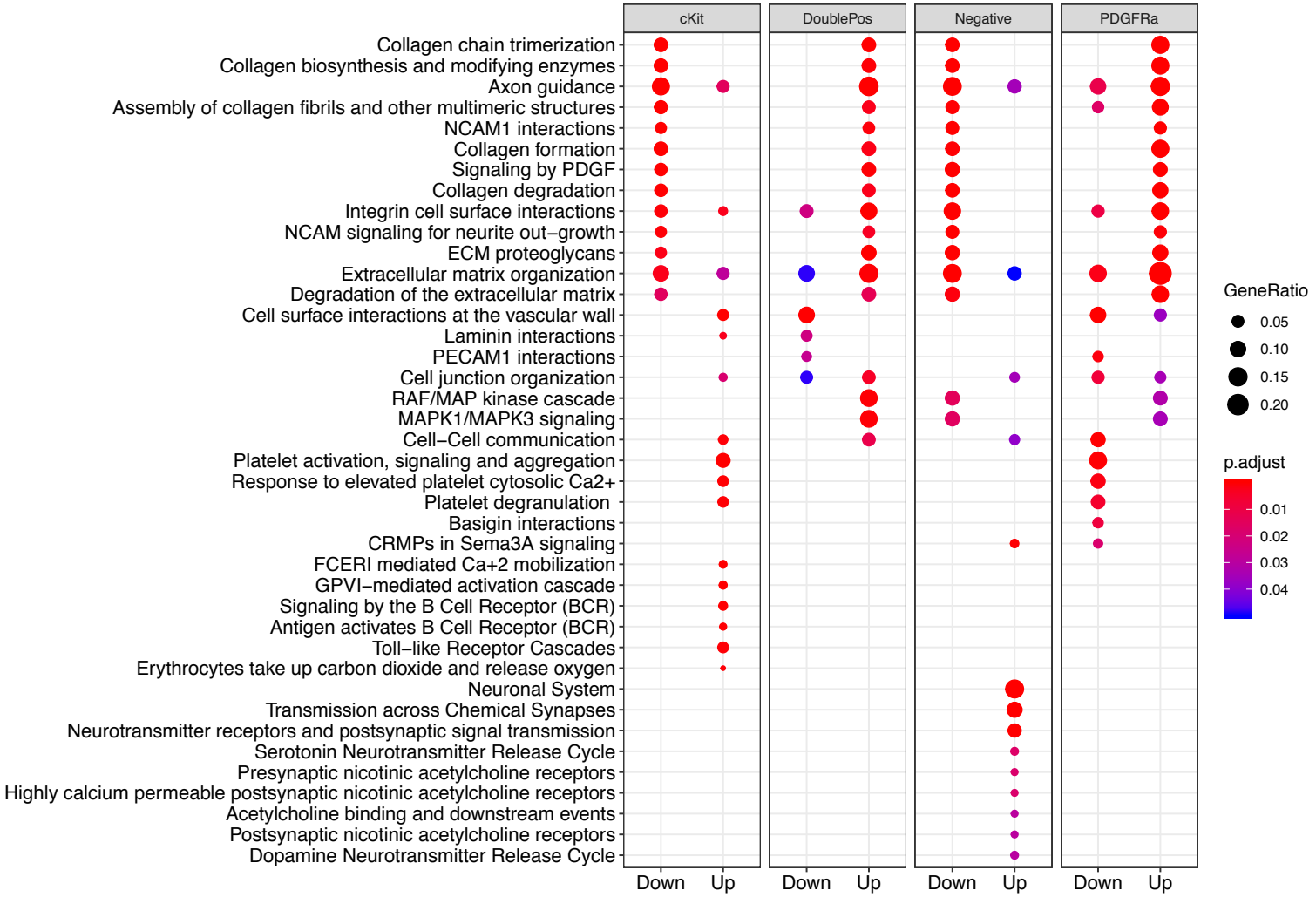
cKit
DoublePos
Negative
PDGFRa
Collagen chain trimerization
Collagen biosynthesis and modifying enzymes
Axon guidance
Assembly of collagen fibrils and other multimeric structures
NCAM1 interactions
Collagen formation
Signaling by PDGF
Collagen degradation
Integrin cell surface interactions
NCAM signaling for neurite out−growth
ECM proteoglycans
Extracellular matrix organization
Degradation of the extracellular matrix
Cell surface interactions at the vascular wall
Laminin interactions
PECAM1 interactions
Cell junction organization
RAF/MAP kinase cascade
MAPK1/MAPK3 signaling
Cell−Cell communication
Platelet activation, signaling and aggregation
Response to elevated platelet cytosolic Ca2+
Platelet degranulation
Basigin interactions
CRMPs in Sema3A signaling
FCERI mediated Ca+2 mobilization
GPVI−mediated activation cascade
Signaling by the B Cell Receptor (BCR)
Antigen activates B Cell Receptor (BCR)
Toll−like Receptor Cascades
Erythrocytes take up carbon dioxide and release oxygen
Neuronal System
Transmission across Chemical Synapses
Neurotransmitter receptors and postsynaptic signal transmission
Serotonin Neurotransmitter Release Cycle
Presynaptic nicotinic acetylcholine receptors
Highly calcium permeable postsynaptic nicotinic acetylcholine receptors
Acetylcholine binding and downstream events
Postsynaptic nicotinic acetylcholine receptors
Dopamine Neurotransmitter Release Cycle
Down
Up
Down
Up
Down
Up
Down
Up
GeneRatio
0.05
0.10
0.15
0.20
p.adjust
0.01
0.02
0.03
0.04

Figure 4-6: E12.5 enriched Reactome pathways

Enriched Reactome pathways obtained from the list of DEGs of each population against the average of the other three populations. For each population enriched Reactome pathways were calculated from the upregulated (i.e. "Up") or downregulated (i.e. "Down") DEGs and the first 10 were plotted. Dot size corresponds to the GeneRatio defined as the number of DEGs in one list (e.g. DEGs upregulated in cKit) mapping to one specific Reactome pathway divided by the total number of DEGs in that list mapping to all Reactome pathways. Colour code corresponds to adjusted p-value, calculated taking into account multiple comparisons against all groups.

Analysis performed at E14.5 revealed a similar signature for the cKit and Negative populations compared with analysis at E12.5 (Fig. 4-7). Indeed, immune signals and neuronal signals were evidenced among the enriched Reactome pathways within the up-regulated genes in cKit and Negative cells, respectively. For example, "cytokine signalling in immune system" and "Regulation of complement cascade" were present within the cKit group and "Neuronal System" and pre and post synaptic receptors were identified in the Negative group.

In contrast to the high similarity among PDGFRa and DoublePos cells highlighted at E12.5, at E14.5 these subpopulations showed different enriched Reactome pathways within their up-regulated DEGs. In particular, while enriched pathways within the DEGs of PDGFRa were mainly associated with the ECM, as shown previously during development, a more defined set of enriched pathways associated with MAPK pathway and "muscle contraction" was evidenced within the up-regulated DEGs in the DoublePos group.

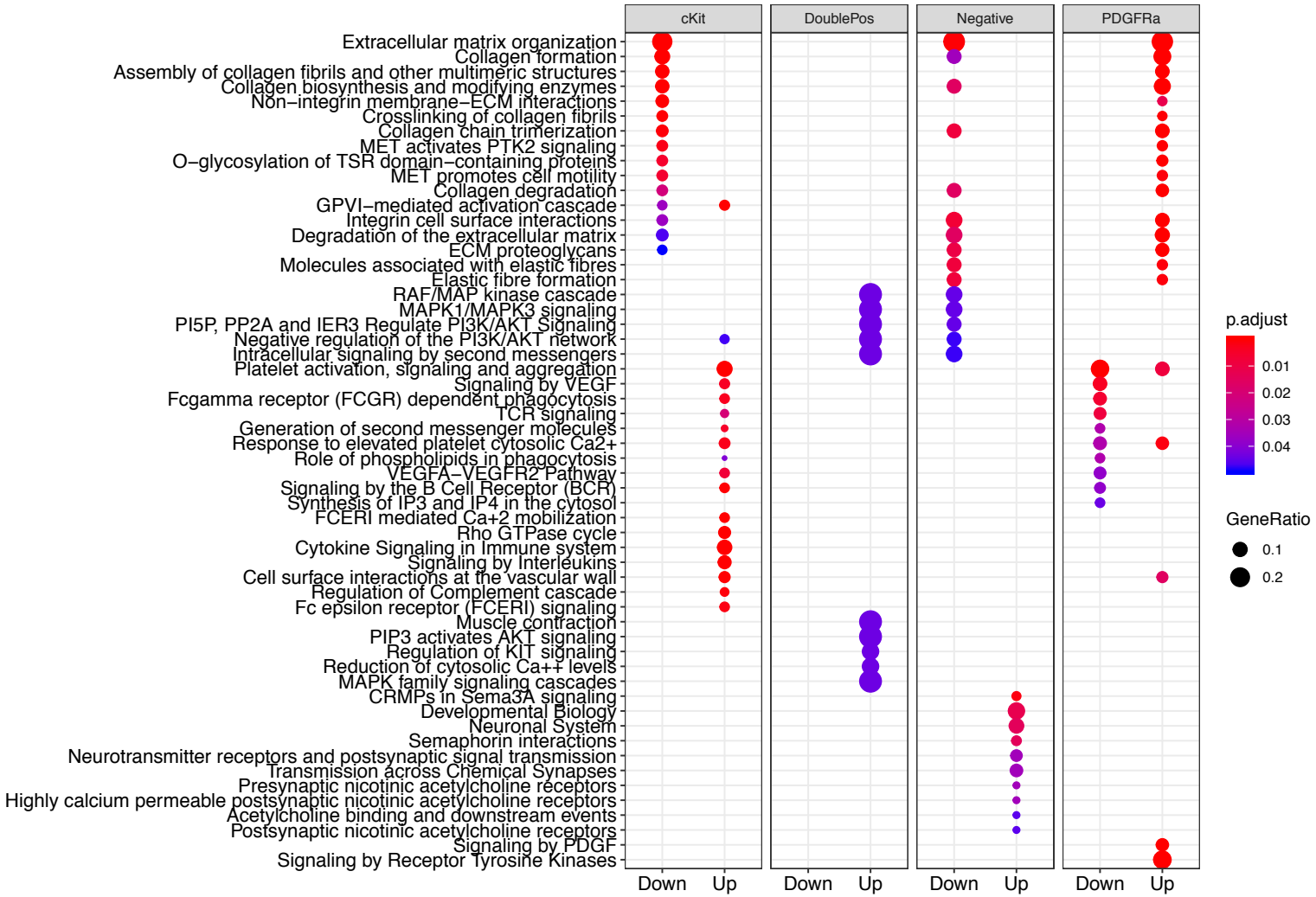
cKit
DoublePos
Negative
PDGFRa
Extracellular matrix organization
Collagen formation
Assembly of collagen fibrils and other multimeric structures
Collagen biosynthesis and modifying enzymes
Non−integrin membrane−ECM interactions
Crosslinking of collagen fibrils
Collagen chain trimerization
MET activates PTK2 signaling
O−glycosylation of TSR domain−containing proteins
MET promotes cell motility
Collagen degradation
GPVI−mediated activation cascade
Integrin cell surface interactions
Degradation of the extracellular matrix
ECM proteoglycans
Molecules associated with elastic fibres
Elastic fibre formation
RAF/MAP kinase cascade
MAPK1/MAPK3 signaling
PI5P, PP2A and IER3 Regulate PI3K/AKT Signaling
Negative regulation of the PI3K/AKT network
Intracellular signaling by second messengers
Platelet activation, signaling and aggregation
Signaling by VEGF
Fcgamma receptor (FCGR) dependent phagocytosis
TCR signaling
Generation of second messenger molecules
Response to elevated platelet cytosolic Ca2+
Role of phospholipids in phagocytosis
VEGFA−VEGFR2 Pathway
Signaling by the B Cell Receptor (BCR)
Synthesis of IP3 and IP4 in the cytosol
FCERI mediated Ca+2 mobilization
Rho GTPase cycle
Cytokine Signaling in Immune system
Signaling by Interleukins
Cell surface interactions at the vascular wall
Regulation of Complement cascade
Fc epsilon receptor (FCERI) signaling
Muscle contraction
PIP3 activates AKT signaling
Regulation of KIT signaling
Reduction of cytosolic Ca++ levels
MAPK family signaling cascades
CRMPs in Sema3A signaling
Developmental Biology
Neuronal System
Semaphorin interactions
Neurotransmitter receptors and postsynaptic signal transmission
Transmission across Chemical Synapses
Presynaptic nicotinic acetylcholine receptors
Highly calcium permeable postsynaptic nicotinic acetylcholine receptors
Acetylcholine binding and downstream events
Postsynaptic nicotinic acetylcholine receptors
Signaling by PDGF
Signaling by Receptor Tyrosine Kinases
Down
Up
Down
Up
Down
Up
Down
Up
p.adjust
0.01
0.02
0.03
0.04
GeneRatio
0.1
0.2

Figure 4-7: E14.5 enriched Reactome pathways

Enriched Reactome pathways obtained from the list of DEGs of each population against the average of the other three populations. For each population enriched Reactome pathways were calculated from the upregulated (i.e. “Up”) or downregulated (i.e. “Down”) DEGs and the first 10 were plotted. Dot size corresponds to the GeneRatio defined as the number of DEGs in one list (e.g. DEGs upregulated in cKit) mapping to one specific Reactome pathway divided by the total number of DEGs in that list mapping to all Reactome pathways. Colour code corresponds to adjusted p-value, calculated taking into account multiple comparisons against all groups.

At E18.5, analysis of the enriched Reactome pathways, showed very similar results regarding the populations of cKit and PDGFRa, as previously evidenced at both E12.5 and E14.5 (Fig. 4-8). However, it was interesting to note a major change in the enrichment of the Negative subpopulation. For instance, several pathways associated with muscle tissue were enriched in the up-regulated DEGs within this population (i.e. “muscle contraction”, “smooth muscle contraction”, “striated muscle contraction”). Finally, no enriched pathways were observed within the up-regulated DEGs within the DoublePos group, probably due to the low number of DEGs within the group (Tab. 4-1).


cKit
DoublePos
Negative
PDGFRa
Extracellular matrix organization
Collagen biosynthesis and modifying enzymes
Collagen formation
Collagen chain trimerization
MET activates PTK2 signaling
Assembly of collagen fibrils and other multimeric structures
ECM proteoglycans
MET promotes cell motility
Integrin cell surface interactions
Collagen degradation
NCAM1 interactions
Degradation of the extracellular matrix
Axon guidance
Muscle contraction
Smooth Muscle Contraction
Striated Muscle Contraction
Molecules associated with elastic fibres
Elastic fibre formation
EPHB–mediated forward signaling
EPH–Ephrin signaling
Platelet activation, signaling and aggregation
GPVI–mediated activation cascade
Fcgamma receptor (FCGR) dependent phagocytosis
Signaling by the B Cell Receptor (BCR)
Signaling by VEGF
FCERI mediated Ca+2 mobilization
Antigen processing–Cross presentation
Cell surface interactions at the vascular wall
Fc epsilon receptor (FCERI) signaling
FCGR activation
TCR signaling
PECAM1 interactions
Cell–Cell communication
Cell junction organization
Regulation of TLR by endogenous ligand
Generation of second messenger molecules
Response to elevated platelet cytosolic Ca2+
Cardiac conduction
Ion homeostasis
RHO GTPases activate PAKs
Down
Up
p.adjust
0.01
0.02
0.03
0.04
GeneRatio
0.25
0.50
0.75
1.00

Figure 4-8: E18.5 enriched Reactome pathways

Enriched Reactome pathways obtained from the list of DEGs of each population against the average of the other three populations. For each population enriched Reactome pathways were calculated from the upregulated (i.e. "Up") or downregulated (i.e. "Down") DEGs and the first 10 were plotted. Dot size corresponds to the GeneRatio defined as the number of DEGs in one list (e.g. DEGs upregulated in cKit) mapping to one specific Reactome pathway divided by the total number of DEGs in that list mapping to all Reactome pathways. Colour code corresponds to adjusted p-value, calculated taking into account multiple comparisons against all groups.

As the development of the intestine moved forward from E14.5 to E18.5, enriched pathways linked to muscle shifted from DoublePos at E14.5 to Negative at E18.5. This suggested that the Negative cell population at E18.5 comprised many DEGs mapping to SM, which could be explained by the fact that both intestinal SM layers are developed by E18.5 and that intestinal mature SMCs do not express cKit or PDGFRα. However, specific muscle signal within the first 10 enriched Reactome pathways was absent in all groups at E12.5. Due to the fact that it has been shown that both cKit and PDGFRα cells have a role in the development of SMCs of the longitudinal SM layer (Kluppel et al., 1998; Kurahashi et al., 2008; Torihashi et al., 1997), further investigation, using additional datasets were performed to identify potential muscle signals at E12.5.

Analysis on the Kegg pathways dataset showed very similar results to previous Reactome pathways' analyses at E12.5. However, it additionally showed the presence of the pathway "vascular smooth muscle contraction" enriched in both the PDGFRa and DoublePos up-regulated DEGs (Fig. 4-9). Furthermore, in the same groups, the "Wnt signalling pathway" was also enriched.


cKit
DoublePos
Negative
PDGFRa
Wnt signaling pathway
Axon guidance
Basal cell carcinoma
Signaling pathways regulating pluripotency of stem cells
Focal adhesion
Human papillomavirus infection
Hedgehog signaling pathway
ECM–receptor interaction
Proteoglycans in cancer
Protein digestion and absorption
Renin secretion
cGMP–PKG signaling pathway
PI3K–Akt signaling pathway
Central carbon metabolism in cancer
Gap junction
MAPK signaling pathway
Vascular smooth muscle contraction
Regulation of actin cytoskeleton
Cell adhesion molecules (CAMs)
Leukocyte transendothelial migration
Hematopoietic cell lineage
Ras signaling pathway
HIF−1 signaling pathway
Rap1 signaling pathway
Tight junction
AGE–RAGE signaling pathway in diabetic complications
Arrhythmogenic right ventricular cardiomyopathy (ARVC)
Prion diseases
Fluid shear stress and atherosclerosis
Natural killer cell mediated cytotoxicity
Staphylococcus aureus infection
Complement and coagulation cascades
Osteoclast differentiation
Leishmaniasis
Malaria
Chemokine signaling pathway
Viral protein interaction with cytokine and cytokine receptor
Cytokine–cytokine receptor interaction
Tuberculosis
Cholinergic synapse
Dopaminergic synapse
Synaptic vesicle cycle
Circadian entrainment
Insulin secretion
Retrograde endocannabinoid signaling
Down
Up
p.adjust
0.01
0.02
0.03
0.04
GeneRatio
0.05
0.10
0.15
0.20

Figure 4-9: E12.5 enriched Kegg pathways

Enriched Kegg pathways obtained from the list of DEGs of each population against the average of the other three populations. For each population enriched Kegg pathways were calculated from the upregulated (i.e. “Up”) or downregulated (i.e. “Down”) DEGs and the first 10 were plotted. Dot size corresponds to the GeneRatio defined as the number of DEGs in one list (e.g. DEGs upregulated in cKit) mapping to one specific Kegg pathway divided by the total number of DEGs in that list mapping to all Kegg pathways. Colour code corresponds to adjusted p-value, calculated taking into account multiple comparisons against all groups.

Interestingly, the additional muscle signals were present also in the analyses of the different gene ontology (GO) domains: cellular component (CC; Fig. 4-10), molecular function (MF; Fig. 4-11) and biological process (BP; Fig. 4-12) at E12.5. In fact, the enriched CC GO categories, such as “contractile fibre part”, “stress fibre” and “contractile actin filament”, were present in the up-regulated DEGs within the PDGFRa and the DoublePos cells (Fig. 4-10) and in the BP GO categories group, “skeletal muscle development” and “muscle cell proliferation” were evidenced among the 10 most enriched categories in these two groups (Fig. 4-11).

Finally, enriched GO categories within the up-regulated DEGs of cKit and Negative cells confirmed previous associations to the immune system and the neuronal compartment, respectively.

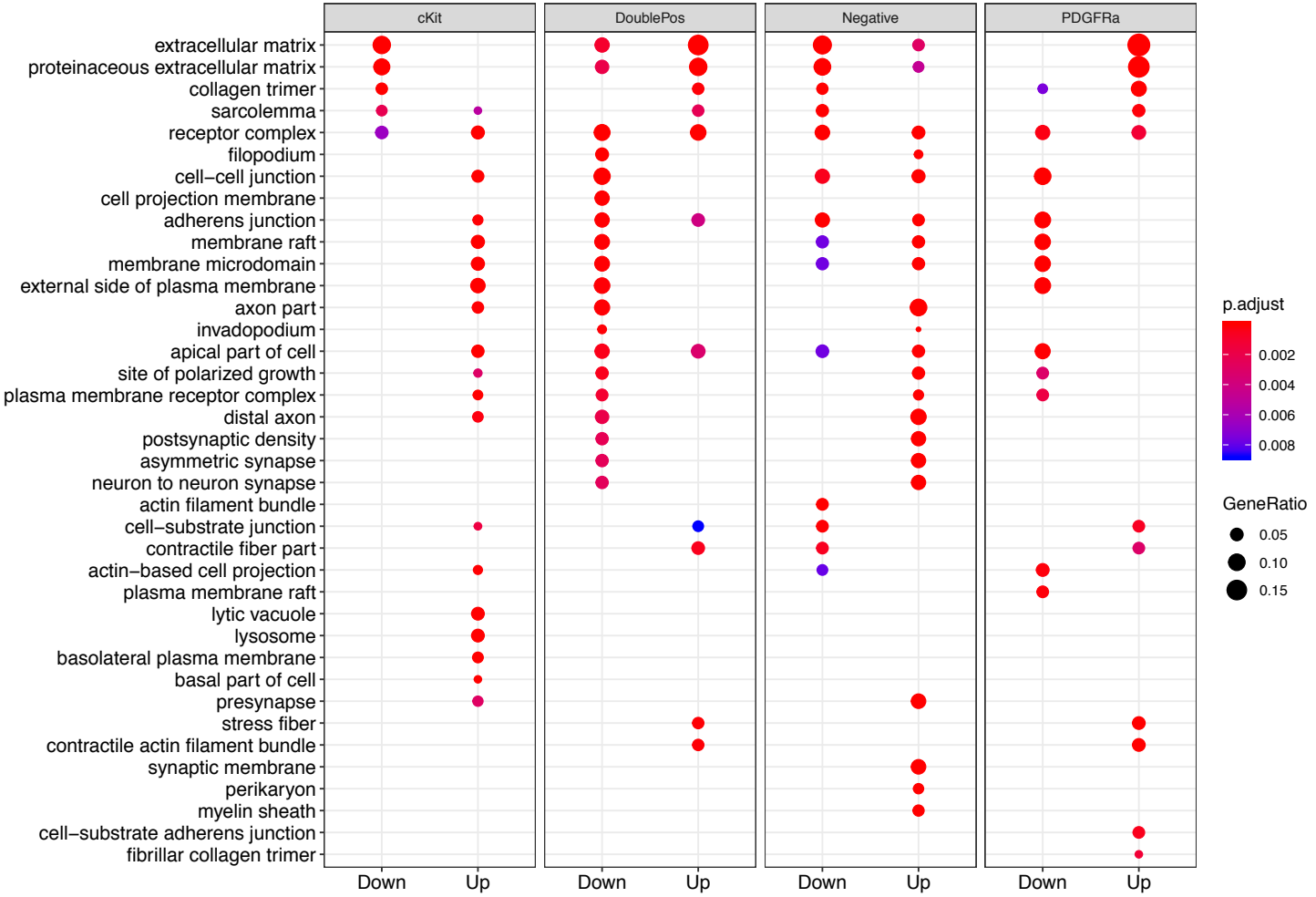

Figure 4-10: E12.5 enriched Cellular Component (CC) GO categories (legend overleaf)

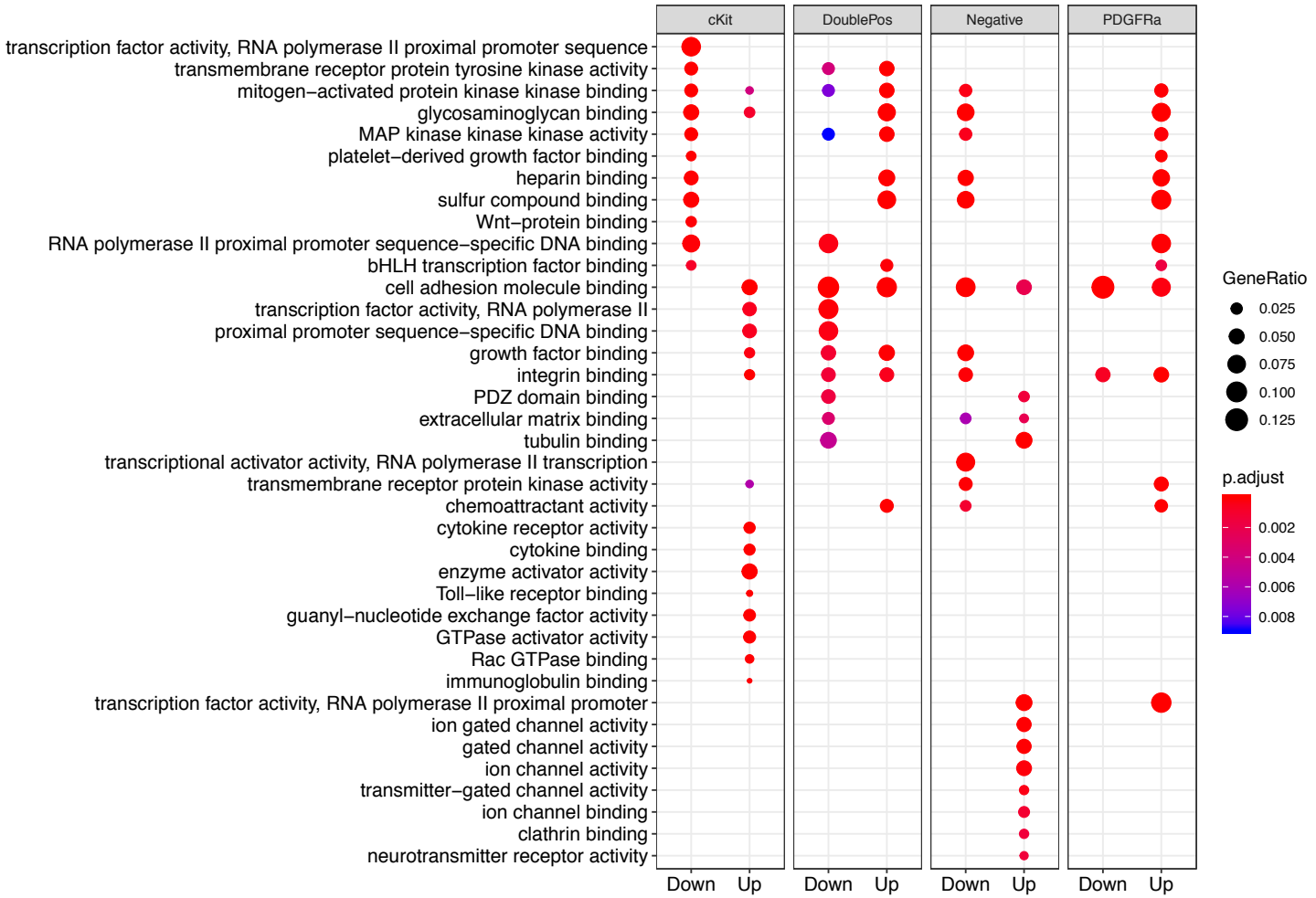

Figure 4-11: E12.5 enriched Molecular Function (MF) GO categories (legend overleaf)

Figure 4-12: E12.5 enriched Biological Process (BP) GO categories (legend overleaf)

Figure 4-10: E12.5 enriched Cellular Component (CC) GO categories

Enriched CC GO categories obtained from the list of DEGs of each population against the average of the other three populations. For each population enriched CC GO categories were calculated from the upregulated (i.e. “Up”) or downregulated (i.e. “Down”) DEGs and the first 10 were plotted. Dot size corresponds to the GeneRatio defined as the number of DEGs in one list (e.g. DEGs upregulated in cKit) mapping to one specific CC GO categories divided by the total number of DEGs in that list mapping to all CC GO categories. Colour code corresponds to adjusted p-value, calculated taking into account multiple comparisons against all groups.

Figure 4-11: E12.5 enriched Molecular Function (MF) GO categories

Enriched MF GO categories obtained from the list of DEGs of each population against the average of the other three populations. For each population enriched MF GO categories were calculated from the upregulated (i.e. “Up”) or downregulated (i.e. “Down”) DEGs and the first 10 were plotted. Dot size corresponds to the GeneRatio defined as the number of DEGs in one list (e.g. DEGs upregulated in cKit) mapping to one specific MF GO categories divided by the total number of DEGs in that list mapping to all MF GO categories. Colour code corresponds to adjusted p-value, calculated taking into account multiple comparisons against all groups.

Figure 4-12: E12.5 enriched Biological Process (BP) GO categories

Enriched BP GO categories obtained from the list of DEGs of each population against the average of the other three populations. For each population enriched BP GO categories were calculated from the upregulated (i.e. “Up”) or downregulated (i.e. “Down”) DEGs and the first 10 were plotted. Dot size corresponds to the GeneRatio defined as the number of DEGs in one list (e.g. DEGs upregulated in cKit) mapping to one specific BP GO categories divided by the total number of DEGs in that list mapping to all BP GO categories. Colour code corresponds to adjusted p-value, calculated taking into account multiple comparisons against all groups.

Recently, Gurdziel et al. (2016) published a list of genes which are specifically expressed by SMCs of the circular SM layer of E14.5 mice. In order to assess which of the different population sorted in this work were closer (from a gene expression point of view) to the phenotype of the cells described by Gurdziel et al. (2016), the expression levels of such genes among the different populations were investigated. In order to do so, separately for each developmental stage (i.e. E12.5, E14.5 and E18.5), all up-regulated DEGs found from all four comparisons (see Tab. 4-1) were screened against the list of

Gurdziel et al. (2016) and only genes present in both lists were retained and plotted (Fig. 4-13; 4-14; 4-15).

At E12.5 a total of 40 genes from Gurdziel et al. (2016) were found up-regulated in at least one population (Fig. 4-13). The clustering of samples clearly indicated that cKit cells were separated from the remaining populations, while PDGFRa and DoublePos were the closest. A higher expression of 19 genes was evident in PDGFRa and DoublePos, compared to cKit and Negative cells; among these genes several important smooth muscle genes such as *Actg2*, *Acta2* and *Cnn1* were present.

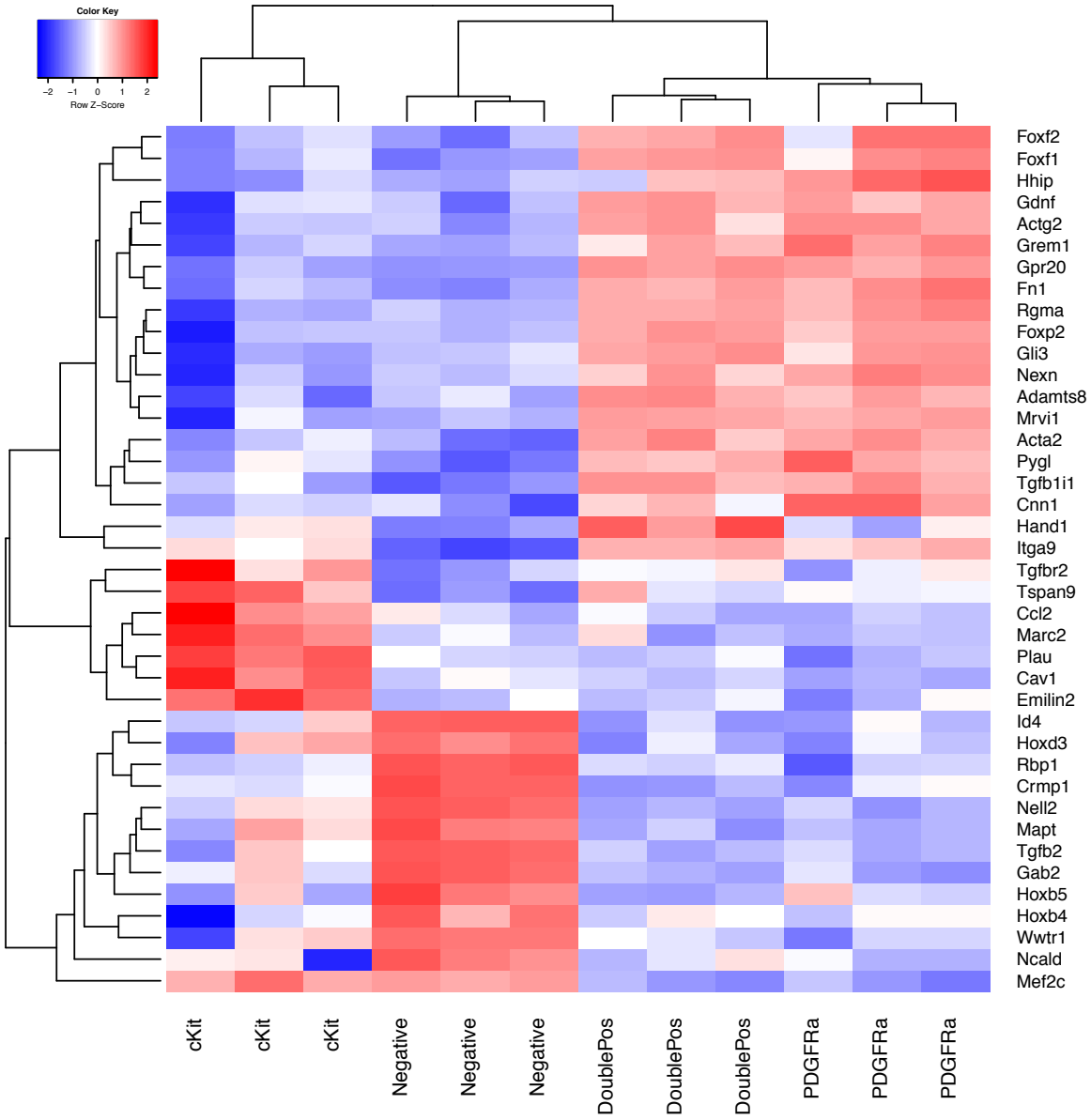

Figure 4-13: Intestinal smooth muscle related DEGs at E12.5

Heatmap showing the genes identified by Gurdziel et al., (2016) which were found as DEGs at E12.5 in at least one of the four comparisons. Expression levels are expressed as $\log_2$(CPM) scaled to have mean =0 and SD =1 and are colour coded, with higher expression levels in red and lower in blue.

At E14.5 a lower number of genes from Gurdziel et al. (2016) were found (Fig. 4-14). Almost all these genes were expressed at low levels in cKit cells while, on the other hand, they were highly expressed in the Negative cells. The expression in PDGFRa and DoublePos cells was similar among the two groups and was intermediate between cKit and Negative cells, suggesting that,

throughout the development, the number of SMCs within the Negative population was increasing.

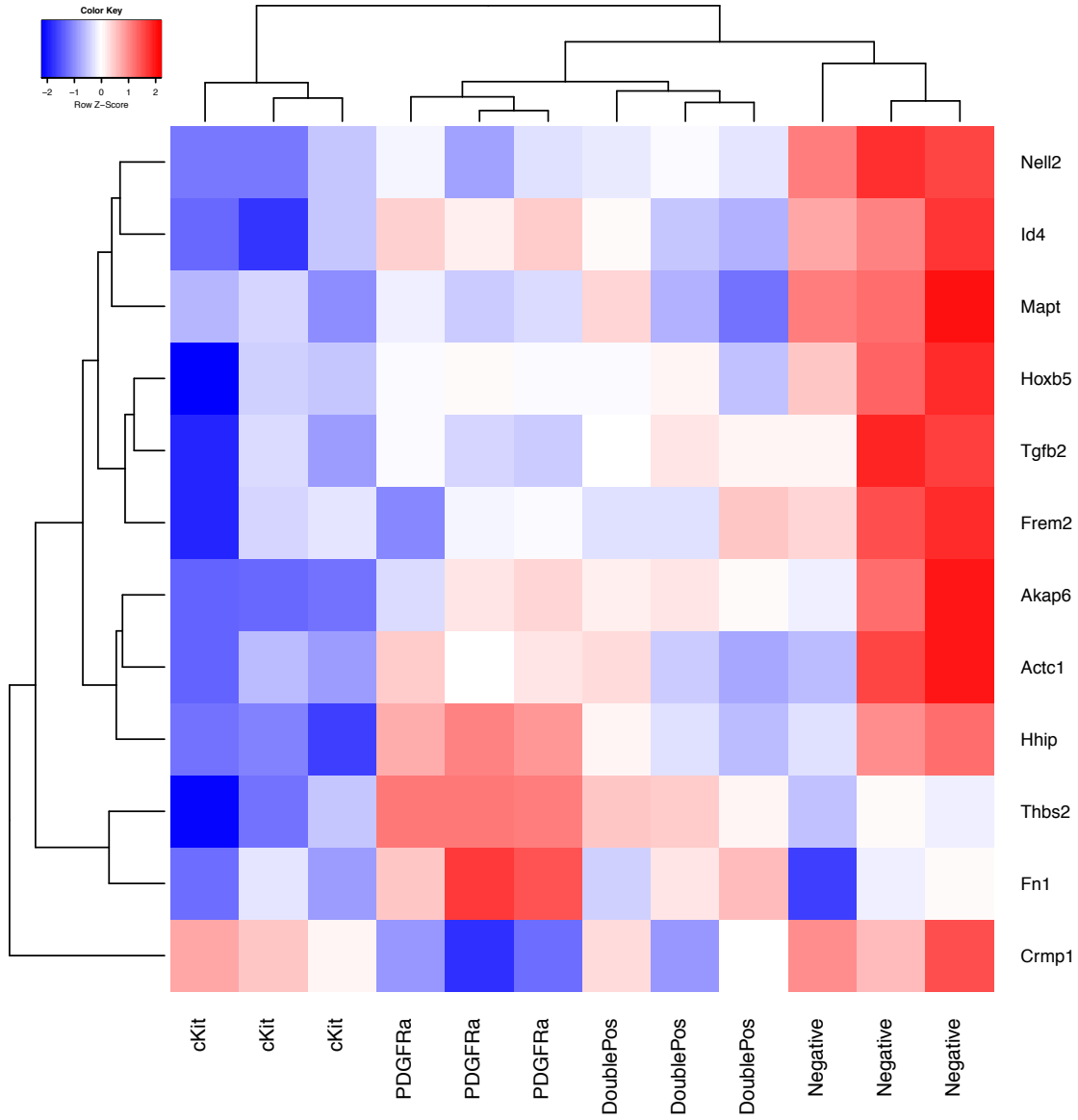

Figure 4-14: Intestinal smooth muscle related DEGs at E14.5

Heatmap showing the genes identified by Gurdziel et al., (2016) which were found as DEGs at E14.5 in at least one of the four comparisons. Expression levels are expressed as $\log_2$(CPM) scaled to have mean =0 and SD =1 and are colour coded, with higher expression levels in red and lower in blue.

At E18.5, the majority of up-regulated DEG within the genes identified by Gurdziel et al. (2016) were highly expressed in the Negative population (Fig. 4-15), confirming the previous observations that, during development, SMCs become abundant in the double negative population.

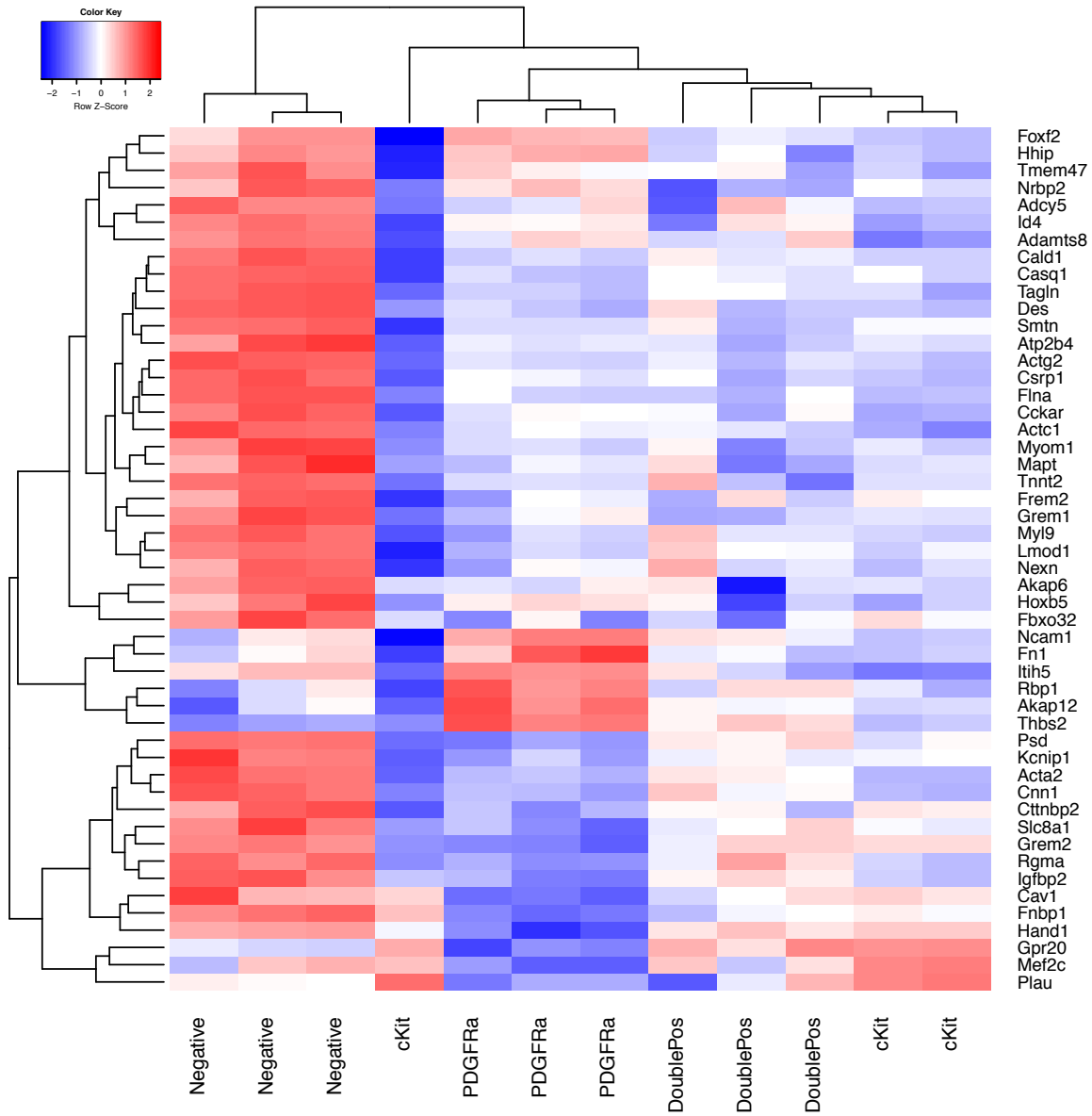

Figure 4-15: Intestinal smooth muscle related DEGs at E18.5

Heatmap showing the genes identified by Gurdziel et al., (2016) which were found as DEGs at E18.5 in at least one of the four comparisons. Expression levels are expressed as $\log_2$(CPM) scaled to have mean =0 and SD =1 and are colour coded, with higher expression levels in red and lower in blue.

Overall, these results suggest that cKit population greatly differed (from a gene expression point of view) from the profile described by Gurdziel et al. (2016), while, at the earliest stage of development considered in this study (i.e. E12.5), cells from PDGFRa and DoublePos populations more closely resembled this profile and that differentiated SMCs were present among the Negative cells.

4.3 Discussion

Attention was drawn to the origin of enteric SMCs only in the past 30 years, giving rise to a series of studies that identified different putative cell sources contributing to the formation of the SMCs of the intestine (Carmona et al., 2013; Kluppel et al., 1998; Kurahashi et al., 2008; Rinkevich et al., 2012; Torihashi et al., 1997; Wilm et al., 2005). However, a clear identification of the cellular profile of cells that during the development give rise to both the circular and the longitudinal SM layer is still missing. In fact, all studies performed focused on cells originating the longitudinal SM layer, which in the murine embryo appears much later than the circular SM layer, with a delay of 5-6 days (Torihashi et al., 1997).

The identification of cells positive for cKit (Torihashi et al., 1997) and PDGFRα (Kurahashi et al., 2008) in the outer layer of the developing mouse guts at E12, outside the already formed circular SM layer, suggested that those cells could be the precursors of the longitudinal SMCs. Overall, immunofluorescence analyses performed in this study using αSMA, cKit and PDGFRα expression at E12.5, E14.5, E16.5 and E18.5 were in accordance with the literature (Kurahashi et al., 2008; Torihashi et al., 1997), confirming the presence of only the circular SM layer at E12.5 and the appearance of an organised longitudinal SM layer between E16.5 and E18.5.

The characterisation of the expression profile of the aforementioned receptors cKit (CD117) and PDGFRα (CD140a) in the mouse embryonic gut by means of flow cytometry and RNA-Seq revealed interesting results. From the counterplots of the expression profiles of CD117 and CD140a positive cells, a different pattern could be evidenced between the different stages of development. In particular, at E12.5 the double positive population for cKit and PDGFRα ($CD117^{+}/CD140a^{+}$) was part of a single population of $CD140a^{+}$ cells, some of which were expressing CD117 while others were not (Fig. 4-3A; 4-4B). This could explain the overall gene expression similarity (i.e. proximity) between PDGFRa and DoublePos cells evidenced at MDS plot at E12.5 (Fig. 4-5). At later embryonic stages, the double positive cells were part of two different populations, one showing high expression of CD140a and low expression of CD117, the other

showing low expression of CD140a and high expression of CD117 (Fig. 4-3A). This could explain the disposition of these populations at the MDS plot from the RNA-Seq data. In fact, at E14.5 and E18.5, DoublePos cells were located between PDGFRa and cKit cells in the MDS plot, suggesting for these cells an intermediate expression profile between PDGFRa and cKit cells.

In general, the number of double positive cells decreased sharply throughout development. Simultaneously, an overall increase with time (from E12.5 to E18.5) in the percentage of double negative cells was evidenced. As demonstrated in this work and previously reported in the literature (Kurahashi et al., 2008; Torihashi et al., 1997), at E12.5 cells expressing cKit and PDGFRα were present in the outer layer of the gut, where the longitudinal SM layer will arise. In the light of this it could be hypothesized that the sharp decrease of the double positive population and increase of the negative population (Fig. 4-4B and C) observed with flow cytometry, is due to a loss of expression of the two receptors in the former cell population that consequently transformed into cells that enriched the negative population. Thanks to whole transcriptome analysis, this theory could be further investigated.

Analyses of the Reactome pathways enriched in the up-regulated genes of each cell population analysed, allowed to identify specific characteristics of each population. For example, it was identified that enriched pathways from the cKit group were associated with the immune system, independently of the stage analysed. This result could be explained by the fact that cKit is a tyrosine kinase receptor expressed by several cell types, and among them ICCs (Blair et al., 2014; Komuro, 2006; Torihashi et al., 1995; Ward et al., 1994), as well as cells of the immune system, such as hematopoietic stem cells, lymphocytes and mast cells (Thorén et al., 2008). Probably, this immune related signal, evidenced at gene expression level, was due to the presence, within the cKit population, of mast cells and lymphocytes that were localised in the mucosa and submucosa of the intestine. Unfortunately, the lack of a negative sort for these specific cell types could have interfered with the signal of the single positive cKit cells that during development give rise to the ICCs colonising the gut. Therefore, a more detailed analysis on the cKit positive cells should be performed to investigate whether the

immune signal identified in the pathway analysis, derived from a contamination from immune cells present in the gut or was due to an unknown role of cKit cells (i.e. future ICCs) in the immune regulation.

Instead, PDGFRa cells in all the developmental stages evaluated were enriched for Reactome pathways mainly associated with the extracellular matrix. Interestingly, at E12.5, few more enriched pathways were evidenced in the PDGFRa group when looking at the GO and Kegg pathway datasets (Fig. 4-9; 4-10; 4-11; 4-12). These pathways, ascribable to muscle tissue, were enriched also in the DoublePos population. The presence of enriched hits for muscle tissue in both populations could suggest that the putative smooth muscle precursor cells may lie within these two populations. However, it would be difficult to discriminate which of the cells, between the DoublePos and the PDGFRa cells, contain the precursors. Nevertheless, the fact that at E14.5 enrichment for muscle tissue was present only in the DoublePos group, would support the hypothesis of the DoublePos cells containing the precursors of the longitudinal SM layer of the intestine.

It is well known that SMCs, following injury or particular physiological states, have the ability to revert from their differentiated phenotype back into an undifferentiated one (Alexander and Owens, 2012; Rensen et al., 2007) where they can extensively proliferate (e.g. the uterine growth during pregnancy) and differentiate again to meet the demands of the body. In this context, this ability of SMCs to switch between phenotypes and proliferate would support the hypothesis of the absence of precursor cells which reside in the gut after birth providing new SMCs, as this role would be carried out by SMCs themselves. The development of SM layers within the gut is fully achieved by E18.5 and mice are born shortly after that. Therefore, the absence of enriched categories within the up-regulated genes of the DoublePos cells at E18.5, could support the idea of the absence of a precursor population that remains throughout the entire intestinal development and is present after birth in the intestine to replenish SMCs during post-natal life. In fact, all the enriched pathways associated with muscle tissue, such as “smooth muscle contraction”, were identified at E18.5 within the Negative cells. This could be viewed in the light of the process of differentiation

towards SMCs. In this case, longitudinal SM precursors (hypothetically present in the DoublePos population at earlier stages of development), while differentiating towards SMCs, would lose the expression of cKit and PDGFRα therefore becoming part of the negative cell population in this setting and, hence, would have been sorted in the Negative population.

Recently, Gurdziel et al. (2016) was able to identify a list of genes that were described as specific to the circular SM layer. By comparing their list of genes with the up-regulated DEGs identified in this study, it was possible to identify at each time point which cells more closely resembled circular SMCs. As expected, the highest number of genes was identified at E18.5 and their expression was proved higher in the Negative population compared with all other cell populations. This further confirmed the idea that at E18.5 the Negative group mainly contained SMCs of both circular and longitudinal SM layers. Looking at earlier developmental stages, it would have been expected to see a high number of these genes highly expressed in the Negative population, which contained the circular SM layer. However, at E14.5 and E12.5, when only the circular smooth muscle layer was fully developed, the main signal detected from the Reactome pathway analysis within the Negative cells was ascribable to the neuronal system. This could probably be explained by the presence of enteric neural crest cells within the Negative population that were putatively present in a higher proportion compared to SMCs at E12.5 and E14.5, thus “masking” the signal from SMCs. On the other hand, at E18.5 the abundance of SMCs was putatively higher than neural cells, therefore explaining the enrichment for muscle categories observed at this stage. In spite of this, at E12.5 the majority of genes from Gurdziel et al. (2016) were more highly expressed in DoublePos and PDGFRa cells, confirming previous results from Kegg and GO categories.

Overall, the results showed in this chapter contributed to the idea that, during development, longitudinal SMCs may arise from a precursor expressing cKit and PDGFRα. However, data collected in this study could not conclusively identify the specific population containing these precursors. A more detailed analysis on the differences between PDGFRα and double positive cells should

be performed to determine where the precursor cells come from and what other markers could be used to identify these cells.

Chapter 5

Human small intestinal mesoangioblast-like cells (hSI_MABs): isolation, characterisation and regenerative medicine application

5. Human small intestinal mesoangioblast-like cells (hSI_MABs): isolation, characterisation and regenerative medicine application

5.1 Introduction

Paediatric intestinal failure (IF) occurs when the intestine is not able to fulfil the nutritional demands of the body and, unfortunately, this condition affects ten out of thousand children worldwide (Duggan and Jaksic, 2017). Intestinal transplantation is, to date, mostly performed in children as a consequence of IF, especially when caused by short bowel syndrome or gastrointestinal motility disorders (Boluda, 2015). However, success rate and quality of life after intestinal transplantation remains poor (Boluda, 2015), and an alternative strategy is essential. The generation of a functional bio-engineered small intestine would be beneficial and could overcome most of the limitations of today's transplants.

The absence of an appropriate enteric SM precursor has prompted several labs to use different sources and approaches when considering the appropriate cell type to be used for the generation of an engineered intestine (Clevers et al., 2019; Zakhem et al., 2019). As previously mentioned in section 1.6.3, mesoangioblasts (MABs) and pericyte-derived cells are thought to be able to generate both vascular SMCs and the mesodermal tissue from which they are isolated (Minasi et al., 2002; Sacchetti et al., 2016). Therefore, it was hypothesised that MABs isolated from the intestine would be able to generate only SMCs and therefore be ideal candidates for tissue engineering the intestine.

In this chapter, for the first time the isolation, characterisation and potential use of human small intestinal mesoangioblast-like cells (hSI_MABs), from both foetal and paediatric intestine is described.

5.2 Results

5.2.1 Human small intestinal mesoangioblast-like cells (hSI_MABs): isolation and characterisation

In order to obtain an alternative source of enteric SMCs for intestinal TE approaches, hSI_MABs were isolated and characterised. Human foetal (hFtSI_MABs) and paediatric (hPaedSI_MABs) small intestinal MABs were isolated from 7 out of 7 samples (100%), 5 derived from foetal midguts staged between 12 and 20 pcw, and 2 from post-natal ileal biopsies from children in their first year of life undertaking surgeries at the Great Ormond Street Hospital (UK). The biopsies were plated and the duration of cell outgrowth from intestinal muscle layer biopsies (i.e. the time that cells needed to come out from the biopsy before being detached) was sample specific, varying from 5 to 10 days (Fig 5-1A). By using a selective growth medium (Megacell added with 5% FBS, 1% Pen/Strep, 1% L-glu and 5ng/ml bFGF), enrichment of hSI_MABs and loss of other cells types, such as neural stem cells, smooth muscle cells and fibroblasts, was obtained after 1-2 passages. In culture flasks, hSI_MABs had two different phenotypes: one attached to the flask's surface and a rounded floating one as shown in Figure 5-1A.

hSI_MABs showed high proliferative capacity: the percentage of Ki67 positive cells over the total number of cells, determined by DAPI counterstaining (Fig 5-1B), was 66.4 ±9.1% (n= 5) for hFtSI_MABs, while it was 69% (n= 2) for hPaedSI_MABs (Fig 5-1C). hSI_MABs were maintained in culture up to passage 8 and both cumulative cell population doubling and cumulative cell number were measured (Fig 5-1D). Growth rates of foetal (n= 3) and paediatric (n= 2) cells were compared by means of linear regression: analysis revealed that the slopes of the two regression lines were different ($F_{1,13}$=14.18, p-value=0.0024), with hPaedSI_MABs cells growing 20% faster.

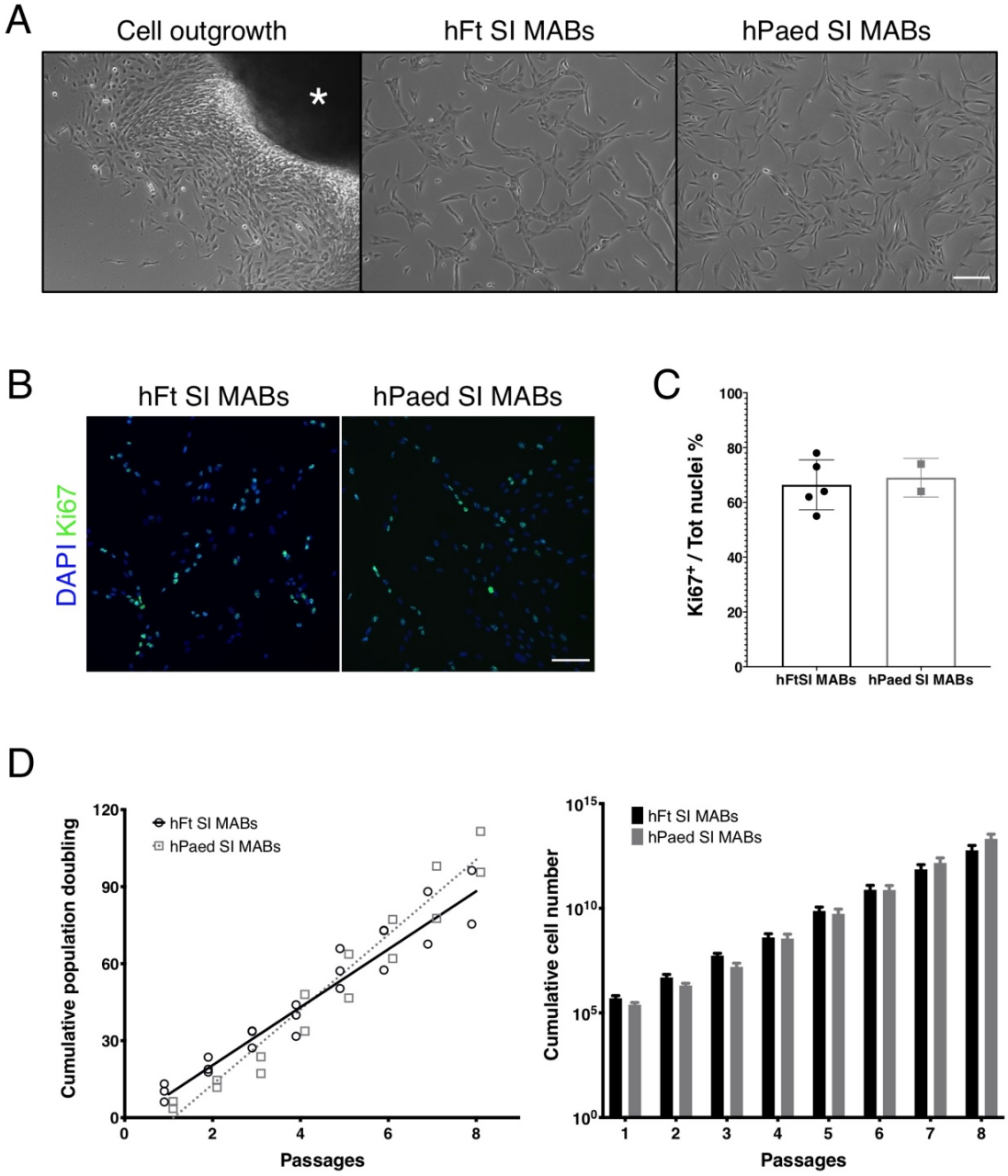

Figure 5-1: hSI_MABs isolation and culture

A) Representative bright field images of outgrowth and cells at passage 3 (star shows biopsy). Scale bar 100 μm. **B)** Immunostaining of hSI_MABs for Ki67 in green and DAPI nuclei in blue. Scale bar 100 μm. **C)** Percentage of proliferating cells ($Ki67^+$) over total number of cells ($DAPI^+$) per field of view. Each dot represents the mean of 5 fields of view per sample. **D)** Left graph: cumulative population doubling of foetal (black circles, n= 3 biological samples for each time point) and paediatric (grey squares, n= 2 biological samples for each time point) of hSI_MABs. Lines represent the linear regressions fitted for each group; right graph: cumulative cell number of the same samples.

To evaluate the genomic stability of cells kept in culture for 7-8 passages, a High-Density SNP genotyping array was performed on two hFtSI_MABs samples (Fig 5-2). No variation in copy number was detected.

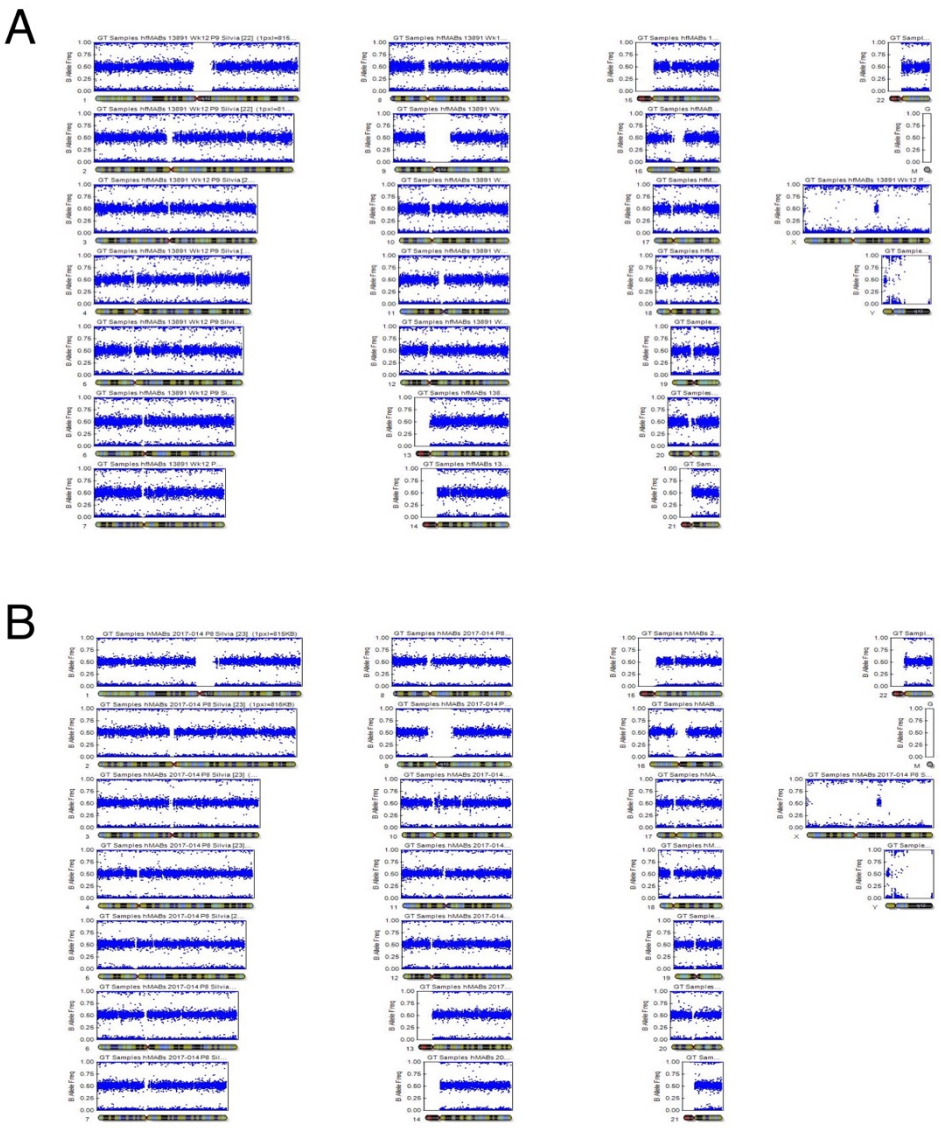

Figure 5-2: hFtSI_MABs SNP genotyping array

A, B) Figures show no major alteration in the genotype of cells from two foetal samples respectively.

In order to better characterise the isolated hSI_MABs, cells were analysed by immunofluorescence for the expression of pericyte markers after 3-4 passages in culture (Fig. 5-3), and with flow cytometry analysis for an in-depth characterisation (Fig. 5-4). As shown in Figure 5-3, all hSI_MABs, both of foetal

or paediatric origin, stained positively for alpha-smooth muscle actin (αSMA), the majority of them also for Neuron-Glial antigen 2 (NG2) and some for platelet-derived growth factor-beta (PDGFRß). No expression of alkaline phosphatase (AP) was evidenced in both hFtSI_MABs and hPaedSI_MABs.

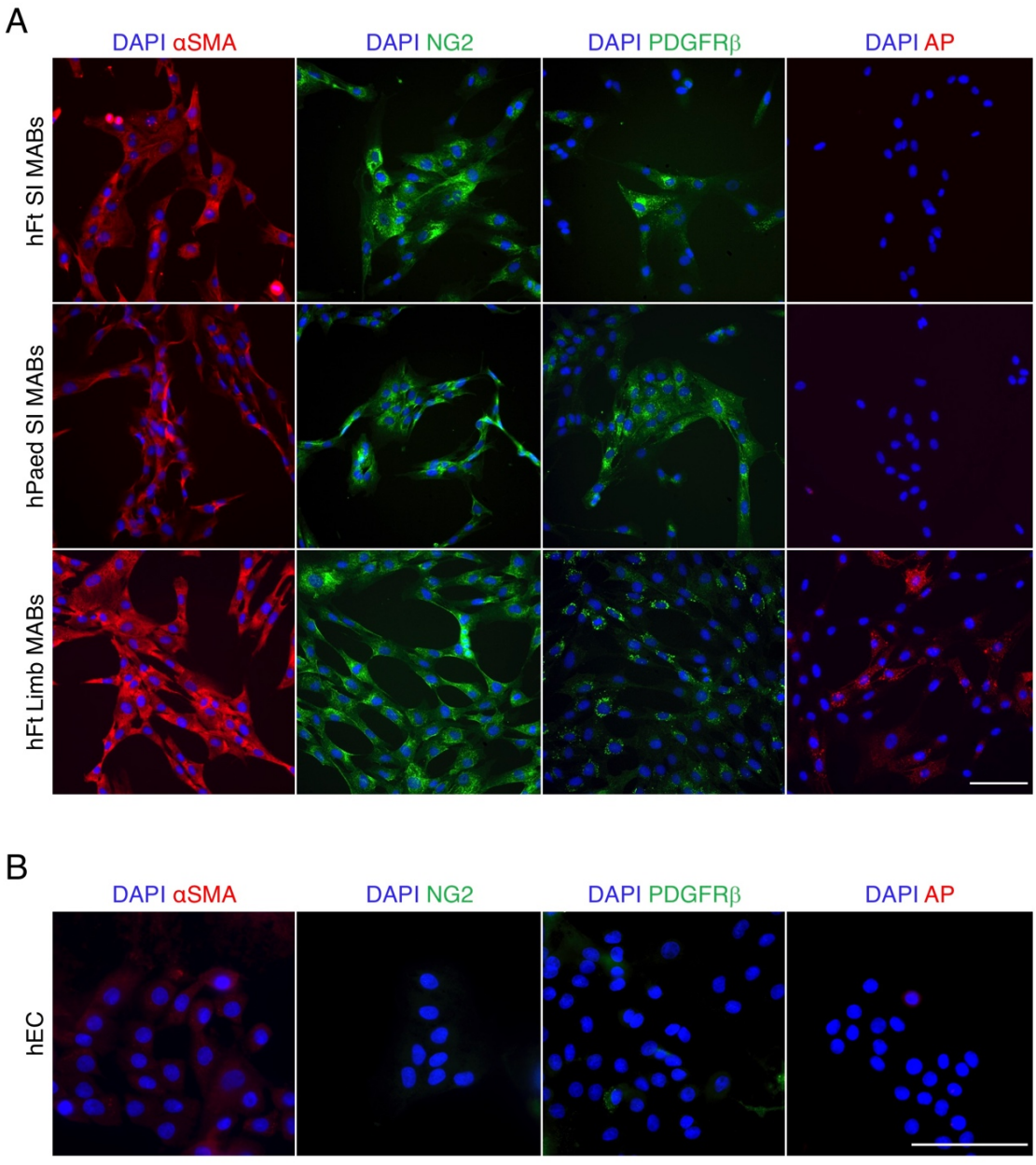

Figure 5-3: hSI_MABs IF characterisation

A) hSI_MABs (top and middle panels) and hFtLimb_MABs (positive control: bottom panel) were stained for pericyte markers: alpha-smooth muscle actin (αSMA), Neuron-glial antigen 2 (NG2), platelet-derived growth factor beta (PDGFRß) and alkaline phosphatase (AP). Scale bar 100 μm. **B)** Human epithelial cells (hEC) were stained for αSMA, NG2, PDGFRß and AP as negative control. Scale bar 100 μm.

Flow cytometry analysis revealed that hSI_MABs cells were highly positive for the mesenchymal marker CD90 with foetal cells being 98.6 ±1.3% positive (Fig. 5-4 B) and paediatric cells 99.85% (Fig. 5-4 C). Focusing on the pericyte markers, CD146 (Melanoma Cell Adhesion Molecule, MCAM) was expressed by 98.0 ±1.7% of hFtSI_MABs (Fig. 5-4 B), while only by 65.9% of the hPaedSI_MABs (Fig. 5-4 C). Another pericyte marker, NG2, was high for all tested samples (88.6 ±10.6% in hFtSI_MABs (Fig. 5-4 B) and 90.3% in hPaedSI_MABs (Fig. 5-4 C)), while the expression of PDGFRß, also known as CD140b, differed widely among foetal samples, varying between 88.6% and 1.8%, with a mean value of 51.6% ±39.8 in hFtSI_MABs (Fig. 5-4 B) and being expressed only in 9.5% of hPaedSI_MABs (Fig. 5-4 C). It is worth noting that only one foetal sample showed positive cells (12.5%) for alkaline phosphatase (AP) (Fig. 5-4 B). Similarly, the hematopoietic and endothelial marker CD34 was detected only in one of the foetal samples, with 4% positive cells (Fig. 5-4 C). Interestingly, CD56, also known as Neural Cell Adhesion Molecule (NCAM), expressed by neurons, glia and skeletal muscle cells, was present in all samples in different amounts. Younger foetal samples tended to have a greater positivity for this marker, with a maximum of 23.5%, while paediatric samples showed almost no positivity for it (Fig 5-4).

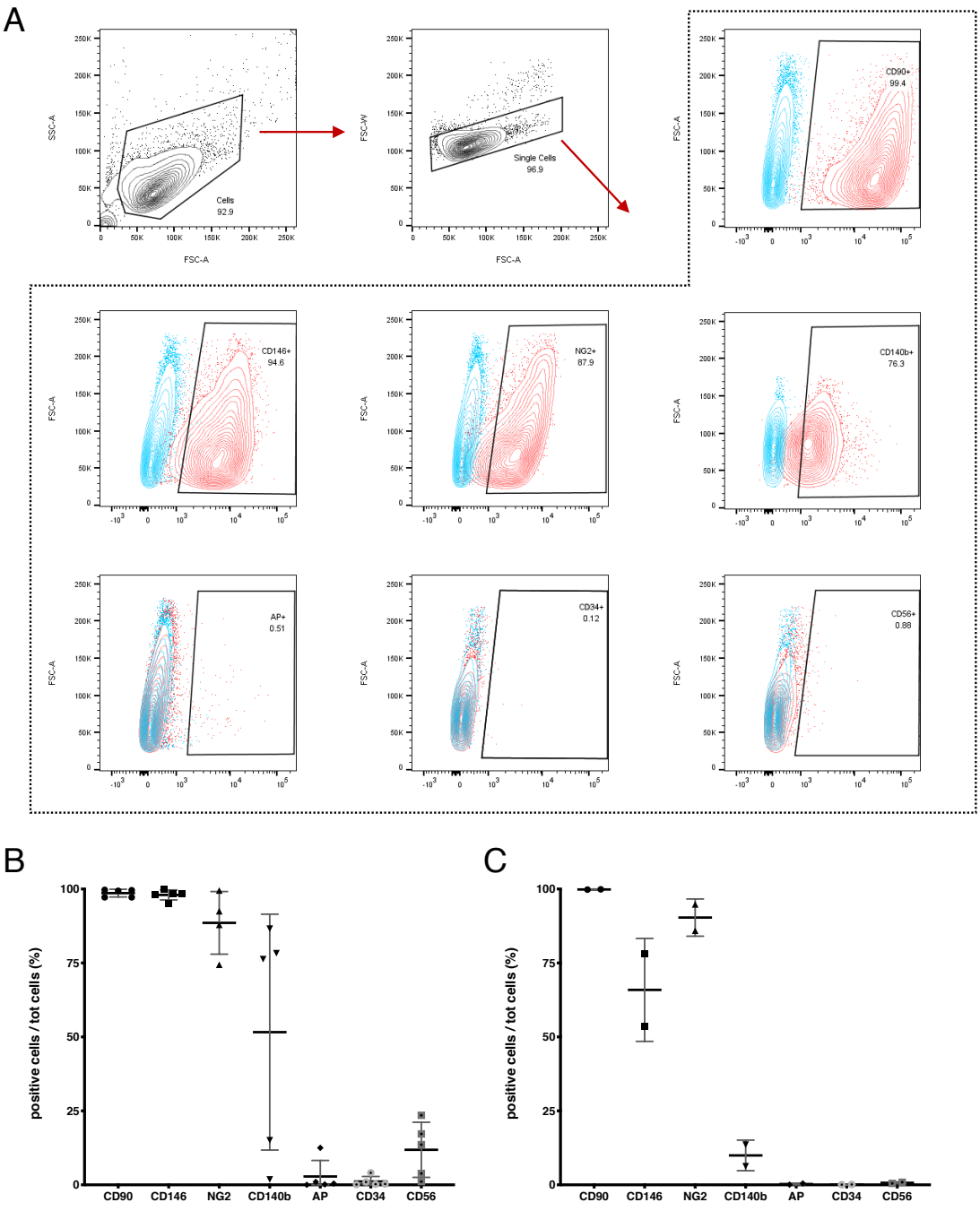

Figure 5-4: hSI_MABs flow cytometry characterisation

A) Representative counter plots of hSI_MABs from top left to bottom right: black and white counter plots of cells gating and single cells gating; followed by coloured counter plots (light blue clouds show negative unstained cells superimposed on red clouds showing stained cells) for each marker (CD90, CD146, NG2, CD140b [PDGFRß], AP, CD34 and CD56). **B, C)** Whisker plots showing the percentage of positive cells for each marker relative to the total number of single cells of hFtSI_MABs (**B**) and hPaedSI_MABs (**C**), respectively. For each marker n= 5 hFtSI_MABs (in B) and n= 2 hPaedSI_MABs (in C) samples were used.

5.2.2 hSI_MABs: muscle differentiation

In order to assess the potential use of hSI_MABs for intestinal TE approaches, cells first were tested *in vitro* for their ability to proliferate and differentiate into SMCs in different culture conditions. The standard differentiation protocol used to generate SMCs from mesoangioblast (Tonlorenzi et al., 2007) consists of a total of 8 days of culture: in the first one, just after passaging, cells are kept in their proliferation medium (enriched Megacell), while for the following 7 days in 2% HS with a daily addition of 5 ng/ml of TGFß.

At first, a test to determine cell proliferation capacity in prolonged (up to 13 days) cell culture differentiation condition was assessed. When cultured in their proliferation medium (Megacell) for up to 13 days, cells grew exponentially (Fig. 5-5; orange line), while when cultured in 2% horse serum containing differentiation media (with or without TGFβ) for the same length of time, their growth rate followed a linear pattern (Fig. 5-5; maroon and green lines).

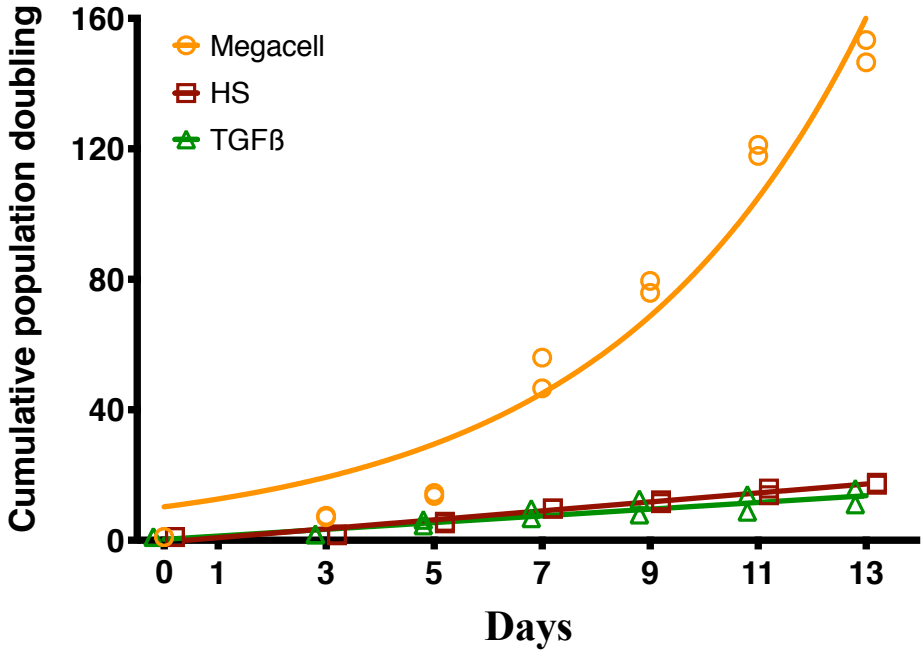

Figure 5-5: hSI_MABs proliferation during differentiation assay

Cumulative population doubling of hSI_MABs cultured in three different media: Megacell, (orange circles); 2% Horse Serum (maroon squares); 2% Horse Serum + TGFß (green triangles). For each medium n= 2 biological replicates were assessed at each time point. Lines show the best fit curve for each condition (linear regression for 2% HS (HS) and 2% HS + TGFß (TGFß); exponential curve for proliferation medium (Megacell)).

To assess mature SM differentiation, immunochemical characterisation showed that hSI_MABs cultured for 8 days (1 day in proliferation medium, Megacell, and the following 7 days in 2% HS medium with or without daily addition of TGFß), expressed smooth muscle proteins, such as SM22 and calponin (Fig. 5-6A). The number of differentiated cells (i.e. SM22 and Calponin positive cells) was assessed counting positive cells over total cells per high magnification field (n =3 foetal samples and n =2 paediatric samples). Both foetal and paediatric hSI_MABs, when cultured with TGFß addition, were able to generate 92 ±6% and 99% SM22 positive cells respectively, as well as 89 ±5% and 97% Calponin positive cells respectively. Cells cultured in 2% HS only, still generated 64 ±18 SM22 positive and 45 ±18% Calponin positive foetal cells, while only 44% SM22 positive and 23% Calponin positive paediatric hSI_MABs were generated. Among the foetal samples Calponin positive cells were statistically different between 2% HS and 2% HS + TGFß treatments, with a higher expression in the latter (Fig. 5-6B). The capacity of hSI_MABs to differentiate into skeletal muscle cells was tested with immunochemical analysis and showed no expression of both MyoD and skeletal MHC when cells were cultured in 2% HS, a culture condition that allowed myotubes formation from human foetal limb MABs (hFtLimb_MABs; Fig. 5-7A). To further confirm inability of hSI_MABs to generate skeletal muscle, GFP-labelled cells were co-cultured for up to 12 days with a mouse myoblasts cell line, C2C12, and the mixture of cells which formed myotubes was assessed via immunofluorescence staining using anti GFP (to identify labelled MABs) and skeletal MHC (Fig. 5-7B). No co-staining was detected in any culture. However, to further confirm this result, a positive control, ideally co-culturing hFtLimb_MABs together with C2-C12, should have also been performed.

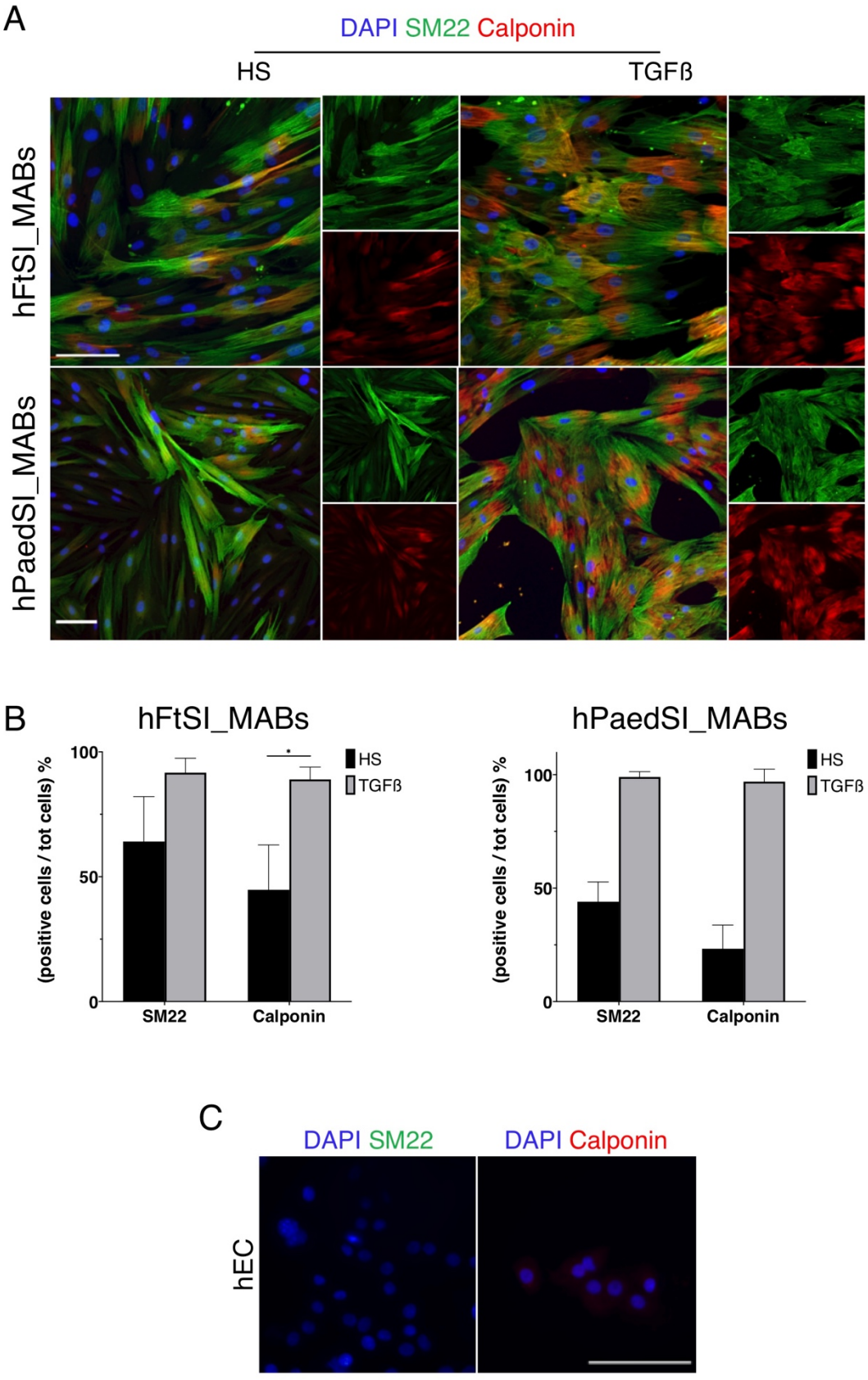

Figure 5-6: hSI_MABs smooth muscle differentiation

A) Staining for SM22 in green and Calponin in red of both foetal and paediatric hSI_MABs cultured in HS or HS+TGFß. Nuclei stained with DAPI, in blue. Scale bar 100 μm. **B)** Percentage of cells

positive for SM22 and Calponin over total cells per high power field of view from foetal (n =3) and paediatric (n =2) cells, left and right graph respectively. Data: mean ±SD. t-test: * p-val≤ 0.05. **C)** Human epithelial cells stained with SM22 and Calponin as negative control. DAPI in blue. Scale bar 100 μm.

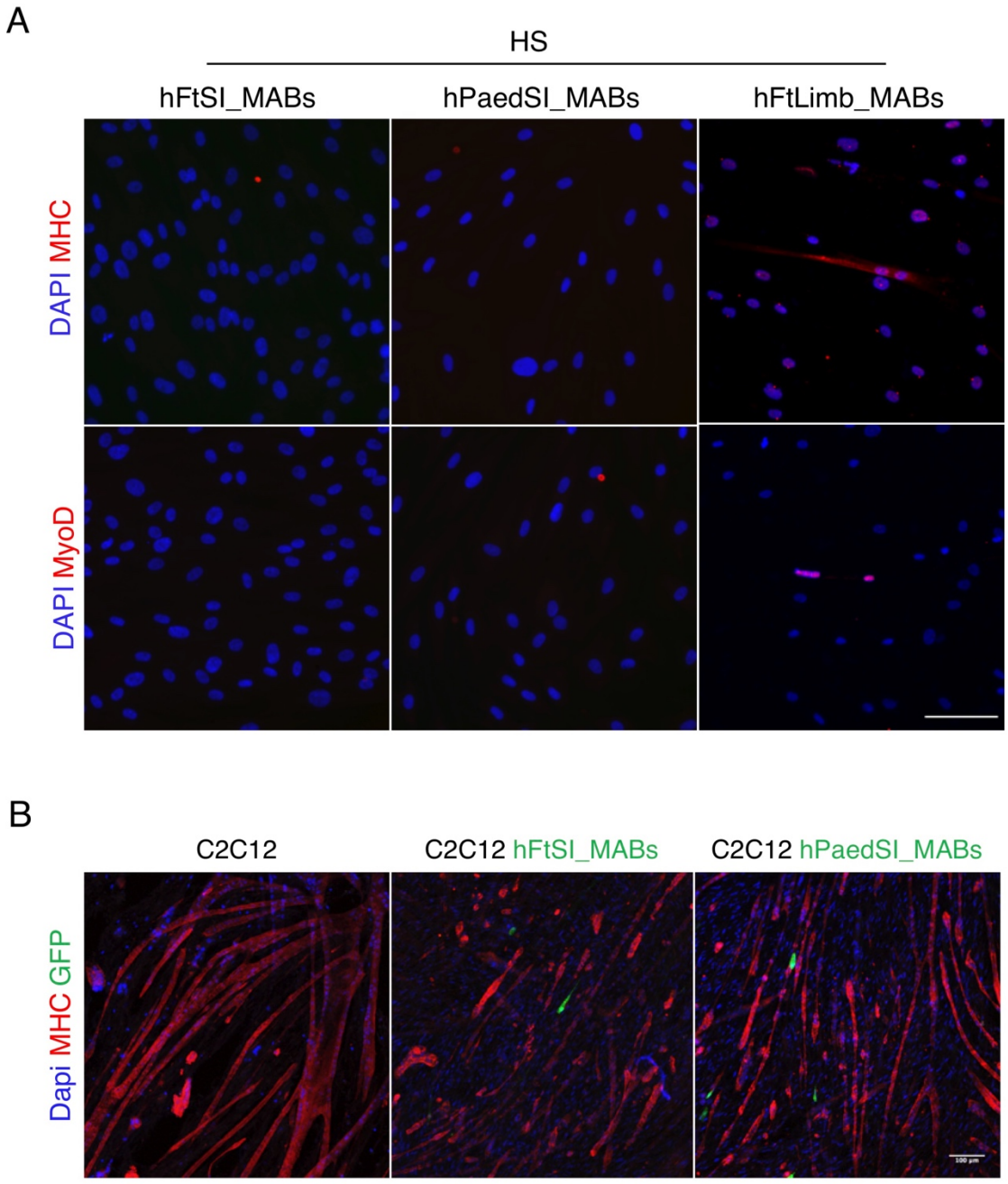

Figure 5-7: hSI_MABs skeletal muscle differentiation

A) MHC, in red, and MyoD, in green, staining of foetal and paediatric cells cultured for 8 days (1 day in Megacell and 7 days in 2%HS with/without TGFß). Human foetal limb MABS (hFtLimb_MABs), as positive control. Nuclei stained with DAPI in blue. Scale bar 100 μm. **B)** Co-culture of GFP-labelled hSI_MABs with C2C12 mouse myoblasts for 12 days. Formed myotubes are stained in red for MHC. Scale bar 100 μm.

Functional analysis, following SM differentiation, was performed for calcium intracellular flushing by calcium imaging in response to local application of Carbachol. In all treatments, cells exhibited a basal activity of intracellular calcium movement (Fig. 5-8A, B). Following Carbachol application for 10 seconds (vertical dashed lines between T = 20 sec and T = 30 sec, Fig. 5-8B), no response was detected in cells kept in the proliferation medium, Megacell. On the other hand, cells cultured in 2% HS medium, with or without daily addition of TGFß, showed a clear flushing. As an example, the response of a single cell in each condition is shown in figure 5-8B. Single cell fluorescent peak responses have been quantified as the fluorescent peak value over the fluorescent level at the beginning of recording. Analysis confirmed response to Carbachol only in cells cultured in 2% HS medium, with or without TGFß addition (non-parametric Kruskal-Wallis Test with multiple comparisons was performed using Megacell as reference; total of 7 ROI (one for each cell) per experiment were measured, n =2 different experiments; Fig. 5-8C).

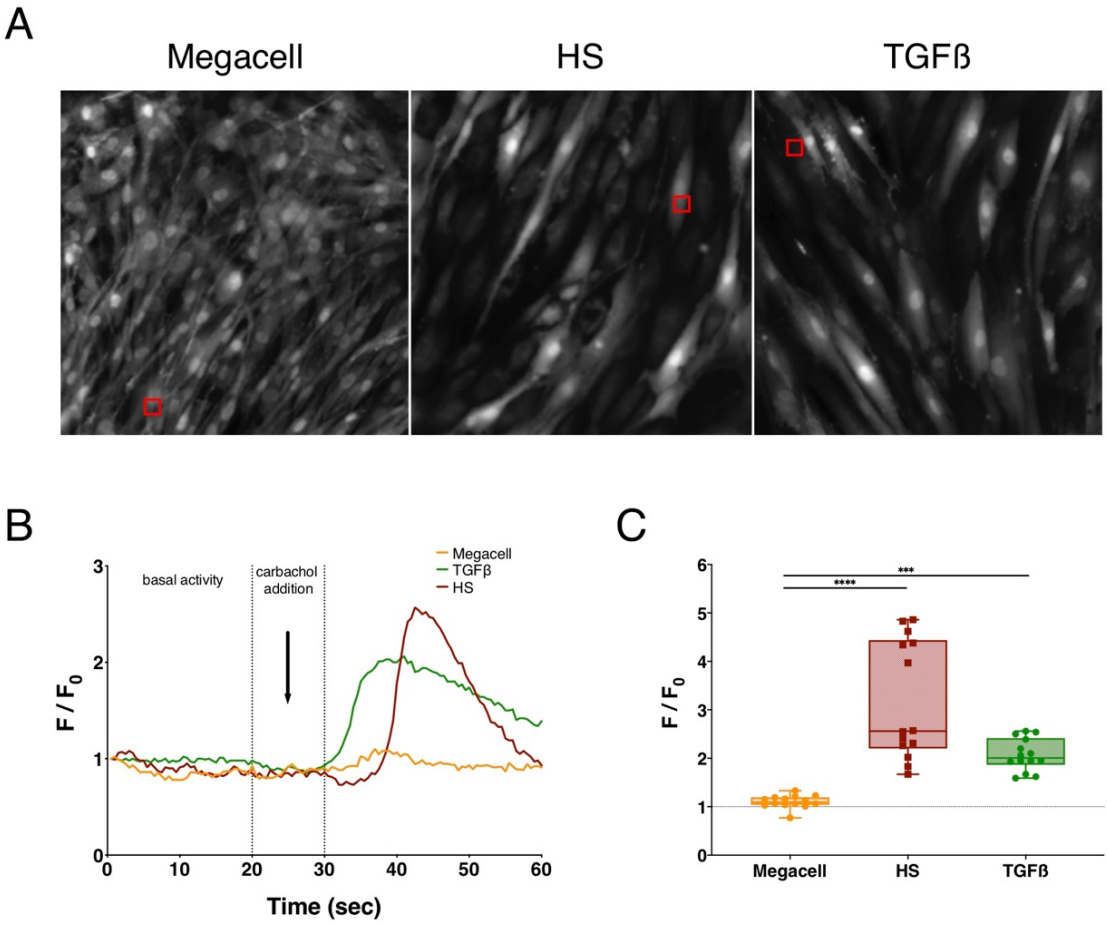

Figure 5-8: hSI_MABs functional analysis

A) Representative images of calcium activity in cells cultured in proliferation medium, Megacell (left), 2% HS + TGFß (middle) and 2% HS (right). Red boxes refer to the ROI in which fluorescence induced by intracellular calcium transit was plotted in figure 5-8B. **B)** Representative fluorescence activity, relative to fluorescence at time 0, of a single cell taken from each culture condition. Cell basal activity was recorded for the first 20 seconds, then Carbachol was supplied for 10 seconds. **C)** Maximum response after Carbachol supply measured from 7 cells from each condition in n =2 experiments. Data: Box and whiskers plot, symbols represent each measurement. Kruskal-Wallis multiple comparisons test: ***p-val <0.001, ****p-val <0.0001.

5.2.3 hSI_MABs differentiation on mouse small intestine in ex vivo culture

With the aim of studying integration of transplanted cells in the gut, and also maintain the vitality of the tissue and avoid tissue contraction, an *ex vivo* culture system using pieces of mouse intestine was set up in the lab. In brief, the dissected mouse gut was flat opened along the mesentery with the serosa surface facing up, then a metal ring was inserted below the tissue and a black

rubber ring was used to secure the intestinal tissue around the metal ring without creases, as shown in figure 5-9.

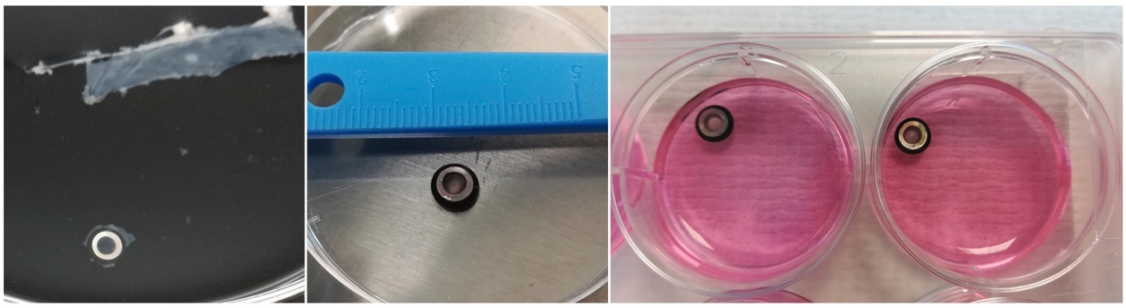

Figure 5-9: *Ex vivo* experimental set up

This set up was used to determine hSI_MABs potency to integrate and generate SMCs when seeded on top of a cryo-injured mouse intestinal gut. In order to track cells, hSI_MABs were transduced with a GFP-lentivirus to get a multiplicity of infection (MOI) of 1-2, and sorted using GFP fluorescence (Fig. 5-10).

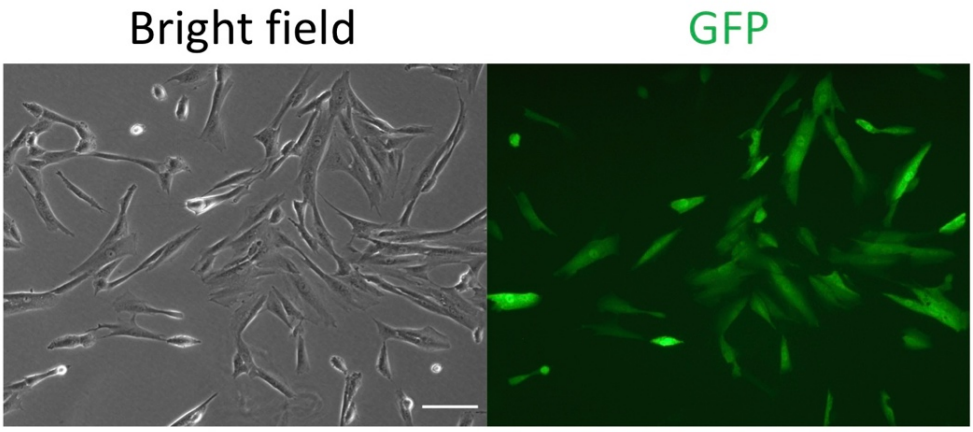

Figure 5-10: GFP labelled hSI_MABs

Bright-field and fluorescent images of GFP transduced cells. Scale bar 100 μm.

In total, 20 pieces of mouse small intestine were secured onto the rings, of which 16 were cryo-injured and 4 were not. Subsequently all 20 rings were seeded with 50'000 GFP-labelled hFtSI_MABs each. These were cultured in plain high glucose DMEM medium after 2-3 hours post-seeding. After the period of culture (10 days), viable cells were visible in only 50% of the uninjured guts,

whereas cells were identified in 75% of the injured ones (Fig. 5-11). As shown in figure 5-11B, both in injured and uninjured guts, GFP cells, located in the middle, were identified after culture. Parallel staining with SM22 (in red in Fig. 5-11B), showed no cells co-staining with GFP in any of the cases. Only very few GFP cells (3-4 cells per ring), among all the guts analysed, co-stained with SM22.

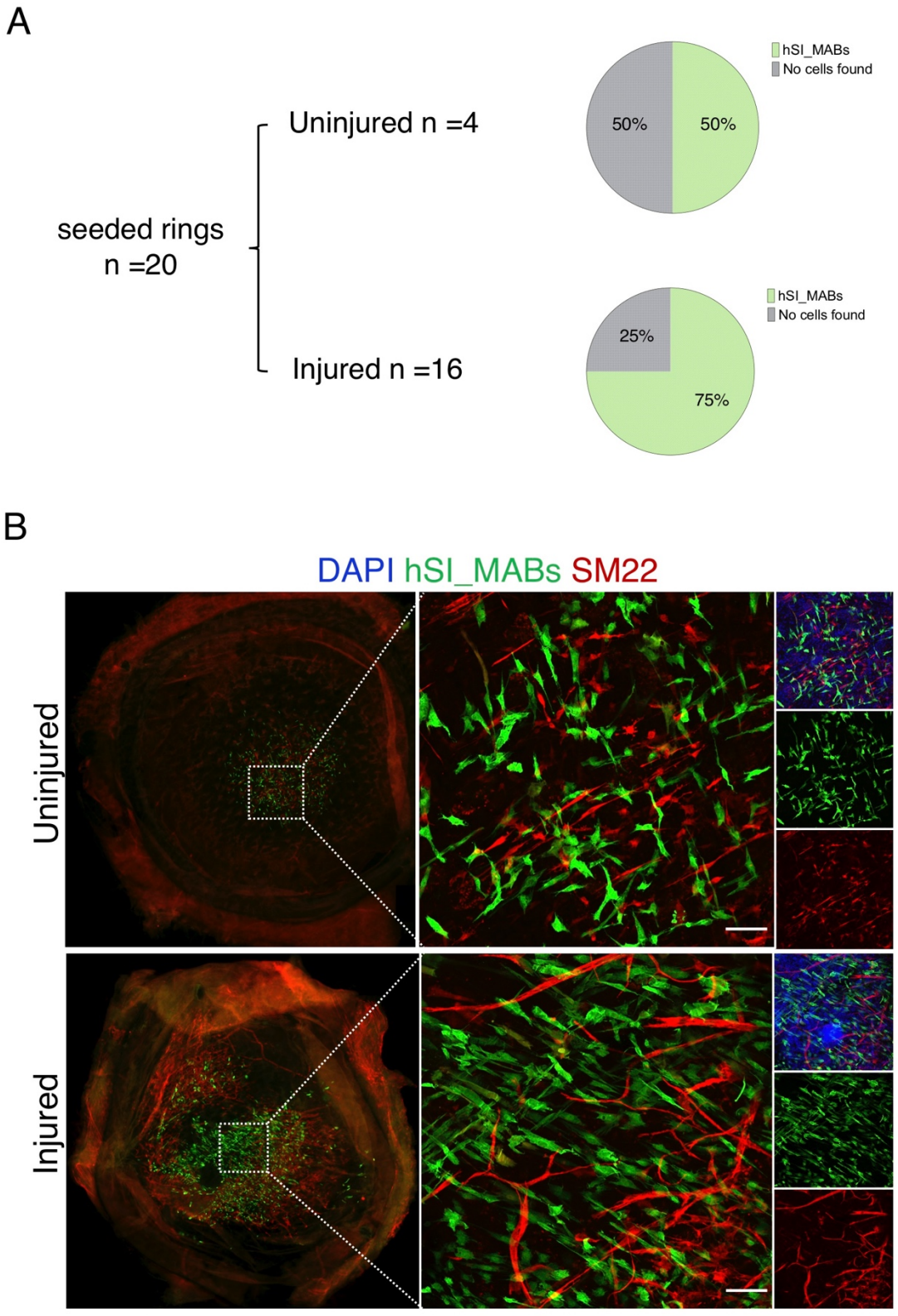

Figure 5-11: *Ex vivo* culture of transplanted hFtSI_MABs

A) Schematic of samples analysed in the experiment after 10 days of *ex vivo* culture. Pie-charts show cell engraftment in uninjured and injured guts, respectively. **B)** Magnified images of uninjured and injured guts showing engraftment of GFP-labelled cells. Magnifications show SM22 in red, GFP in green and DAPI for nuclei in blue. 100 μm scale bar.

5.2.4 hSI_MABs mouse intestinal transplantation: a Pilot in vivo study

A pilot *in vivo* transplantation study was performed to determine if hSI_MABs, both foetal and paediatric, were able to differentiate into SMCs in their native environment. GFP-labelled cells were transplanted into the terminal ileum (last 5 cm) of $Rag2^{-}/\gamma c^{-}/C5^{-}$ knockout mice (total n= 5, 3 with foetal and 2 with paediatric cells) and intestines were dissected 4 weeks post-transplantation. As evidenced by whole mount staining shown in figure 5-12A, GFP-labelled cells were visible on the surface of all dissected intestines. Furthermore, some of the hSI_MABs transplanted differentiated into SMCs, as determined by co-expression of SM22 (white arrows: elongated yellow cells in the central panel of Fig. 5-12A). However, some of the GFP-labelled cells identified in the tissue clearly did not differentiate into SMCs as shown in the right panel of figure 5-12A.

Cryosections of the transplanted ileums, showed that hSI_MABs were localised on the outer surface of the gut, external to the longitudinal SM layer. Among these cells, as shown from whole mount staining, some cells co-stained with both SM22 and Calponin (Fig. 5-12B, white arrows), while others did not (Fig. 5-12B, arrow-heads).

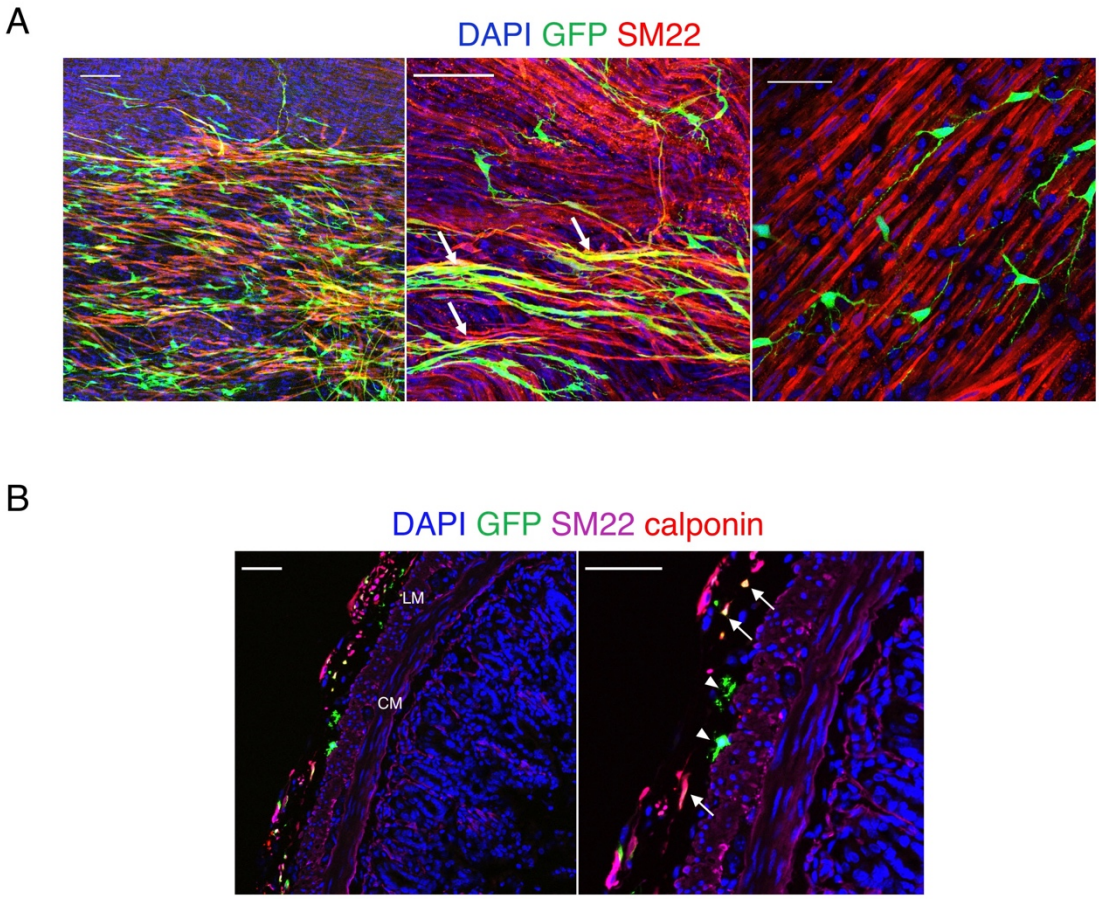

Figure 5-12: *In vivo* transplantation of hSI_MABs

A) Whole mount staining of dissected transplanted ileums 4 weeks after transplantation with GFP-labelled hSI_MABs in green, SM22 in red and nuclei (DAPI) in blue. White arrows indicate elongated GFP-SM22 positive cells. Scale bars 100 μm. **B)** Cryosection images of transplanted intestines showing, GFP-labelled transplanted hSI_MABs in green, SM22 in magenta, Calponin in red and nuclei counterstain in blue. LM= Longitudinal Muscle, CM= Circular Muscle. White arrows indicate cells co-labelling for GFP, SM22 and Calponin; arrow-heads indicate GFP cells. Scale bars 50 μm.

5.2.5 in vitro seeding of hSI_MABs onto human foetal decellularised intestine

As a proof of principle study to demonstrate the usability of hSI_MABs for intestinal TE, a re-cellularisation experiment was designed. Foetal decellularised midguts were used as scaffolds in which 10^6 hFtSI_MABs per cm^2 were injected and cultured for a total of 9 days (2 days in Megacell proliferation medium and 7 days in 2% HS + TGFß).

One cycle of decellularisation was sufficient to generate white, translucent pieces of human foetal midgut acellular matrix (2-3 cm length), that preserved the

size and shape of the fresh tissue (Fig. 5-13A). Removal of nuclear components in the scaffolds following decellularisation was evidenced by the absence of DAPI staining on cryosections of the scaffolds (Fig. 5-13B). Residual DNA content of the scaffolds was quantified and showed a significant reduction compared to fresh tissue (Fig. 5-13C).

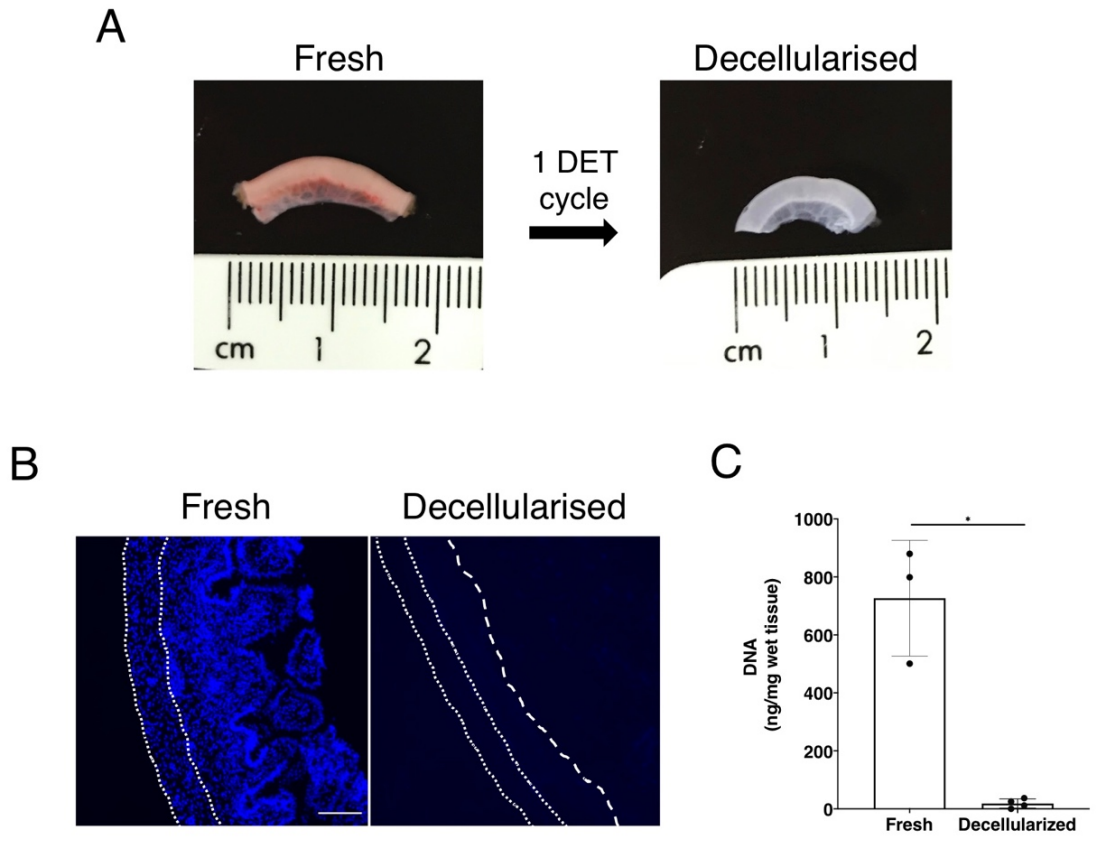

Figure 5-13: Human foetal midguts decellularisation

A) Gross appearance of fresh and decellularized human foetal midguts after 1 cycle of DET. **B)** Staining for DAPI to identify nuclei. Dot lines demarcates muscle wall; dashed line marks remaining of the submucosa layer. Scale bar: 100µm. **C)** DNA content of fresh (n= 3 biological samples) and decellularized (n= 4 biological samples) scaffolds. Data: mean ±SD. t-test: * p-val ≤0.05.

After the culture period, the presence, engraftment and spreading of cells were assessed. Whole mount staining confirmed that in all scaffolds (n= 4) cells were present after the culture period and were spread on the entire scaffold (Fig. 5-14A). On the other hand, decellularized scaffolds cultured without hSI_MABs (n= 1) showed the absence of cells over the entire scaffold (data not showed).

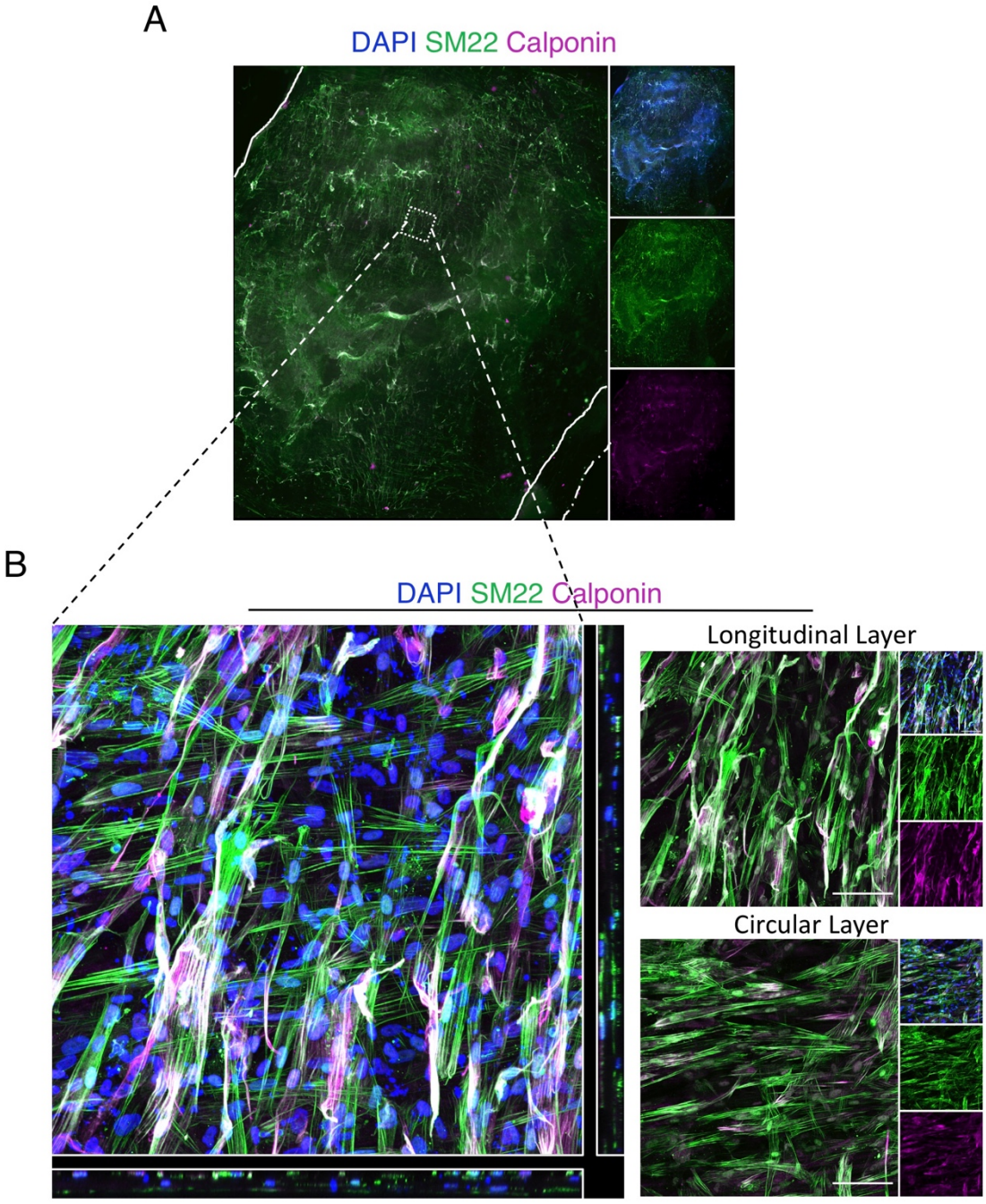
A
DAPI SM22 Calponin
B
DAPI SM22 Calponin
Longitudinal Layer
Circular Layer
C
cells per layer / total cells (%)
80
60
40
20
0
***
Longitudinal
Circular
positive cells / cells per layer (%)
80
60
40
20
0
*
*
Longitudinal
Circular
SM22
Calponin

Figure 5-14: Human foetal midgut muscle re-cellularisation

A) Whole mount staining of a re-cellularised scaffold showing the presence and spreading of hSI_MABs cells in blue (DAPI) throughout the scaffold. SM22 (green) and Calponin (magenta) hSI_MABs positive cells were also observed in the whole scaffold. White lines demarcate the gut scaffold, while dashed-dot white line delimits the mesentery region for tissue orientation. White square shows the area from which the magnification in B was taken. **B)** Left: orthogonal view of z-stack images showing cellular distribution inside the scaffold. Right: images of cells oriented into the outer/longitudinal and inner/circular layers. DAPI (blue), SM22 (green), Calponin (magenta). Scale bar 100 μm. **C)** Left: Graph showing the distribution of cells inside the scaffold as percentage of DAPI positive cells per layer over the total amount of DAPI positive cells per z-stack of high magnification field of view. Five random areas/images from n= 2 scaffolds were evaluated. Data: mean ±SD. t-test: *** p-val≤ 0.0001; Right: Graph showing the distribution of differentiated cells as percentage of SM22 or Calponin positive cells per layer, over the total amount of DAPI positive cells in the layer. Five random areas/images from n= 2 scaffolds were evaluated. Data: mean ±SD. t-test: * p-val≤ 0.05.

Further analysis of the whole mount staining allowed to determine that many of the cells present in the scaffold differentiated into SMCs, staining for SM22 and calponin (Fig. 5-14A). In addition, z-stack high magnification imaging showed that differentiated cells inside the scaffolds were located at two different levels along the thickness of the scaffold and oriented in a perpendicular manner. More specifically, cells of the outer layer were oriented along the mesentery axis of the scaffold, while deeper cells were orthogonal to it (Fig. 5-14B).

In order to determine whether cells preferentially distributed into one of the two layers, for each layer cells were counted from five high magnification images taken from random spots on the scaffolds (n =2 scaffolds). A significantly higher percentage of cells was found on the outer, longitudinal layer (60 ±9%) compared to the inner, circular layer (40 ±9%; Fig. 5-14C, left graph). Moreover, the percentage of differentiated cells in each layer was determined and showed that the longitudinal layer had more SM22 positive cells (60 ±15%) than Calponin positive cells (30 ±10%) compared to the circular layer (40 ±13% for SM22 and 19 ±6% for Calponin; Fig. 5-14C, right graph). Finally, the overall percentage of SM22 positive cells was higher than that of Calponin positive cells in the scaffolds, irrespective of their location in the two layers as determined by two-way ANOVA with multiple comparisons.

5.3 Discussion

In this work, the aim was to determine whether intestinal mesoangioblasts could be used as a source for enteric visceral SM. The contribution of the vascular compartment to enteric SM has never been proved, and only recently the feasibility of isolating mesoangioblasts from the intestine was proven in mice (Perin et al., 2019). However, studies on isolation and in-depth characterisation of intestinal mesoangioblasts and their differentiation capacity from human are still missing. In order to fulfil this aim, a preliminary isolation and characterisation of human intestinal mesoangioblast-like cells from foetal and paediatric intestinal biopsies was conducted. Following an established protocol (Tonlorenzi et al., 2007), hSI_MABs were successfully isolated and showed good proliferation capacity, maintaining an exponential growth rate at least for almost 40 days (i.e. 8 passages). Interestingly, hPaedSI_MABs seemed to grow at a faster rate compared to foetal cells. However, this finding could potentially have been biased by the low number of replicates used in the analysis, mainly due to the paucity of paediatric samples (Fig. 5-1).

Characterisation of hSI_MABs obtained with immunofluorescence and flow cytometry analyses revealed that these cells have a mesenchymal origin, as suggested by their expression of CD90, while expression of pericyte markers was variable amongst the samples, similarly to what shown for MABs isolated from skeletal muscle (Cappellari and Cossu, 2013). Whilst almost all cells expressed CD146 and NG2, the latter being visible with both immunofluorescence and flow cytometry analyses, the expression of PDGFRβ differed among samples and AP was present only in one of the seven samples analysed. It has been suggested that characterisation of pericytes is quite difficult given that the expression of their markers is not consistent and can differ over the lifetime of these cells (Armulik et al., 2011). Since it is agreed that the identification of pericytes should rely on the presence of two or more pericyte markers (Armulik et al., 2011), it can be argued that hSI_MABs isolated in this study can be considered pericytes. In fact, they have characteristics used to identify pericytes of several organs as described by Crisan et al. (2008). In example they express two pericyte markers

CD146 and NG2, show variable expression of CD140b (PDGFRß) and do not express the hematopoietic and endothelial marker, CD34.

In vitro, the ability of hSI_MABs to differentiate towards SM was assessed by means of immunofluorescence and calcium intracellular transit in response to Carbachol. In agreement with previous studies from the literature, hSI_MABs, when subjected to serum starvation with the additional supply of TGFβ, showed the capacity to differentiate into SMCs (Tonlorenzi et al., 2007) by expressing SM22 and Calponin. Interestingly, in the absence of TGFβ, SM differentiation was also observed. These results are in agreement with the concept of mesoangioblasts being tissue-specific mesodermal progenitors and also being able to generate vascular SMCs (Minasi et al., 2002; Sacchetti et al., 2016). In fact, as Dellavalle et al. (2011) showed, mesoangioblasts isolated from skeletal muscle biopsies could generate SMCs *in vitro* as well as contribute to the generation of skeletal muscle cells both *in vitro* and *in vivo*. In the present study, since cells were isolated from the intestine, their ability to generate SMCs was expected, while skeletal muscle differentiation was indeed not seen.

Remarkably, the ability of cells to generate mature SMCs was additionally proved with a functional assay. In fact, the capacity of differentiated cells to respond to Carbachol, a cholinergic agonist, was proven for cells cultured in differentiation media, with or without TGFβ, while the absence of response was observed in undifferentiated hSI_MABs. Interestingly, hSI_MABs cultured without TGFβ were able to positively respond to Carbachol, suggesting that TGFβ may not be essential for their differentiation towards SMCs. Moreover, the results seem to suggest a delayed and higher response to Carbachol in cells cultured in 2% HS alone, compared to cells cultured in 2% HS + TGFβ. However, the delayed peak in response detected in 2% HS in comparison to TGFß (Fig. 5-8C) could be attributed to the experimental set-up, and in particular to a difference in the position of the Carbachol injector relative to the camera. In fact, arguably a higher distance between the two elements would require a higher time lapse between Carbachol injection and the onset of cellular flushing. Furthermore, given the fact that only two experiments were performed and that a high variability in cellular response in 2% HS was present compared to other conditions,

additional experiments would be required to assess whether there is a difference in response between HS and TGFß treatments.

After assessing the *in vitro* characteristics of hSI_MABs, focus was put on their capacity to generate SMCs in *ex vivo* and *in vivo* settings. Cultures of small intestinal pieces were performed taking advantage of a new tissue culture system developed in the lab using a combination of metal and rubber rings (unpublished work). In this system, guts were kept alive using a simple basal media supplemented only with antibiotics to avoid culture contaminations. Moreover, gut contraction was avoided by maintaining the tissue adequately stretched on the aforementioned metal ring and exposing a flat portion of the gut wall which was used as an injury site and cell seeding site.

Although the system proved adequate for studying the integration of transplanted hSI_MABs in the intestine, it was not efficient in inducing their SM differentiation. In fact, cells, transplanted on both injured and uninjured guts, did not differentiate towards SM22 positive cells within 10 days of culture. The lack of differentiation could be due to an insufficient period of culture, even if cells have proven to be able to efficiently become SMCs *in vitro* within 7 days. However, while for differentiation *in vitro,* cells were provided with necessary nutrients and factors added to the medium of HS and TGFß (Guo and Chen, 2012; Tonlorenzi et al., 2007), the *ex vivo* system was conceived in a way that all chemical cues to induce hSI_MABs differentiation would be provided by the recipient mouse tissue (Zakhem et al., 2019). Given the scarce differentiation of hSI_MABs observed in this *ex vivo* system, it could be hypothesised that either hSI_MABs do not have the ability to generate SMCs when transplanted or the system does not provide sufficient cues (or the right cues) to stimulate differentiation of hSI_MABs within 10 days of culture.

Furthermore, by securing the tissue in place between a metal and a rubber ring, another important stimulus, the repetitive mechanical stretching, was prevented as this would have affected seeding, culture and traceability of cells. However, several studies have shown that mechanical stretch can positively affect cell growth and differentiation and indeed this factor has been taken into consideration while improving TE approaches (Riehl et al., 2012). In our *ex vivo*

system, removal of this very important mechanical cue, could have arguably reduced or delayed the differentiation of hSI_MABs.

In light of the limitations of the *ex vivo* system, a pilot transplantation study was performed in order to determine the *in vivo* potential of hSI_MABs to become SMCs. hSI_MABs were transplanted, via laparotomy, into the distal portion of the ileum of five $Rag2^{-}/\gamma c^{-}/C5^{-}$ mice. Four weeks after transplantation, it was noticed that GFP-transduced cells were spread over the distal portion of the dissected ileum. Although cells had not penetrated the gut wall and were located at the surface of the longitudinal muscle layer, many cells showed positivity for SM22. This proved the ability of hSI_MABs to generate SM in an *in vivo* setting, where some or all the right signalling cues, both chemical and physical, were provided. In order to test the role of hSI_MABs in the process of intestinal SM regeneration, an injury should be created on the gut wall prior the injection of these cells. Unfortunately, limitations in the animal licence did not allow muscular gut injury *in vivo* and hence restricted our investigation.

The absence of an injury, which resulted in an intact gut wall, constituted a physical barrier for hSI_MABs, blocking their migration inside the tissue and resulting in hSI_MABs' spreading only on the surface of the gut. The fact that intestinal MABs migrate is an important quality for intestinal TE. Urbani et al. (2018) demonstrated that mesoangioblasts isolated from skeletal muscle benefited from co-seeding together with fibroblasts to enhance the colonisation of a rat tissue engineered oesophagus. In contrast, hSI_MABs showed the capacity to colonise a long portion of the mouse ileum, suggesting that if singly seeded on the scaffold, they could colonize the whole patch, facilitating the process of creation of an engineered intestine.

As already mentioned, the intestine is a complex multi-layered organ, and its generation with TE approaches remains a challenge that researchers are trying to overcome (Clevers et al., 2019; Zakhem et al., 2019). Several successful experiments have regenerated the intestinal epithelial layer after implantation of synthetic and decellularised scaffolds seeded with intestinal organoids (Grant et al., 2015; Grikscheit et al., 2004; Kitano et al., 2017; Levin et al., 2013; Sala et al., 2011). However, as per its structure, different components need to be

generated and among them, a functional neuro-muscular wall constitutes a necessary aspect for the correct functioning of a tissue engineered intestine (Bitar et al., 2014; Zakhem et al., 2019). Given the lack of an established culture of smooth muscle precursors of the intestine, in this work, hSI_MABs were tested as a source of SMCs in a TE approach.

To begin with, human foetal midguts were chosen for decellularisation to derive scaffolds to test hSI_MABs potency in a TE context. Recently, Kajbafzadeh et al. (2018) used, for the first time, decellularised scaffolds derived from human foetal intestines as a bio-scaffold for augmentation cystoplasty in rabbits. Although using slightly different protocols, decellularised scaffolds were successfully generated in this study with one cycle of a detergent-enzymatic protocol, previously proven successful in generating different decellularised organs (Totonelli et al., 2012; Urbani et al., 2018; Urciuolo et al., 2018). Concerning intestinal muscular wall generation, as mentioned above, the correct orientation of the two muscle layers is of primary importance. Decellularised scaffolds, preserving the native extracellular matrix, are of great value because they maintain the structural, mechanical and biomolecular cues helpful in guiding cell proliferation, migration and differentiation (Bitar et al., 2014; Zakhem et al., 2019).

Cells were seeded on the flat open midgut scaffold, similarly to that shown by Urbani et al. (2018). After 9 days of culture, cells had colonised the entire scaffold. It was interesting to note that, in addition to the high migratory capacity that cells exhibited on the scaffold, they demonstrated SM differentiation potential as well as highlighted by immunostaining for early and mid-differentiation SM proteins, such as SM22 and Calponin (Rensen et al., 2007). Moreover, cells were able to orientate themselves inside the scaffold, orientating into two perpendicular layers of cells that resembled the native longitudinal and circular SM layers. Previous work attempting to produce an engineered intestinal muscular wall, failed to generate this spatial orientation without implementing several steps. For example, the creation of synthetic scaffolds mimicking the longitudinal and circular orientation of the two muscle layers has been attempted separately (Raghavan et al., 2010; Somara et al., 2009) or combined together (Kobayashi

et al., 2015). In contrast, to the best of my knowledge, here, it was shown for the first time that the simultaneous generation of orthogonally orientated SM layers could be obtained by simple seeding of a singular cell type, the hSI_MABs, into a decellularised human foetal midgut. More importantly, the newly observed layers were oriented in accordance with the scaffold orientation, with the external longitudinal layer following the major orientation of the intestine and the inner circular one the circumferential orientation. Arguably, the architecture of the extracellular matrix of the decellularised scaffold guided and oriented cells along the correct spatial location and helped inducing their differentiation without the need of additional mechanical cues. Furthermore, as previously suggested, extracellular matrix can provide important molecular cues for cell differentiation preserving the cellular niche of the native tissue (Martin et al., 2018). In fact, it was already shown that a decellularized intestine could preserve all the intestinal extracellular components and allow epithelia cell adherence (Totonelli et al., 2012).

This result is of great value, and is the foundation for future work aiming to assess the functionality of these muscle layers that could also benefit from the co-seeding with other cell types, including enteric neural crest cells, in order to fulfil the need of a fully functional neuro-muscular wall.

Chapter 6

Human small intestinal mesoangioblast-like cells (hSI_MABs): smooth muscle differentiation

6. Human small intestinal mesoangioblast-like cells (hSI_MABs): smooth muscle differentiation

6.1 Introduction

In the early 2000s, MABs were isolated from the dorsal aorta and characterized as a population of vessel-associated stem cells with the ability to generate mesoderm cell types (Minasi et al., 2002). Since then, MABs isolated from the vasculature of different tissues have been used to generate different mesodermal tissues, including smooth muscle cells (Tagliafico et al., 2004), and were used to repair dystrophic skeletal muscle (Galvez et al., 2006). However, as mentioned in the previous chapter, the isolation of human small intestinal MABs (hSI_MABs), from both foetal and paediatric intestine, as an alternative source of SMCs had never been performed and hence an in-depth characterization of their phenotype when subjected to differentiation towards SMCs was required.

With the emergence of Next-generation Sequencing, a steep increase in the number of publications using RNA-Seq technology was observed. This technique is extremely powerful and optimized to study whole transcriptomic differences between tissues and/or cell types and can be used to characterize the phenotype of cells at the molecular level. To the best of my knowledge, so far, no study has assessed the complete transcriptome of MABs using Next-Generation sequencing techniques. Moreover, only few studies focussed on the characterization of visceral, and in particular intestinal SM (Gurdziel et al., 2016; Larsson et al., 2008; Lee et al., 2015).

In this chapter, hSI_MABs subjected to four different culture conditions with the aim of generating SMCs, were studied and characterized at different levels by means of immunofluorescence, Western-blotting, RNA-Seq and quantitative-PCR.

6.2 Results

6.2.1 hSI_MABs FACS

The main focus of this chapter was to assess SM differentiation capacity of hSI_MABs. In order to reduce the risk of contamination when assessing characteristics of hSI_MABs at the transcriptomic level, cells were sorted in order to purify the population of study. According to the flow cytometry analyses performed and discussed in Chapter 5 section 5.2.1, some samples contained a low percentage of CD56 positive cells that could have been of neuronal origin. Therefore, a flow activated cell sorting (FACS) strategy was designed to remove possible neural contaminants from the culture. An additional cell surface marker, p75, expressed by enteric neural crest cells (NCCs) and their derivatives, was added to the list of markers previously used. After gating to remove debrides, and possible doublets, a negative selection for CD56 and p75 was performed, followed by a positive selection for the mesenchymal marker CD90 and the pericyte marker NG2 (Fig. 6-1A). No selection for CD140b or CD146 was performed to maintain a certain level of variability for the pericyte markers. The level of such variability was assessed in the sorted populations ($CD56^-$ / $p75^-$ / $CD90^+$ / $NG2^+$; Fig. 6-1B). The percentage of CD146 positive cells was 56 ±29%, while CD140b positive cells were 15 ±28% (Fig. 6-1C).

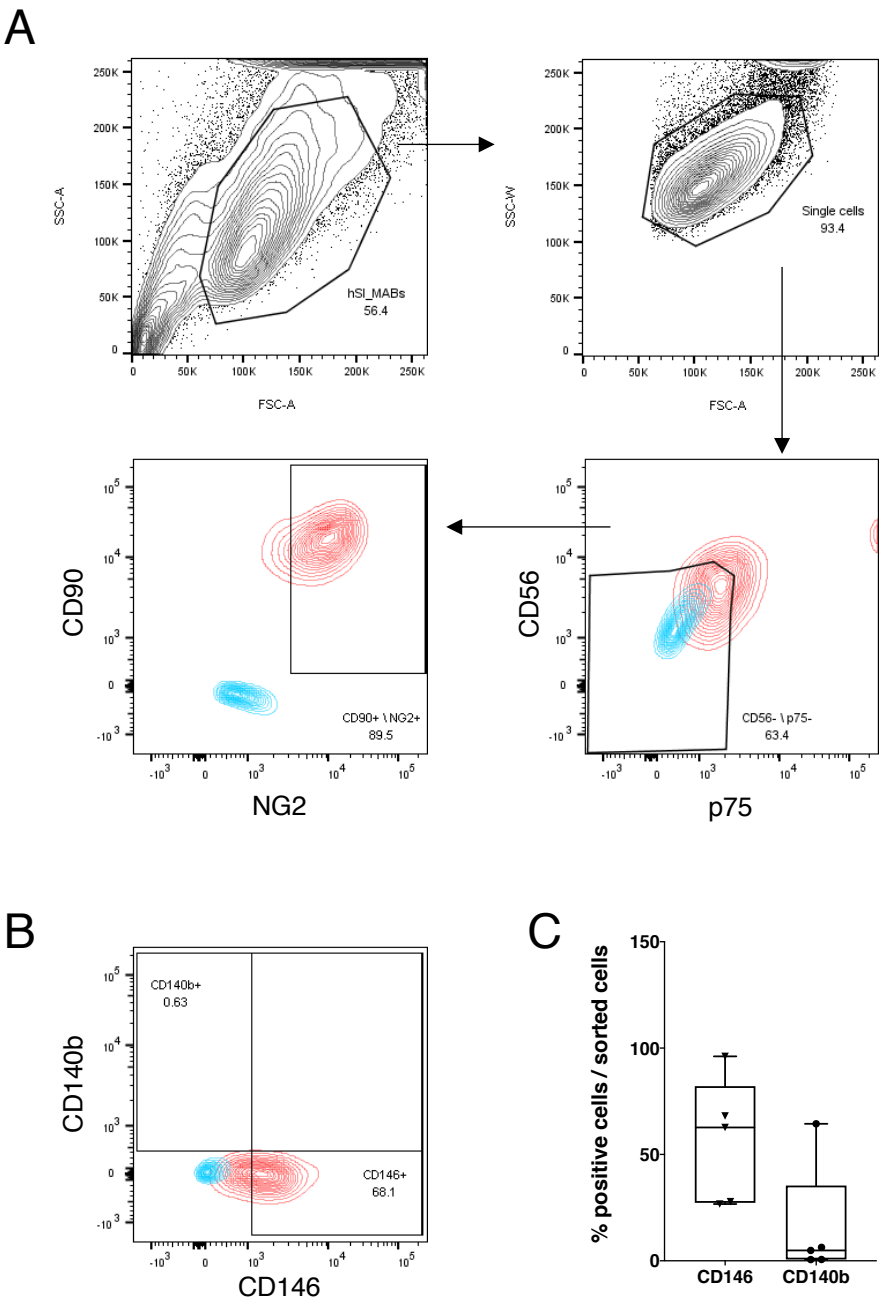

Figure 6-1: hSI_MABs FACS

A) Representative counter plot images showing gating strategy of hSI_MABs FACS. Cells were selected to remove debris, then to remove doublets. Negative selection for CD56 and p75 and positive selection for CD90 and NG2. (blue clouds represent unstained cells which are superimposed on red clouds stained samples) were then performed. **B)** Representative counter plot image of sorted cells showing positivity for the pericytes' markers CD146 and CD140b (blue clouds represent unstained cells, red clouds stained sample). **C)** Box and whiskers plots showing percentage of positive cells for pericytes' markers CD146 and CD140b in the sorted populations (n =5 biological samples).

6.2.2 hFtSI_MABs RNA-Seq

To better understand the mechanism of small intestinal mesoangioblasts differentiation towards SMCs, an RNA-Seq experiment was performed. In this experiment, proliferating hFtSI_MABs cultivated in Megacell (hereafter called “M”) were compared with cells differentiated with the three different conditions (2% HS =“H”, 2% HS + TGFß =“T”, 2%HS + TGFß-I =”I”) for 7 days, where HS is horse serum, TGFb is Transforming growth factor ß and I is TGFb inhibitor . For each treatment three biological replicates were sequenced using a 3’-tag approach.

In total, between 4.3 and 9.2 million raw reads were obtained per sample and after trimming, all replicates had more than 97% high quality reads. Between 74 and 79% of clean reads were mapped without ambiguity onto the human genome (Ensembl assembly version GRCh38.p12 96.38) and were used to generate the count matrix. Only genes with count per million (CPM) >1 in at least two libraries were considered for analysis (total number of genes 14,822).

To explore differences between libraries, a two dimensional principal component analysis (PCA) was performed (Fig. 6-2A). The figure shows that replicate samples from the same treatment cluster together and that proliferating cells (M) are separated from the other groups, followed by the group T, while group H and I sit closer in the PCA plot.

Subsequently, differences in gene expression were assessed by means of a general linear model in which the differentiated conditions (i.e. H, T, I) were compared with M (i.e. the reference). In total 3,414 genes were found as differentially expressed genes (DEGs), with a cut-off false discovery rate FDR ≤0.01 and a fold change ≥l1.5l. To confirm PCA results, the relative distances between samples were assessed by plotting a dendrogram (Fig. 6-2B), which showed that M was the most distant compared to the other treatments, and I and H the closest.

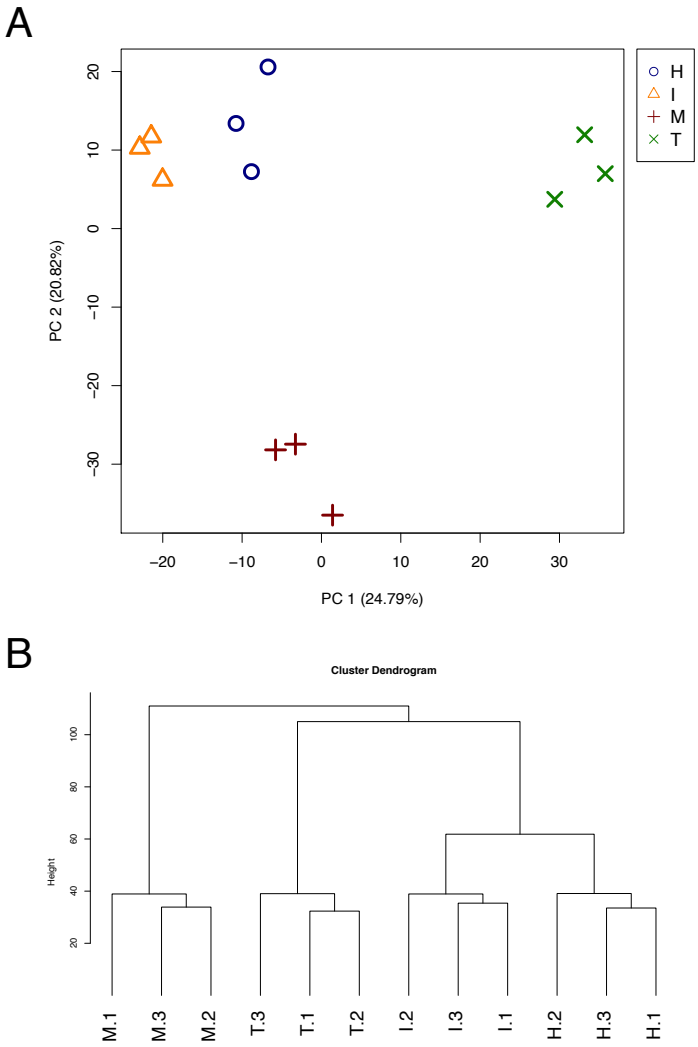

Figure 6-2: PCA and samples clustering

A) PCA showing differences between libraries (M =Megacell, H =2% HS, T =2% HS + TGFß, I =2% HS + TGFß-I). Each symbol represents a biological replicate (n =3 per treatment). **B)** Dendrogram of all samples based on all DEGs identified with a general linear model (cut-off p-value ≤0.01 and a fold change ≥|1.5|).

A heatmap of all 3,414 genes was then plotted and DEGs were divided into clusters based on similar expression levels. The dendrogram of the genes was cut off at the height of 90% and such cut generated eight different clusters (Fig. 6-3). The average expression level in each cluster is depicted in figure 6-4. Overall, clusters contained a variable number of genes, varying from a minimum of 25 genes in cluster 8 to a maximum of 844 genes in cluster 1. Cluster 1, the most numerous, contained genes highly expressed in T compared to other treatments, whereas genes expressed at low levels in T were found in cluster 5;

cluster 2 contained genes highly expressed in M and less expressed in T and cluster 3 was composed of genes expressed at low levels in I and H, in comparison to T and M. Finally, genes highly expressed in H and I were found in cluster 4 and also cluster 6, where genes were highly expressed in T as well. Finally, clusters 7 and 8 contained less than 50 genes each, with a variable expression in the different treatments.

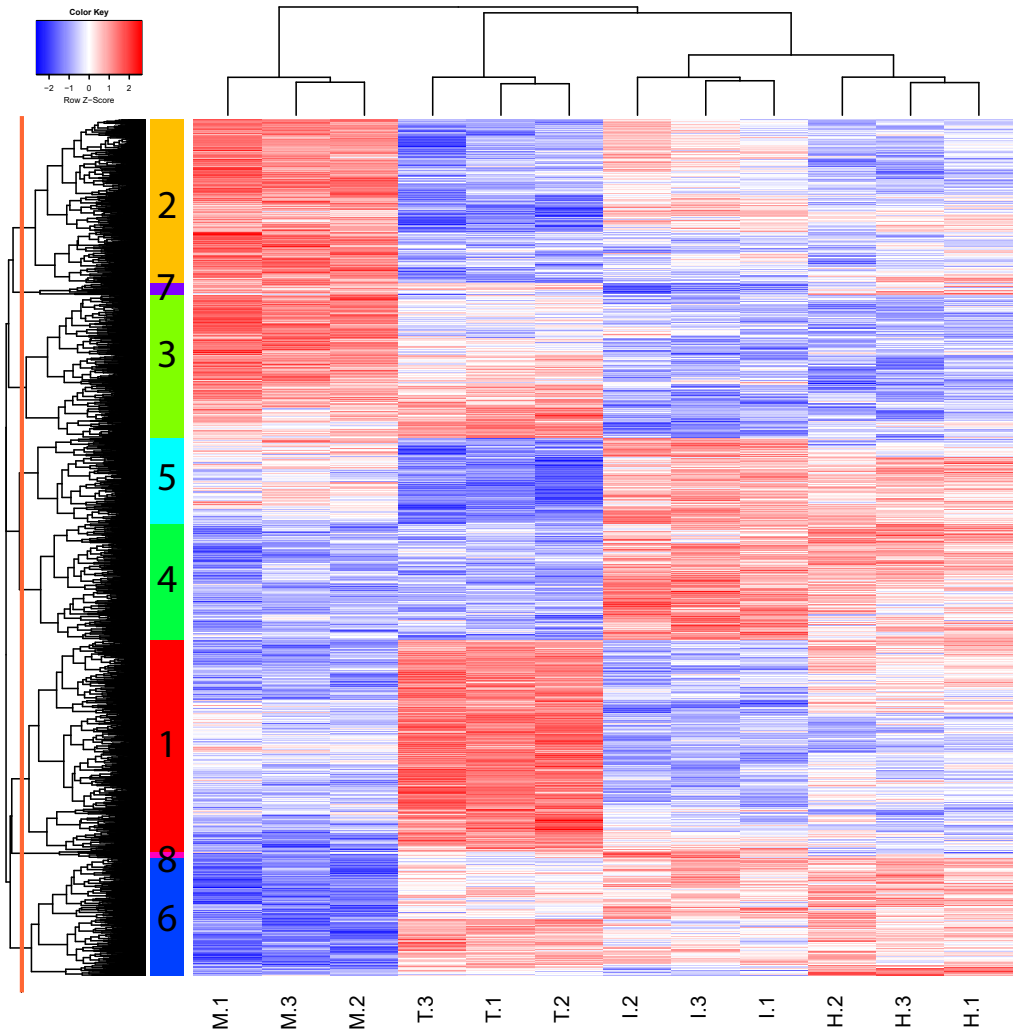

Figure 6-3: DEGs' heatmap

Heatmap of all DEGs identified from the general linear model (cut-off p-value ≤0.01 and a fold change ≥|1.5|). Expression levels are expressed as $\log_2$(CPM) scaled to have mean =0 and SD =1, and are colour coded, with higher expression in red and lower in blue. Coloured column between the dendrogram of the genes and the heatmap highlights the subdivision into clusters with each cluster being represented by one colour and one number (cluster numbers refer to Figure 6-4). Clusters were generated by cutting the gene dendrogram at 90% of its height (vertical orange line).

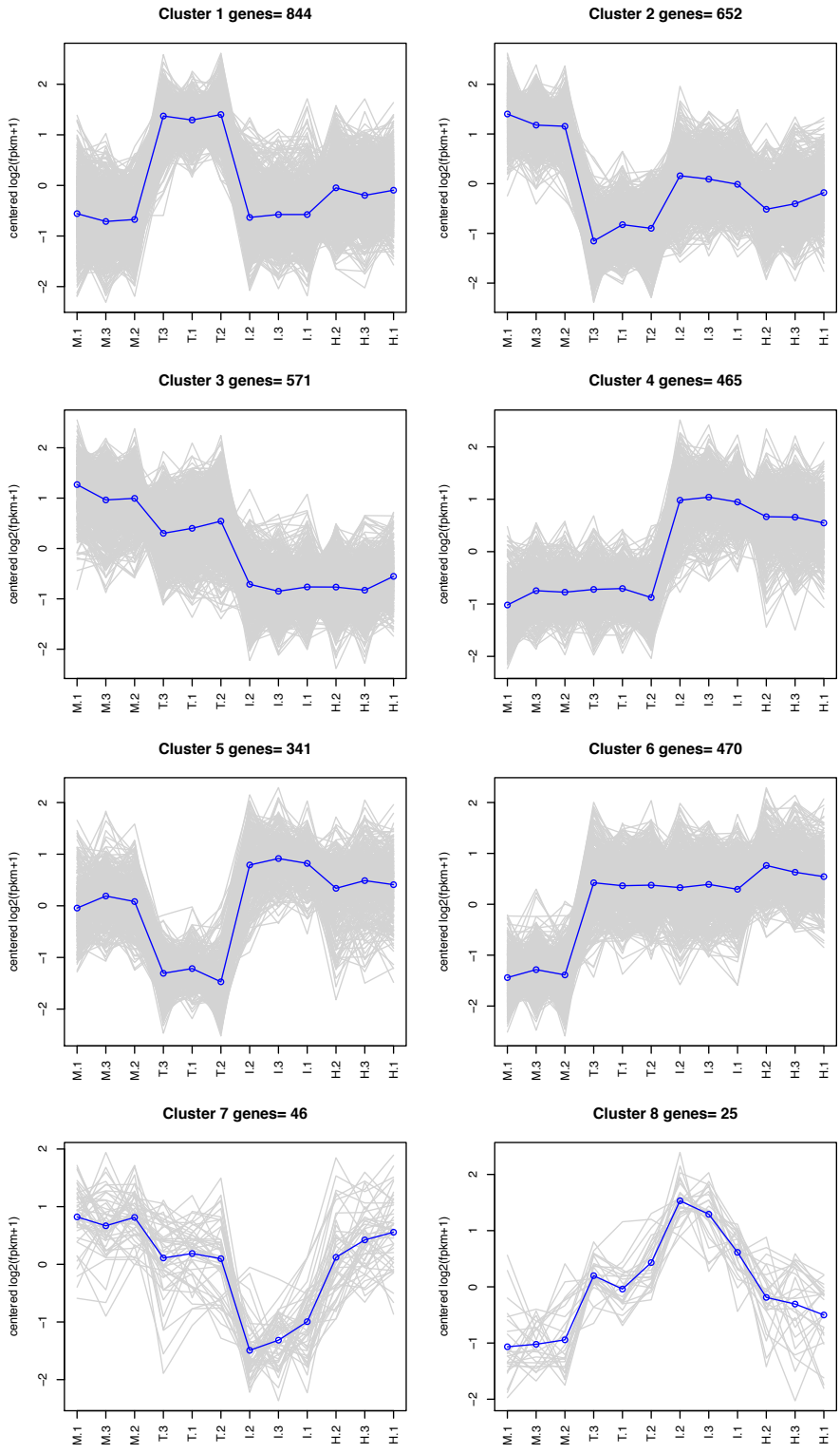

Figure 6-4: Clusters of gene expression

Expression levels of genes belonging to each cluster identified in the DEGs' heatmap. Grey lines represent expression levels of each single gene in each sample. Blue dots are the average expression levels of all genes in the cluster in each sample with blue line connecting each dot.

To define, at molecular level, the main features of cells in each group, a test for gene ontology (GO) categories over-represented in clusters was performed. In particular, attention was drawn to cluster 1 and 2 because they contained genes highly expressed in T and M respectively (Fig. 6-5; 6-6; 6-7 and Fig. 6-8; 6-9; 6-10), allowing description of the main characteristics of T (i.e. cluster 1) and the differences between T and M (i.e. cluster 2). Similarly, analyses focused on cluster 4 for a better understanding of common features in H and I (Fig. 6-11; 6-12; 6-13) and on cluster 6 for characteristics peculiar to the three differentiated cells, H, I and T, in comparison to M (Fig. 6-14; 6-15; 6-16).

Cellular component domain in cluster 1 was enriched for GO categories mainly associated with endoplasmic reticulum and cytoskeletal components, commonly seen in muscle cells, and cell-cell and cell-matrix adhesion complexes (Fig. 6-6). In contrast, cluster 2 was enriched for GO categories belonging to cell division, mitosis and DNA transcription (Fig. 6-8). In cluster 2, similar categories involved in cell proliferation were evidenced also when looking at the molecular function and biological process domains (Fig. 6-9; 6-10). For example, DNA replication initiation and stem cell population maintenance were two of the biological process GO categories identified as enriched in cluster 2 (Fig. 6-10). Cluster 1, on the other hand, was enriched for GO associated with the TGFß pathway, as evidenced by the presence of TGFß and SMAD binding categories (Fig. 6-6). Moreover, muscle GO categories (e.g. muscle contraction and vascular smooth muscle development) were also enriched among the biological process categories (Fig. 6-7), together with GO associated with ion activity in the cell (e.g. calcium ion transmembrane transport activity; Fig. 6-6).

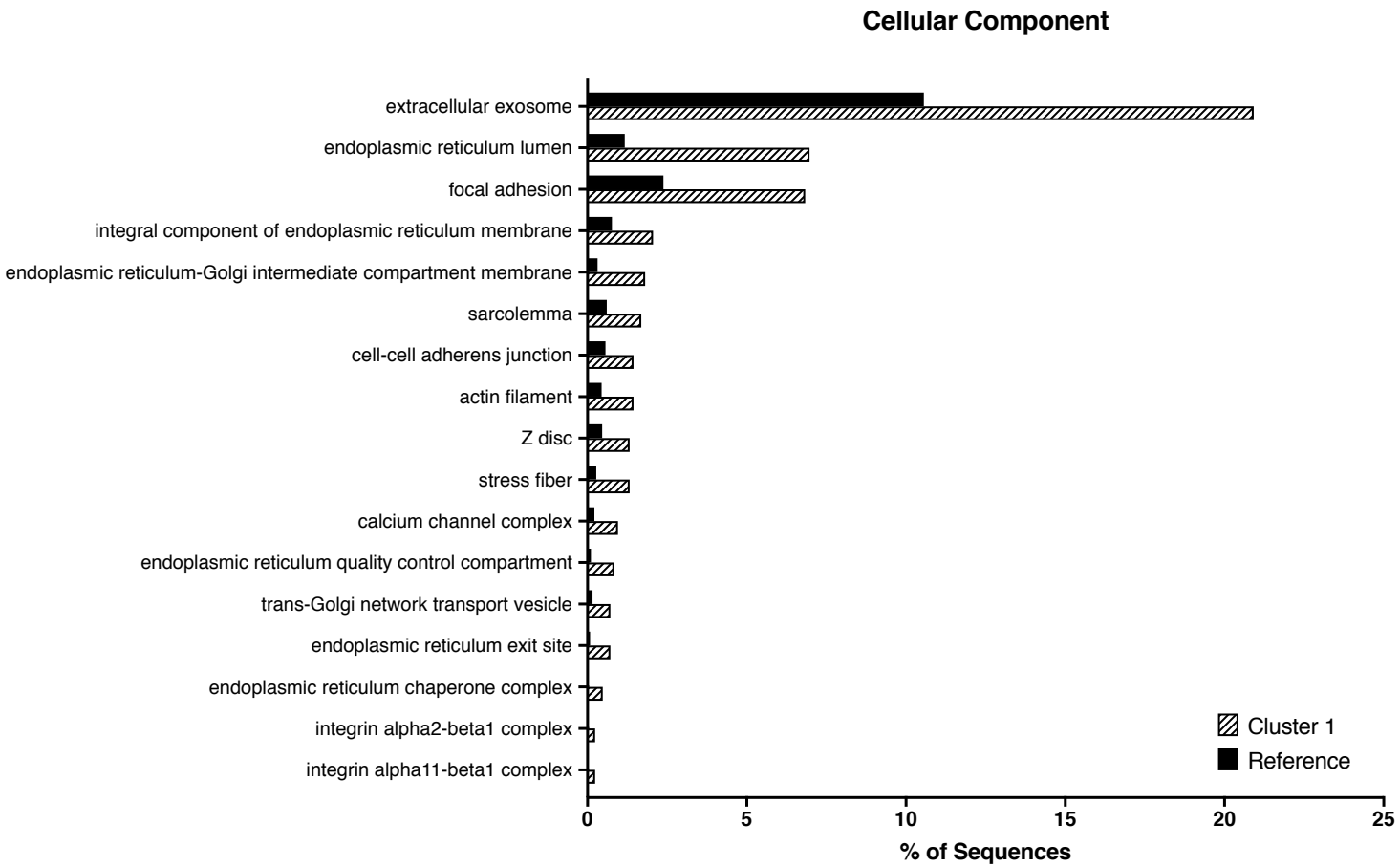

Figure 6-5: Over-represented Cellular Component GO categories in cluster 1

Enrichment analysis on DEGs from cluster 1 in comparison to the reference transcriptome (i.e. all genes except genes from cluster 1; “reference” in the figure). Enriched GO categories were analysed using Fisher’s exact test and considered significant with a p-value <0.01. Selected GO categories plotted in the figure.

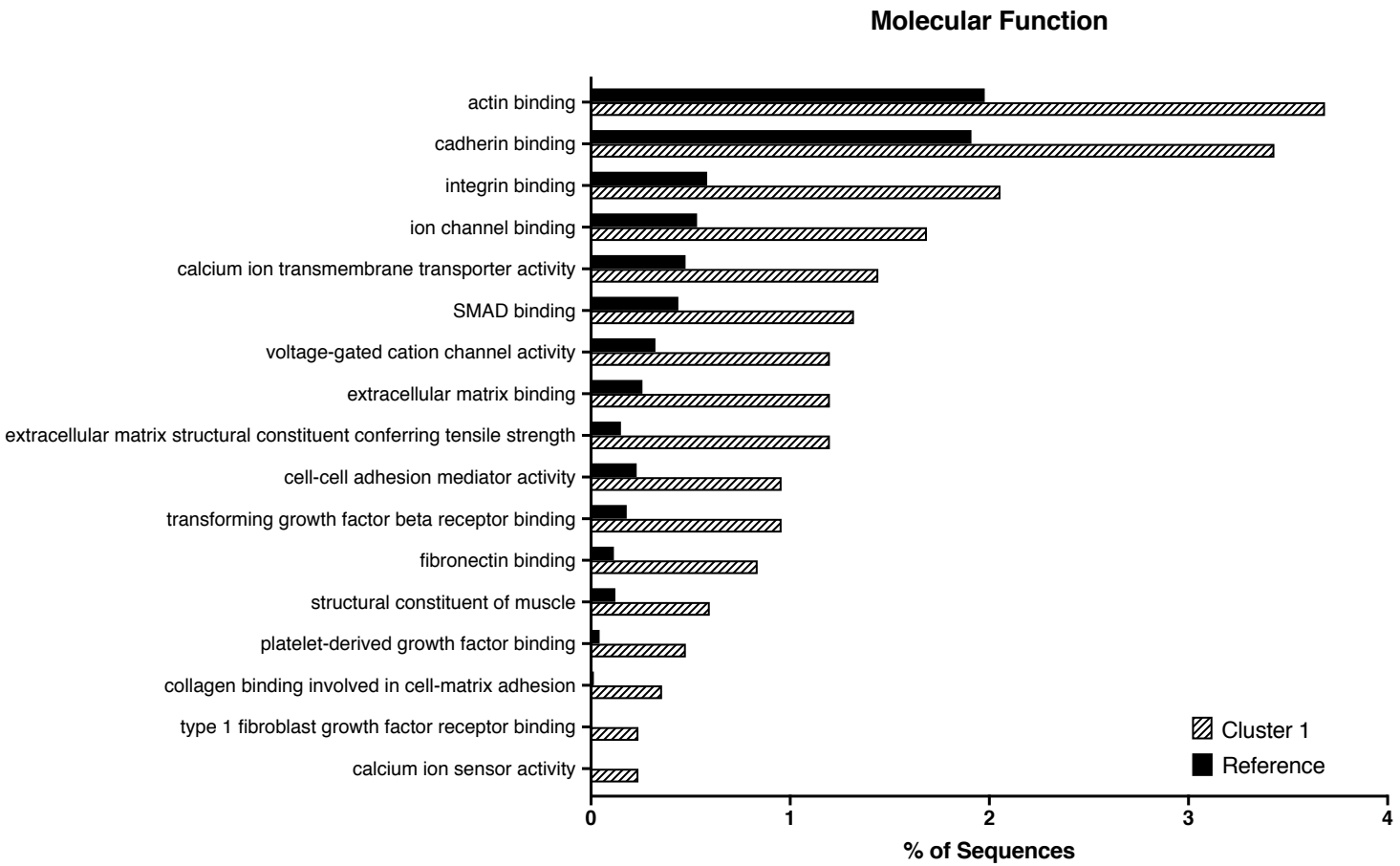

Figure 6-6: Over-represented Molecular Function GO categories in cluster 1

Enrichment analysis on DEGs from cluster 1 in comparison to the reference transcriptome (i.e. all genes except genes from cluster 1; “reference” in the figure). Enriched GO categories were analysed using Fisher’s exact test and considered significant with a p-value <0.01. Selected GO categories plotted in the figure.

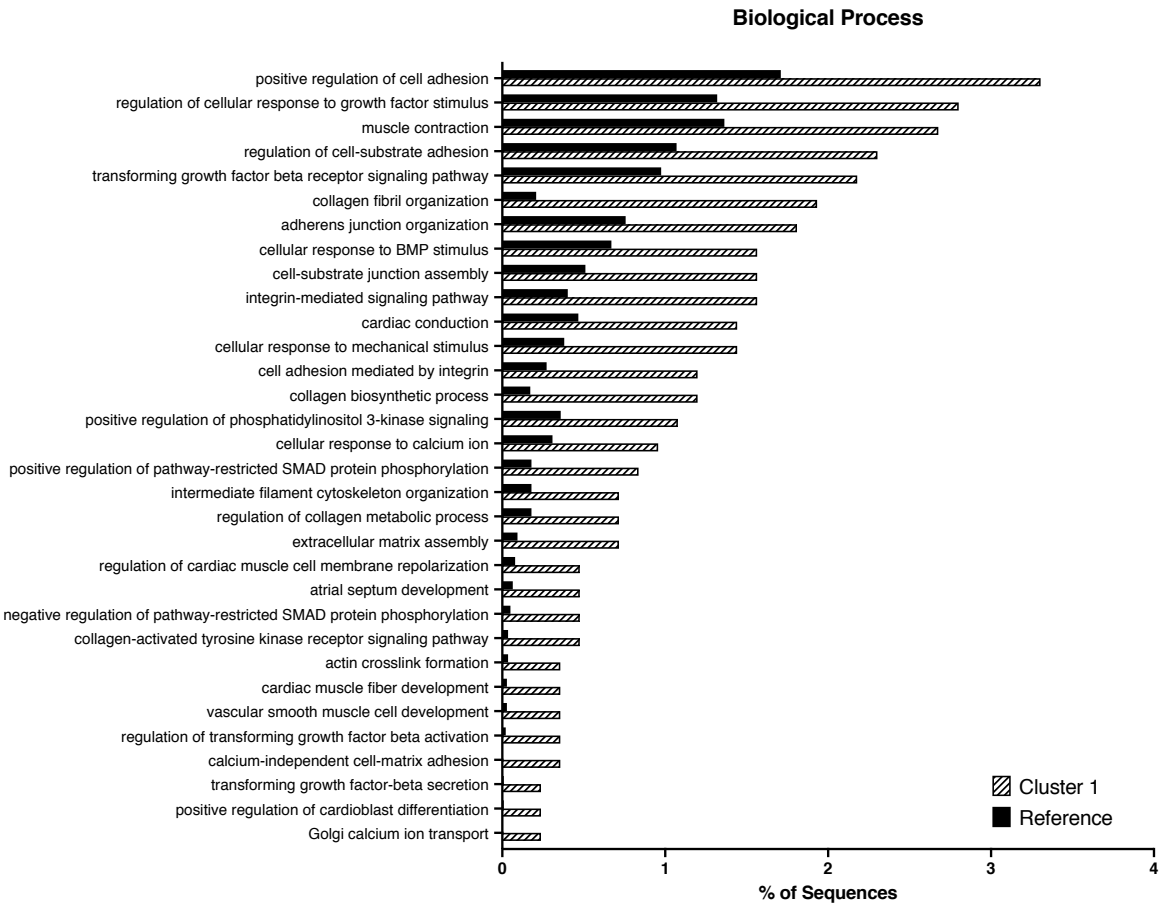

Figure 6-7: Over-represented Biological Process GO categories in cluster 1

Enrichment analysis on DEGs from cluster 1 in comparison to the reference transcriptome (i.e. all genes except genes from cluster 1; “reference” in the figure). Enriched GO categories were analysed using Fisher’s exact test and considered significant with a p-value <0.01. Selected GO categories plotted in the figure.

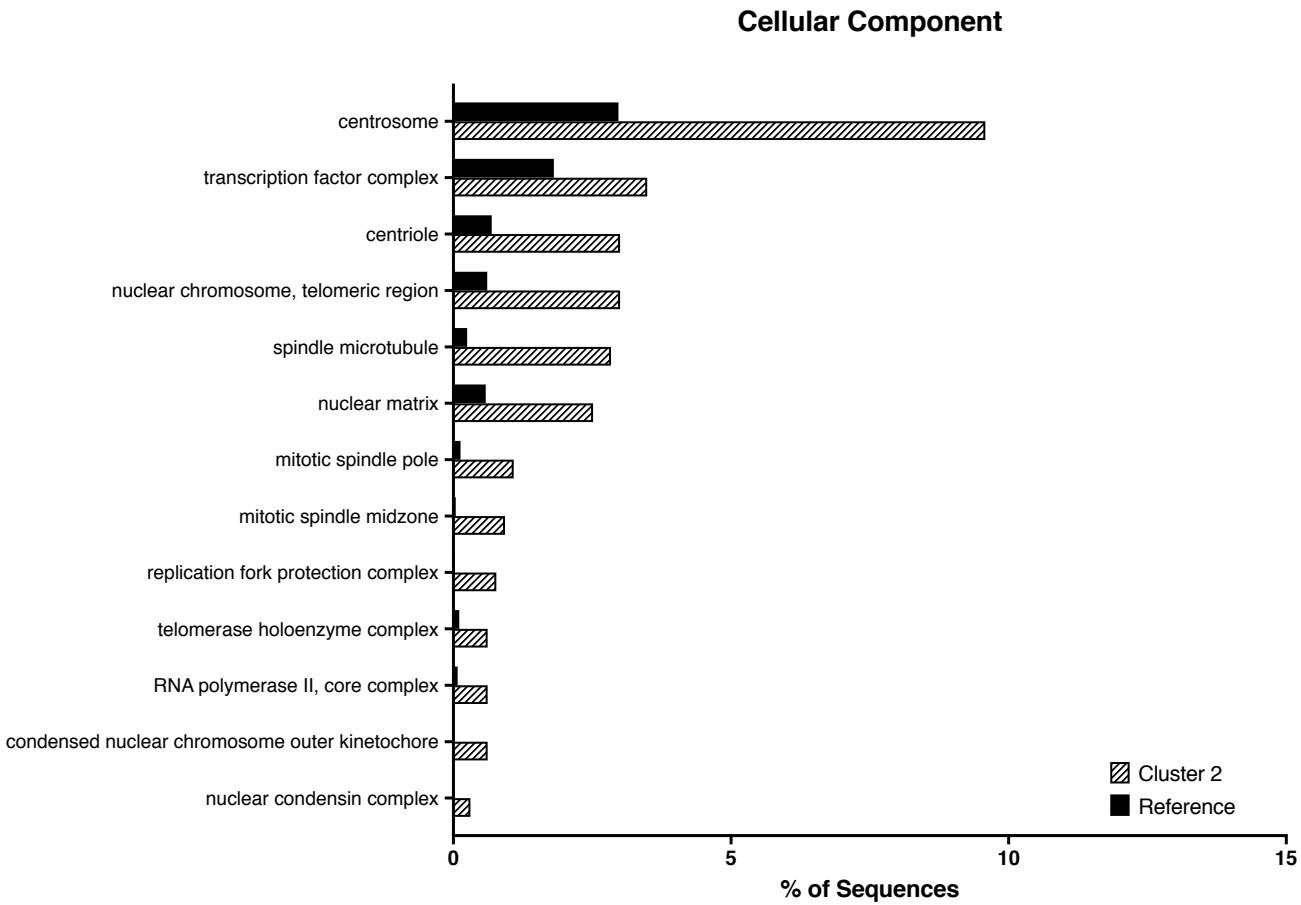

Figure 6-8: Over-represented Cellular Component GO categories in cluster 2

Enrichment analysis on DEGs from cluster 2 in comparison to the reference transcriptome (i.e. all genes except genes from cluster 2; “reference” in the figure). Enriched GO categories were analysed using Fisher’s exact test and considered significant with a p-value <0.01. Selected GO categories plotted in the figure.

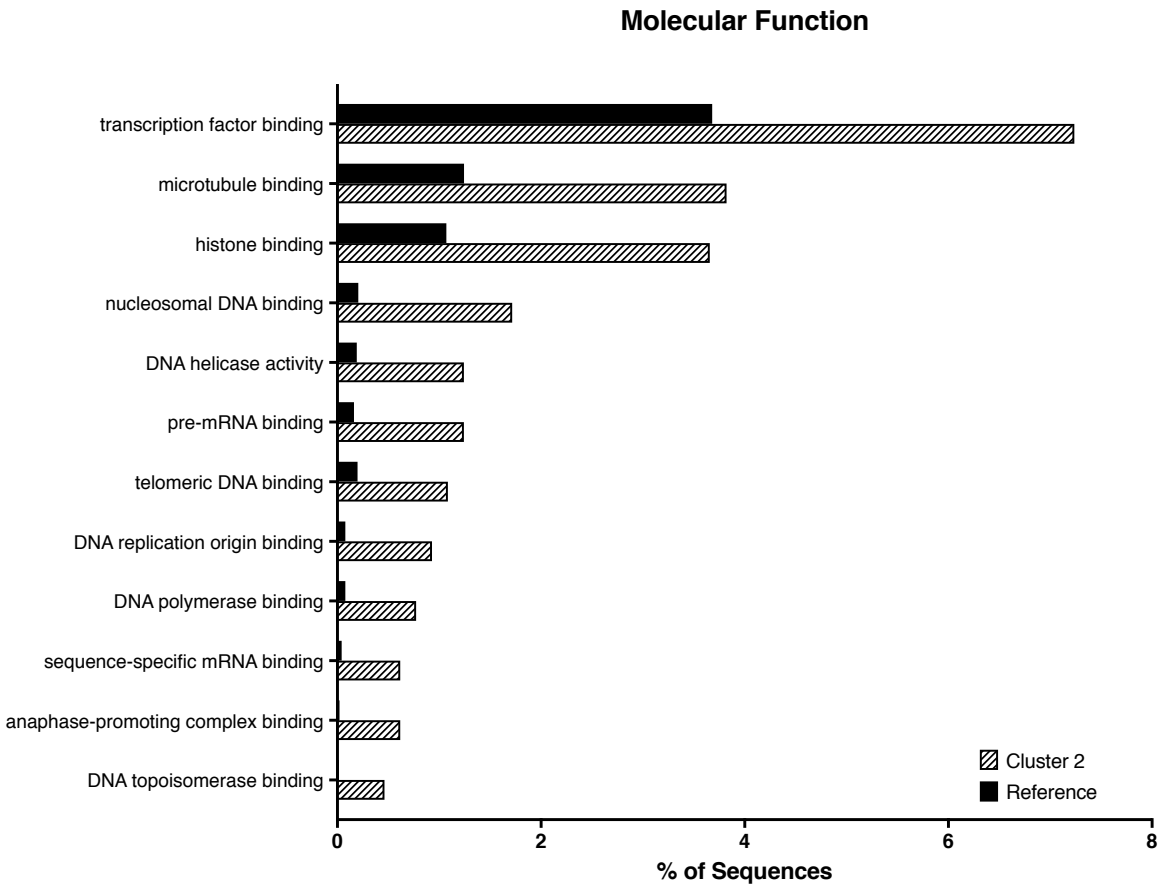

Figure 6-9: Over-represented Molecular Function GO categories in cluster 2

Enrichment analysis on DEGs from cluster 2 in comparison to the reference transcriptome (i.e. all genes except genes from cluster 2; “reference” in the figure). Enriched GO categories were analysed using Fisher’s exact test and considered significant with a p-value <0.01. Selected GO categories plotted in the figure.

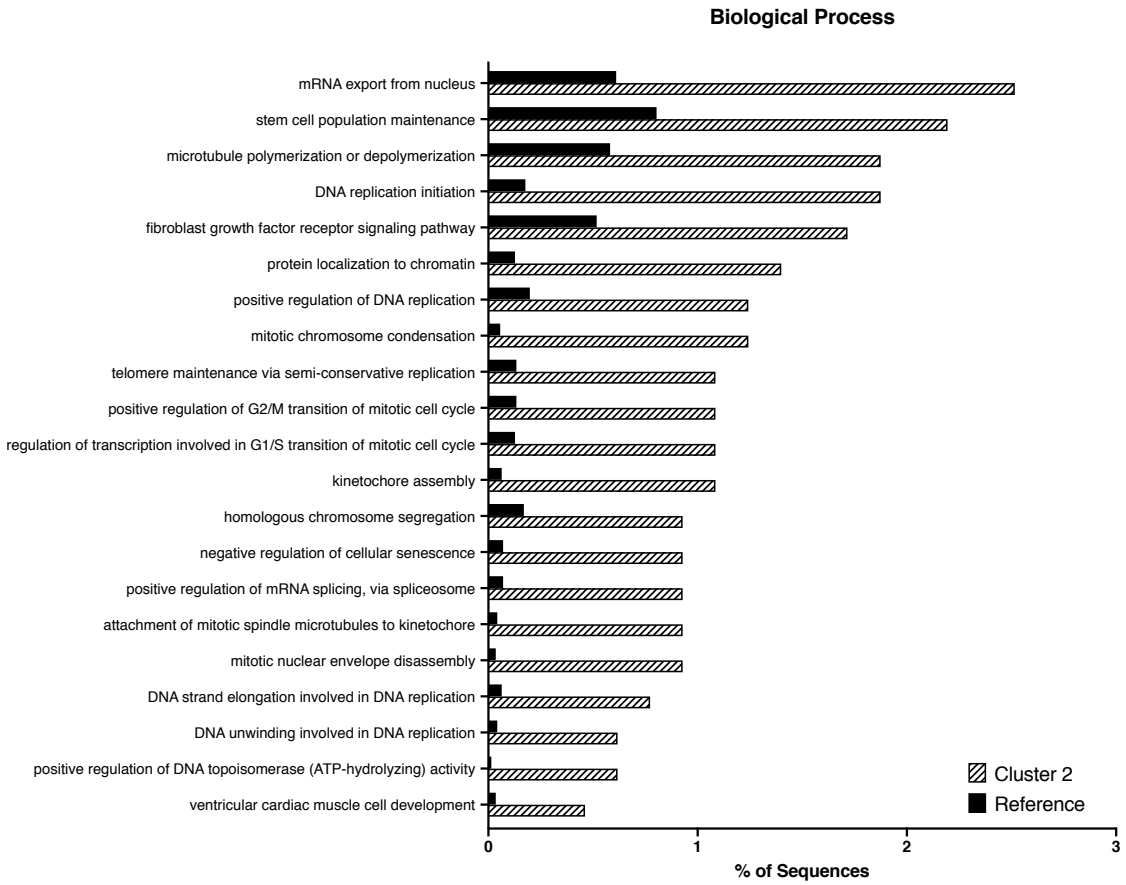

Figure 6-10: Over-represented Biological Process GO categories in cluster 2

Enrichment analysis on DEGs from cluster 2 in comparison to the reference transcriptome (i.e. all genes except genes from cluster 2; “reference” in the figure). Enriched GO categories were analysed using Fisher’s exact test and considered significant with a p-value <0.01. Selected GO categories plotted in the figure.

Cluster 4 showed enriched GO categories belonging to cytoplasmic messengers of several signalling pathways, such as inositol-phosphate and G-proteins. Among the enriched pathways, MAPK, EGF and IGF pathways were identified (Fig. 6-11; 6-12). Similar to cluster 1, several GO mapping to the cell interaction with the extracellular matrix, were enriched in cluster 4, such as smooth muscle cell-matrix adhesion. In addition, enrichment for cell migration processes was found in cluster 4.

Interestingly, in both cluster 4 (Fig. 6-11; 6-12) and cluster 6 (Fig. 6-13; 6-14; 6-15), enriched GO that could be ascribed to muscle cells were present. These were associated with several aspects of muscle physiology, in particular muscle contraction and smooth muscle cell proliferation. Moreover, other similarities were evidenced at the level of signalling pathways, in particular the presence of enriched GOs related to the insulin-growth factor pathway, insulin binding, the regulation of MAP kinase and ERK cascade. Additionally, cluster 4 was also enriched for stem cell proliferation.

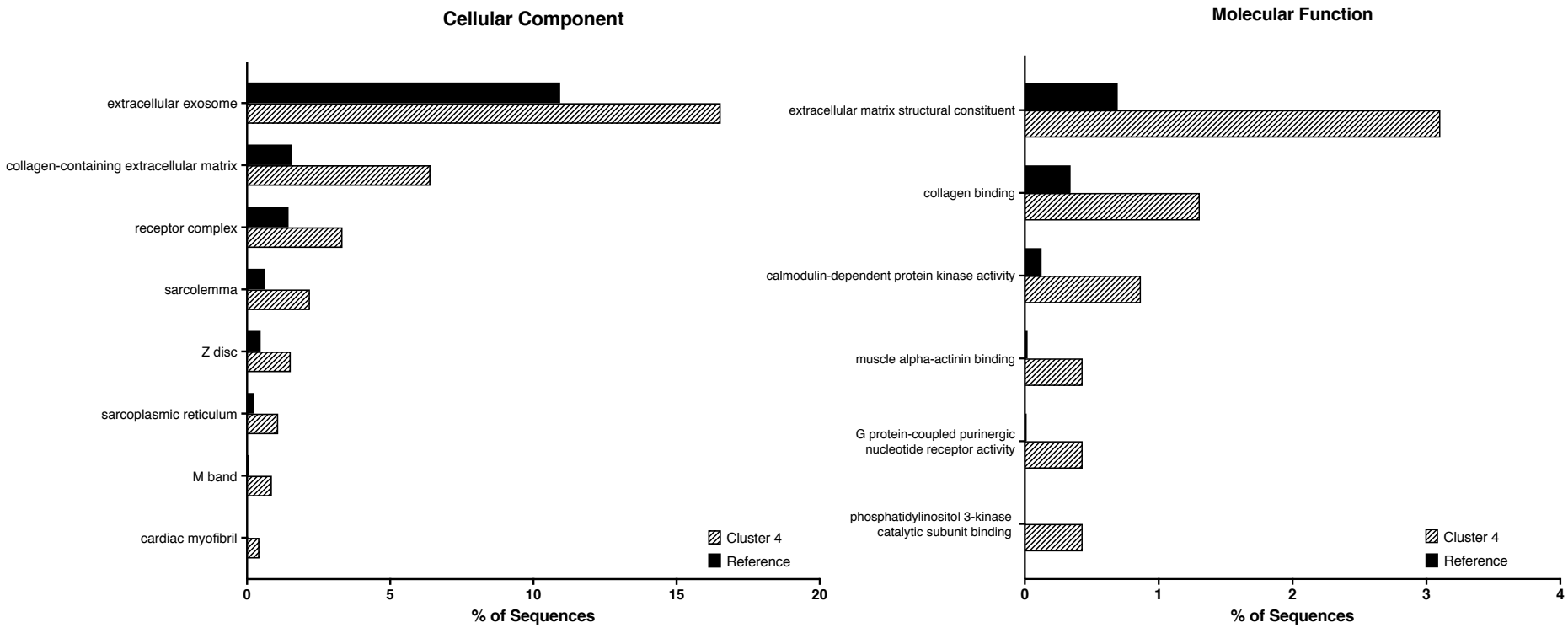

Figure 6-11: Over-represented Cellular Component and Molecular Function GO categories in cluster 4

Enrichment analysis on DEGs from cluster 4 in comparison to the reference transcriptome (i.e. all genes except genes from cluster 4; “reference” in the figure). Enriched GO categories were analysed using Fisher’s exact test and considered significant with a p-value <0.01. Selected GO categories plotted in the figure were subdivided according to two domains of the GO classification: Cellular Component (left) and Molecular Function (right).

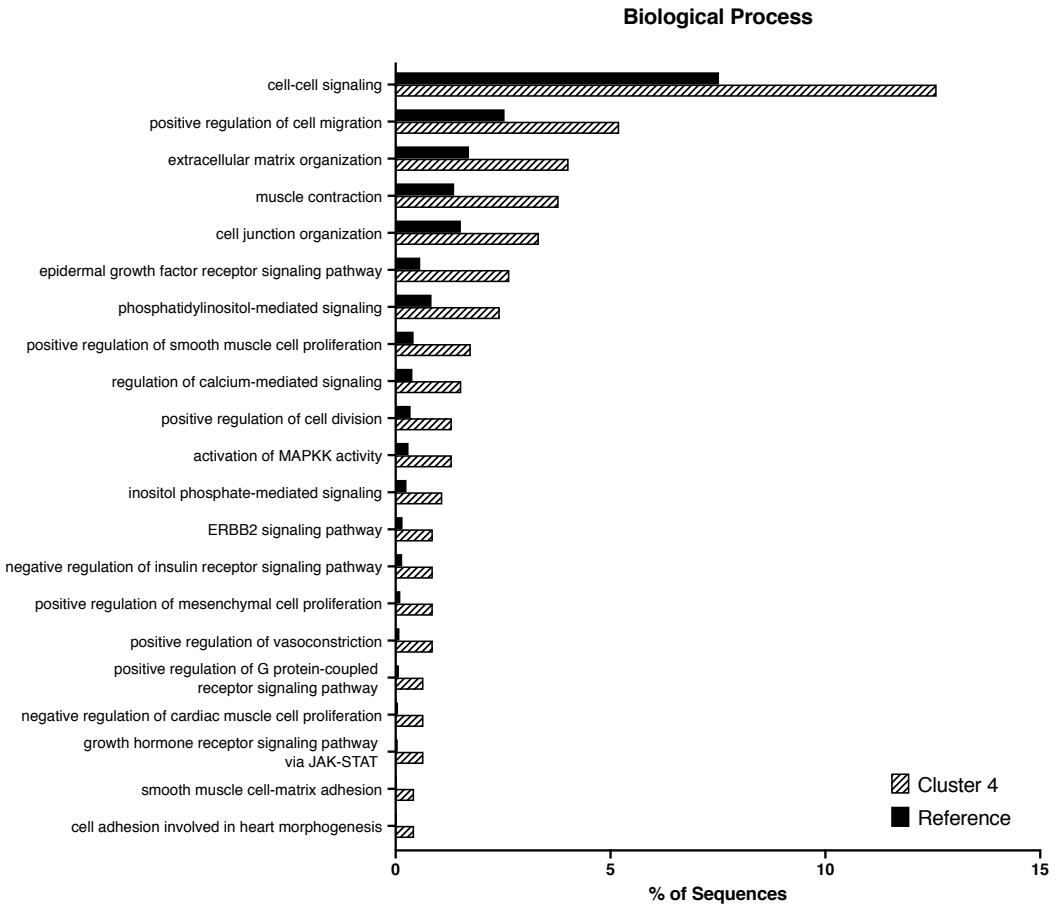

Figure 6-12: Over-represented Biological Process GO categories in cluster 4

Enrichment analysis on DEGs from cluster 4 in comparison to the reference transcriptome (i.e. all genes except genes from cluster 4; “reference” in the figure). Enriched GO categories were analysed using Fisher’s exact test and considered significant with a p-value <0.01. Selected GO categories plotted in the figure.

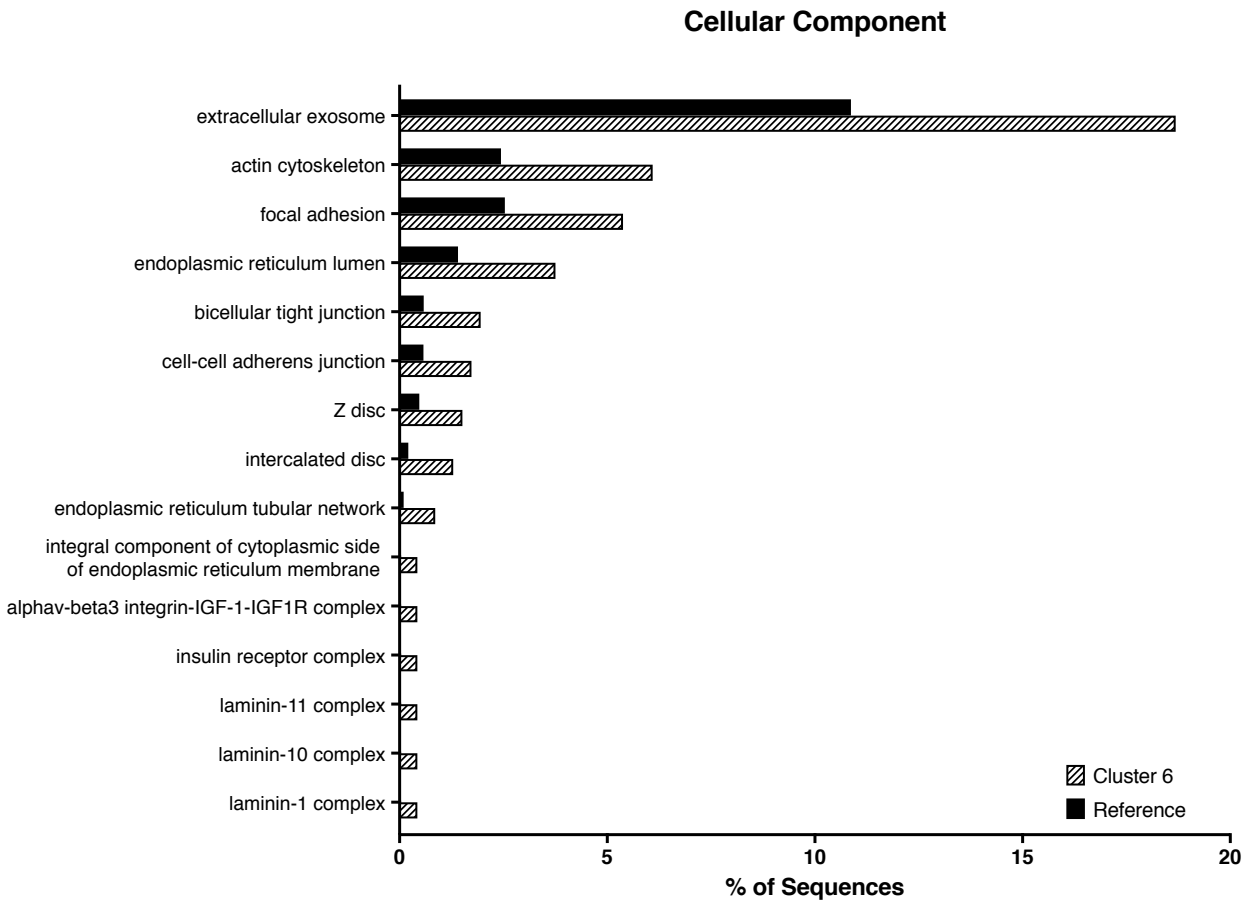

Figure 6-13: Over-represented Cellular Component GO categories in cluster 6

Enrichment analysis on DEGs from cluster 6 in comparison to the reference transcriptome (i.e. all genes except genes from cluster 6; "reference" in the figure). Enriched GO categories were analysed using Fisher's exact test and considered significant with a p-value <0.01. Selected GO categories plotted in the figure.

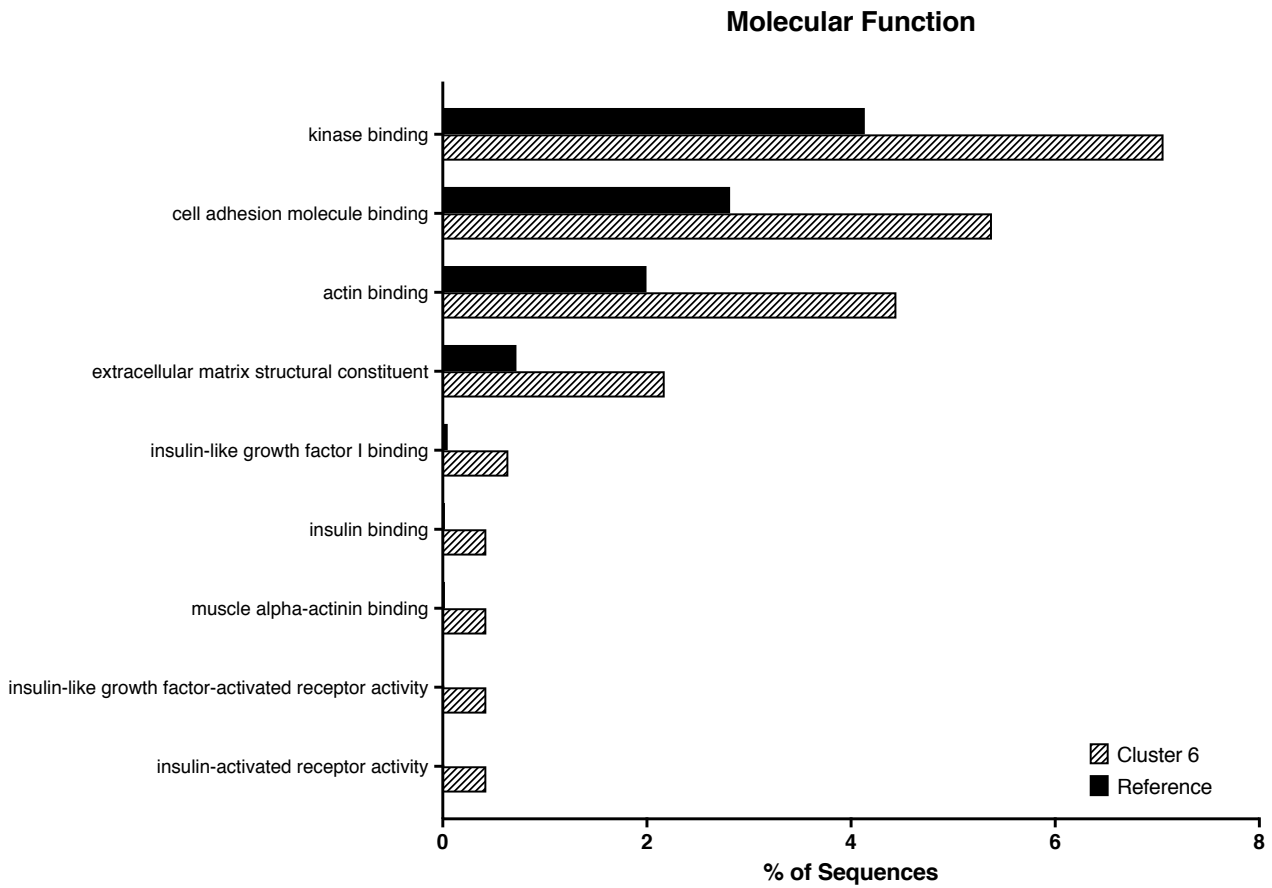

Figure 6-14: Over-represented Molecular Function GO categories in cluster 6

Enrichment analysis on DEGs from cluster 6 in comparison to the reference transcriptome (i.e. all genes except genes from cluster 6; “reference” in the figure). Enriched GO categories were analysed using Fisher’s exact test and considered significant with a p-value <0.01. Selected GO categories plotted in the figure.

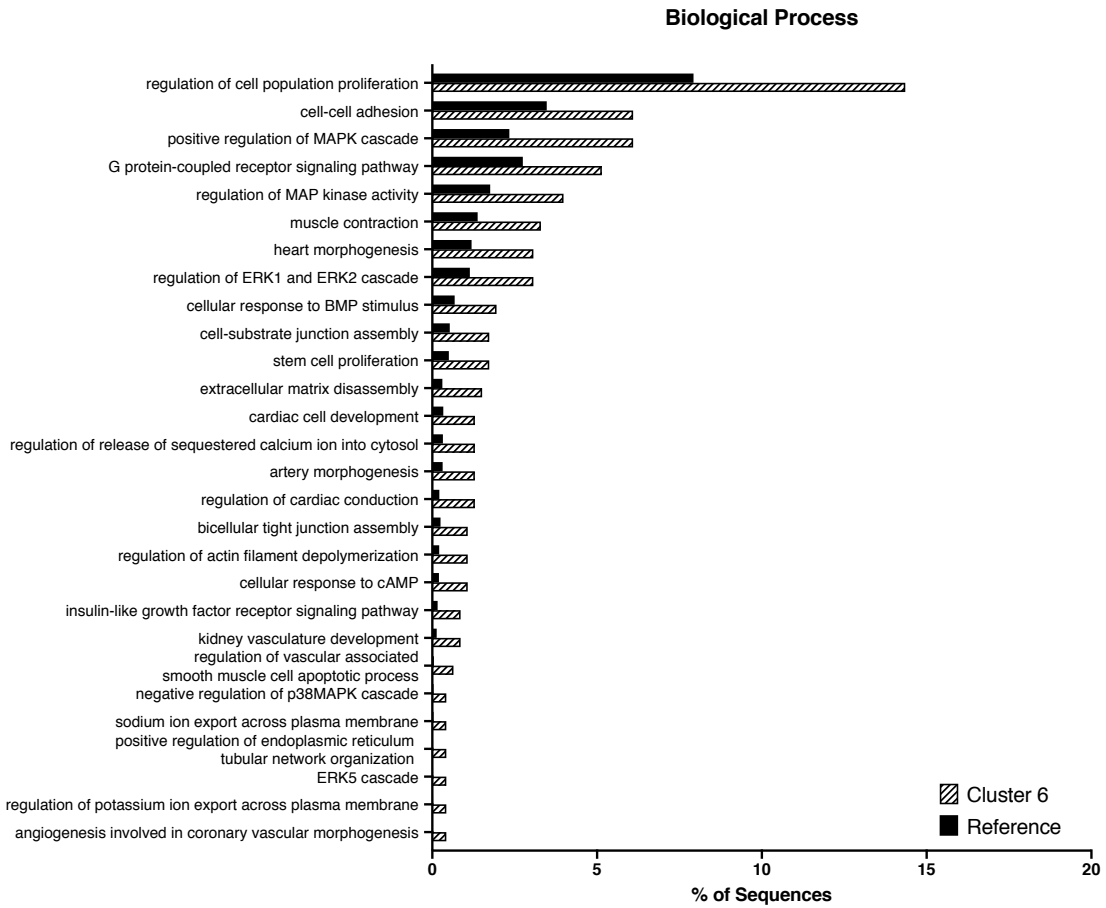

Figure 6-15: Over-represented Biological Process GO categories in cluster 6

Enrichment analysis on DEGs from cluster 6 in comparison to the reference transcriptome (i.e. all genes except genes from cluster 6; “reference” in the figure). Enriched GO categories were analysed using Fisher’s exact test and considered significant with a p-value <0.01. Selected GO categories plotted in the figure.

Different analyses were then performed to determine whether gene expression profile of differentiated hFtSI_MABs closely resembled mature intestinal SMCs. First, a list of intestinal SM specific markers from Lee et al. (2015) was taken and, within the DEGs, the expression of those genes checked (Fig. 6-16). Most of these genes encode for cytoskeletal proteins known to be involved in muscle contraction, such as the smooth muscle specific myosin heavy chain-11 (MYH11), and calponin1 (CNN1). From the original list, 11 out of 13 genes were found among the DEGs and were all highly expressed in T (apart from desmin, DES). Interestingly, group H also showed relevant expression of these genes, clustering together with T. On the other hand, group M showed very low levels of expression of the same genes.

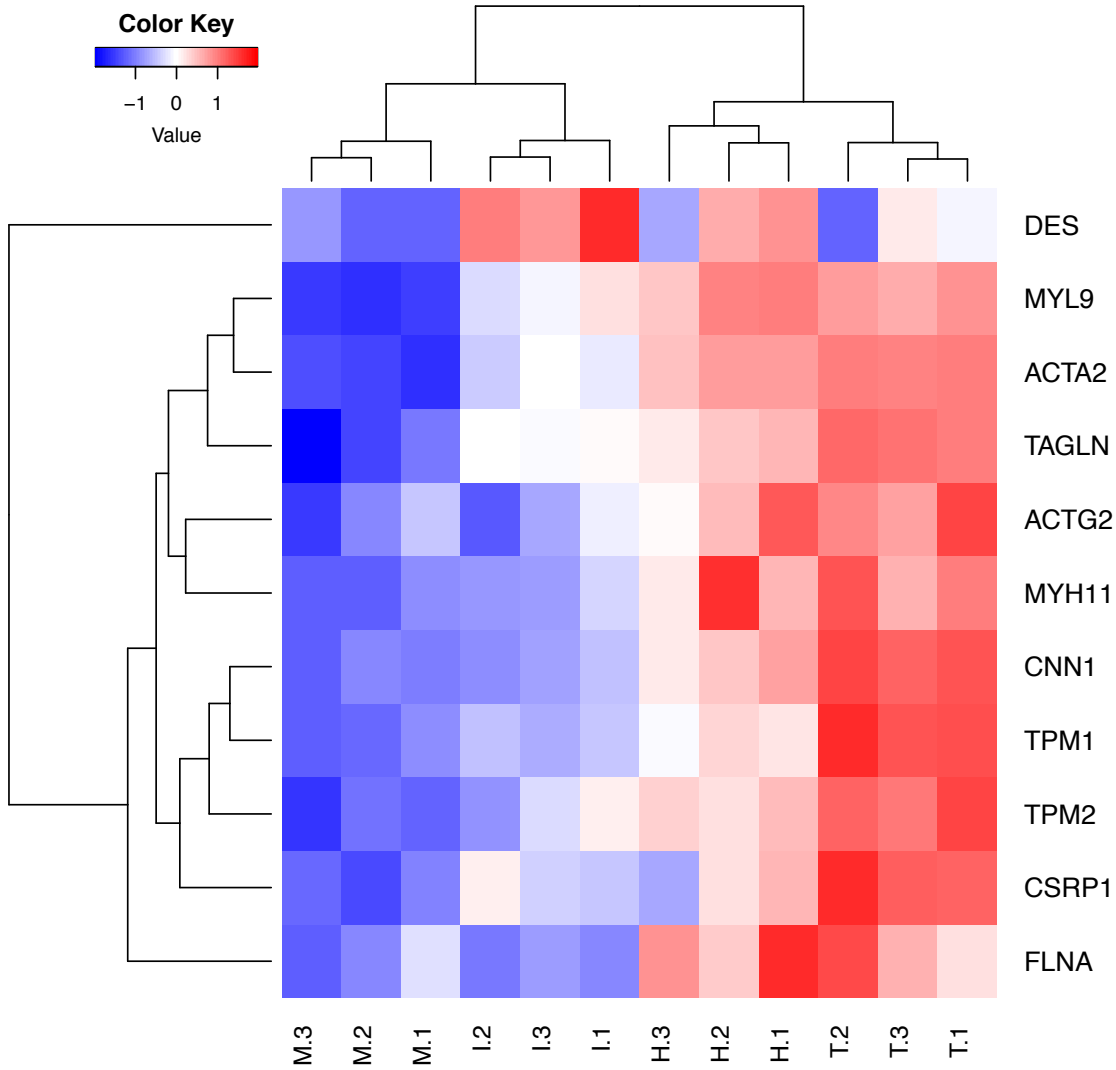

Figure 6-16: Intestinal SMCs specific genes

Heatmap showing DEGs specific to intestinal SMCs in the different treatments. Expression levels are expressed as $\log_2$(CPM) scaled to have mean =0 and SD =1, and are colour coded, with higher expression in red and lower in blue. The list of genes was taken from Lee et al. (2015).

To further evaluate the degree of SM differentiation among the different groups, all DEGs belonging to the Reactome pathway related to SM contraction were plotted (Fig. 6-17). In accordance with Fig 6-16, samples from T clustered together with H and were separated from M and I. The majority of genes from the Reactome pathway of contraction were highly expressed in T (~12 out of 16) and H (~10 out of 16) in comparison to I and M. Interestingly a restricted group of four genes followed an opposite pattern, and were more expressed in M and I compared to H and T. It is interesting to note that the group of four genes less expressed in T were isoforms of genes highly expressed in T: for example two

isoforms of Calmodulin, a calcium-binding messenger protein which mediates calcium regulation (Walsh, 1994), were more expressed in M and I (i.e. CALM1 and CALM3) while a third isoform was highly expressed in T (i.e. CALM2). In a similar way Tropomyosin 3 (TPM3), a protein coding for a gene which binds to actin and regulates SM contraction via interaction with caldesmon (CALD1, here higher in T), was higher in M while TPM1 and TPM2 were higher in T.

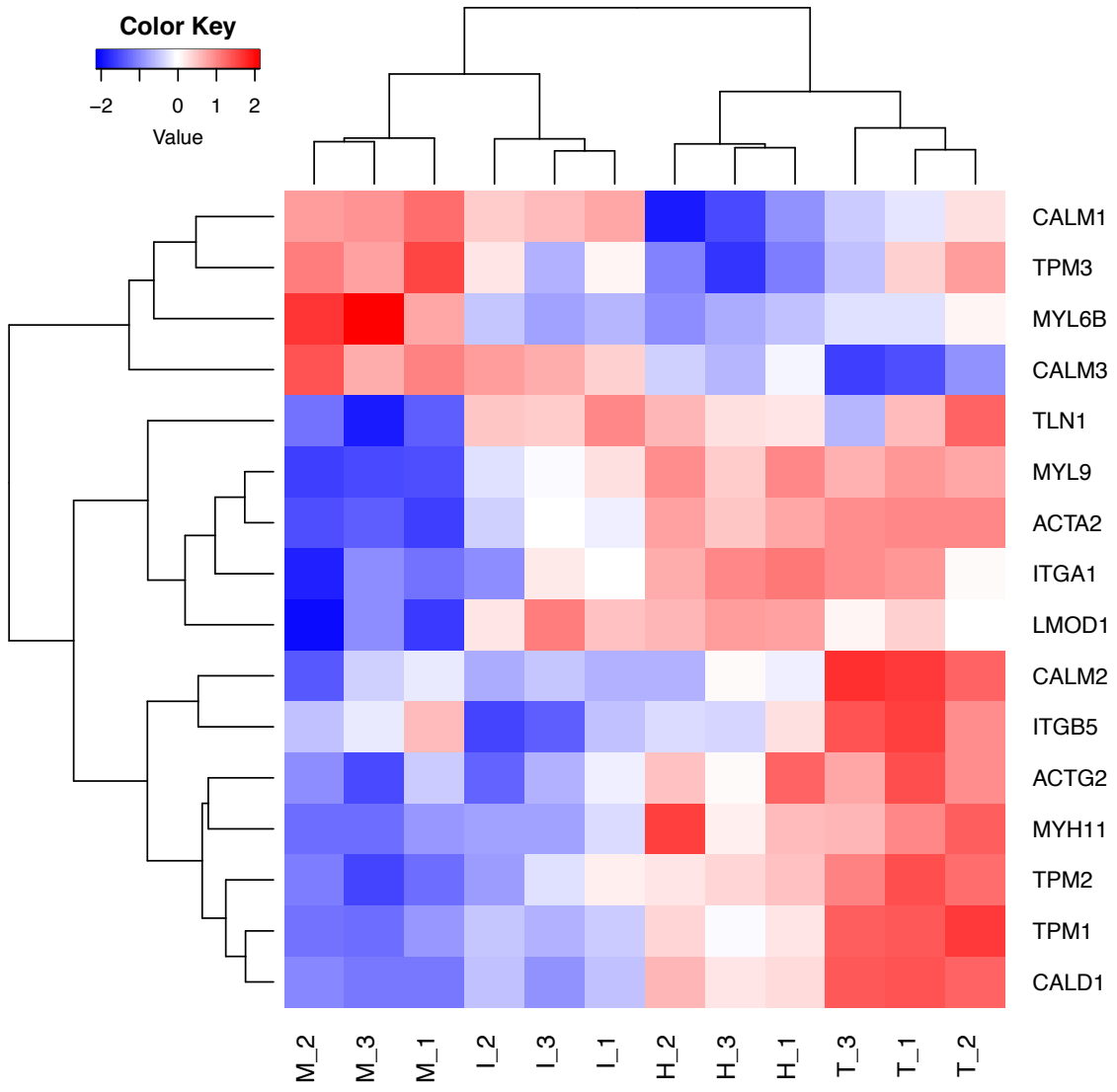

Figure 6-17: REACTOME Smooth muscle contraction

Heatmap showing DEGs belonging to the Reactome pathway of “Smooth muscle contraction”, in the different treatments. Expression levels are represented as $\log_2$(CPM) scaled to have mean =0 and SD =1, and are colour coded, with higher expression in red and lower in blue.

Since it is known that SMCs do not terminally differentiate and are very plastic, having two different phenotypes, a synthetic and a contractile one, which depend on external cues, a test was performed to assess the phenotype of cells cultured in different treatments. Taking advantage of the work from Larsson et al. (2008), who identified two modules (i.e. set of genes) that helped in the discrimination between the two SMC phenotypes, the same approach was applied in this context. The two modules from Larsson are known as the “ECM matrix module” (E), usually associated in SMCs with the contractile phenotype, and the “cell cycle module” (C), usually more expressed in SMCs in the synthetic phenotype. In this work, all genes (i.e. not only DEGs) included in the two modules were plotted on two separate heatmaps (Fig. 6-18) to assess the phenotype of the cultured cells. In the heatmap with the cell cycle module, genes in M were expressed at higher level compared to all other treatments (Fig. 6-18A). On the other hand, the heatmap of module E showed an opposite distribution for the treatments, with T expressing most of the genes at higher level compared with the other treatments and therefore clustering separately from them (Fig. 6-18B). Interestingly, in both heatmaps, a gradient in the levels of gene expression among treatments was evident, with a similar but opposite pattern. This was better seen when, from each sample, the average expression level of all genes from module E was plotted against the average expression level of genes belonging to module C (Fig. 6-19). The distribution of samples in the plot followed an anti-correlation relationship such that when a sample had a high C value, it had a low E value (or vice versa). This anti-correlation was tested by Pearson correlation coefficient and revealed to be statistically significant ($p\text{-val} < 0.001$, $n= 12$, $r= -0.86$). Interestingly, the distribution of samples along the gradient from high C/low E to high E/low C was: M, I, H and T, suggesting that I and H exhibited an intermediate phenotype between the synthetic and contractile phenotypes.

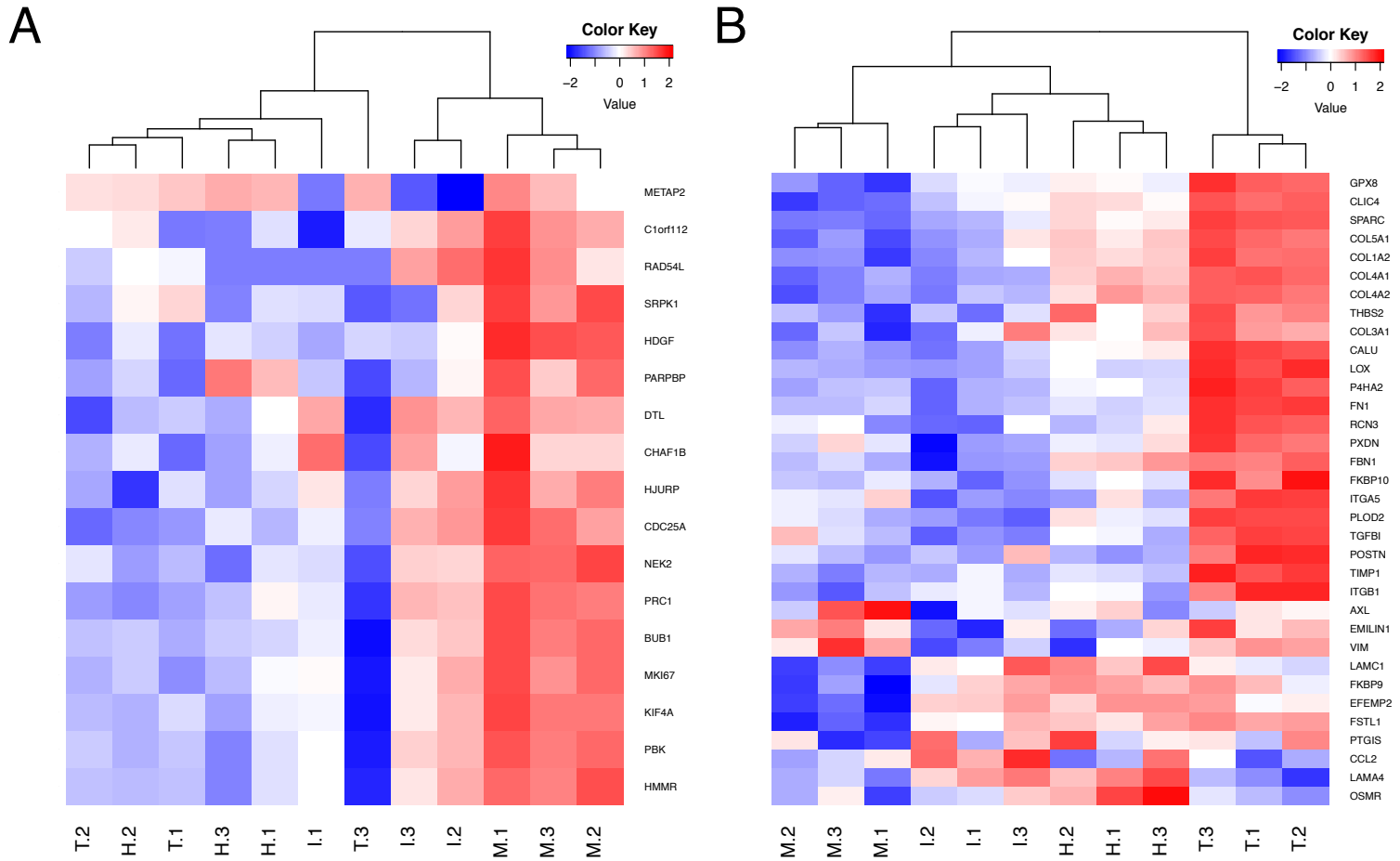

Figure 6-18: Heatmaps of SMCs gene modules

A, B) Heatmaps showing all genes belonging to cell cycle regulation module (A) or ECM module (B) in the different treatments. Expression levels are expressed as $\log_2$(CPM) scaled to have mean =0 and SD =1, and are colour coded, with higher expression in red and lower in blue.

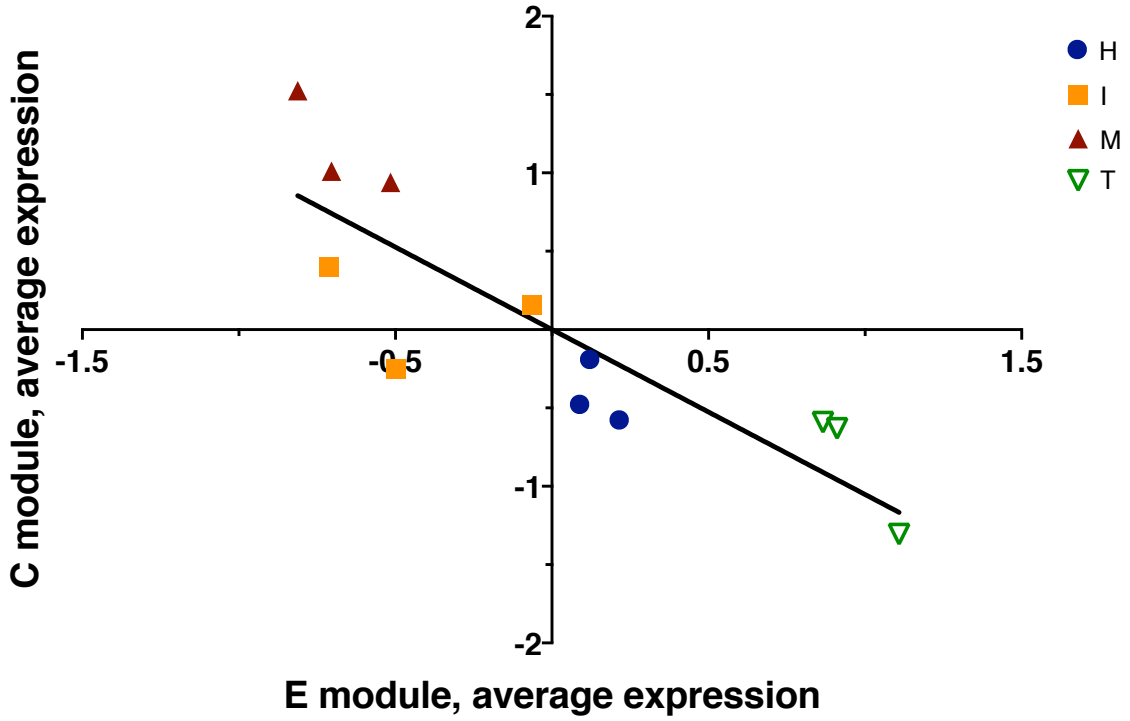

Figure 6-19: SMCs gene modules

C-E plot showing the degree of synthetic or contractile phenotype expressed by cells in different treatments. E and C values are expressed as the Log_2(CPM) average expression level of the E module (X axis) versus the log_2(CPM) average expression level of the C module (Y axis). Straight line represents the linear regression that could be fitted using all samples (p-value < 0.001, R^2 = 0.74).

To verify the results of the RNA-Seq analysis, a set of 5 DEGs (i.e. Smooth Muscle Actin Alpha 2 [*ACTA2*], Smooth Muscle Actin Gamma 2 [*ACTG2*], Smooth Muscle Protein 22 Alpha or Transgelin [*TAGLN*], Calponin 1 [*CNN1*] and Myosin Heavy Chain 11 [*MYH11*]) and 1 non-DEG (i.e. Smoothelin [*SMTN*]) were chosen and their expression was analysed by means of quantitative-PCR. The expression levels of all genes were normalised using two housekeeping genes (i.e. Ribosomal Protein L 30 [*RPL30*] and Ornithine Decarboxylase Antizyme 1 [*OAZ1*]) and were therefore expressed as Normalised Relative Quantities (NRQ), in agreement with Hellemans et al. (2007). The expression levels from the RNA-Seq analysis for all genes is reported in Figure 6-20A, while the expression levels from the qPCR analysis is reported in Figure 6-20B. Overall, qPCR results confirmed the results obtained with the RNA-Seq approach for all genes. In particular, *SMTN*, which was not differentially expressed (DE) from the

transcriptomics analysis, was also not DE at qPCR level (One-way ANOVA, p-val = 0.62). On the other hand, for each of the remaining genes, expression levels in at least one of the differentiating conditions (i.e. H, I or T) were statistically higher than those in M (One-way ANOVA with Dunnett's multiple comparisons, p-val < 0.05), confirming the results obtained at transcriptomic level.

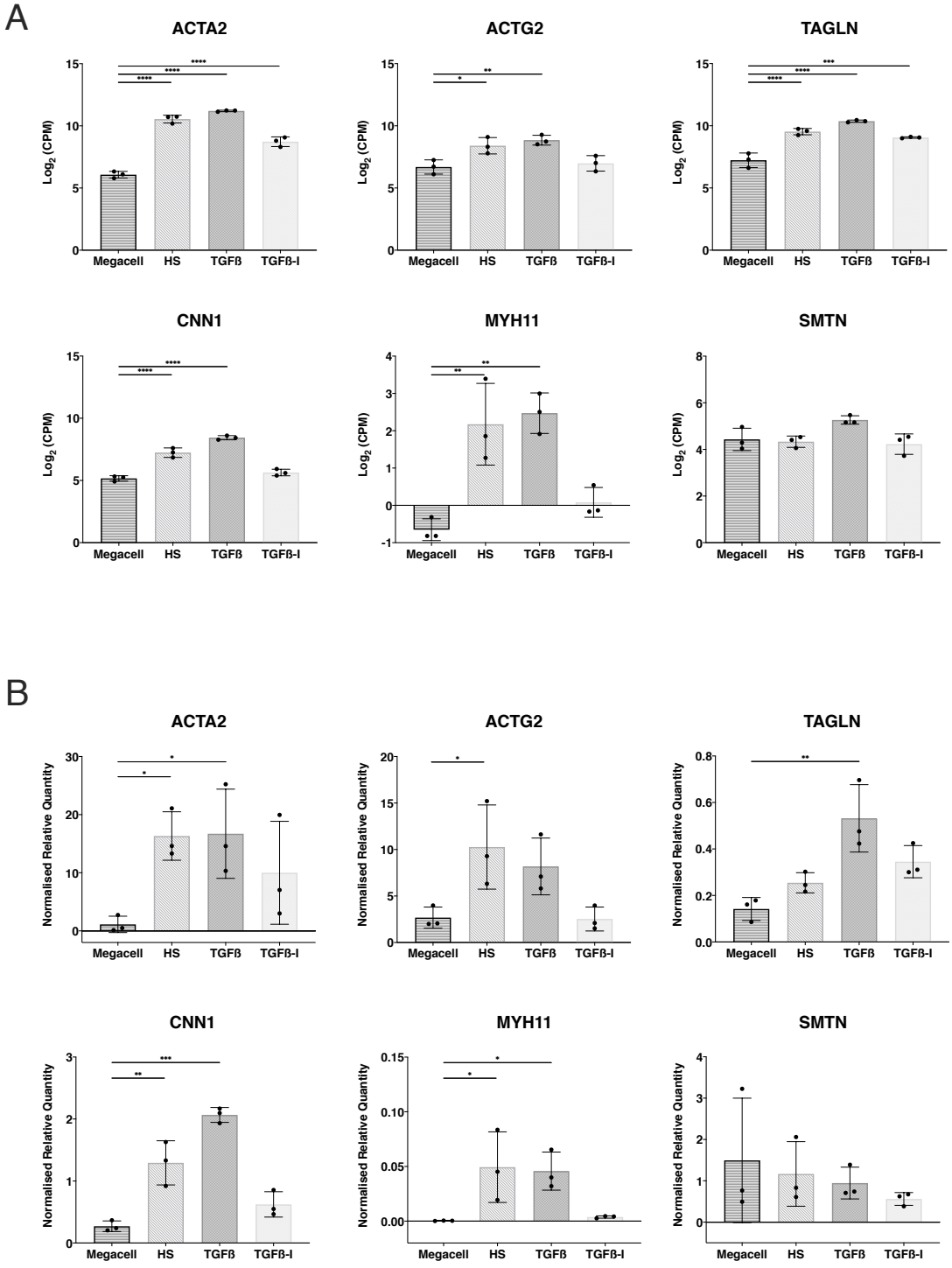

Figure 6-20: Quantitative-PCR validation of transcriptomics analysis

A) Expression levels, expressed as log_2(CPM), of 5 selected genes deemed as DE and one gene not-DE (i.e. SMTN) following transcriptomics analysis (One-way ANOVA with Dunnett's multiple comparisons: * p-val ≤0.05; ** p-val ≤0.01; *** p-val ≤0.001; **** p-val ≤0.0001). In the graph, treatments "Megacell", "HS", "TGFß" and "TGFß-I" correspond to treatments "M", "H", "T" and "I" of the RNA-Seq. **B)** Normalised Relative Quantities on the same genes from A) following qPCR analysis, using RPL30 and OAZ1 as housekeeping genes. Statistical differences were assessed by means of One-way ANOVA with Dunnett's multiple comparisons (* p-val ≤0.05; ** p-val ≤0.01; *** p-val ≤0.001).

6.2.3 hSI_MABs smooth muscle differentiation

Cell differentiation capacity was further investigated by culturing cells in 2% HS alone, with addition of TGFß or addition of TGFß inhibitor for 7 (standard differentiation protocol) or 14 days. Differences in cell morphology among the different treatments were visible in brightfield as evidenced in Figure 6-21. Cells treated with TGFß (Fig. 6-21A, B central panel), appeared flatter compared with cells of other treatments, with presumed actin-myosin filaments visible with brightfield imaging. Cells cultured in 2% HS only, had a similar phenotype at 7 days of culture to TGFß treated cells (Fig. 6-21A), although recognition of cytoskeletal filaments was less evident, while in long term culture, probably due to over proliferation, cells became more elongated. Similarly, cells cultured with daily addition of TGFß-inhibitor, showed, at both 7 and 14 days of culture, a more elongated phenotype with only few patches of cells resembling cells cultured with TGFß (data not shown).

To determine SM differentiation, hSI_MABs after 7 and 14 days of culture were double immunolabelled with SM22 and calponin (Fig. 6-22). Cells cultured in TGFß confirmed previous results described in chapter 5, with the additional information that SMCs differentiation was maintained also after 14 days of culture. Interestingly, while SM differentiation was achieved by most cells in HS at 7 days of differentiation, fewer cells seemed to maintain the expression of SM proteins at 14 days of differentiation, especially among the paediatric hSI_MABs. Curiously, when the TGFß-inhibitor was added to the culture, SM differentiation was still observed, although in fewer cells than in the other treatments at both 7 and 14 days of differentiation. This was more evident in paediatric samples,

where SM differentiation in the presence of TGFß-inhibitor seemed to be almost abolished, with only few patches of cells expressing SM22 and Calponin.

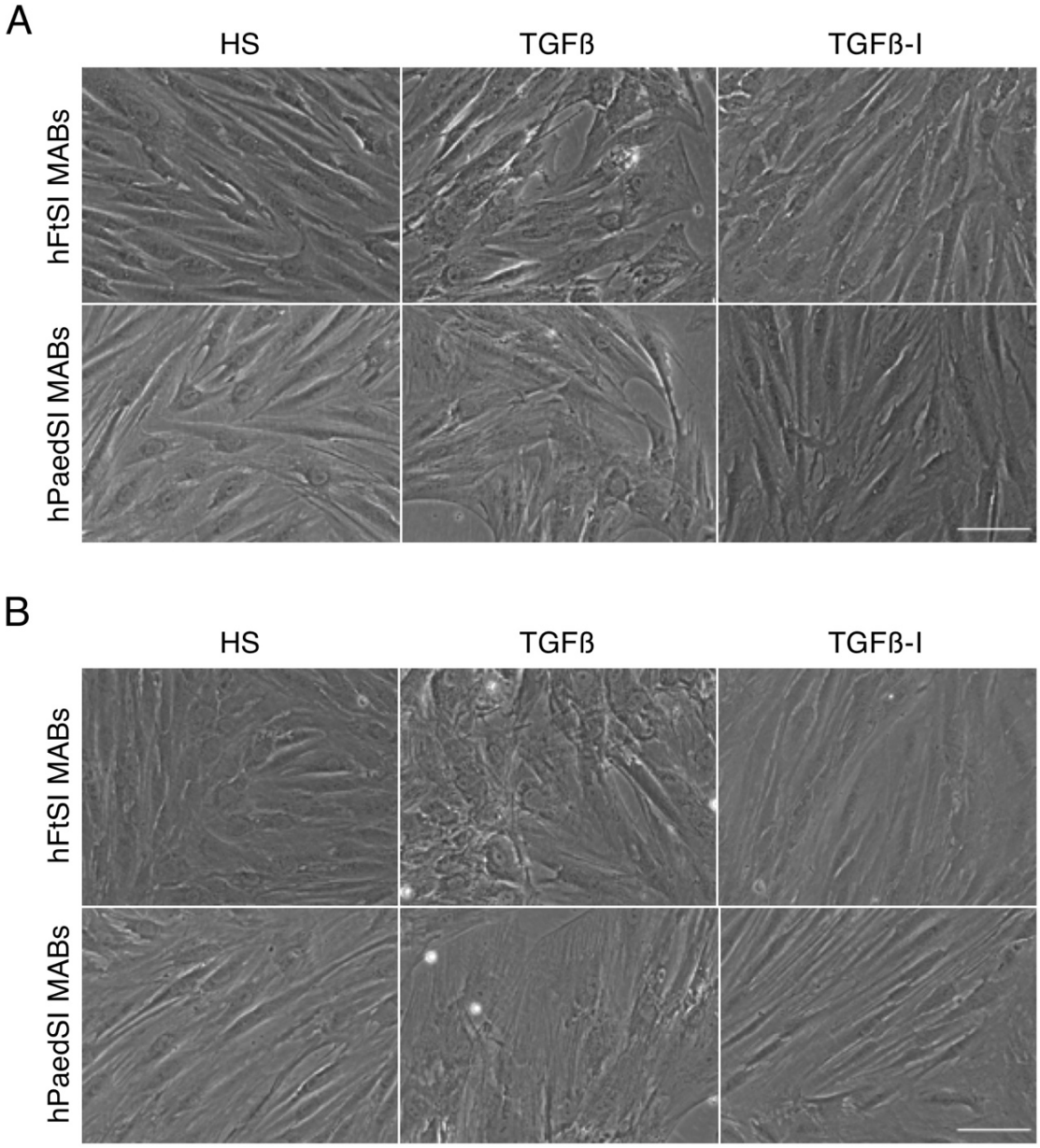

Figure 6-21: Bright field morphological appearance of differentiated hSI_MABs

A) Representative brightfield images of hFtSI_MABs and hPaedSI_MABs cultured for 7 days in 2% HS (HS) alone, with daily addition of 5 ng/ml of TGFß (TGFß) or with daily addition of TGFß-inhibitor (TGFß-I) to a final concentration of 5 μM. Scale bar 100 μm. **B)** Representative brightfield images of cells cultured for 14 days in the same conditions as in panel A. Scale bar 100 μm.

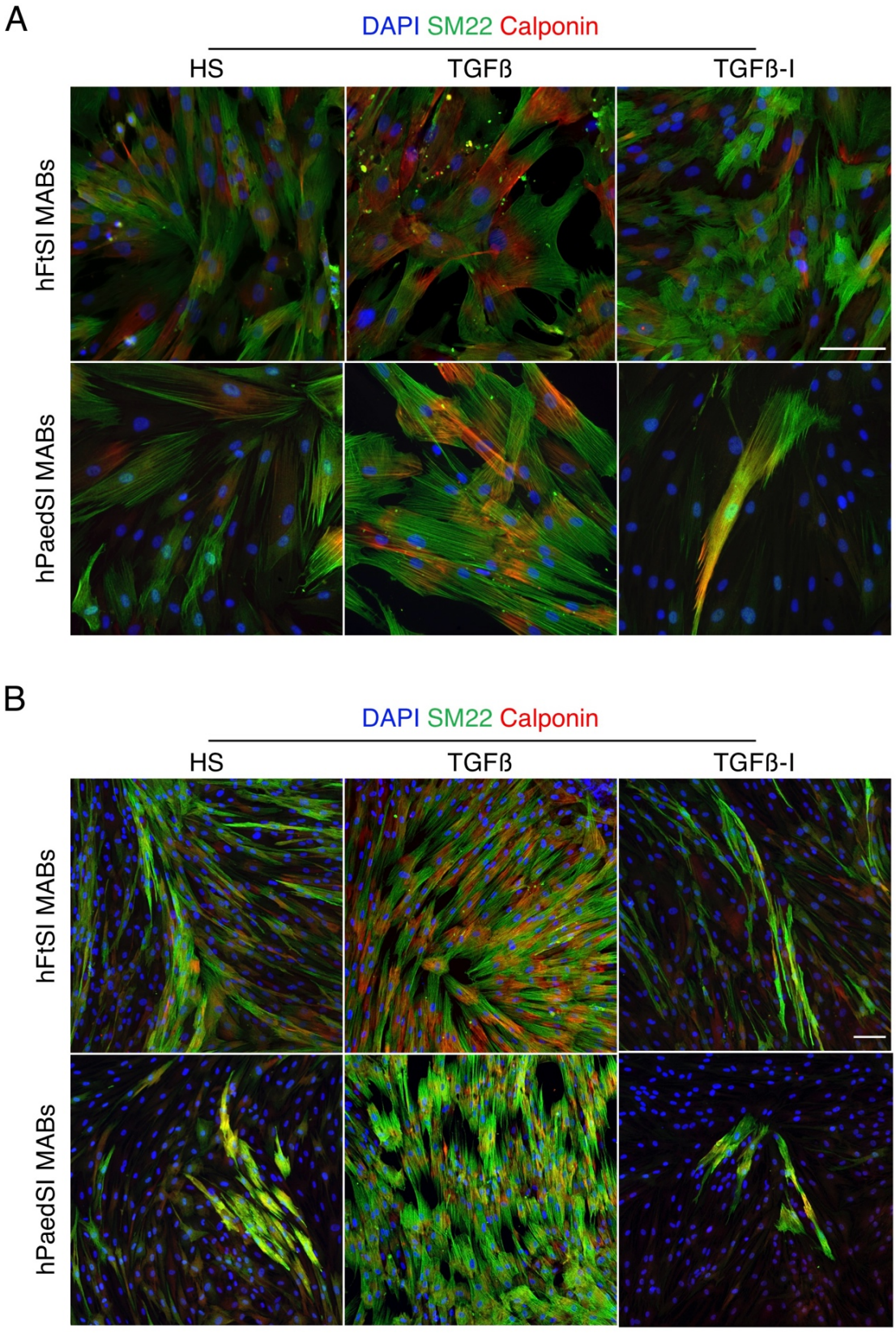

Figure 6-22: hSI_MABs 7 and14 days differentiation

A) Representative images of immunostaining for SM22 in green and Calponin in red of foetal and paediatric hSI_MABs cultured for 7 days in 2% HS (HS) alone, with daily addition of 5 ng/ml of TGFß (TGFß) or of TGFß-inhibitor (TGFß-I) to a final concentration of 5 μM. Nuclei stained with

DAPI in blue. Scale bar 100 μm. **B)** Representative immunofluorescent images of cells cultured for 14 days in the same conditions as in panel A. Scale bar 100 μm.

In order to quantify the level of differentiation in the various treatments observed with immunofluorescence imaging, western blots for SM22, Calponin and also SM-MHC, was performed on cells cultured for 7 and 14 days (Fig. 6-23 foetal cells and Fig. 6-24 paediatric cells). In total 4 μg of proteins were loaded for each sample and bands from immunoblotting images were quantified with ImageJ using ß-actin as reference. Proper statistical quantification was possible only for hFtSI_MABs, since only 2 biological samples were available of hPaedSI_MABs. As evidenced in Figure 6-23B, after 7 days of culture, hFtSI_MABs showed a significantly higher amount of SM22 and SM-MHC in all treatments compared to undifferentiated cells, confirming the successful generation of SMCs. The amount of Calponin was significantly higher only in cells treated with TGFß. At 14 days of culture, a statistically higher amount of Calponin was still evident only for cells cultured with TGFß, while for all other proteins, no statistically significant difference was recognised in any treatments (Fig. 6-23C), probably due to high variability among biological samples.

A similar trend could be hypothesised for hPaedSI_MABs, with a higher amount of Calponin in TGFß treated cells and putatively for SM22 in both TGFß and HS treated cells (Fig. 6-24A, B). However, statistical differences could not be tested due to paucity in number of samples.

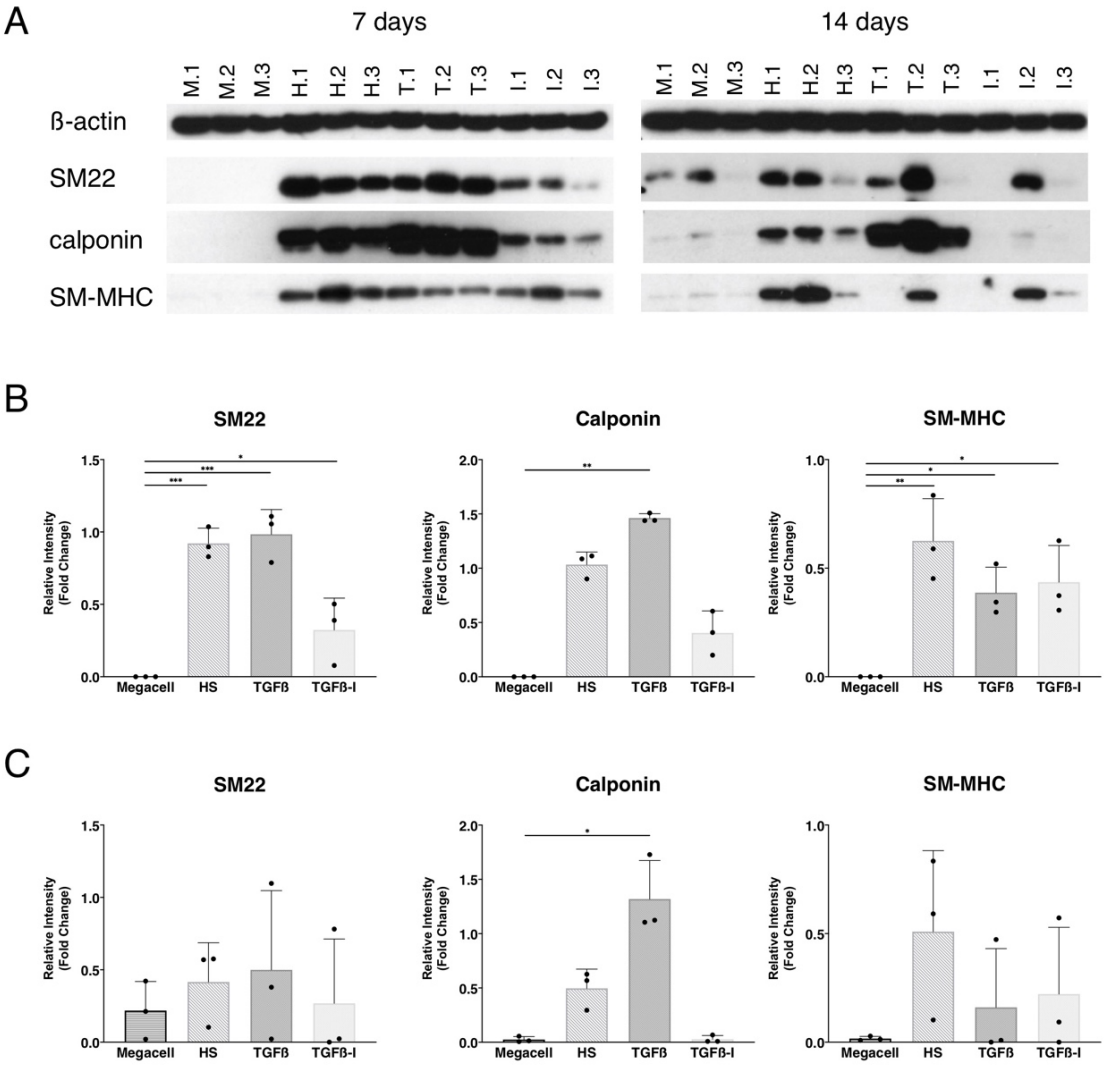

Figure 6-23: Western Blot analysis of SM differentiation of hFtSI_MABs

A) Immunoblot images obtained with 4 μg of protein per sample for ßactin, SM22, Calponin, SH-MHC. Samples were differentaiated for 7 (left) and 14 days (right). Sample names are reported above the pictures. **B)** Relative quantification of SM22, Calponin and SM-MHC content normalised using ßactin in cells cultured for 7 days or **C)** 14 days. Depending on normality of data, assessed with Shapiro-Wilk normality test, statistical differences among treatments were tested by means of One-way ANOVA with Holm-Sidak's multiple comparisons against Megacell as reference or by means of Kruskal-Wallis test with Dunn's multiple comparisons against Megacell as reference (n =3 for each treatment). (* p-val ≤0.05; ** p-val ≤0.01; *** p-val ≤0.001)

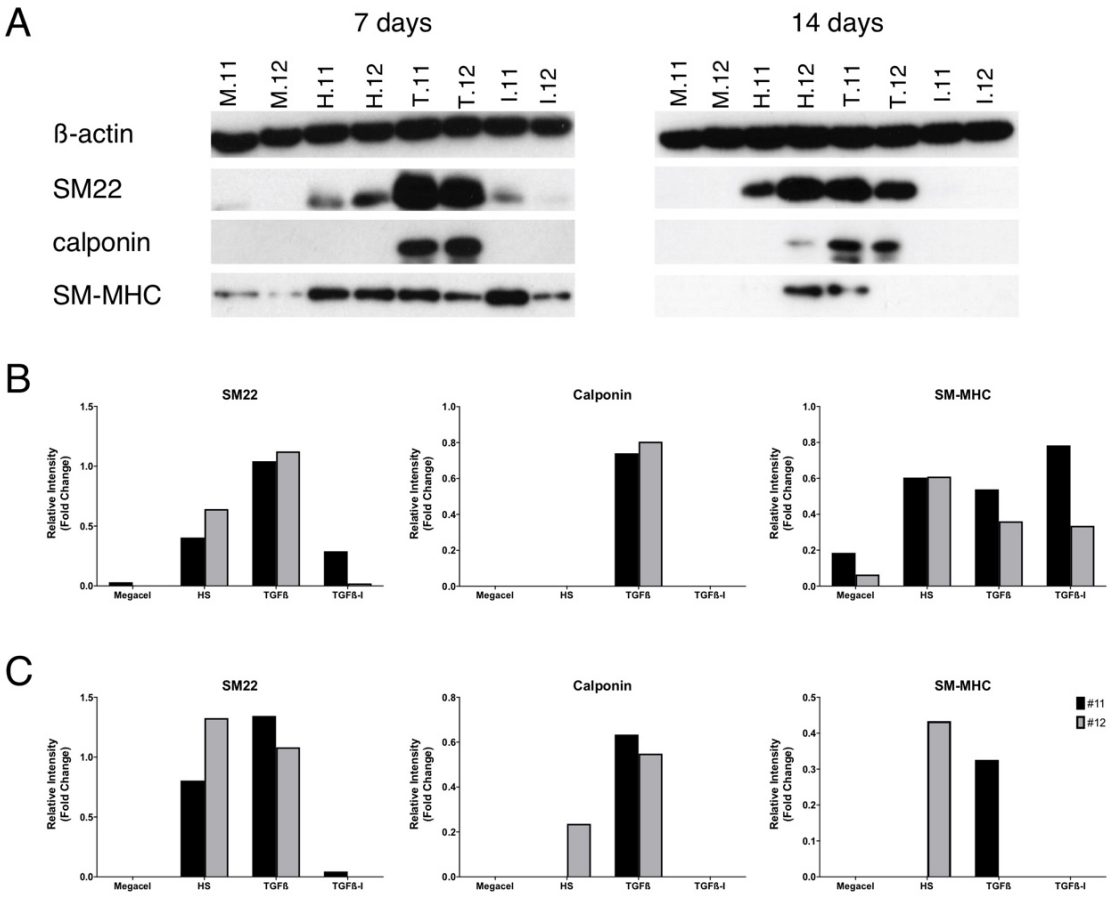

Figure 6-24: Western Blot analysis of SM differentiation of hPaedSI_MABs

A) Immunoblot images obtained with 4 μg of protein per sample for ßactin, SM22, calponin, SH-MHC. Samples were differentaiated for 7 (left) and 14 days (right). Sample names are reported above the pictures. **B)** Relative quantification of SM22, Calponin and SM-MHC content normalised using ßactin in cells cultured for 7 days or **C)** 14 days. Statistical differences among treatments were not tested due to the lack of sufficient biologial samples (n =2).

6.3 Discussion

As it was shown in chapter 5, hSI_MABs were able to generate SMCs when TGFß was added to the culture medium (i.e. 2% HS + TGFß = "T"). SM differentiation, although at lower level, was achieved also when cells were cultured in serum starvation conditions without TGFß addition (i.e. 2% HS = "H"). To confirm that TGFß pathway was the main pathway involved in the SM differentiation of hSI_MABs, a third culture condition was added in order to assess the outcome of cells when cultured with the inhibitor of TGFß (i.e. 2% HS + TGFß-I = "I"). An RNA-Seq experiment was performed to assess SM

differentiation with the standard protocol using TGFß (Tonlorenzi et al., 2007) and the major gene expression differences amongst other treatments, in order to understand to what degree hSI_MABs cultured in 2% HS and 2% HS + TGFß-I were able to generate SMCs. This approach was possible only for foetal hSI_MABs, while additional experiments, such as immunofluorescence and western blotting aimed at evaluating SM differentiation ability, were performed with both foetal and paediatric hSI_MABs.

In order to obtain the best results from all experiments, a cell purification step was performed to avoid possible contaminations from neural cells. In fact, some neural cells could have contaminated the culture from the outgrowth and may have survived throughout the culturing passages, despite the selective conditions of the growth media. Hence, to ensure that putative contaminants were removed, cells were negatively sorted for CD56 and Neurotrophin Receptor p75 (Young et al., 1999), to remove possible neural crest cells. In addition, during the sorting step, to preserve the heterogeneity of hSI_MABs population for the expression of CD146 and CD140b, cells were positively sorted only for CD90 and NG2 (both highly expressed by hSI_MABs as shown in section 5.2.1).

The sequencing of proliferating foetal hSI_MABs (i.e. M) and differentiated foetal hSI_MABs cultured for 7 days in different media (i.e. H, T and I) revealed that cells from T highly expressed most markers characteristics of SMCs, as evidenced when considering the Reactome pathway “SM contraction” (Fig. 6-17). In addition, the same genes were more expressed in H compared with the other two treatments, I and M. From this analysis it was clear that upon TGFß treatment hFtSI_MABs were able to generate cells resembling SMCs, confirming previous results in Chapter 5, and that H treated cells resembled those cultured in T.

The main interest of this work was to demonstrate that hSI_MABs are a good source of enteric SMCs progenitors that can be used in TE approaches. As shown in section 5.2.2, these cells were able to generate SMCs capable of responding to Carbachol, which laid the foundation to the hypothesis that derived SMCs could potentially respond *in vivo* to cholinergic stimuli, which are the main physiological mediators of enteric SM contraction (Montgomery et al., 2016). At transcriptomic level, cells from treatments T and H, expressed at high levels the

same genes that are specifically expressed in intestinal SMCs (Lee et al., 2015). Work done by Ro's lab generated specific transcriptome profiles of different mouse intestinal cells (i.e. , SMCs, ICCs and PDGFRα cells), isolated from three different mouse reporter lines, constituting the SIP syncytium (Ha et al., 2017; Lee et al., 2017; Lee et al., 2015). By comparing the expression levels among SMCs, ICCs and PDGFRα cells, Lee et al. (2015) managed to identify genes that are specific to enteric SMCs. In this work, cells from group T expressed 11 out of 13 genes identified by Lee et al. (2015) at higher levels compared to the other treatments, followed by cells from group H, further confirming that hFtSI_MABs which differentiated in T and H probably closely resembled enteric SMCs at transcriptomic level.

Most of the knowledge about SMCs' phenotype and behaviour has been discovered studying vascular SMCs. These cells are not terminally differentiated and are believed to possess, *in vitro* and *in vivo,* a variety of phenotypes ranging from a proliferative/synthetic to a contractile phenotype (Alexander and Owens, 2012; Rensen et al., 2007). It has been hypothesised that the existence of these two phenotypes would describe the function of SM tissues. In example, SMCs adapt to generate tonic contractions of vessels to adjust lumen diameter (hence regulating blood pressure) but can also proliferate, for example during uterine growth in pregnancy or while repairing damaged blood vessels following injuries (Rensen et al., 2007). As stated by Rensen et al. (2007), these two phenotypes constitute the ends of a range of phenotypes with intermediate characteristics. On the other hand, less is known regarding this mechanism in enteric SMCs, although recently some investigations have confirmed a similar behaviour (Scirocco et al., 2016). Similarly, while there is a paucity of studies underling the molecular aspects of intestinal SMCs, more extensive work has been done to characterise vascular SMCs (Scirocco et al., 2016). In this study, by building on work from Larsson et al. (2008), it was possible to demonstrate that hFtSI_MABs and differentiated cells could be defined as SMCs in various differentiation states between the synthetic and contractile phenotypes. More in detail, Larsson et al. (2008) showed that an anti-correlation model between the expression levels of the two gene modules, the cell cycle regulation module (C, usually associated

with the synthetic phenotype) and the ECM module (E, usually associated with the contractile phenotype), does exist and described SMCs in their different phenotypes. Similar to their work, an anti-correlation was evident for hFtSI_MABs belonging to the different treatments (i.e. M, I, H and T) based on the average expression levels of module C and E. In this work, the phenotype of proliferating M cells resembled more a synthetic phenotype, while differentiated T cells a contractile one, with I and H sitting between these two extremes: H more closely to T and I to M. This observation is in agreement with results from Larsson et al. (2008), who concluded that SMCs can be found at various levels of differentiation between two “opposite” phenotypes (i.e. synthetic and contractile).

The analysis performed on all 3,414 DEGs identified using the general linear model, further corroborated the hypothesis of undifferentiated hFtSI_MABs (i.e. M) and differentiated cells in T being two opposite phenotypes. In fact, enriched GO categories identified in cluster 2, which consisted of genes highly expressed in M, could nicely describe the synthetic phenotype of SMCs, with the enrichment of GO relative to stem cells proliferation. On the other hand, cluster 1, which represented cells differentiated with TGFß, showed GO category enriched for muscle contraction, cell-cell and cell-matrix interaction, typical aspects of the contractile phenotype.

Analysis on cluster 4, which represented genes expressed more in H and I, revealed the presence of a more variable combination of enriched GO categories. Assuming that group H and I include cells that are found at different degrees of differentiation between the two extreme SMCs phenotypes, then this could explain the presence in this cluster of GO categories enriched for all the different aspect of SMCs: smooth muscle contraction, proliferation and cell migration. It is interesting to note that in this cluster, as well as in cluster 6, which contained genes highly expressed in T, H and I, GO of different signalling pathways were enriched, leading to the idea that other pathways, beside the canonical TGFß pathway, could be involved in hFtSI_MABs SM differentiation.

Experiments testing protein content upon different SM differentiation treatments confirmed that TGFß treated cells after 7 days were the most mature group of derived SMCs, showing significantly higher content of all SM related

proteins evaluated (i.e. SM22, Calponin and SM-MHC). Moreover, a higher content of SM22 and SM-MHC was also evidenced in the other two differentiation treatments of hFtSI_MABs, (i.e. H and I) compared to the proliferative condition (i.e. M) leading to the conclusion that a certain level of differentiation was evident also in the absence of TGFß. Thanks to immunofluorescence images, it could be argued that the different protein content evidenced among treatments with western blot analysis, was due to a different number of cells that differentiated following the treatments. Several mechanisms could be hypothesised to explain how cells in H and I differentiated in comparison to cells in T. For example, cells could produce their own TGFß (e.g. in an autocrine manner) and induce their own differentiation. In this scenario, cells could be differentiating through the canonical TGFß pathway, and addition of TGFß-inhibitor should completely block SM differentiation. However, some cells in treatment I still showed capacity to differentiate, suggesting the presence of an alternative pathway inducing their differentiation.

Among the pathways evidenced by the enriched GO categories, as expected, TGFß pathway was enriched in cluster 1 confirming the effectiveness of treatment with TGFß in hFtSI_MABs SM differentiation (Guo and Chen, 2012; Tagliafico et al., 2004). However, in cluster 4 it was interesting to note an enrichment for the MAPK pathway and for the EGF and IGF pathways. The mitogen-activated protein kinase pathway (MAPK), which can be activated by several signalling pathways including many growth factors, is known to be involved in the regulation of several cell functions, such as proliferation, differentiation and apoptosis (Pearson et al., 2001). Despite the fact that an in-depth analysis of its activation has not being assessed, it could be hypothesised that cells from groups H and I responded to IGF, via activation of the phosphatidylinositol-3 kinase (a component of MAPK) to induce the contractile phenotype. This assumption is supported by evidence of the IGF signalling being involved in airways SMCs hypertrophy and contraction (Halayko et al., 2004; Schaafsma et al., 2007). In particular, these studies demonstrated that upon insulin treatment in a serum-free environment, there was an accumulation of SM contractile proteins in bovine and canine airway SMCs. Other studies

investigated the role of insulin signalling in the equilibrium between the synthetic and contractile SM phenotypes and concluded that SMCs differently responded to the IGF signals according to the phenotypic state which the cells were in, when stimulated. Therefore, IGF could sustain the production of SM contractile proteins in contractile SMCs, and could maintain proliferation in synthetic SMCs (Hayashi et al., 2004). Further in-depth analysis is required in order to clearly determine which specific pathways are activated in this context: one such pathway could be the IGF-pathway, but more in-depth analysis might reveal additional pathways that affect SM differentiation.

Chapter 7

Final Discussion

7. Final Discussion

7.1 Discussion

Despite the encouraging advances that have been made in the field of whole organ tissue-engineering (Orlando et al., 2012), the production of a fully functional intestine has still not been achieved. The possibility to decellularise organs, a process by which tissues and organs are cleared of their cellular compartment (Badylak et al., 2011) but maintain the shape, size and biomechanical properties of the native organs, is crucial when approaching this field (Martin et al., 2018). Several studies have demonstrated the possibility to successfully generate decellularised tissues and organs such as skeletal muscles, oesophagus, stomach, lung, trachea and also the intestine (Elliott et al., 2012; Maghsoudlou et al., 2013; Totonelli et al., 2012; Urbani et al., 2018; Urciuolo et al., 2018; Zambaiti et al., 2019). Furthermore, their successful use in clinic (Elliott et al., 2012) show promise for their possible role as organ replacements for future treatments of many congenital malformations and organ failures.

To produce a functional intestine, all the different layers that compose it have to be recreated. For this reason, the choice of the appropriate cell types to be seeded onto the scaffold, preferably organ-specific and with a certain degree of immaturity (i.e. precursor potential), is also of critical importance for the achievement of this goal (Martin et al., 2018; Orlando et al., 2012). As previously described (section 1.1) the intestine has several functions; including absorption of nutrients and water, performed by a specialised epithelium (Mowat and Agace, 2014), of which the stem/precursor cells responsible for its constant regeneration have been extensively studied (Barker et al., 2007b; Gehart and Clevers, 2019). However, the intestine is mainly a tubular structure and the transit of food is attributed to its neuromuscular wall (section 1.2), which is necessary to stir and move food along its entire length and to finally eliminate waste. The presence of the enteric nervous system together with the SMC / ICC / PDGFRα^{+} cells syncytium allows this process (Sanders et al., 2014). While the origin of the ENS,

mainly from the vagal neural crest cells, and the isolation of neuronal precursors from intestinal biopsies (Bondurand et al., 2003; Burns et al., 2016) has been well established, the exact origin of intestinal SMCs and the possible presence of a precursor population residing in the gut is still a debated subject, although some studies have been made for the progression of this field (section 1.6). In this study, several advances have been made to understand the origin of intestinal SMCs during human and mouse development. Also, the potential use of SMCs precursors of a vascular origin, that can be successfully isolated from human intestinal biopsies, for regenerative medicine purposes, is described.

7.1.1 Origin of Intestinal SMCs

Previous studies on human intestine development described the advent of the different components of the neuromuscular wall, with particular attention to the enteric NCCs, as well as ICCs and SMCs (Fu et al., 2004; Wallace and Burns, 2005). However, from this study, it was highlighted that the onset of SMCs, as well as cKit and PDGFRα expressing cells can be variable from sample to sample, due to some degree of biological variability that is present during development. In particular, regarding the longitudinal SM layer, it was possible to narrow down its appearance to week 8 of gestation (where at least 50% of the samples analysed show positive immunostaining for αSMA, SM22 and Calponin in the region of the longitudinal SM layer, see Tab. 3-1), while its maturation was completed by week 10 (where all samples showed a positive immunostaining for SM-MHC in the longitudinal SM layer, Tab. 3-1), in contrast with what was reported in the literature (Fu et al., 2004; Wallace and Burns, 2005).

In addition, it was possible to confirm some previous data observed in mice (Kurahashi et al., 2008; Torihashi et al., 1997), regarding the expression of cKit and PDGFRα in cells located in the region where the longitudinal SM layer will arise, suggesting a role for these cells in the development of SMCs. Subsequently, more in-depth analyses were then performed on mouse developing guts at different embryonic stages to understand, at molecular level, the specific transcriptome of the putative intestinal longitudinal SM precursors, as suggested in previous (Kurahashi et al., 2008; Torihashi et al., 1997) and in the

current study in Chapter 4. Results indicated that the sorted cKit$^+$ cells did not constitute a SM precursor population due to the fact that enriched pathways in this population were mainly associated with immune functions with no specific connection to SM. However, the lack of negative sorting for mast cells and lymphocytes may have arguably interfered with the proper assessment of cKit+ cells (see 7.2 Limitations and future work section). On the other hand, identification of muscle related signals in the PDGFRα$^+$/cKit$^+$ (i.e. DoublePos) and PDGFRα$^+$ populations at E12.5, confirmed the presence of cells putatively identified as the enteric SM precursors, among these populations.

7.1.2 Intestinal SMCs precursors of a vascular origin

The presence of several SM precursors in the human intestine has never been investigated. However, the idea that the mural wall of vessels can be considered a mosaic from a developmental point of view (Armulik et al., 2011), could be arguably implied also for the intestinal SM wall. This concept has been in part already determined, thanks to studies in mouse, showing a partial contribution of mesothelial cells to the generation of both vascular and intestinal SMCs during development (Carmona et al., 2013; Rinkevich et al., 2012; Wilm et al., 2005), a phenomenon also described for heart and lung (Que et al., 2008; Smits et al., 2018).

However, another major contribution to SMCs of the intestine that, so far, has not been taken into consideration, could be found in vasculature. In this case, the idea of a vascular contribution to the intestinal SMCs came from studies on mesoangioblasts. Mesoangioblasts are mesoderm-derived stem cells, that were first isolated from the mouse embryonic dorsal aorta (De Angelis et al., 1999; Minasi et al., 2002) and subsequently from human post-natal skeletal muscles (Dellavalle et al., 2007; Tonlorenzi et al., 2007). They share common features with pericytes, such as the expression of pericytes markers and the anatomical location in capillaries and small vessels (Quattrocelli et al., 2012). Of note is the ability of mesoangioblast to generate SMCs of the vasculature as well as several mesodermal tissues, including skeletal muscle (when isolated from it) (Dellavalle et al., 2011). Following these results, a hypothesis was developed, that if

mesoangioblasts were isolated from the intestine, they would successfully generate enteric SMCs. In this way, they would constitute an accessible source of SM precursors for the generation of a bioengineered intestine. Furthermore, their safety *in vivo* has already been established in a Phase I/II clinical trial for the treatment of Duchenne muscular dystrophy (Cossu et al., 2015), therefore making them a perfect candidate for tissue engineering approaches.

So far no reports seem to exist regarding isolation of mesoangioblasts from human intestine, even though recently we successfully managed to isolate them from mouse intestine (Perin et al., 2019). However, their full characterisation was still necessary for a complete assessment of their characteristics. As expected, isolated human small intestinal mesoangioblast-like cells (hSI_MABs), both from foetal or paediatric intestinal biopsies, showed a phenotype similar to pericytes, with the characteristic expression of some of the pericytes markers (Armulik et al., 2011; Crisan et al., 2008). Moreover, *in vitro* they showed growth capability, without reaching a plateau, at least within 40 days of culture, maintaining at the same time a genomic stability necessary for their translational use (Attwood and Edel, 2019). Unfortunately, the protocol used to isolate cells (Tonlorenzi et al., 2007) in this work, used animal derivates, such as Matrigel (Hughes et al., 2010), which makes the process unsafe for clinical translation. However, thanks to the characterisation performed on the isolated cells, future work could be done by direct isolation of cells via FACS, therefore eliminating culture steps in Matrigel and making the process clinically safe.

The generation of SMCs from hSI_MABs was tested and the phenotypical characteristics of hSI_MABs and derived SMCs, both at protein and molecular levels, revealed that cells from different treatment groups (i.e. undifferentiated cells, “M”; and differentiated cells cultured only in 2% HS, “H”; in 2% HS + TGFß, “T”; in 2% HS + TGFß-inhibitor, “I”) represented SMCs in different states between a synthetic and a contractile phenotype (Alexander and Owens, 2012; Rensen et al., 2007). In SM tissues the presence of cells showing intermediate characteristics between these two ends of a range of phenotypes, has already been postulated (Rensen et al., 2007). Further, the presence of SMCs in different phenotypical stages is believed to have an important role in SM tissues, such as

in vessel contraction to adjust lumen diameter and for proliferation in uterine growth during pregnancy (Rensen et al., 2007). A similar behaviour was also observed for enteric SMCs (Scirocco et al., 2016). Therefore, the capacity of hSI_MABs to generate SMCs with a range of phenotypes is pivotal if they are to be used to regenerate an intestinal substitute, because they could generate necessary phenotypic variability within the organ to accomplish its functions. An important addition is that, SMCs derived from hSI_MABs showed a positive response to the acetylcholine agonist Carbachol, suggesting their capacity to respond to the major signalling involved in SM contraction of the gut (Montgomery et al., 2016).

Several cell types have been used in the past years to generate SM components of different organs. The direct use of SMCs has not been validated yet for clinical applications, therefore their use to engineer grafts, might be an obstacle to human translation. In addition, the use of autologous tissue-specific (Grikscheit et al., 2003) or bone marrow-derived mesenchymal stem-cells (MSCs) was attempted for the generation of different organs (Park et al., 2016; Tan et al., 2013). However, although the paracrine activity of MSCs was observed for tissue remodelling, a clear contribution to muscle regeneration was not supported by the authors.

The remarkable results achieved when hSI_MABs were seeded onto decellularised foetal midguts, showing the ability to self-orientate into the two orthogonal SM layers constituting the *muscularis propria* of the intestine, was encouraging and is the basis for the future use of these cells to produce an engineered intestine. In fact, as mentioned in Chapter 5, such a result has never been accomplished with a simple seeding of cells into a scaffold, but always required multiple steps (Kobayashi et al., 2015; Raghavan et al., 2010; Somara et al., 2009). This result is of critical importance for the generation of a functional contractile intestine as it simplifies the experimental protocol including co-seeding with other cell types of the neuromuscular wall thus being beneficial in generating a fully functional intestine.

7.2 Strengths, limitations and future work

In Chapter 3 the development of human intestinal layers was studied in order to characterize the timing of appearance and maturation of the different components of the intestinal smooth muscle compartment. The strength of this work resided in the use of multiple different biological samples, which allowed to evidence some degree of variability (especially in the timing of appearance) between foetuses. While, on the one hand, this variability could be due to inaccurate staging of the embryos (e.g. arguably there are differences between an early and a late week 8 embryo), it is also true that some variability during embryogenesis might occur. In the light of this, in order to obtain a more accurate estimation of the timing of appearance and maturation of the different components of the intestine, additional samples would be required.

In addition, from a physiological point of view, the presence of SM proteins in the cells, does not automatically guarantee that SMCs are able to function properly (i.e. contract). This study has only focused on the first appearance of the muscle layers of the small intestine and concentrated on their maturation by looking at different SM proteins. However, proper functional analyses should be performed to determine the exact timing of SMCs activation as was recently done for ENCCs (McCann et al., 2019). In fact, by knowing the exact timing we could further investigate the mechanism that are responsible for the correct activation of intestinal contraction and this could be pivotal to help understanding at least some of the various phenotypes of enteric myopathies (see section 1.4; (De Giorgio et al., 2004; Knowles et al., 2004; Koh et al., 2008; Munoz-Yague et al., 2006; Smith and Milla, 1997)).

In Chapter 4 the origin of longitudinal SM layer in mouse was investigated by studying different subpopulations of cells (based on the expression of cKit and PDGFRα) by means of flow cytometry and RNA-seq technology. However, during the isolation phase, the absence of a negative sort for mast cells as well as lymphocytes, known to express the receptor cKit (Thorén et al., 2008), has probably been the main limitation to a full assessment of the molecular signature of the subgroup of cells that express cKit and that are thought to be the precursors of both longitudinal SMCs and of ICCs (Torihashi et al., 1997). In fact, the

presence of mast cells and lymphocytes within the sorted cKit$^+$ population likely masked the signal originated from the precursors of ICCs, thus partly limiting the current analysis.

In spite of this limitation, results from the analysis suggested that PDGFRα$^+$/cKit$^+$ (i.e. DoublePos) and PDGFRα$^+$ populations at E12.5 constitute a putative pool of enteric SM precursors, due to their high enrichment in muscle GO categories and Kegg pathways within their differentially expressed genes. A confirmation of these results could be made via lineage tracing studies using inducible mouse reporter lines for PDGFRα and for double positive cells. In this way, the direct tracing of cells derived from PDGFRα$^+$ cells or DoublePos cells could definitely confirm their role as SM precursors. However, the generation of such transgenic mice could be time consuming. A quicker way to assess the potential of these cells to effectively generate intestinal SMCs could be tested by using C57BL/6-(ACTB-EGFP)/J mice (Okabe et al., 1997), where EGFP is constitutively expressed under the promoter of ß-actin, therefore being express in all cell types. This line could be used to isolate PDGFRα$^+$ and double positive cells, which will constitutively express GFP and transplant them into developing (i.e. embryonic) WT mouse guts cultured *ex vivo* (Au - Walton and Au - Kolterud, 2014). In this way, by tracing and characterising GFP$^+$ cells after a few days of culture, the generation of SMCs could be verified.

Future work could be done also by analysing the transcriptome of different developmental stages at single cell level, to determine clusters of cells with similar molecular signatures, which may help to identify the specific precursor population (Robson, 2014; Treutlein et al., 2014). Another option could be to combine the present flow cytometry approach with single cell RNA-sequencing using a new method that has been recently developed (Stoeckius et al., 2017). This method combines multiplexed detection of protein markers, by flow cytometry, with unbiased transcriptome profiling of thousands of cells, by single cell RNA-sequencing, called cellular indexing of transcriptomes and epitopes by sequencing – CITE-seq (Stoeckius et al., 2017), allowing a better identification of the cellular phenotypes compared to single transcriptome data. In this way we could possibly identify additional superficial markers (e.g. comparing the

molecular profile of precursor cells with the surfaceome dataset (Bausch-Fluck et al., 2015)), to be used for the isolation of these precursors and the evaluation of their presence in the gut during post-natal life.

In Chapter 5, hSI_MABs were successfully isolated, characterised and proved to generate functional SMCs *in vitro*. However, when transplanted *in vivo*, even though they showed capacity to differentiate into SMCs, as discussed in Chapter 5, hSI_MABs were unable to penetrate the intact gut wall and limitations in the animal licence did not allow muscular gut injury *in vivo*, restricting our investigation. A new licence allowing to perform such action would be the ideal starting point to investigate the ability of these cells to restore the damaged tissue by migrating in the injury and differentiating into SM cells.

The remarkable result of this chapter is the demonstration that, when hSI_MABs are seeded on a decellularized scaffold, they self-generate two orthogonally orientated SM layers that resemble the native SM layers. However, this study was limited to the demonstration of the presence of differentiated SMCs via the expression of some SM muscle proteins. To determine the efficiency of these cells to generate a functional gut wall for TE applications, the functionality of the orthogonal layers should be further investigated. This could be performed by studying the responses to Carbachol via calcium imaging as well as via measuring contractile activity using organ bath contractility (Montgomery et al., 2016). Furthermore, the full regeneration of the gut wall should be promoted by co-seeding of the different cell types that compose it, such as the NCCs and the interstitial cells (i.e. ICCs and PDGFRα cells) that together with the SMCs constitute the SIP syncytium (Sanders et al., 2014).

In Chapter 6, the molecular signature of hSI_MABs cultured in different condition media was investigated by means of RNA-seq technology. Analyses performed on the transcriptome of cells showed an enrichment of gene ontology categories associated with the MAPK pathway, and in particular its activation through different growth factors (i.e. EGF and IGF), showing an intermediate phenotype between the synthetic and the contractile one (i.e. H and I treatments). Studies on airway SMCs have already demonstrated the involvement of insulin signalling in the complex equilibrium of the SMC phenotypes (Halayko et al.,

2004; Hayashi et al., 2004; Schaafsma et al., 2007), therefore a putative role of MAPK in SM differentiation of hSI_MABs should be further investigated.

The lack of a direct comparison of hSI_MABs with human intestinal SMCs in the design of the RNA-seq experiment was one of the main limitations to a definitive demonstration of the derivation of intestinal SMCs from hSI_MABs. However, upon TGFß treatment, the generation of SMCs expressing most of the genes identified as specific for intestinal SMCs in mouse (Lee et al., 2015) was of crucial importance, especially with the intent to use these cells for the regeneration of intestinal muscle layers in a tissue engineering context.

7.3 Conclusion

Up to now intestinal substitution remains the ultimate option for intestinal failure as a consequence of several intestinal diseases, such as short bowel syndrome and severe intestinal motility disorders (Chandra and Kesavan, 2018). Unfortunately, success rate of intestinal transplantation in children is still very poor and is mainly associated with very high morbidity and mortality (Andres et al., 2010; Boluda, 2015). Moreover, donor shortage (Glotzbach et al., 2011), in particular for organs of the right size for children, and the need of life-long immunosuppression, persists as one of the major constraints for this approach. In this context, the ability to produce a custom-made functional organ of the right size, possibly using the patient's own cells, via a tissue engineering approach, could be an ideal strategy to overcome all major restrictions of bowel transplantation.

Within this framework, my work focussed on intestinal SMCs, a cell type that has not been particularly investigated in comparison to other cell types (e.g. intestinal epithelial cells). The objectives of the PhD were twofold: *i)* investigate human and mouse early developmental stages in order to identify the precursor cells from which SM layers of the gut originate; *ii)* explore additional sources of SMCs for the reconstruction of gut SM layers.

Results from the first part of this work underlined that double positive cells (for cKit and PDGFRa) were the most suitable precursors of the enteric

longitudinal SM layer due to their gene expression profile and their histological and temporal location in the longitudinal SM region before SM protein could be identified. In the second part of this work, human intestinal MABs were successfully isolated and showed their capacity to generate mature SMCs *in vitro, in vivo* and in a decellularised scaffold. In particular, within the scaffold their self-disposition in two orthogonal layers, resembling the native circular and longitudinal layers of the gut, suggests that these cells are the best candidate source so far identified for SM regeneration of the intestine.

Bibliography

Alexander, M.R., Owens, G.K., 2012. Epigenetic control of smooth muscle cell differentiation and phenotypic switching in vascular development and disease. Annu Rev Physiol 74, 13-40.

Anderson, R.B., Stewart, A.L., Young, H.M., 2006. Phenotypes of neural-crest-derived cells in vagal and sacral pathways. Cell and tissue research 323, 11-25.

Andres, A.M., Santamaria, M.L., Ramos, E., Sarria, J., Molina, M., Hernandez, F., Encinas, J.L., Larrauri, J., Prieto, G., Tovar, J.A., 2010. Graft-vs-host disease after small bowel transplantation in children. Journal of pediatric surgery 45, 330-336; discussion 336.

Antonucci, A., Fronzoni, L., Cogliandro, L., Cogliandro, R.F., Caputo, C., De Giorgio, R., Pallotti, F., Barbara, G., Corinaldesi, R., Stanghellini, V., 2008. Chronic intestinal pseudo-obstruction. World J Gastroenterol 14, 2953-2961.

Aranishi, H., Kunisawa, Y., Komuro, T., 2009. Characterization of interstitial cells of Cajal in the subserosal layer of the guinea-pig colon. Cell and tissue research 335, 323-329.

Armulik, A., Genove, G., Betsholtz, C., 2011. Pericytes: developmental, physiological, and pathological perspectives, problems, and promises. Developmental cell 21, 193-215.

Asahara, T., Murohara, T., Sullivan, A., Silver, M., van der Zee, R., Li, T., Witzenbichler, B., Schatteman, G., Isner, J.M., 1997. Isolation of putative progenitor endothelial cells for angiogenesis. Science (New York, N.Y.) 275, 964-967.

Asahina, K., Zhou, B., Pu, W.T., Tsukamoto, H., 2011. Septum transversum-derived mesothelium gives rise to hepatic stellate cells and perivascular mesenchymal cells in developing mouse liver. Hepatology (Baltimore, Md.) 53, 983-995.

Attwood, S.W., Edel, M.J., 2019. iPS-Cell Technology and the Problem of Genetic Instability-Can It Ever Be Safe for Clinical Use? J Clin Med 8.

Au - Walton, K.D., Au - Kolterud, Å., 2014. Mouse Fetal Whole Intestine Culture System for Ex Vivo Manipulation of Signaling Pathways and Three-dimensional Live Imaging of Villus Development. JoVE, e51817.

Babensee, J.E., McIntire, L.V., Mikos, A.G., 2000. Growth factor delivery for tissue engineering. Pharm Res 17, 497-504.

Badylak, S.F., Taylor, D., Uygun, K., 2011. Whole-organ tissue engineering: decellularization and recellularization of three-dimensional matrix scaffolds. Annu Rev Biomed Eng 13, 27-53.

Barker, N., van Es, J.H., Kuipers, J., Kujala, P., van den Born, M., Cozijnsen, M., Haegebarth, A., Korving, J., Begthel, H., Peters, P.J., Clevers, H., 2007a. Identification of stem cells in small intestine and colon by marker gene Lgr5. Nature 449, 1003-1007.

Barker, N., van Es, J.H., Kuipers, J., Kujala, P., van den Born, M., Cozijnsen, M., Haegebarth, A., Korving, J., Begthel, H., Peters, P.J., Clevers, H., 2007b. Identification of stem cells in small intestine and colon by marker gene Lgr5. Nature 449, 1003-1007.

Battle, M.A., Bondow, B.J., Iverson, M.A., Adams, S.J., Jandacek, R.J., Tso, P., Duncan, S.A., 2008. GATA4 is essential for jejunal function in mice. Gastroenterology 135, 1676-1686 e1671.

Bausch-Fluck, D., Hofmann, A., Bock, T., Frei, A.P., Cerciello, F., Jacobs, A., Moest, H., Omasits, U., Gundry, R.L., Yoon, C., Schiess, R., Schmidt, A., Mirkowska, P., Hartlova, A., Van Eyk, J.E., Bourquin, J.P., Aebersold, R., Boheler, K.R., Zandstra, P., Wollscheid, B., 2015. A mass spectrometric-derived cell surface protein atlas. PloS one 10, e0121314.

Bengal, E., 2017. TAZ is involved in transcriptional complexes regulating smooth muscle cell differentiation. FEBS J 284, 1628-1630.

Beuling, E., Aronson, B.E., Tran, L.M.D., Stapleton, K.A., ter Horst, E.N., Vissers, L.A.T.M., Verzi, M.P., Krasinski, S.D., 2012. GATA6 is required for proliferation, migration, secretory cell maturation, and gene expression in the mature mouse colon. Molecular and Cellular Biology 32, 3392-3402.

Beuling, E., Baffour-Awuah, N.Y., Stapleton, K.A., Aronson, B.E., Noah, T.K., Shroyer, N.F., Duncan, S.A., Fleet, J.C., Krasinski, S.D., 2011. GATA factors regulate proliferation, differentiation, and gene expression in small intestine of mature mice. Gastroenterology 140, 1219-1229 e1211-1212.

Bianchi, A., 1984. Intestinal lengthening: an experimental and clinical review. Journal of the Royal Society of Medicine 77 Suppl 3, 35-41.

Bianco, P., Robey, P.G., 2001. Stem cells in tissue engineering. Nature 414, 118-121.

Bitar, K.N., 2003. Function of gastrointestinal smooth muscle: from signaling to contractile proteins. The American Journal of Medicine 115, 15-23.

Bitar, K.N., Raghavan, S., Zakhem, E., 2014. Tissue engineering in the gut: developments in neuromusculature. Gastroenterology 146, 1614-1624.

Blair, P.J., Rhee, P.L., Sanders, K.M., Ward, S.M., 2014. The significance of interstitial cells in neurogastroenterology. J Neurogastroenterol Motil 20, 294-317.

Bolger, A.M., Lohse, M., Usadel, B., 2014. Trimmomatic: a flexible trimmer for Illumina sequence data. Bioinformatics 30, 2114-2120.

Bolte, C., Ren, X., Tomley, T., Ustiyan, V., Pradhan, A., Hoggatt, A., Kalin, T.V., Herring, B.P., Kalinichenko, V.V., 2015. Forkhead box F2 regulation of platelet-derived growth factor and myocardin/serum response factor signaling is essential for intestinal development. J Biol Chem 290, 7563-7575.

Boluda, E.R., 2015. Pediatric small bowel transplantation. Current opinion in organ transplantation 20, 550-556.

Bondurand, N., Natarajan, D., Thapar, N., Atkins, C., Pachnis, V., 2003. Neuron and glia generating progenitors of the mammalian enteric nervous system isolated from foetal and postnatal gut cultures. Development (Cambridge, England) 130, 6387-6400.

Bosse, T., Piaseckyj, C.M., Burghard, E., Fialkovich, J.J., Rajagopal, S., Pu, W.T., Krasinski, S.D., 2006. Gata4 is essential for the maintenance of jejunal-ileal identities in the adult mouse small intestine. Mol Cell Biol 26, 9060-9070.

Bradford, M.M., 1976. A rapid and sensitive method for the quantitation of microgram quantities of protein utilizing the principle of protein-dye binding. Analytical biochemistry 72, 248-254.

Brown, M.A., Iyer, R.K., Radisic, M., 2008. Pulsatile perfusion bioreactor for cardiac tissue engineering. Biotechnol Prog 24, 907-920.

Brown, M.E., Rondon, E., Rajesh, D., Mack, A., Lewis, R., Feng, X., Zitur, L.J., Learish, R.D., Nuwaysir, E.F., 2010. Derivation of induced pluripotent stem cells from human peripheral blood T lymphocytes. PloS one 5, e11373.

Bullen, P., Wilson, D., 1997. The Carnegie staging of human embryos: a practical guide, Molecular genetics of early human development. Bios Scientific publishers, pp. 27-35.

Burns, A.J., Douarin, N.M., 1998. The sacral neural crest contributes neurons and glia to the post-umbilical gut: spatiotemporal analysis of the development of the enteric nervous system. Development (Cambridge, England) 125, 4335-4347.

Burns, A.J., Goldstein, A.M., Newgreen, D.F., Stamp, L., Schafer, K.H., Metzger, M., Hotta, R., Young, H.M., Andrews, P.W., Thapar, N., Belkind-Gerson, J., Bondurand, N., Bornstein, J.C., Chan, W.Y., Cheah, K., Gershon, M.D., Heuckeroth, R.O., Hofstra, R.M., Just, L., Kapur, R.P., King, S.K., McCann, C.J., Nagy, N., Ngan, E., Obermayr, F., Pachnis, V., Pasricha, P.J., Sham, M.H., Tam, P., Vanden Berghe, P., 2016. White paper on guidelines concerning enteric nervous system stem cell therapy for enteric neuropathies. Dev Biol 417, 229-251.

Burns, A.J., Lomax, A., Torihashi, S., Sanders, K.M., Ward, S.M., 1996. Interstitial cells of Cajal mediate inhibitory neurotransmission in the stomach. Proceedings of the National Academy of Sciences 93, 12008-12013.

Burns, A.J., Thapar, N., 2014. Neural stem cell therapies for enteric nervous system disorders. Nature reviews. Gastroenterology & hepatology 11, 317-328.

Bustin, S.A., Benes, V., Garson, J.A., Hellemans, J., Huggett, J., Kubista, M., Mueller, R., Nolan, T., Pfaffl, M.W., Shipley, G.L., Vandesompele, J., Wittwer, C.T., 2009. The MIQE guidelines: minimum information for publication of quantitative real-time PCR experiments. Clinical chemistry 55, 611-622.

Cajal, R.y.S., 1911. Histologie du système nerveux de l'homme et des vertébrés. Maloine, Paris 2, 153-173.

Cajal, S., 1893. Sur les ganglions et plexus nerveux de l'intestin. CR soc Biol. Paris 45, 217-223.

Caplan, A.I., 1991. Mesenchymal stem cells. Journal of orthopaedic research : official publication of the Orthopaedic Research Society 9, 641-650.

Cappellari, O., Cossu, G., 2013. Pericytes in development and pathology of skeletal muscle. Circulation research 113, 341-347.

Carmona, R., Cano, E., Mattiotti, A., Gaztambide, J., Munoz-Chapuli, R., 2013. Cells derived from the coelomic epithelium contribute to multiple gastrointestinal tissues in mouse embryos. PloS one 8, e55890.

Cervantes, S., Yamaguchi, T.P., Hebrok, M., 2009. Wnt5a is essential for intestinal elongation in mice. Dev Biol 326, 285-294.

Chandra, R., Kesavan, A., 2018. Current treatment paradigms in pediatric short bowel syndrome. Clinical journal of gastroenterology 11, 103-112.

Chang, P.S., Li, L., McAnally, J., Olson, E.N., 2001. Muscle specificity encoded by specific serum response factor-binding sites. J Biol Chem 276, 17206-17212.

Clevers, H., 2013. The Intestinal Crypt, A Prototype Stem Cell Compartment. Cell 154, 274-284.

Clevers, H., Conder, R.K., Li, V.S.W., Lutolf, M.P., Vallier, L., Chan, S., Grikscheit, T.C., Jensen, K.B., De Coppi, P., 2019. Tissue-Engineering the Intestine: The Trials before the Trials. Cell Stem Cell 24, 855-859.

Collett, G.D., Canfield, A.E., 2005. Angiogenesis and pericytes in the initiation of ectopic calcification. Circulation research 96, 930-938.

Conconi, M.T., De Coppi, P., Di Liddo, R., Vigolo, S., Zanon, G.F., Parnigotto, P.P., Nussdorfer, G.G., 2005. Tracheal matrices, obtained by a detergent-enzymatic method, support in vitro the adhesion of chondrocytes and tracheal epithelial cells. Transpl Int 18, 727-734.

Conesa, A., Götz, S., 2008. Blast2GO: A comprehensive suite for functional analysis in plant genomics. Int J Plant Genomics 2008, 619832-619832.

Cosgrove, B.D., Sacco, A., Gilbert, P.M., Blau, H.M., 2009. A home away from home: challenges and opportunities in engineering in vitro muscle satellite cell niches. Differentiation 78, 185-194.

Cossu, G., Bianco, P., 2003. Mesoangioblasts--vascular progenitors for extravascular mesodermal tissues. Current opinion in genetics & development 13, 537-542.

Cossu, G., Previtali, S.C., Napolitano, S., Cicalese, M.P., Tedesco, F.S., Nicastro, F., Noviello, M., Roostalu, U., Natali Sora, M.G., Scarlato, M., De Pellegrin, M., Godi, C., Giuliani, S., Ciotti, F., Tonlorenzi, R., Lorenzetti, I., Rivellini, C., Benedetti, S., Gatti, R., Marktel, S., Mazzi, B., Tettamanti, A., Ragazzi, M., Imro, M.A., Marano, G., Ambrosi, A., Fiori, R., Sormani, M.P., Bonini, C., Venturini, M., Politi, L.S., Torrente, Y., Ciceri, F., 2015. Intra-arterial transplantation of HLA-matched donor mesoangioblasts in Duchenne muscular dystrophy. EMBO Mol Med 7, 1513-1528.

Cotton, J.L., Li, Q., Ma, L., Park, J.-S., Wang, J., Ou, J., Zhu, L.J., Ip, Y.T., Johnson, R.L., Mao, J., 2017. YAP/TAZ and Hedgehog Coordinate Growth and Patterning in Gastrointestinal Mesenchyme. Developmental cell 43, 35-47.e34.

Crawley, S.W., Mooseker, M.S., Tyska, M.J., 2014. Shaping the intestinal brush border. The Journal of cell biology 207, 441-451.

Crisan, M., Yap, S., Casteilla, L., Chen, C.-W., Corselli, M., Park, T.S., Andriolo, G., Sun, B., Zheng, B., Zhang, L., Norotte, C., Teng, P.-N., Traas, J., Schugar, R., Deasy, B.M., Badylak, S., Bűhring, H.-J., Giacobino, J.-P., Lazzari, L., Huard, J., Péault, B., 2008. A Perivascular Origin for Mesenchymal Stem Cells in Multiple Human Organs. Cell Stem Cell 3, 301-313.

Cserni, T., Takayasu, H., Muzsnay, Z., Varga, G., Murphy, F., Folaranmi, S.E., Rakoczy, G., 2011. New idea of intestinal lengthening and tailoring. Pediatric surgery international 27, 1009-1013.

De Angelis, L., Berghella, L., Coletta, M., Lattanzi, L., Zanchi, M., Cusella-De Angelis, M.G., Ponzetto, C., Cossu, G., 1999. Skeletal myogenic progenitors originating from embryonic dorsal aorta coexpress endothelial and myogenic markers and contribute to postnatal muscle growth and regeneration. The Journal of cell biology 147, 869-878.

De Giorgio, R., Sarnelli, G., Corinaldesi, R., Stanghellini, V., 2004. Advances in our understanding of the pathology of chronic intestinal pseudo-obstruction. Gut 53, 1549-1552.

de Santa Barbara, P., van den Brink, G.R., Roberts, D.J., 2002. Molecular etiology of gut malformations and diseases. American journal of medical genetics 115, 221-230.

de Santa Barbara, P., van den Brink, G.R., Roberts, D.J., 2003. Development and differentiation of the intestinal epithelium. Cell Mol Life Sci 60, 1322-1332.

De Santa Barbara, P., Williams, J., Goldstein, A.M., Doyle, A.M., Nielsen, C., Winfield, S., Faure, S., Roberts, D.J., 2005. Bone morphogenetic protein signaling pathway plays multiple roles during gastrointestinal tract development. Developmental dynamics : an official publication of the American Association of Anatomists 234, 312-322.

Dellavalle, A., Maroli, G., Covarello, D., Azzoni, E., Innocenzi, A., Perani, L., Antonini, S., Sambasivan, R., Brunelli, S., Tajbakhsh, S., Cossu, G., 2011. Pericytes resident in postnatal skeletal muscle differentiate into muscle fibres and generate satellite cells. Nature communications 2, 499.

Dellavalle, A., Sampaolesi, M., Tonlorenzi, R., Tagliafico, E., Sacchetti, B., Perani, L., Innocenzi, A., Galvez, B.G., Messina, G., Morosetti, R., Li, S., Belicchi, M., Peretti, G., Chamberlain, J.S., Wright, W.E., Torrente, Y., Ferrari, S., Bianco, P., Cossu, G., 2007. Pericytes of human skeletal muscle are myogenic precursors distinct from satellite cells. Nature cell biology 9, 255-267.

Dessimoz, J., Opoka, R., Kordich, J.J., Grapin-Botton, A., Wells, J.M., 2006. FGF signaling is necessary for establishing gut tube domains along the anterior-posterior axis in vivo. Mech Dev 123, 42-55.

Di Nardo, G., Blandizzi, C., Volta, U., Colucci, R., Stanghellini, V., Barbara, G., Del Tacca, M., Tonini, M., Corinaldesi, R., De Giorgio, R., 2008. Review article: molecular, pathological and therapeutic features of human enteric neuropathies. Aliment Pharmacol Ther 28, 25-42.

Dobin, A., Davis, C.A., Schlesinger, F., Drenkow, J., Zaleski, C., Jha, S., Batut, P., Chaisson, M., Gingeras, T.R., 2013. STAR: ultrafast universal RNA-seq aligner. Bioinformatics 29, 15-21.

Duggan, C.P., Jaksic, T., 2017. Pediatric Intestinal Failure. The New England journal of medicine 377, 666-675.

Duluc, I., Freund, J.N., Leberquier, C., Kedinger, M., 1994. Fetal endoderm primarily holds the temporal and positional information required for mammalian intestinal development. The Journal of cell biology 126, 211-221.

Durbec, P.L., Larsson-Blomberg, L.B., Schuchardt, A., Costantini, F., Pachnis, V., 1996. Common origin and developmental dependence on c-ret of subsets of enteric and sympathetic neuroblasts. Development (Cambridge, England) 122, 349-358.

Elliott, M.J., De Coppi, P., Speggiorin, S., Roebuck, D., Butler, C.R., Samuel, E., Crowley, C., McLaren, C., Fierens, A., Vondrys, D., Cochrane, L., Jephson, C., Janes, S., Beaumont, N.J., Cogan, T., Bader, A., Seifalian, A.M., Hsuan, J.J., Lowdell, M.W., Birchall, M.A., 2012. Stem-cell-based, tissue engineered tracheal replacement in a child: a 2-year follow-up study. Lancet 380, 994-1000.

Evans, M.J., Kaufman, M.H., 1981. Establishment in culture of pluripotential cells from mouse embryos. Nature 292, 154-156.

Fang, R., Olds, L.C., Sibley, E., 2006. Spatio-temporal patterns of intestine-specific transcription factor expression during postnatal mouse gut development. Gene Expr Patterns 6, 426-432.

Faussone Pellegrini, M., 1977. Ultrastructure of the tunica muscularis of the cardial portion of the human esophagus and stomach, with special reference to the so-called Cajal's interstitial cells. Arch Ital Anat Embryol 82, 157-177.

Faussone Pellegrini, M.S., Cortesini, C., 1984. Ultrastructural peculiarities of the inner portion of the circular layer of colon. I. Research in the human. Acta anatomica 120, 185-189.

Fredriksson, L., Li, H., Eriksson, U., 2004. The PDGF family: four gene products form five dimeric isoforms. Cytokine & growth factor reviews 15, 197-204.

Frongia, G., Kessler, M., Weih, S., Nickkholgh, A., Mehrabi, A., Holland-Cunz, S., 2013. Comparison of LILT and STEP procedures in children with short bowel syndrome -- a systematic review of the literature. Journal of pediatric surgery 48, 1794-1805.

Fu, M., Tam, P.K., Sham, M.H., Lui, V.C., 2004. Embryonic development of the ganglion plexuses and the concentric layer structure of human gut: a topographical study. Anatomy and embryology 208, 33-41.

Furness, J.B., 2012. The enteric nervous system and neurogastroenterology. Nature Reviews Gastroenterology &Amp; Hepatology 9, 286.

Gabella, G., 2002. Development of visceral smooth muscle. Results and problems in cell differentiation 38, 1-37.

Galvez, B.G., Sampaolesi, M., Brunelli, S., Covarello, D., Gavina, M., Rossi, B., Constantin, G., Torrente, Y., Cossu, G., 2006. Complete repair of dystrophic skeletal muscle by mesoangioblasts with enhanced migration ability. The Journal of cell biology 174, 231-243.

Gao, N., White, P., Kaestner, K.H., 2009. Establishment of Intestinal Identity and Epithelial-Mesenchymal Signaling by Cdx2. Developmental cell 16, 588-599.

Gehart, H., Clevers, H., 2019. Tales from the crypt: new insights into intestinal stem cells. Nature reviews. Gastroenterology & hepatology 16, 19-34.

Gerrelli, D., Lisgo, S., Copp, A.J., Lindsay, S., 2015. Enabling research with human embryonic and fetal tissue resources. Development (Cambridge, England) 142, 3073-3076.

Gerritsen, J., Smidt, H., Rijkers, G.T., de Vos, W.M., 2011. Intestinal microbiota in human health and disease: the impact of probiotics. Genes Nutr 6, 209-240.

Geske, M.J., Zhang, X., Patel, K.K., Ornitz, D.M., Stappenbeck, T.S., 2008. Fgf9 signaling regulates small intestinal elongation and mesenchymal development. Development (Cambridge, England) 135, 2959-2968.

Glotzbach, J.P., Wong, V.W., Gurtner, G.C., Longaker, M.T., 2011. Regenerative medicine. Curr Probl Surg 48, 148-212.

Goldstein, A.M., Thapar, N., Karunaratne, T.B., De Giorgio, R., 2016. Clinical aspects of neurointestinal disease: Pathophysiology, diagnosis, and treatment. Dev Biol 417, 217-228.

Grant, C.N., Mojica, S.G., Sala, F.G., Hill, J.R., Levin, D.E., Speer, A.L., Barthel, E.R., Shimada, H., Zachos, N.C., Grikscheit, T.C., 2015. Human and mouse tissue-engineered small intestine both demonstrate digestive and absorptive function. American journal of physiology. Gastrointestinal and liver physiology 308, G664-677.

Grikscheit, T., Ochoa, E.R., Srinivasan, A., Gaissert, H., Vacanti, J.P., 2003. Tissue-engineered esophagus: experimental substitution by onlay patch or interposition. J Thorac Cardiovasc Surg 126, 537-544.

Grikscheit, T.C., Siddique, A., Ochoa, E.R., Srinivasan, A., Alsberg, E., Hodin, R.A., Vacanti, J.P., 2004. Tissue-engineered small intestine improves recovery after massive small bowel resection. Annals of surgery 240, 748-754.

Guiu, J., Jensen, K.B., 2015. From Definitive Endoderm to Gut-a Process of Growth and Maturation. Stem Cells Dev 24, 1972-1983.

Guo, X., Chen, S.-Y., 2012. Transforming growth factor-β and smooth muscle differentiation. World journal of biological chemistry 3, 41-52.

Gurdziel, K., Vogt, K.R., Walton, K.D., Schneider, G.K., Gumucio, D.L., 2016. Transcriptome of the inner circular smooth muscle of the developing mouse intestine: Evidence for regulation of visceral smooth muscle genes by the hedgehog target gene, cJun. Developmental dynamics : an official publication of the American Association of Anatomists 245, 614-626.

Ha, S.E., Lee, M.Y., Kurahashi, M., Wei, L., Jorgensen, B.G., Park, C., Park, P.J., Redelman, D., Sasse, K.C., Becker, L.S., Sanders, K.M., Ro, S., 2017. Transcriptome analysis of PDGFRalpha+ cells identifies T-type Ca2+ channel CACNA1G as a new pathological marker for PDGFRalpha+ cell hyperplasia. PloS one 12, e0182265.

Halayko, A.J., Kartha, S., Stelmack, G.L., McConville, J., Tam, J., Camoretti-Mercado, B., Forsythe, S.M., Hershenson, M.B., Solway, J., 2004. Phophatidylinositol-3 kinase/mammalian target of rapamycin/p70S6K regulates contractile protein accumulation in airway myocyte differentiation. Am J Respir Cell Mol Biol 31, 266-275.

Hao, M.M., Foong, J.P.P., Bornstein, J.C., Li, Z.L., Vanden Berghe, P., Boesmans, W., 2016. Enteric nervous system assembly: Functional integration within the developing gut. Developmental Biology 417, 168-181.

Hayashi, K., Shibata, K., Morita, T., Iwasaki, K., Watanabe, M., Sobue, K., 2004. Insulin receptor substrate-1/SHP-2 interaction, a phenotype-dependent switching machinery of insulin-like growth factor-I signaling in vascular smooth muscle cells. J Biol Chem 279, 40807-40818.

Hellemans, J., Mortier, G., De Paepe, A., Speleman, F., Vandesompele, J., 2007. qBase relative quantification framework and software for management and automated analysis of real-time quantitative PCR data. Genome Biol 8, R19.

Huang, H., Cotton, J.L., Wang, Y., Rajurkar, M., Zhu, L.J., Lewis, B.C., Mao, J., 2013. Specific requirement of Gli transcription factors in Hedgehog-mediated intestinal development. J Biol Chem 288, 17589-17596.

Hughes, C.S., Postovit, L.M., Lajoie, G.A., 2010. Matrigel: a complex protein mixture required for optimal growth of cell culture. Proteomics 10, 1886-1890.

Huycke, T.R., Miller, B.M., Gill, H.K., Nerurkar, N.L., Sprinzak, D., Mahadevan, L., Tabin, C.J., 2019. Genetic and Mechanical Regulation of Intestinal Smooth Muscle Development. Cell 179, 90-105.e121.

Iino, S., Horiguchi, K., Horiguchi, S., Nojyo, Y., 2009. c-Kit-negative fibroblast-like cells express platelet-derived growth factor receptor alpha in the murine gastrointestinal musculature. Histochem Cell Biol 131, 691-702.

Jeong, S.I., Kwon, J.H., Lim, J.I., Cho, S.W., Jung, Y., Sung, W.J., Kim, S.H., Kim, Y.H., Lee, Y.M., Kim, B.S., Choi, C.Y., Kim, S.J., 2005. Mechano-active tissue engineering of vascular smooth muscle using pulsatile perfusion bioreactors and elastic PLCL scaffolds. Biomaterials 26, 1405-1411.

Jeppesen, P.B., 2012. Teduglutide, a novel glucagon-like peptide 2 analog, in the treatment of patients with short bowel syndrome. Therapeutic Advances in Gastroenterology 5, 159-171.

Kajbafzadeh, A.M., Khorramirouz, R., Masoumi, A., Keihani, S., Nabavizadeh, B., 2018. Decellularized human fetal intestine as a bioscaffold for regeneration of the rabbit bladder submucosa. Journal of pediatric surgery 53, 1781-1788.

Kappus, M., Diamond, S., Hurt, R.T., Martindale, R., 2016. Intestinal Failure: New Definition and Clinical Implications. Current gastroenterology reports 18, 48.

Kapur, R.P., 2000. Colonization of the murine hindgut by sacral crest-derived neural precursors: experimental support for an evolutionarily conserved model. Dev Biol 227, 146-155.

Katari, R.S., Peloso, A., Orlando, G., 2014. Tissue engineering. Advances in surgery 48, 137-154.

Kedinger, M., Duluc, I., Fritsch, C., Lorentz, O., Plateroti, M., Freund, J.N., 1998. Intestinal epithelial-mesenchymal cell interactions, Annals of the New York Academy of Sciences, pp. 1-17.

Kim, H.B., Fauza, D., Garza, J., Oh, J.T., Nurko, S., Jaksic, T., 2003. Serial transverse enteroplasty (STEP): a novel bowel lengthening procedure. Journal of pediatric surgery 38, 425-429.

Kim, T.H., Kim, B.M., Mao, J., Rowan, S., Shivdasani, R.A., 2011. Endodermal Hedgehog signals modulate Notch pathway activity in the developing digestive tract mesenchyme. Development (Cambridge, England) 138, 3225-3233.

Kitano, K., Schwartz, D.M., Zhou, H., Gilpin, S.E., Wojtkiewicz, G.R., Ren, X., Sommer, C.A., Capilla, A.V., Mathisen, D.J., Goldstein, A.M., Mostoslavsky, G., Ott, H.C., 2017. Bioengineering of functional human induced pluripotent stem cell-derived intestinal grafts. Nature communications 8, 765.

Kluppel, M., Huizinga, J.D., Malysz, J., Bernstein, A., 1998. Developmental origin and Kit-dependent development of the interstitial cells of cajal in the mammalian small intestine. Developmental dynamics : an official publication of the American Association of Anatomists 211, 60-71.

Knowles, C.H., Silk, D.B., Darzi, A., Veress, B., Feakins, R., Raimundo, A.H., Crompton, T., Browning, E.C., Lindberg, G., Martin, J.E., 2004. Deranged smooth muscle alpha-actin as a biomarker of intestinal pseudo-obstruction: a controlled multinational case series. Gut 53, 1583-1589.

Kobayashi, M., Lei, N.Y., Wang, Q., Wu, B.M., Dunn, J.C., 2015. Orthogonally oriented scaffolds with aligned fibers for engineering intestinal smooth muscle. Biomaterials 61, 75-84.

Koh, S., Bradley, R.F., French, S.W., Farmer, D.G., Cortina, G., 2008. Congenital visceral myopathy with a predominantly hypertrophic pattern treated by multivisceral transplantation. Hum Pathol 39, 970-974.

Kohlnhofer, B.M., Thompson, C.A., Walker, E.M., Battle, M.A., 2016. GATA4 regulates epithelial cell proliferation to control intestinal growth and development in mice. Cell Mol Gastroenterol Hepatol 2, 189-209.

Kolterud, A., Grosse, A.S., Zacharias, W.J., Walton, K.D., Kretovich, K.E., Madison, B.B., Waghray, M., Ferris, J.E., Hu, C., Merchant, J.L., Dlugosz, A.A., Kottmann, A.H., Gumucio, D.L., 2009. Paracrine Hedgehog signaling in stomach and intestine: new roles for hedgehog in gastrointestinal patterning. Gastroenterology 137, 618-628.

Komuro, T., 2006. Structure and organization of interstitial cells of Cajal in the gastrointestinal tract. J Physiol 576, 653-658.

Kurahashi, M., Niwa, Y., Cheng, J., Ohsaki, Y., Fujita, A., Goto, H., Fujimoto, T., Torihashi, S., 2008. Platelet-derived growth factor signals play critical roles in differentiation of longitudinal smooth muscle cells in mouse embryonic gut. Neurogastroenterology and motility : the official journal of the European Gastrointestinal Motility Society 20, 521-531.

Kurahashi, M., Zheng, H., Dwyer, L., Ward, S.M., Koh, S.D., Sanders, K.M., 2011. A functional role for the 'fibroblast-like cells' in gastrointestinal smooth muscles. J Physiol 589, 697-710.

Lander, A.D., Kimble, J., Clevers, H., Fuchs, E., Montarras, D., Buckingham, M., Calof, A.L., Trumpp, A., Oskarsson, T., 2012. What does the concept of the stem cell niche really mean today? BMC Biology 10, 19.

Langer, R., Vacanti, J.P., 1993. Tissue engineering. Science (New York, N.Y.) 260, 920-926.

Larsson, E., McLean, S.E., Mecham, R.P., Lindahl, P., Nelander, S., 2008. Do two mutually exclusive gene modules define the phenotypic diversity of mammalian smooth muscle? Molecular Genetics and Genomics 280, 127.

Le Douarin, N.M., Teillet, M.A., 1973. The migration of neural crest cells to the wall of the digestive tract in avian embryo. Journal of embryology and experimental morphology 30, 31-48.

Lee, H.T., Hennig, G.W., Fleming, N.W., Keef, K.D., Spencer, N.J., Ward, S.M., Sanders, K.M., Smith, T.K., 2007. Septal interstitial cells of Cajal conduct pacemaker activity to excite muscle bundles in human jejunum. Gastroenterology 133, 907-917.

Lee, M.Y., Ha, S.E., Park, C., Park, P.J., Fuchs, R., Wei, L., Jorgensen, B.G., Redelman, D., Ward, S.M., Sanders, K.M., Ro, S., 2017. Transcriptome of interstitial cells of Cajal reveals unique and selective gene signatures. PloS one 12, e0176031.

Lee, M.Y., Park, C., Berent, R.M., Park, P.J., Fuchs, R., Syn, H., Chin, A., Townsend, J., Benson, C.C., Redelman, D., Shen, T.W., Park, J.K., Miano, J.M., Sanders, K.M., Ro, S., 2015. Smooth Muscle Cell Genome Browser: Enabling the Identification of Novel Serum Response Factor Target Genes. PloS one 10, e0133751.

Levin, D.E., Barthel, E.R., Speer, A.L., Sala, F.G., Hou, X., Torashima, Y., Grikscheit, T.C., 2013. Human tissue-engineered small intestine forms from postnatal progenitor cells. Journal of pediatric surgery 48, 129-137.

Li, X., Udager, A.M., Hu, C., Qiao, X.T., Richards, N., Gumucio, D.L., 2009. Dynamic patterning at the pylorus: formation of an epithelial intestine-stomach boundary in late fetal life. Developmental dynamics : an official publication of the American Association of Anatomists 238, 3205-3217.

Liao, Y., Smyth, G.K., Shi, W., 2014. featureCounts: an efficient general purpose program for assigning sequence reads to genomic features. Bioinformatics 30, 923-930.

Liu, L.S., Ng, C.K., Thompson, A.Y., Poser, J.W., Spiro, R.C., 2002. Hyaluronate-heparin conjugate gels for the delivery of basic fibroblast growth factor (FGF-2). J Biomed Mater Res 62, 128-135.

Loh, Y.H., Hartung, O., Li, H., Guo, C., Sahalie, J.M., Manos, P.D., Urbach, A., Heffner, G.C., Grskovic, M., Vigneault, F., Lensch, M.W., Park, I.H., Agarwal, S., Church, G.M., Collins, J.J., Irion, S., Daley, G.Q., 2010. Reprogramming of T cells from human peripheral blood. Cell Stem Cell 7, 15-19.

Ma, F., Fuqua, B.K., Hasin, Y., Yukhtman, C., Vulpe, C.D., Lusis, A.J., Pellegrini, M., 2019. A comparison between whole transcript and 3' RNA sequencing methods using Kapa and Lexogen library preparation methods. BMC Genomics 20, 9.

Madison, B.B., Braunstein, K., Kuizon, E., Portman, K., Qiao, X.T., Gumucio, D.L., 2005. Epithelial hedgehog signals pattern the intestinal crypt-villus axis. Development (Cambridge, England) 132, 279-289.

Maghsoudlou, P., Georgiades, F., Tyraskis, A., Totonelli, G., Loukogeorgakis, S.P., Orlando, G., Shangaris, P., Lange, P., Delalande, J.M., Burns, A.J., Cenedese, A., Sebire, N.J., Turmaine, M., Guest, B.N., Alcorn, J.F., Atala, A., Birchall, M.A., Elliott, M.J., Eaton, S., Pierro, A., Gilbert, T.W., De Coppi, P., 2013. Preservation of micro-architecture and angiogenic potential in a pulmonary acellular matrix obtained using intermittent intra-tracheal flow of detergent enzymatic treatment. Biomaterials 34, 6638-6648.

Maherali, N., Sridharan, R., Xie, W., Utikal, J., Eminli, S., Arnold, K., Stadtfeld, M., Yachechko, R., Tchieu, J., Jaenisch, R., Plath, K., Hochedlinger, K., 2007. Directly reprogrammed fibroblasts show global epigenetic remodeling and widespread tissue contribution. Cell Stem Cell 1, 55-70.

Mangalat, N., Teckman, J., 2018. Pediatric Intestinal Failure Review. Children (Basel, Switzerland) 5.

Mao, J., Kim, B.M., Rajurkar, M., Shivdasani, R.A., McMahon, A.P., 2010. Hedgehog signaling controls mesenchymal growth in the developing mammalian digestive tract. Development (Cambridge, England) 137, 1721-1729.

Martin, G.R., Wiley, L.M., Damjanov, I., 1977. The development of cystic embryoid bodies in vitro from clonal teratocarcinoma stem cells. Dev Biol 61, 230-244.

Martin, I., Wendt, D., Heberer, M., 2004. The role of bioreactors in tissue engineering. Trends Biotechnol 22, 80-86.

Martin, L.Y., Ladd, M.R., Werts, A., Sodhi, C.P., March, J.C., Hackam, D.J., 2018. Tissue engineering for the treatment of short bowel syndrome in children. Pediatric research 83, 249-257.

Mauro, A., Adams, W.R., 1961. The structure of the sarcolemma of the frog skeletal muscle fiber. J Biophys Biochem Cytol 10(4)Suppl, 177-185.

McCann, C.J., Alves, M.M., Brosens, E., Natarajan, D., Perin, S., Chapman, C., Hofstra, R.M., Burns, A.J., Thapar, N., 2019. Neuronal Development and Onset of Electrical Activity in the Human Enteric Nervous System. Gastroenterology 156, 1483-1495 e1486.

McCann, C.J., Cooper, J.E., Natarajan, D., Jevans, B., Burnett, L.E., Burns, A.J., Thapar, N., 2017. Transplantation of enteric nervous system stem cells rescues nitric oxide synthase deficient mouse colon. Nature communications 8, 15937.

Minasi, M.G., Riminucci, M., De Angelis, L., Borello, U., Berarducci, B., Innocenzi, A., Caprioli, A., Sirabella, D., Baiocchi, M., De Maria, R., Boratto, R., Jaffredo, T., Broccoli, V., Bianco, P., Cossu, G., 2002. The meso-angioblast: a multipotent, self-renewing cell that originates from the dorsal aorta and differentiates into most mesodermal tissues. Development (Cambridge, England) 129, 2773-2783.

Mizuno, T., Yasugi, S., 1990. Susceptibility of epithelia to directive influences of mesenchymes during organogenesis: uncoupling of morphogenesis and cytodifferentiation. Cell Differ Dev 31, 151-159.

Mo, R., Kim, J.H., Zhang, J., Chiang, C., Hui, C.C., Kim, P.C., 2001. Anorectal malformations caused by defects in sonic hedgehog signaling. The American journal of pathology 159, 765-774.

Montgomery, L.E., Tansey, E.A., Johnson, C.D., Roe, S.M., Quinn, J.G., 2016. Autonomic modification of intestinal smooth muscle contractility. Adv Physiol Educ 40, 104-109.

Montgomery, R.K., Mulberg, A.E., Grand, R.J., 1999. Development of the human gastrointestinal tract: Twenty years of progress. Gastroenterology 116, 702-731.

Moore KL, TVN, P., MG, T., 2016. The Developing Human, 10th Edition.

Mowat, A.M., Agace, W.W., 2014. Regional specialization within the intestinal immune system. Nat Rev Immunol 14, 667-685.

Munoz-Yague, M., Marín, J., Colina, F., Ibarrola, C., López-Alonso, G., Martín, M., Herruzo, J.S., 2006. Chronic primary intestinal pseudo-obstruction from visceral myopathy. Revista Espanola de Enfermedades Digestivas 98, 292.

Nagy, N., Goldstein, A.M., 2017. Enteric nervous system development: A crest cell's journey from neural tube to colon. Semin Cell Dev Biol 66, 94-106.

Nataf, V., Lecoin, L., Eichmann, A., Le Douarin, N.M., 1996. Endothelin-B receptor is expressed by neural crest cells in the avian embryo. Proceedings of the National Academy of Sciences of the United States of America 93, 9645-9650.

Natarajan, D., Cooper, J., Choudhury, S., Delalande, J.M., McCann, C., Howe, S.J., Thapar, N., Burns, A.J., 2014. Lentiviral labeling of mouse and human enteric nervous system stem cells for regenerative medicine studies. Neurogastroenterology and motility : the official journal of the European Gastrointestinal Motility Society 26, 1513-1518.

Natarajan, D., Marcos-Gutierrez, C., Pachnis, V., de Graaff, E., 2002. Requirement of signalling by receptor tyrosine kinase RET for the directed migration of enteric nervous system progenitor cells during mammalian embryogenesis. Development (Cambridge, England) 129, 5151-5160.

Nerurkar, N.L., Mahadevan, L., Tabin, C.J., 2017. BMP signaling controls buckling forces to modulate looping morphogenesis of the gut. Proceedings of the National Academy of Sciences of the United States of America 114, 2277-2282.

Nillesen, S.T., Geutjes, P.J., Wismans, R., Schalkwijk, J., Daamen, W.F., van Kuppevelt, T.H., 2007. Increased angiogenesis and blood vessel maturation in acellular collagen-heparin scaffolds containing both FGF2 and VEGF. Biomaterials 28, 1123-1131.

Notarnicola, C., Rouleau, C., Le Guen, L., Virsolvy, A., Richard, S., Faure, S., De Santa Barbara, P., 2012. The RNA-Binding Protein RBPMS2 Regulates Development of Gastrointestinal Smooth Muscle. Gastroenterology 143, 687-697.e689.

Offield, M.F., Jetton, T.L., Labosky, P.A., Ray, M., Stein, R.W., Magnuson, M.A., Hogan, B.L.M., Wright, C.V.E., 1996. PDX-1 is required for pancreatic outgrowth and differentiation of the rostral duodenum. Development (Cambridge, England) 122, 983-995.

Okabe, M., Ikawa, M., Kominami, K., Nakanishi, T., Nishimune, Y., 1997. 'Green mice' as a source of ubiquitous green cells. FEBS Lett 407, 313-319.

Okita, K., Ichisaka, T., Yamanaka, S., 2007. Generation of germline-competent induced pluripotent stem cells. Nature 448, 313-317.

Olson, L.E., Soriano, P., 2011. PDGFRbeta signaling regulates mural cell plasticity and inhibits fat development. Developmental cell 20, 815-826.

Orlando, G., Garcia-Arraras, J.E., Soker, T., Booth, C., Sanders, B., Ross, C.L., De Coppi, P., Farney, A.C., Rogers, J., Stratta, R.J., 2012. Regeneration and bioengineering of the gastrointestinal tract: current status and future perspectives. Dig Liver Dis 44, 714-720.

Ostrer, H., Wilson, D.I., Hanley, N.A., 2006. Human embryo and early fetus research. Clin Genet 70, 98-107.

Pachnis, V., Mankoo, B., Costantini, F., 1993. Expression of the c-ret proto-oncogene during mouse embryogenesis. Development (Cambridge, England) 119, 1005-1017.

Pagiatakis, C., Sun, D., Tobin, S.W., Miyake, T., McDermott, J.C., 2017. TGFbeta-TAZ/SRF signalling regulates vascular smooth muscle cell differentiation. FEBS J 284, 1644-1656.

Park, S.Y., Choi, J.W., Park, J.K., Song, E.H., Park, S.A., Kim, Y.S., Shin, Y.S., Kim, C.H., 2016. Tissue-engineered artificial oesophagus patch using three-dimensionally printed polycaprolactone with mesenchymal stem cells: a preliminary report. Interact Cardiovasc Thorac Surg 22, 712-717.

Pattyn, A., Morin, X., Cremer, H., Goridis, C., Brunet, J.F., 1999. The homeobox gene Phox2b is essential for the development of autonomic neural crest derivatives. Nature 399, 366-370.

Pearson, G., Robinson, F., Beers Gibson, T., Xu, B.E., Karandikar, M., Berman, K., Cobb, M.H., 2001. Mitogen-activated protein (MAP) kinase pathways: regulation and physiological functions. Endocr Rev 22, 153-183.

Peri, L.E., Sanders, K.M., Mutafova-Yambolieva, V.N., 2013. Differential expression of genes related to purinergic signaling in smooth muscle cells, PDGFRalpha-positive cells, and interstitial cells of Cajal in the murine colon. Neurogastroenterology and motility : the official journal of the European Gastrointestinal Motility Society 25, e609-620.

Perin, S., McCann, C.J., Borrelli, O., De Coppi, P., Thapar, N., 2017. Update on Foregut Molecular Embryology and Role of Regenerative Medicine Therapies. Frontiers in pediatrics 5, 91.

Perin, S., McCann, C.J., De Coppi, P., Thapar, N., 2019. Isolation and characterisation of mouse intestinal mesoangioblasts. Pediatric surgery international 35, 29-34.

Perkins, J.R., Dawes, J.M., McMahon, S.B., Bennett, D.L., Orengo, C., Kohl, M., 2012. ReadqPCR and NormqPCR: R packages for the reading, quality checking and normalisation of RT-qPCR quantification cycle (Cq) data. BMC Genomics 13, 296.

Pipes, G.C., Creemers, E.E., Olson, E.N., 2006. The myocardin family of transcriptional coactivators: versatile regulators of cell growth, migration, and myogenesis. Genes Dev 20, 1545-1556.

Place, E.S., George, J.H., Williams, C.K., Stevens, M.M., 2009. Synthetic polymer scaffolds for tissue engineering. Chemical Society reviews 38, 1139-1151.

Quattrocelli, M., Palazzolo, G., Perini, I., Crippa, S., Cassano, M., Sampaolesi, M., 2012. Mouse and human mesoangioblasts: isolation and characterization from adult skeletal muscles. Methods in molecular biology (Clifton, N.J.) 798, 65-76.

Que, J., Wilm, B., Hasegawa, H., Wang, F., Bader, D., Hogan, B.L., 2008. Mesothelium contributes to vascular smooth muscle and mesenchyme during lung development. Proceedings of the National Academy of Sciences of the United States of America 105, 16626-16630.

R Development Core Team, 2008. R: A Language and Environment for Statistical Computing. R Foundation for Statistical Computing, Vienna, Austria.

Raghavan, S., Lam, M.T., Foster, L.L., Gilmont, R.R., Somara, S., Takayama, S., Bitar, K.N., 2010. Bioengineered three-dimensional physiological model of colonic longitudinal smooth muscle in vitro. Tissue engineering. Part C, Methods 16, 999-1009.

Ramalho-Santos, M., Melton, D.A., McMahon, A.P., 2000. Hedgehog signals regulate multiple aspects of gastrointestinal development. Development (Cambridge, England) 127, 2763-2772.

Rangarajan, S., Madden, L., Bursac, N., 2014. Use of flow, electrical, and mechanical stimulation to promote engineering of striated muscles. Ann Biomed Eng 42, 1391-1405.

Rensen, S.S., Doevendans, P.A., van Eys, G.J., 2007. Regulation and characteristics of vascular smooth muscle cell phenotypic diversity. Netherlands heart journal : monthly journal of the Netherlands Society of Cardiology and the Netherlands Heart Foundation 15, 100-108.

Riehl, B.D., Park, J.-H., Kwon, I.K., Lim, J.Y., 2012. Mechanical stretching for tissue engineering: two-dimensional and three-dimensional constructs. Tissue Eng Part B Rev 18, 288-300.

Rinkevich, Y., Mori, T., Sahoo, D., Xu, P.X., Bermingham, J.R., Jr., Weissman, I.L., 2012. Identification and prospective isolation of a mesothelial precursor lineage giving rise to smooth muscle cells and fibroblasts for mammalian internal organs, and their vasculature. Nature cell biology 14, 1251-1260.

Roberts, R.R., Ellis, M., Gwynne, R.M., Bergner, A.J., Lewis, M.D., Beckett, E.A., Bornstein, J.C., Young, H.M., 2010. The first intestinal motility patterns in fetal mice are not mediated by neurons or interstitial cells of Cajal. The Journal of physiology 588, 1153-1169.

Roberts, R.R., Murphy, J.F., Young, H.M., Bornstein, J.C., 2007. Development of colonic motility in the neonatal mouse-studies using spatiotemporal maps. American journal of physiology. Gastrointestinal and liver physiology 292, G930-938.

Robinson, M.D., McCarthy, D.J., Smyth, G.K., 2010. edgeR: a Bioconductor package for differential expression analysis of digital gene expression data. Bioinformatics 26, 139-140.

Robinson, M.D., Oshlack, A., 2010. A scaling normalization method for differential expression analysis of RNA-seq data. Genome Biol 11, R25.

Robson, P., 2014. Deciphering developmental processes from single-cell transcriptomes. Developmental cell 29, 260-261.

Sacchetti, B., Funari, A., Remoli, C., Giannicola, G., Kogler, G., Liedtke, S., Cossu, G., Serafini, M., Sampaolesi, M., Tagliafico, E., Tenedini, E., Saggio, I., Robey, P.G., Riminucci, M., Bianco, P., 2016. No Identical "Mesenchymal Stem Cells" at Different Times and Sites: Human Committed Progenitors of Distinct Origin and Differentiation Potential Are Incorporated as Adventitial Cells in Microvessels. Stem cell reports 6, 897-913.

Sadler, T.W., 2011. Langman's medical embryology. Lippincott Williams & Wilkins.

Sailaja, B.S., He, X.C., Li, L., 2016. The regulatory niche of intestinal stem cells. The Journal of Physiology 594, 4827-4836.

Sakiyama, J.-i., Yokouchi, Y., Kuroiwa, A., 2001. HoxA and HoxB cluster genes subdivide the digestive tract into morphological domains during chick development. Mechanisms of Development 101, 233-236.

Sala, F.G., Matthews, J.A., Speer, A.L., Torashima, Y., Barthel, E.R., Grikscheit, T.C., 2011. A multicellular approach forms a significant amount of tissue-engineered small intestine in the mouse. Tissue engineering. Part A 17, 1841-1850.

Sanders, K.M., Koh, S.D., Ro, S., Ward, S.M., 2012. Regulation of gastrointestinal motility--insights from smooth muscle biology. Nature reviews. Gastroenterology & hepatology 9, 633-645.

Sanders, K.M., Ward, S.M., Koh, S.D., 2014. Interstitial cells: regulators of smooth muscle function. Physiol Rev 94, 859-907.

Sasselli, V., Pachnis, V., Burns, A.J., 2012. The enteric nervous system. Developmental Biology 366, 64-73.

Sato, T., Stange, D.E., Ferrante, M., Vries, R.G., Van Es, J.H., Van den Brink, S., Van Houdt, W.J., Pronk, A., Van Gorp, J., Siersema, P.D., Clevers, H., 2011. Long-term expansion of epithelial organoids from human colon, adenoma, adenocarcinoma, and Barrett's epithelium. Gastroenterology 141, 1762-1772.

Saund, R.S., Kanai-Azuma, M., Kanai, Y., Kim, I., Lucero, M.T., Saijoh, Y., 2012. Gut endoderm is involved in the transfer of left-right asymmetry from the node to the lateral plate mesoderm in the mouse embryo. Development (Cambridge) 139, 2426-2435.

Schaafsma, D., McNeill, K.D., Stelmack, G.L., Gosens, R., Baarsma, H.A., Dekkers, B.G.J., Frohwerk, E., Penninks, J.-M., Sharma, P., Ens, K.M., Nelemans, S.A., Zaagsma, J., Halayko, A.J., Meurs, H., 2007. Insulin increases the expression of contractile phenotypic markers in airway smooth muscle. American Journal of Physiology-Cell Physiology 293, C429-C439.

Schlieve, C.R., Fowler, K.L., Thornton, M., Huang, S., Hajjali, I., Hou, X., Grubbs, B., Spence, J.R., Grikscheit, T.C., 2017. Neural Crest Cell Implantation Restores Enteric Nervous System Function and Alters the Gastrointestinal Transcriptome in Human Tissue-Engineered Small Intestine. Stem cell reports 9, 883-896.

Scirocco, A., Matarrese, P., Carabotti, M., Ascione, B., Malorni, W., Severi, C., 2016. Cellular and Molecular Mechanisms of Phenotypic Switch in Gastrointestinal Smooth Muscle. Journal of Cellular Physiology 231, 295-302.

Seki, T., Yuasa, S., Oda, M., Egashira, T., Yae, K., Kusumoto, D., Nakata, H., Tohyama, S., Hashimoto, H., Kodaira, M., Okada, Y., Seimiya, H., Fusaki, N., Hasegawa, M., Fukuda, K., 2010. Generation of induced pluripotent stem cells from human terminally differentiated circulating T cells. Cell Stem Cell 7, 11-14.

Sekimoto, T., Yoshinobu, K., Yoshida, M., Kuratani, S., Fujimoto, S., Araki, M., Tajima, N., Araki, K., Yamamura, K.-i., 1998. Region-specific expression of murine Hox genes implies the Hox code-mediated patterning of the digestive tract. Genes to Cells 3, 51-64.

Serbedzija, G.N., Burgan, S., Fraser, S.E., Bronner-Fraser, M., 1991. Vital dye labelling demonstrates a sacral neural crest contribution to the enteric nervous system of chick and mouse embryos. Development (Cambridge, England) 111, 857-866.

Shamblott, M.J., Axelman, J., Wang, S., Bugg, E.M., Littlefield, J.W., Donovan, P.J., Blumenthal, P.D., Huggins, G.R., Gearhart, J.D., 1998. Derivation of pluripotent stem cells from cultured human primordial germ cells. Proceedings of the National Academy of Sciences of the United States of America 95, 13726-13731.

Sherwood, R.I., Chen, T.Y.A., Melton, D.A., 2009. Transcriptional dynamics of endodermal organ formation. Developmental Dynamics 238, 29-42.

Sherwood, R.I., Maehr, R., Mazzoni, E.O., Melton, D.A., 2011. Wnt signaling specifies and patterns intestinal endoderm. Mechanisms of Development 128, 387-400.

Shi, S., Gronthos, S., 2003. Perivascular niche of postnatal mesenchymal stem cells in human bone marrow and dental pulp. Journal of bone and mineral research : the official journal of the American Society for Bone and Mineral Research 18, 696-704.

Smith, V.V., Milla, P.J., 1997. Histological phenotypes of enteric smooth muscle disease causing functional intestinal obstruction in childhood. Histopathology 31, 112-122.

Smits, A.M., Dronkers, E., Goumans, M.-J., 2018. The epicardium as a source of multipotent adult cardiac progenitor cells: Their origin, role and fate. Pharmacological Research 127, 129-140.

So, W.-K., Cheung, T.H., 2018. Molecular Regulation of Cellular Quiescence: A Perspective from Adult Stem Cells and Its Niches, in: Lacorazza, H.D. (Ed.), Cellular Quiescence: Methods and Protocols. Springer New York, New York, NY, pp. 1-25.

Somara, S., Gilmont, R.R., Dennis, R.G., Bitar, K.N., 2009. Bioengineered Internal Anal Sphincter Derived From Isolated Human Internal Anal Sphincter Smooth Muscle Cells. Gastroenterology 137, 53-61.

Somlyo, A.P., Himpens, B., 1989. Cell calcium and its regulation in smooth muscle. FASEB journal : official publication of the Federation of American Societies for Experimental Biology 3, 2266-2276.

Spangrude, G.J., Heimfeld, S., Weissman, I.L., 1988. Purification and characterization of mouse hematopoietic stem cells. Science (New York, N.Y.) 241, 58-62.

Squires, R.H., Duggan, C., Teitelbaum, D.H., Wales, P.W., Balint, J., Venick, R., Rhee, S., Sudan, D., Mercer, D., Martinez, J.A., Carter, B.A., Soden, J., Horslen, S., Rudolph, J.A., Kocoshis, S., Superina, R., Lawlor, S., Haller, T., Kurs-Lasky, M., Belle, S.H., 2012. Natural history of pediatric intestinal failure: initial report from the Pediatric Intestinal Failure Consortium. The Journal of pediatrics 161, 723-728.e722.

Staerk, J., Dawlaty, M.M., Gao, Q., Maetzel, D., Hanna, J., Sommer, C.A., Mostoslavsky, G., Jaenisch, R., 2010. Reprogramming of human peripheral blood cells to induced pluripotent stem cells. Cell Stem Cell 7, 20-24.

Standring, S., 2016. Gray's Anatomy: the anatomical basis of clinical practice, Forty-first edition ed. Elsevier Limited, United States.

Stoeckius, M., Hafemeister, C., Stephenson, W., Houck-Loomis, B., Chattopadhyay, P.K., Swerdlow, H., Satija, R., Smibert, P., 2017. Simultaneous epitope and transcriptome measurement in single cells. Nature methods 14, 865.

Sugii, S., Kida, Y., Kawamura, T., Suzuki, J., Vassena, R., Yin, Y.Q., Lutz, M.K., Berggren, W.T., Izpisua Belmonte, J.C., Evans, R.M., 2010. Human and mouse adipose-derived cells support feeder-independent induction of pluripotent stem cells. Proceedings of the National Academy of Sciences of the United States of America 107, 3558-3563.

Sukegawa, A., Narita, T., Kameda, T., Saitoh, K., Nohno, T., Hideo, I., Yasugi, S., Fukuda, K., 2000. The concentric structure of the developing gut is regulated by Sonic hedgehog derived from endodermal epithelium. Development (Cambridge, England) 127, 1971-1980.

Sun, N., Panetta, N.J., Gupta, D.M., Wilson, K.D., Lee, A., Jia, F., Hu, S., Cherry, A.M., Robbins, R.C., Longaker, M.T., Wu, J.C., 2009. Feeder-free derivation of induced pluripotent stem cells from adult human adipose stem cells. Proceedings of the National Academy of Sciences of the United States of America 106, 15720-15725.

Suzuki, H., Ward, S., Bayguinov, Y., Edwards, F., Hirst, G., 2003. Involvement of intramuscular interstitial cells in nitrergic inhibition in the mouse gastric antrum. The Journal of physiology 546, 751-763.

Tagliafico, E., Brunelli, S., Bergamaschi, A., De Angelis, L., Scardigli, R., Galli, D., Battini, R., Bianco, P., Ferrari, S., Cossu, G., Ferrari, S., 2004. TGFbeta/BMP activate the smooth muscle/bone differentiation programs in mesoangioblasts. J Cell Sci 117, 4377-4388.

Takahashi, K., Tanabe, K., Ohnuki, M., Narita, M., Ichisaka, T., Tomoda, K., Yamanaka, S., 2007. Induction of pluripotent stem cells from adult human fibroblasts by defined factors. Cell 131, 861-872.

Takahashi, K., Yamanaka, S., 2006. Induction of pluripotent stem cells from mouse embryonic and adult fibroblast cultures by defined factors. Cell 126, 663-676.

Tan, B., Wei, R.Q., Tan, M.Y., Luo, J.C., Deng, L., Chen, X.H., Hou, J.L., Li, X.Q., Yang, Z.M., Xie, H.Q., 2013. Tissue engineered esophagus by mesenchymal stem cell seeding for esophageal repair in a canine model. J Surg Res 182, 40-48.

Tang, Y., Urs, S., Boucher, J., Bernaiche, T., Venkatesh, D., Spicer, D.B., Vary, C.P.H., Liaw, L., 2010. Notch and Transforming Growth Factor-β (TGFβ) Signaling Pathways Cooperatively Regulate Vascular Smooth Muscle Cell Differentiation. Journal of Biological Chemistry 285, 17556-17563.

Tang, Y., Urs, S., Liaw, L., 2008. Hairy-related transcription factors inhibit Notch-induced smooth muscle alpha-actin expression by interfering with Notch intracellular domain/CBF-1 complex interaction with the CBF-1-binding site. Circulation research 102, 661-668.

Taxi, J., 1952. Cellules de Schwann et cellules interstitielles de cajal au niveau des plexusnerveus de la musculeus inteestinale du Cobaye: retour aux definitions. Arch Anat microscmorphol Exp 41 281, 304.

Thapar, N., Saliakellis, E., Benninga, M.A., Borrelli, O., Curry, J., Faure, C., De Giorgio, R., Gupte, G., Knowles, C.H., Staiano, A., Vandenplas, Y., Di Lorenzo, C., 2018. Paediatric Intestinal Pseudo-obstruction: Evidence and Consensus-based Recommendations From an ESPGHAN-Led Expert Group. J Pediatr Gastroenterol Nutr 66, 991-1019.

Thorén, L.A., Liuba, K., Bryder, D., Nygren, J.M., Jensen, C.T., Qian, H., Antonchuk, J., Jacobsen, S.-E.W., 2008. Kit Regulates Maintenance of Quiescent Hematopoietic Stem Cells. The Journal of Immunology 180, 2045.

Tonlorenzi, R., Dellavalle, A., Schnapp, E., Cossu, G., Sampaolesi, M., 2007. Isolation and characterization of mesoangioblasts from mouse, dog, and human tissues. Current protocols in stem cell biology Chapter 2, Unit 2B.1.

Torihashi, S., Hattori, T., Hasegawa, H., Kurahashi, M., Ogaeri, T., Fujimoto, T., 2009. The expression and crucial roles of BMP signaling in development of smooth muscle progenitor cells in the mouse embryonic gut. Differentiation 77, 277-289.

Torihashi, S., Nishi, K., Tokutomi, Y., Nishi, T., Ward, S., Sanders, K.M., 1999. Blockade of kit signaling induces transdifferentiation of interstitial cells of cajal to a smooth muscle phenotype. Gastroenterology 117, 140-148.

Torihashi, S., Ward, S.M., Nishikawa, S., Nishi, K., Kobayashi, S., Sanders, K.M., 1995. c-kit-dependent development of interstitial cells and electrical activity in the murine gastrointestinal tract. Cell and tissue research 280, 97-111.

Torihashi, S., Ward, S.M., Sanders, K.M., 1997. Development of c-Kit-positive cells and the onset of electrical rhythmicity in murine small intestine. Gastroenterology 112, 144-155.

Totonelli, G., Maghsoudlou, P., Garriboli, M., Riegler, J., Orlando, G., Burns, A.J., Sebire, N.J., Smith, V.V., Fishman, J.M., Ghionzoli, M., Turmaine, M., Birchall, M.A., Atala, A., Soker, S., Lythgoe, M.F., Seifalian, A., Pierro, A., Eaton, S., De Coppi, P., 2012. A rat decellularized small bowel scaffold that preserves villus-crypt architecture for intestinal regeneration. Biomaterials 33, 3401-3410.

Treutlein, B., Brownfield, D.G., Wu, A.R., Neff, N.F., Mantalas, G.L., Espinoza, F.H., Desai, T.J., Krasnow, M.A., Quake, S.R., 2014. Reconstructing lineage hierarchies of the distal lung epithelium using single-cell RNA-seq. Nature 509, 371.

Urbani, L., Camilli, C., Phylactopoulos, D.E., Crowley, C., Natarajan, D., Scottoni, F., Maghsoudlou, P., McCann, C.J., Pellegata, A.F., Urciuolo, A., Deguchi, K., Khalaf, S., Aruta, S.F., Signorelli, M.C., Kiely, D., Hannon, E., Trevisan, M., Wong, R.R., Baradez,

M.O., Moulding, D., Virasami, A., Gjinovci, A., Loukogeorgakis, S., Mantero, S., Thapar, N., Sebire, N., Eaton, S., Lowdell, M., Cossu, G., Bonfanti, P., De Coppi, P., 2018. Multi-stage bioengineering of a layered oesophagus with in vitro expanded muscle and epithelial adult progenitors. Nature communications 9.

Urciuolo, A., Urbani, L., Perin, S., Maghsoudlou, P., Scottoni, F., Gjinovci, A., Collins-Hooper, H., Loukogeorgakis, S., Tyraskis, A., Torelli, S., Germinario, E., Fallas, M.E.A., Julia-Vilella, C., Eaton, S., Blaauw, B., Patel, K., De Coppi, P., 2018. Decellularised skeletal muscles allow functional muscle regeneration by promoting host cell migration. Sci Rep 8, 8398.

van der Flier, L.G., Haegebarth, A., Stange, D.E., van de Wetering, M., Clevers, H., 2009a. OLFM4 Is a Robust Marker for Stem Cells in Human Intestine and Marks a Subset of Colorectal Cancer Cells. Gastroenterology 137, 15-17.

van der Flier, L.G., van Gijn, M.E., Hatzis, P., Kujala, P., Haegebarth, A., Stange, D.E., Begthel, H., van den Born, M., Guryev, V., Oving, I., van Es, J.H., Barker, N., Peters, P.J., van de Wetering, M., Clevers, H., 2009b. Transcription Factor Achaete Scute-Like 2 Controls Intestinal Stem Cell Fate. Cell 136, 903-912.

Van Der Werf, C.S., Sribudiani, Y., Verheij, J.B.G.M., Carroll, M., O'Loughlin, E., Chen, C.H., Brooks, A.S., Liszewski, M.K., Atkinson, J.P., Hofstra, R.M.W., 2013. Congenital short bowel syndrome as the presenting symptom in male patients with FLNA mutations. Genetics in Medicine 15, 310-313.

Vanderwinden, J.M., Rumessen, J.J., Bernex, F., Schiffmann, S.N., Panthier, J.J., 2000. Distribution and ultrastructure of interstitial cells of Cajal in the mouse colon, using antibodies to Kit and Kit(W-lacZ) mice. Cell and tissue research 302, 155-170.

Varelas, X., 2014. The Hippo pathway effectors TAZ and YAP in development, homeostasis and disease. Development (Cambridge, England) 141, 1614-1626.

Vasita, R., Katti, D.S., 2006. Growth factor-delivery systems for tissue engineering: a materials perspective. Expert Rev Med Devices 3, 29-47.

Viotti, M., Niu, L., Shi, S.H., Hadjantonakis, A.K., 2012. Role of the gut endoderm in relaying left-right patterning in mice. PLoS Biology 10.

Walker, E.M., Thompson, C.A., Kohlnhofer, B.M., Faber, M.L., Battle, M.A., 2014. Characterization of the developing small intestine in the absence of either GATA4 or GATA6. BMC Research Notes 7.

Wallace, A.S., Burns, A.J., 2005. Development of the enteric nervous system, smooth muscle and interstitial cells of Cajal in the human gastrointestinal tract. Cell and tissue research 319, 367-382.

Walsh, M.P., 1994. Calmodulin and the regulation of smooth muscle contraction. Molecular and Cellular Biochemistry 135, 21-41.

Wang, D.Z., Li, S., Hockemeyer, D., Sutherland, L., Wang, Z., Schratt, G., Richardson, J.A., Nordheim, A., Olson, E.N., 2002. Potentiation of serum response factor activity by

a family of myocardin-related transcription factors. Proceedings of the National Academy of Sciences of the United States of America 99, 14855-14860.

Wang, S., Walton, K.D., Gumucio, D.L., 2019. Chapter Two - Signals and forces shaping organogenesis of the small intestine, in: Wellik, D.M. (Ed.), Current Topics in Developmental Biology. Academic Press, pp. 31-65.

Wang, X., Chan, A.K., Sham, M.H., Burns, A.J., Chan, W.Y., 2011. Analysis of the sacral neural crest cell contribution to the hindgut enteric nervous system in the mouse embryo. Gastroenterology 141, 992-1002.e1001-1006.

Ward, S.M., Burns, A.J., Torihashi, S., Sanders, K.M., 1994. Mutation of the proto-oncogene c-kit blocks development of interstitial cells and electrical rhythmicity in murine intestine. J Physiol 480 (Pt 1), 91-97.

Ward, S.M., Sanders, K.M., 1990. Pacemaker activity in septal structures of canine colonic circular muscle. American Journal of Physiology-Gastrointestinal and Liver Physiology 259, G264-G273.

Wernig, M., Meissner, A., Foreman, R., Brambrink, T., Ku, M., Hochedlinger, K., Bernstein, B.E., Jaenisch, R., 2007. In vitro reprogramming of fibroblasts into a pluripotent ES-cell-like state. Nature 448, 318-324.

Wilm, B., Ipenberg, A., Hastie, N.D., Burch, J.B., Bader, D.M., 2005. The serosal mesothelium is a major source of smooth muscle cells of the gut vasculature. Development (Cambridge, England) 132, 5317-5328.

Wilson, Y.M., Richards, K.L., Ford-Perriss, M.L., Panthier, J.J., Murphy, M., 2004. Neural crest cell lineage segregation in the mouse neural tube. Development (Cambridge, England) 131, 6153-6162.

Wong, V.W., Wan, D.C., Gurtner, G.C., Longaker, M.T., 2012. Regenerative surgery: tissue engineering in general surgical practice. World J Surg 36, 2288-2299.

Wu, X., Wang, S., Chen, B., An, X., 2010. Muscle-derived stem cells: isolation, characterization, differentiation, and application in cell and gene therapy. Cell and tissue research 340, 549-567.

Yamada, M., Udagawa, J., Matsumoto, A., Hashimoto, R., Hatta, T., Nishita, M., Minami, Y., Otani, H., 2010. Ror2 is required for midgut elongation during mouse development. Developmental Dynamics 239, 941-953.

Yau, T.M., Li, G., Zhang, Y., Weisel, R.D., Mickle, D.A., Li, R.K., 2005. Vascular endothelial growth factor receptor upregulation in response to cell-based angiogenic gene therapy. Ann Thorac Surg 79, 2056-2063.

Yin, H., Price, F., Rudnicki, M.A., 2013. Satellite cells and the muscle stem cell niche. Physiol Rev 93, 23-67.

Yntema, C.L., Hammond, W.S., 1954. The origin of intrinsic ganglia of trunk viscera from vagal neural crest in the chick embryo. J Comp Neurol 101, 515-541.

Young, H.M., Ciampoli, D., Hsuan, J., Canty, A.J., 1999. Expression of Ret-, p75(NTR)-, Phox2a-, Phox2b-, and tyrosine hydroxylase-immunoreactivity by undifferentiated neural crest-derived cells and different classes of enteric neurons in the embryonic mouse gut. Developmental dynamics : an official publication of the American Association of Anatomists 216, 137-152.

Yu, G., Wang, L.-G., Han, Y., He, Q.-Y., 2012. clusterProfiler: an R package for comparing biological themes among gene clusters. OMICS 16, 284-287.

Yu, J., Vodyanik, M.A., Smuga-Otto, K., Antosiewicz-Bourget, J., Frane, J.L., Tian, S., Nie, J., Jonsdottir, G.A., Ruotti, V., Stewart, R., Slukvin, II, Thomson, J.A., 2007. Induced pluripotent stem cell lines derived from human somatic cells. Science (New York, N.Y.) 318, 1917-1920.

Zacharias, W.J., Madison, B.B., Kretovich, K.E., Walton, K.D., Richards, N., Udager, A.M., Li, X., Gumucio, D.L., 2011. Hedgehog signaling controls homeostasis of adult intestinal smooth muscle. Developmental Biology 355, 152-162.

Zakhem, E., Raghavan, S., Suhar, R.A., Bitar, K.N., 2019. Bioengineering and regeneration of gastrointestinal tissue: where are we now and what comes next? Expert Opin Biol Ther 19, 527-537.

Zambaiti, E., Scottoni, F., Rizzi, E., Russo, S., Deguchi, K., Eaton, S., Pellegata, A.F., De Coppi, P., 2019. Whole rat stomach decellularisation using a detergent-enzymatic protocol. Pediatric surgery international 35, 21-27.

Zheng, X.L., 2014. Myocardin and smooth muscle differentiation. Archives of biochemistry and biophysics 543, 48-56.

Zuk, P.A., Zhu, M., Mizuno, H., Huang, J., Futrell, J.W., Katz, A.J., Benhaim, P., Lorenz, H.P., Hedrick, M.H., 2001. Multilineage cells from human adipose tissue: implications for cell-based therapies. Tissue engineering 7, 211-228.

Acknowledgments

I would like to offer my sincere thanks to my supervisors, Dr Nikhil Thapar and Professor Paolo De Coppi, for their guidance and insight. You trusted me and gave me the freedom to pursue my own ideas, and for this I want to express to you my gratitude.
Thanks, Nikhil, for welcoming me in your wonderful lab where I got the chance to meet and work with extraordinary people. Our late lunches (calling them dinners would have been outrageous!!!) made me feel like being part of a family, but most importantly taught me that a Christmas party without “Thai calamari” is not worth it!
Thanks, Paolo, for introducing me to the world of research and for all the advice for my future medical career.

Thanks to Professor Allan Goldstein and Professor Andrew Copp for the stimulating discussion and thoughtful comments on my work.

A special thank goes to Dr Dipa Natarajan, who started and finished this journey with me. Your enthusiasm and your energy have inspired me. Despite that we undertook different paths, you have always been there, encouraging and supporting me every single time I needed help. You are such a good friend, something I will never forget!
To Dr Conor McCann, for having taught me that the most important thing in science is to have good ideas and be very organised and determined. It is not always a matter of how many hours we spend in the lab, but how we use our time there. For always having a good comment and new ideas to share with me, I will never thank you enough.
My gratitude also goes to Dr Anna Urciuolo. If it wasn’t for you, I’ll probably would not even have started this journey!
Dipa, Conor, Anna, even if you are very different people, you all inspired me so much as scientists and you are the best I could hope to work with!

Thanks to all the people, staff and students who helped me during this journey. Special thanks to Stephanie, Vruti, Sahira and Sindhu: your help has been priceless. I’m very grateful to all the colleagues I had the chance to work with and in particular to all PhD students that shared this journey with me.
Carlotta, for being the first of us to succeed. You gave us all the knowledge and the hope that all this, one day, would finish.
Giulia and Mike, for helping me in this last year of work. I hope I gave you good advice.

Sara and Alfonso, for sharing with me the entire journey, with all its many experiences. For all the laughter and tears and for being there for each other at each single crisis, becoming such good friends. I have no words to express my gratitude.

I would like to thank all the many friends I have in London, the extended Italian family, that made me feel a bit less far from home. I was extraordinary lucky to meet all of you and I will have such good memories of my time here.

Most importantly, I want to thank my family, my parents Lino and Mariagrazia, my brothers Michele and Mauro, my sister in law Marina and my little niece Giulia. Thanks for being always present and supportive in all the difficult moments. All the endless calls and pictures made me feel a bit less far from you all. Thank you for understanding when I couldn't be there. All this would not be possible without you!

Last but not least, I want to thank my husband Luca. You have always been there for me, in every moment of the many years we spent together. Your professional help for this work was invaluable and I will never thank you enough for this. But it was thanks to your love, your support, your advice and your encouragements that I made it through this experience and I could realise all this. This thesis is for you!